Probing human cytochromes P450: mutational and spectroscopic analysis of CYP2D6

Keizers, P.H.J.

2006

document version
Publisher's PDF, also known as Version of record

Probing human cytochromes P450:

mutational and spectroscopic analysis of CYP2D6

Probing human cytochromes P450: mutational and spectroscopic analysis of CYP2D6

Peter H.J. Keizers

For the printing of this thesis the Jurriaanse Stichting and the Nederlandse Vereniging voor Toxicologie (NVT) are acknowledged for their grant and presentation award respectively.

Printed by Printpartners Ipskamp

Cover: steel covered with ironoxide

VRIJE UNIVERSITEIT

Probing human cytochromes P450: mutational and spectroscopic analysis of CYP2D6

ACADEMISCH PROEFSCHRIFT

ter verkrijging van de graad Doctor aan
de Vrije Universiteit Amsterdam,
op gezag van de rector magnificus
prof.dr. T. Sminia,
in het openbaar te verdedigen
ten overstaan van de promotiecommissie
van de faculteit der Exacte Wetenschappen
op maandag 26 juni 2006 om 13.45 uur
in de aula van de universiteit,
De Boelelaan 1105

door

Peter Henricus Jozef Keizers

geboren te Stad Delden

promotoren:	prof.dr. N.P.E. Vermeulen
	prof.dr. S.M. van der Vies
copromotor:	dr. J.N.M. Commandeur

hic igitur, penitus qui in ferrost abditus aeër,
sollicito motu semper iactatur eoque

thus then, this air in iron so deeply stored,
is tossed evermore in vexed motion

Titus Lucretius 50 BC

Leescommissie: prof.dr. M. Ingelman-Sundberg
prof.dr. C. Gooijer
prof.dr. K. Lammertsma
prof.dr. S. de Vries
prof.dr.ir. I.M.C.M. Rietjens

The investigations described in this thesis were carried out in the Leiden Amsterdam Center for Drug Research (LACDR), Division of Molecular Toxicology, Department of Chemistry and Pharmaceutical Sciences, Faculty of Sciences, Vrije Universiteit, De Boelelaan 1083, 1081 HV Amsterdam, the Netherlands.

Contents

Introduction

Chapter 1

General introduction

All organisms express enzymes that can convert both endogenous and exogenous compounds into more water-soluble compounds. This process, known as biotransformation, holds a central position in the detoxification processes in the organisms, but as a paradigm it can also lead to increased toxicity of the parent compound by bioactivation [1, 2]. In man, these enzymes are predominantly expressed in the liver and they determine the fate of compounds like drugs, industrial chemicals, pyrolysis products in cooked food and also plant and animal toxins [3]. Biotransformation, or drug metabolism, is usually divided in to three phases. Phase I reactions involve the introduction of functional groups by hydrolysis, reduction and oxidation. In phase II reactions, cofactors react with the functional groups that were already present on the molecule or that are introduced by phase I reactions. The phase II reactions involved are glucuronidation, sulphonation, acetylation, methylation and conjugation with amino acids or glutathione. As an example, the metabolism of 3,4-methylenedioxymethylamphetamine (MDMA) is shown in Figure 1, showing that in both phase I and phase II reactions several enzymes can be involved in the metabolism of the same substrate. Phase III metabolism involves further modifications of the phase II products in order to facilitate urinary excretion even more. In phase I the most important enzymes are cytochromes P450 (CYPs). These enzymes have been subject of elaborate research over the last thirty years, mainly because of their important role in biotransformation of carcinogens, steroids and drugs. Because of their involvement in drug metabolism, a good understanding of these enzymes at the molecular level would be advantageous in the process of drug discovery and development, to prevent drug-drug interactions and decrease the risks of side effects.

Cytochromes P450

It was in the Netherlands in 1932 that Verkade et al. isolated urinary dicarboxylic acids from dogs and human volunteers after feeding fatty acids [4]. This was the first observation of fatty acid ω-oxidation, where the insertion of the oxygen is at the least reactive position. Whenever biological oxidations occur through unpredictable chemical principles, usually cofactors such as metals or coenzymes or specific amino acid residues are required in the reaction [5]. Later it was found that the oxidation of 2,2-dimethyloctanoic acid occurred in liver tissue, by an unstable membrane bound enzyme system [6]. Using ion exchange column chromatography the components of this enzyme system that was also responsible for ω-hydroxylation of lauric acid, could be purified from rabbit liver and activity could be reconstituted after mixing of the components [7].
The hemeprotein nature of these hepatic enzymes became known by the experiments of Omura and Sato [8]. It was already shown before that mammalian liver pigments could bind CO when reduced, thus giving a typical absorbance maximum at 450 nm [9]. Omura and Sato showed that an unusual cysteine ligated hemeprotein was responsible for this absorption and that this protein was reducible by both NADPH and NADH. The hemeprotein was named cytochrome because it was a pigment (in Greek: chromos) within the cells (in

Greek: cyto), and P450 because the pigment gave a typical absorbance band at 450 nm. Later, it was again Omura who showed that these cytochromes P450 (CYPs) were involved in the hydroxylation of steroids and drugs [10].
The expression of CYPs is not restricted to mammals but can be found in virtually all organisms, in all kinds of tissues. They are involved in synthesis and breakdown of a large variety of different compounds, dependent on the isoenzyme. So far there are about 4500 unique named sequences of CYPs known (drnelson.utmem.edu). They are named according to sequence homology [11-15]. In general, when their amino acid sequences are less then 40% identical, CYPs are assigned to different gene families, indicated by a number. When sequences are between 40 and 55% identical, they are assigned to different subfamilies, indicated by a capital letter. When the sequences are more then 55% identical, they are classified as members of the same subfamily and if the sequences and the function are similar, then they get the same gene number. For instance, a CYP from the family 2, subfamily D, isoenzyme 6 is thus named CYP2D6.

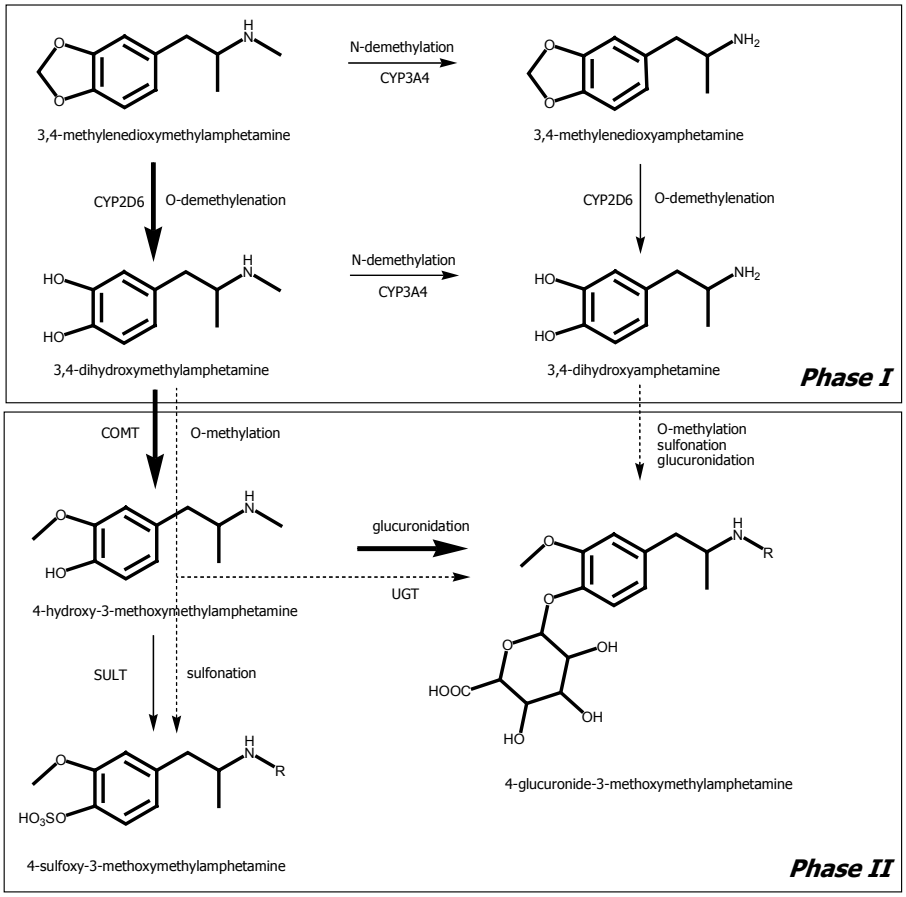

Figure 1: Metabolic fate of 3,4-methylenedioxymethylamphetamine (MDMA or XTC) in man, showing phase I O-demethylenation and N-dealkylation catalyzed by CYPs, and phase II methylation, sulfonation and glucuronidation catalyzed by catechol O-methyl transferase (COMT), sulfotransferase (SULT) and UDP-glucuronyl transferase (UGT), respectively (adapted from de la Torre [16]). The thickness of the arrows indicates the relative importance of the pathway.

Drug metabolism by CYPs

There are currently about 60 different human CYPs known (drnelson.utmem.edu). Approximately a dozen of these are involved in drug metabolism; the CYP isoforms, 1A2, 2A6, 2B6, 2C8, 2C9, 2C19, 2D6, 2E1, 3A4, 3A5 and 3A7 [17]. All together these CYPs account for the phase I metabolism of about 90% of the currently marketed drugs [18]. In Figure 3 the relative amounts of the major human liver CYP isoenzymes involved in drug metabolism in a group of 30 Caucasian patients is shown. CYP3A4 is the most abundant isoenzyme, followed by the CYP2C family members, and than CYP1A [19]. When it comes to the number of metabolized drugs in which a CYP isoenzyme is involved again CYP3A4 takes the largest share, followed by the CYP2C family members and CYP2D6. So although the hepatic concentration of CYP2D6 is relatively low, i.e. an average of 3% of the total amount of CYP, it is involved in the metabolism of 20-30% of the drugs currently on the market [19-21].

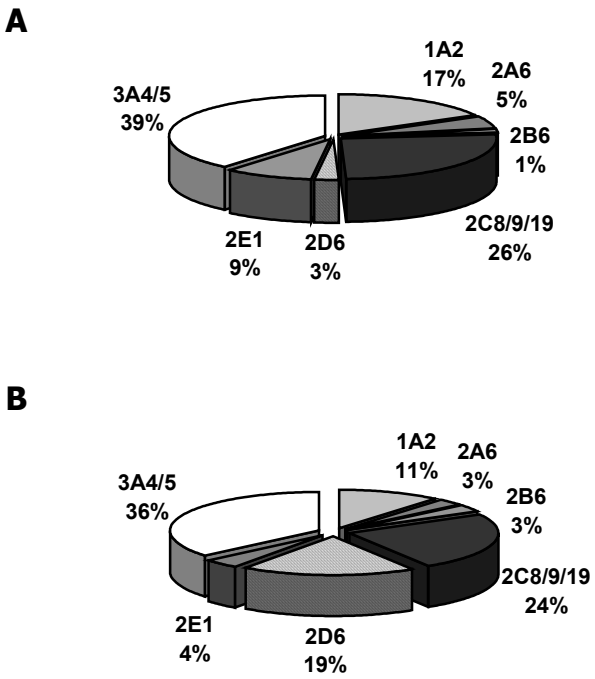

Figure 3: Relative amounts of the drug metabolizing CYPs in human liver (A), and the contribution of these CYPs in the metabolism of the currently prescribed drugs (B) [19, 22].

Polymorphisms of CYPs

The efficacy and pharmacokinetics of a drug can be determined genetically. Genes encoding proteins involved in the functioning, transport, or metabolism of the drug for instance, can be present in the population in two or more allelic forms and can therefore affect the activity of the drug. When at least two alleles have frequencies larger than 1% this is called a genetic polymorphism. In some occasions these polymorphisms are caused by a mutation,

deletion or insertion of just a single nucleotide, thus called single nucleotide polymorphisms (SNPs). Many drug-metabolizing enzymes are known to be polymorphic. Aldehyde dehydrogenase (ALDH) activity for instance, is severely lowered in half of the populations in Japan, China, Korea, Taiwan and Vietnam, due to an ALDH3 deficiency. Other known polymorphic enzymes involved in drug metabolism are: UDP-glucuronyltransferases 2 family members, sulfotransferase SULT1A3, catechol *O*-methyl transferase, *N*-acetyl transferases 1 and 2, glutathion S-transferase M1, and many CYPs [3, 23]. There are as much as 22 human CYPs expressed from different alleles (www.imm.ki.se/CYPalleles). Nevertheless, of these 22 enzymes, only few were found with significant clinical effects caused by the polymorphisms. Minor clinical effects were reported for CYPs 1A2, 2A6, 2B6 and 2C8 polymorphisms, and major effects of polymorphism for CYPs of the 2 family, namely CYP2C9, CYP2C19 and CYP2D6 [24].

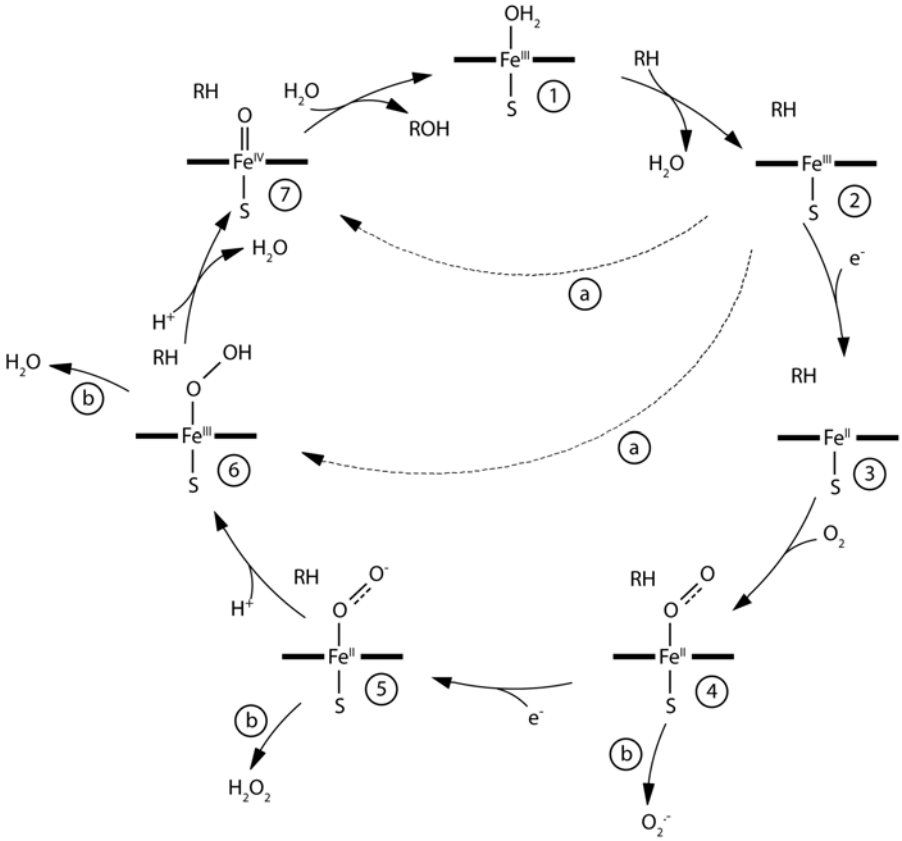

Figure 2: The catalytic cycle of CYPs, adapted from [25-27]. The cycle is subdivided in seven stages (1-7), artificial oxidants short-circuits (a), and uncoupling pathways are indicated (b), the horizontal bars represent the porphyrin ring.

CYP catalytic activity

Although CYPs are involved in what appears to be a multitude of different reactions, the activity of all CYPs can be summarized in a general catalytic cycle [25, 27-29], as shown in

Figure 2. The cycle starts (Stage 1) in the resting state, in which the ferric iron is often bound to a water molecule in the axial position. In most CYPs, the heme iron atom in Stage 1 is predominantly in the low spin state. Then (Stage 2), a substrate enters the active site, displaces the 6^{th} ligand, which often causes the iron spin state to change from low to high. Whether the spin change triggers the next step, followed by the rest of the cycle is still under debate [30, 31]. At Stage 3, the five-coordinated iron accepts the first electron, delivered by the cytochrome P450 NADPH-reductase (CPR), so that to the ferrous iron atom formed can bind molecular oxygen (Stage 4). Subsequently, a second electron is delivered, yielding a negatively charged iron peroxo intermediate (Stage 5). This species is protonated to the hydroperoxo-iron (Stage 6), which after the loss of water yields the oxenoid-iron, also known as compound I, the originally presumed active oxidant species (Stage 7). The oxenoid-iron oxygenates the substrate, the product is released and a water molecule binds again to the ferric iron (Stage 1).
The general catalytic cycle can be short-circuited when artificial oxygen delivering agents are used, such as hydrogen peroxide or organic peroxides. In these cases, the cycle is shortened, and turns immediately from Stage 2 to Stage 6 or 7, depending on the nature of the oxidant, indicated by dashed arrows (a) [29, 32, 33]. On the other hand, uncoupling or autoxidation may occur [34], in which the cycle is started and molecular oxygen is reduced without leading to product formation. These processes are also known as the oxygen reductase activity of a CYP [35], and are indicated by arrows (b). Then superoxide anion can be formed from Stage 4, hydrogen peroxide can be formed from Stage 5, or water can be formed from Stage 6 [26].
Currently it is under debate whether just one oxidant (the oxenoid-iron, Stage 7) can create all the experimentally detected reactivity patterns. The proton needed to form the oxenoid-iron (from Stage 6 to 7) is thought to be delivered by a conserved I-helix threonine residue in the CYP [36]. Mutation of this residue to an alanine in CYPs 2B4 and 2E1 led to a drastically changed regioselectivity in catalysis [37, 38]. While some model activities of the mutated CYPs were decreased, others were increased. This could be explained by hypothesizing the threonine to be responsible for the ultimate proton donation to form Stage 7, and by introducing the iron-oxo species preceding the oxenoid-iron, i.e. the iron-peroxo and the iron hydroperoxo (Stages 5, and 6 respectively) to be reactive oxygenating species as well. Together these multiple oxygenating species were thought to be responsible for the different reactions CYPs can catalyze, each with their own preferences for certain types of reactions, ranging from nucleophilic to electrophilic [39]. The use of alternative oxidants and kinetic isotope studies experimentally strengthened this hypothesis [40]. Furthermore, in recent studies the hydroperoxo-iron was experimentally detected using electron magnetic resonance (EMR) techniques, and shown to be stabilized by the presence of substrates (*vide infra*) [41]. However, the identity of a second (or more) electrophilic oxidant remains speculative. The hydroperoxo-iron is experimentally not yet distinguishable from iron-complexed hydrogen peroxide [42]. Furthermore, it has been suggested from theoretical computational studies that the hydroperoxo-iron is a poor oxidant, not capable to compete with the reactivity of the oxenoid iron [43]. As an alternative, using density functional theoretical studies it has been suggested that the oxenoid-iron exists in degenerate spin states and can therefore act (chameleon wise) like two different oxidants [43, 44].

Reactions catalyzed by CYPs
Although the catalytic activity may be represented in one schematic cycle, it can lead to many reactions: i.e. aromatic and aliphatic hydroxylation, epoxidation, heteroatom

oxygenation, heteroatom dealkylation, dehalogenation, dehydrogenation, cleavage of esters, oxidative group transfer, substrate reduction and oxygen reduction [26]. Examples of these reactions are listed in Table 1. The multitude of reactions CYPs can catalyze makes the enzymes highly versatile.

Table 1: Types of reactions catalyzed by CYPs with examples of each reaction [3, 26, 35].

Reaction	Example
Aliphatic hydroxylation	Lauric acid ω-hydroxylation by CYP4A
Aromatic hydroxylation	Coumarin 7-hydroxylation by CYP2A6
Epoxidation	Verlukast epoxidation by CYP1A1
Heteroatom oxygenation	Omeprazole sulfoxidation by CYP3A4
Heteroatom dealkylation	Dextromethorphan *O*-dealkylation by CYP2D6
Dehalogenation	Halothane to trifluoroacetylchloride by CYP2E1
Dehydrogenation	Acetaminophen to *N*-acetylbenzoquinoneimine by CYP2E1
Cleavage of esters	Loratadine to desloratadine by CYP3A4
Oxidative group transfer	Amphetamine to phenylacetone by CYP2C
Reduction	Dimethylaminoazobenzene reduction by CYP2B
Oxygen reduction	2,3,5,6-tetramethylbenzoquinone by CYP1A

Dynamics of CYPs

It is thought that CYPs need to undergo conformational changes upon substrate binding, substrate conversion and product release for several reasons. At first, substrates can be relatively large and bulky but need to enter the inside of the CYP to reach the active site. So it is thought that substrate entrance channels [45], need to open to accommodate a substrate [46]. Secondly, single CYPs usually have a wide range of compounds that are substrates, so their active site and substrate entrance channels need to be able to adapt their sizes to the substrate. Thirdly, after the oxidative metabolism the physico-chemical character of the substrates has changed from hydrophobic to more hydrophilic. To enable the product to leave the buried active site, a product egress channel needs to be present to accommodate the product on the way out [47]. At fourth, CYPs interact with reducing partner proteins, like the CPR, cytochrome b5 and maybe even other CYPs by forming dimers [48]. Because of the relatively low concentration of CPR in mammalian hepatic membranes, a conformation driven regulation of interaction between CYPs and CPR is likely [49]. Therefore, conformational changes of CPR and/or CYP are thought to take place [50]. For all the reasons listed above, CYPs are thought to be highly dynamic proteins [51]. To measure the dynamics of proteins fast spectroscopic techniques are needed in combination with fast triggers, stop flow or freeze quenching techniques (*vide infra*).

The isoform CYP2D6

The relatively large share CYP2D6 takes in drug oxidation while being a low abundant hepatic CYP, in combination with its polymorphic nature make CYP2D6 one of the most relevant CYPs in human drug metabolism. The history of the enzyme starts in the late seventies. In 1975 it was shown that debrisoquine, an antihypertensive drug, was predominantly 4-hydroxylated in man after oral administration [52]. A few years later, a typical bimorphically distribution was found of this metabolite in the urine of 94 volunteers after a 10 mg oral dose [53, 54]. The 4-hydroxylation of debrisoquine was subsequently shown to be metabolized by a specific CYP, relating polymorphisms with this large family of drug metabolizing enzymes [55]. The rat debrisoquine 4-hydroxylase was purified in 1984

by Larrey *et al.* [56], which was followed by the purification of the responsible human enzyme [57]. It was later found that the gene for this human enzyme was located on chromosome 22 [58]. Two debrisoquine hydroxylase genes were found in the rat and classified in a new family; P450II [59]. In humans the cDNA and amino acid sequences were found of a single gene encoding the debrisoquine hydroxylase and originally named P450IID1 [60].
Soon afterwards, mutant alleles and gene deletions of cytochrome P450IID1 were observed explaining for the deficient metabolism of debrisoquine and other drugs [61]. After establishment of the official cytochrome P450 nomenclature in 1993, the unique name CYP2D6 was given to the human debrisoquine hydroxylase [12]. The high frequency of mutations in the gene was hypothesized to be caused by the presence of a downstream CYP2D7 with a disrupted reading frame and CYP2D8, a pseudogene, likely to transfer mutations easily via gene conversions into CYP2D6 [62]. Currently, the polymorphism of CYP2D6 is characterized by multiple alleles, in total numbering up to more than 80 sequences (www.imm.ki.se/CYPalleles/cyp2d6.htm). The consequence of these different alleles is an interindividually varying activity of the enzyme. Thus 10% of the Caucasians and 1% of the Asians have two null alleles. The resulting poor metabolizer (PM) phenotype is characterized by the inability to use CYP2D6 dependent metabolic pathways. On the other end of the spectrum, 2% of the Caucasians and up to 29% of the Ethiopians display the ultrarapid metabolizer (UM) phenotype, caused by alleles carrying multiple gene copies, or by promotor mutations [63]. Individuals having the UM phenotype are typical in having a high metabolic ratio for CYP2D6 substrates. In between PM and UM are the normal extensive metabolizer (EM) phenotype, with one or two functional genes and the intermediate metabolizer (IM) phenotype, characterized by at least one partially deficient allele.
CYP2D6 is known for its role in drug metabolism. It is involved in the metabolism of about 20-30% of all currently prescribed drugs [19]. These include often prescribed drugs like β-blockers, neuroleptics, antidepressants and antiarythmics [21, 64]. A selection of the drugs that are (partly) metabolized by CYP2D6 dependent pathways is shown in Table 2.

Table 2: Examples of drugs of different therapeutic classes known to be metabolized by CYP2D6, adapted from [3, 64]. A more extended table including the relevant other human drug metabolizing CYPs was made by Rendic [65].

Therapeutic class	Drug	Reaction by CYP2D6
Analgesica/antitussives	Codeine	*O*-demethylation
	Dextromethorphan	*O*-demethylation
	Dihydrocodeine	*O*-demethylation
	Ethylmorphine	*O*-deethylation
	Hydrocodone	*N*-demethylation
	Norcodeine	*O*-demethylation
	Oxycodone	*O*-demethylation
	Tramadol	*O*-demethylation
Anti-ADHD drugs	Atomoxetine	Aromatic hydroxylation
Antiarrhythmics	Aprindine	Aromatic hydroxylation
	Encainide	*O*-demethylation
	Flecainide	*O*-dealkylation (?)
	Mexiletine	Aromatic hydroxylation
	N-propylajmaline	Benzylic hydroxylation
	Procainamide	Arylamine *N*-oxidation
	Propafenone	Aromatic hydroxylation
	Sparteine	Aliphatic hydroxylation

Antidementia drugs	Galanthamine	*O*-demethylation
	Nicergoline	*N*-demethylation
Tricyclic antidepressants	Amitriptyline	Benzylic hydroxylation
	Clomipramine	Aromatic hydroxylation
	Desipramine	Aromatic hydroxylation
	Imipramine	Aromatic hydroxylation
	Nortriptyline	Benzylic hydroxylation
Other antidepressants	Citalopram	*N*-demethylation
	Desmethylcitalopram	*N*-demethylation
	Fluoxetine	*N*-demethylation
	Fluvoxamine	Unclear
	Maprotiline	Unclear
	Mianserin	Aromatic hydroxylation
	Minaprine	Aromatic hydroxylation
	Mirtazapine	Aromatic hydroxylation
	Paroxetine	Demethylenation
	Venlafaxine	*O*-demethylation
Antidiabetics	Phenformine	Aromatic hydroxylation
Antiestrogens	Tamoxifen	Aromatic hydroxylation
Antihypertensives	Debrisoquine	Benzylic hydroxylation
	Guanoxan	Aromatic hydroxylation
	Indoramin	Aromatic hydroxylation
Antiemetics	Dolasetron	Aromatic hydroxylation
	Ondansetron	Aromatic hydroxylation
	Tropisetron	Aromatic hydroxylation
Antihistamines	Mequitazine	Aromatic Hydroxylation
	Promethazine	Aromatic hydroxylation
Antipsychotics	Clozapine	*N*-demethylation
	Haloperidol	*N*-dealkylation
	Perphenazine	*N*-dealkylation
	Remoxipride	Aromatic hydroxylation
	Risperidone	Aliphatic hydroxylation
	Thioridazine	Sulfoxidation
	Trifluperidol	*N*-dealkylation
	Zuclopenthixol	*N*-dealkylation
Appetite suppressants	Dexfenfluramine	*N*-dealkylation
Beta adrenergic blocking agents	Alprenolol	Aromatic hydroxylation
	Bufuralol	Benzylic hydroxylation
	Bunitrolol	Aromatic hydroxylation
	Bupranolol	Aromatic hydroxylation
	Carvedilol	Aromatic hydroxylation
	Metoprolol	Aliphatic hydroxylation
	Propranolol	Aromatic hydroxylation
	Timolol	*O*-dealkylation
Calcium antagonist	Perhexiline	Aliphatic hydroxylation
MAO-inhibitors	Amiflamine	*N*-demethylation
	Brofaromine	*O*-demethylation
	Deprenyl	*N*-demethylation
Recreational drugs	Methoxyamphetamine	*O*-demethylation
	MDMA[1], MDEA[2]	*O*-demethylenation
	Methoxyphenamine	*O*-dealkylation
Vasodilatators	Cinnarizine	Aromatic hydroxylation
	Flunarizine	Aromatic hydroxylation

[1] *3,4-methylenedioxymethylamphetamine,* [2] *3,4-methylenedioxyethylamphetamine*

Sometimes the use of drugs can result in serious side effects that could not be predicted from the prior clinical studies. These so-called adverse drug reactions (ADR's) are a significant cause of morbidity and mortality. Although many ADR's are considered not preventable, it has been suggested that these reactions may be avoided through individualization of drug therapies based on genetic information [66]. Based upon a search on adverse drug reaction studies published between January 1995 and June 2000, it was found that drug therapy based on individual genetic makeup could result in a clinically important reduction in adverse outcomes. In relation to this, it was shown that the polymorphic CYP2D6 is involved in 38% of all ADR's [67].
The highest expression levels of CYP2D6 are found in the human liver, but also in the skin [68], and in the brain significant levels of CYP2D6 mRNA and protein can be found [69]. A frameshift mutation in the pseudogene CYP2D7 leads to a brain specific expression of a splice variant of this enzyme in Indian people [70]. This splice variant was shown to be even more active than CYP2D6 in morphine formation from codeine. Besides roles in drug metabolism, there seem to be endogenous functions for the enzyme as well. It was shown that CYP2D6 selectively metabolizes 5-methoxytryptamine, 5-methoxy-*N,N*-dimethyltryptamine and pinoline, with high turnovers while other structurally similar endogenous compounds were not significantly metabolized [71-73]. The association with serotonin metabolism suggests that the enzyme may influence mood and mental health. This hypothesis was strengthened by clinical studies revealing a high amount of patients with persistent mood disorders having the UM phenotype [74].

Computer modeling of CYP2D6

As outlined above, CYPs play a major role in the disposition of drugs and their pharmacological and toxicological effects. The absorption, distribution, metabolism and excretion (ADME) properties of new drug-like compounds in relation to CYPs can be screened *in vitro*. However, to reduce screening efforts and also to predict the ADME properties of theoretical compounds, *in silico* predictions approaches to study CYP-compound interactions are a necessity [75]. Computational studies on ligand-to-CYP interactions can be divided into two different approaches, one starting from a model based on the known ligands (pharmacophore modeling) and the other starting from a model of the protein. Both approaches were used to examine oxidative metabolism of compounds by CYP2D6 and will shortly be discussed.

Pharmacophore modeling

CYP2D6 is one of the CYP isoforms most extensively studied computationally [75, 76], because of its important role in drug metabolism and being a polymorphic enzyme. As yet, the X-ray structure of CYP2D6 is unknown. Furthermore, the apparent narrow substrate selectivity of this enzyme compared to other CYPs, makes this enzyme suitable for a pharmacophore modeling approach. Practically all compounds that are metabolized by CYP2D6 contain a basic nitrogen atom and at least one aromatic moiety (Table 2). The initial substrate models of CYP2D6 were not in agreement with the distance between the substrate basic nitrogen and the predicted site of oxidation distance being 5 Å [77], or 7 Å [78]. A new substrate model was developed, hypothesizing the presence of a carboxylate group in the protein to interact with the substrate basic nitrogen (Figure 4). The substrate nitrogen atoms were proposed to interact with either one of the two carboxylate oxygen atoms, thus explaining the two different distances between the nitrogen atom and the site

of oxidation [79]. This model had a higher predictive value compared to the previous models. This was further confirmed by experimental validation of the two predicted metabolites of the new compound GBR12909 [80]. Later, the model was extended with a large set of substrates [81]. In this model also the heme moiety and the I-helix containing D301 were incorporated leading to a refined and more restrictive substrate model.

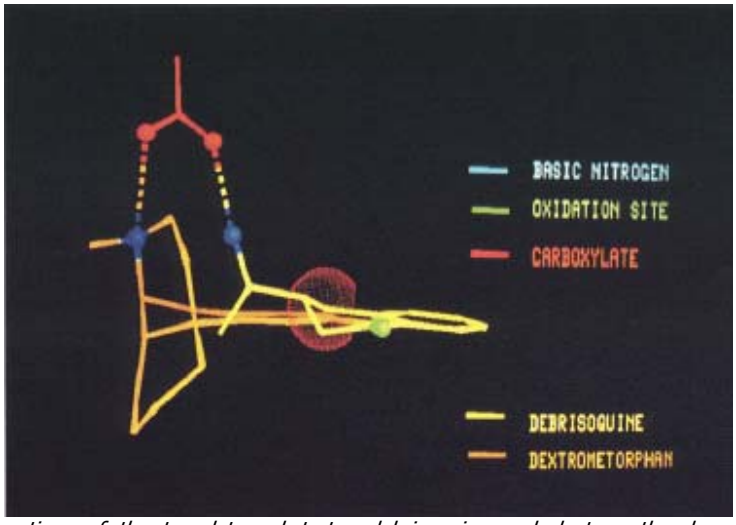

Figure 4: Conformations of the template substrates debrisoquine and dextromethorphan used to construct the pharmacophore model of CYP2D6 [79]. The sites of oxidation are fixed and the dotted surface represents a part in the molecule where all substrates exhibit a negative electrostatic potential. A colored version of this picture is attached in the Appendix of this thesis.

Homology modeling

The availability of crystallographic data of bacterial CYPs made it possible to build protein models of CYP2D6 based upon homology. At first, in the late eighties the crystal structure of bacterial CYP101 was resolved [82-84], and this was used as a template to construct a homology model of CYP2D6 [85]. This protein model was able to accommodate debrisoquine and dextromethorphan, and aspartic acids 100 or 301 were proposed as the carboxylate interacting with the substrate basic nitrogen atoms. However, due to relatively low homology (15%), not all regions of the enzyme could be modeled well. Better templates were the crystal structures of the slightly higher homologous (20%) CYP102 [86, 87], for developing CYP2D6 protein models [88, 89]. Including experimental spectroscopic data strengthened the CYP102 based homology model. The active site orientation of the substrate codeine was determined using the spin lattice relaxation NMR technique (*vide infra*). This codeine active site orientation was then used in the homology model to fixate D301 in the active site in a way that it would interact with the codeine nitrogen atom [88]. It was concluded that CYP2D6 resembled CYP102 more than CYP101 or CYP108 and thus relative positions of active site residues could be better predicted with this model. More modeling studies were performed to compare the different available crystal structures as templates for a CYP2D6 protein model and also parts of structures were combined in order to use the best resolved parts of the crystal structures in order to get better accommodations of the substrates in the enzyme active site [90-92].

To utilize the strengths of the two modeling approaches, pharmacophore modeling and protein modeling, these were also combined. This way, the metabolism of a wide variety of compounds could be correctly predicted, even the relatively often by CYP2D6 catalyzed *N*-dealkylation reactions (Table 2), which were not included before [91, 93, 94].

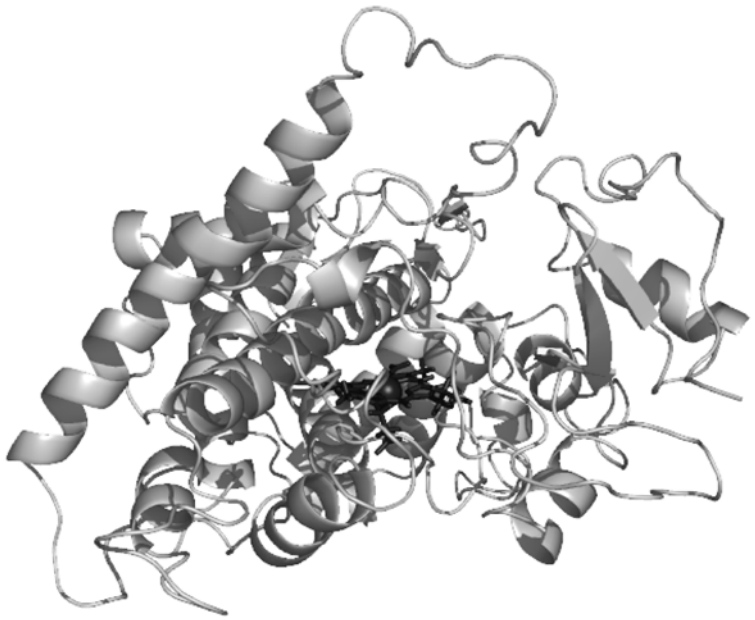

Figure 5: Protein model of CYP2D6 using the crystal-structure of CYP2C5 as a template [95]. The porphyrin ring is depicted (in dark), with the centering iron atom as a sphere.

Further improvement of the protein models of CYP2D6 was possible after the first crystal structure of a mammalian CYP, rabbit CYP2C5, was solved [96]. Because of the higher homology of CYP2C5 with CYP2D6 (40%), compared to CYPs 101 and 102 (15-20%), the predictive quality of the new model could be significantly increased [95, 97]. Rigid docking of substrates in the protein model resulted in orientations with predicted sites of oxidation corresponding to experimental product formation. From the rigid docking of 12 ligands into the protein model, the interacting active site residues were determined. In a comparative study of CYP2 family member sequences, 6 substrate recognition sites (SRS) were appointed [98]. In analogy, these 6 SRS were identified in CYP2D6, containing in total 22 residues in the B/C interhelical loop (SRS 1), helices F G and I (SRS 2, 3 and 4 respectively), the strands 1-4 and 2-1 of betasheets 1 and 2 (SRS 5) and a part of betasheet 4 (SRS 6). This model (shown in Figure 5), was capable of accommodating codeine in the experimentally determined orientation [88], and did place the experimentally validated D301 [99, 100] in the active site, but not as the residue interacting with the basic nitrogen atom. So although the protein model predicted D301 to be located in the active site, in many cases it was not involved in fixation of the substrate basic nitrogen atom, as it was suggested in the previous CYP2D6 models. The residue E216 was subsequently proposed to fulfill this role [95], and later mutagenesis studies confirmed this prediction [101, 102]. It appeared that using the mammalian CYP2C5 crystal structure as a template was indeed a big improvement for the CYP2D6 homology model. The carboxylate of D301 now appeared to

form hydrogen bonds with the backbone nitrogen atoms of V119 and F120. This phenylalanine, F120 and also F483, were thought to be responsible for π-stacking and van der Waals interactions with substrates like codeine, and eventually the experimental evidence for this was delivered (this thesis and [103, 104]).

Table 3: Site-directed mutation studies of CYP2D6.

Residue	Mutated to	Substrates used	Possible roles
P34	S	Debrisoquine, bunitrolol	Known SNP, small effect on metabolism [105].
G42	R K V F S E	Debrisoquine, bunitrolol	Residue appears to be involved with enzyme stability and membrane anchoring [105].
F120	A L T S H W M	Dextromethorphan, bufuralol, MAMC, MDMA	Residue involved in binding and orientation of substrates, although mutation and substrate dependent [103, 104], (this thesis).
W128	F	MAMC	May be involved in porphyrin anchoring (this thesis).
E216	D Q A H F K	Dextromethorphan, bufuralol, diclofenac, testosterone, tolbutamide, nifedepine, spirosulfonamide	Role in fixation of basic nitrogen atom present in typical substrates [101, 102].
E222	A	Bufuralol	Residue just out of active site, might have a role like E216 [104].
R296	C	Debrisoquine, bunitrolol	Known SNP, no effect on metabolism [105].
D301	E N G Q A δ	Dextromethorphan, bufuralol, diclofenac, testosterone, tolbutamide, nifedepine	Residue involved in fixation of substrate basic nitrogen atom, and/or involved in positioning of F120, and contributing to a net negative charge of part of the active site [99-101, 106, 107], (this thesis).
S304	A	Metoprolol, propranolol, debrisoquine	Residue not involved in substrate binding, mutation does not lead to large changes in enzyme activity [108].
T309	V	Dextromethorphan, bufuralol, MAMC, MDMA	Residue involved in activation of iron bound oxygen (this thesis).
T312	V	Dextromethorphan, bufuralol, MAMC, MDMA	Residue not involved in activation of iron bound oxygen, mutation has no effect on activity (this thesis).
M374	V	Metoprolol	Residue seems to be mutated in initial cloning experiments. Mutation does to small extent influence regio- and enantioselective metabolism of metoprolol [109].
F481	Y N G	Metoprolol, debrisoquine, dextromethorphan	Residue seems to be outside active site. However mutation leads to lower affinity to some substrates [110].
F483	I W	Testosterone, dextromethorphan, bufuralol, MAMC, MDMA	Residue involved in binding and orientation of substrates, although mutation and substrate dependent [111], (this thesis).
S486	T	Debrisoquine, bunitrolol	Known SNP, no effect on metabolism [105].

δ = deletion of residue

Novel high resolution crystal structures of CYP2C5 with substrates bound [112, 113], made it recently possible to further optimize the protein model of CYP2D6 (this thesis and [114]). This model does not have D301 positioned in the active site anymore, and the active site has a more closed conformation, due to incorporation of the F/G-loop, which was not resolved in the former CYP2C5 crystal structure. Applications of this new CYP2D6 model show good correlations with experimental data (this thesis and [75, 114]). The new model could be used to rationalize experimental findings with substrate interacting residues like F120, and it could also be used to predict active site residues involved in the mechanism of oxidation (this thesis).

Site directed mutagenesis studies of CYP2D6

Predictions of active site residues crucial for the functioning of CYP2D6, based upon substrate and protein models of CYP2D6 were usually validated by site-directed mutagenesis studies. An overview of these studies is given in Table 3. The residues of interest are listed together with the mutations and the postulated functions of the residues. As yet, D301 is the most studied residue. It was first indicated as the active site carboxylate involved in fixation of the substrate basic nitrogen atom and the first residue subjected to site directed mutagenesis. Although mutation of this amino acid led to a decreased CYP2D6 activity, in the latest models it appears not to be in the active site. Instead, another active site carboxylate, E216, was suggested to be primarily involved in binding of substrate basic nitrogen atom. Besides one or two carboxylates, active site phenylalanines, F120, F481 and F483, were thought to interact with the aromatic moiety present in most CYP2D6 substrates. After mutagenesis of any of these, the catalytic activity of CYP2D6 decreased. The negative effect on the catalytic activity of mutating D301 is thought to be indirect. D301 is suggested to position the active site substrate aromatic moiety interacting F120, thereby affecting substrate binding. Several more distal active site residues are probably also interacting with the larger substrates, so more mutagenesis studies are required still (this thesis).

Table 4: Biophysical techniques used to study the structure and structural changes of CYPs.

Technique	Type of information obtained	CYP studied
X-ray	3D structure [46, 115].	101, 102, 2C5, 2C9, 3A4
UV-Vis	Spin state, oxidation state, active oxygen species, ligand binding, active enzyme quantitation [8, 116, 117].	101 many others
Raman	Spin state, oxidation state, coordination number, ligand binding, porphyrin conformation [118].	101, 102, 1A2, 3A4
Infrared	CO and NO binding, effect substrate binding, active site conformation [119].	101, 102
Mossbauer	Iron electronic stucture [120].	101
NMR	3D structure and substrate active site orientations [121, 122].	101, 102, 1A2, 2C9, 2D6
EMR	Spin state and ligation, oxygenating species lifetimes [123].	101, 102
Fluorescence	Intraprotein distances, protein to ligand distances, protein conformational changes [124].	101, 11A1, 2B4
AFM/STM	Shape and interaction with membrane and other proteins [125].	101, 2B4
Mass spectrometry	Covalent interactions, active site topology [126].	2C9, 2E1
Cyclic voltametry	Iron electronic stucture [127].	2C9
Chemical probes	Topology of active site cavity [128].	101, 2D6, 3A4

Biophysical studies on cytochromes P450

Complementary to mutagenesis studies, structural information on CYPs can also be obtained by using a variety of spectroscopic and other biophysical techniques. The obtained data is usually interpreted in combination with a protein model in order to determine the mechanism by which the CYP is functioning. The most relevant techniques to study CYPs are briefly introduced below and an overview is given in Table 4.

Table 5: Overview of the currently available crystal structures of CYP isoforms. modified from de Graaf et al (2005) [75].

CYP	Species	Ligands	mutants	PDB
101	Pseudomonas putida	*R*- and *S*-camphor, and analogs, 4-phenylimidazole, metyrapone, nisotine, (+)α-pinene	F87W/Y96F/ V247L/C334A, F87W/Y96F, R109K, R112K, D251N, T252I, T252A, C334A, L358P/C334A	2CPP
102	Bacilus megaterium	Palmitoleic acid, *N*-palmitoylglycine	A264E, T268A, F393H	1BU7
107A1	Saccharopolyspora erythrea	9-aminophenanthrene, androstendione, ketoconazole, 6-deoxyerythronolide B	A245S	1JIO
108	Pseudomonas			1CPT
119	Sulfolobus solfactaricus	Imidazole,		1IO7
	Sulfolobus tokodaii	4-phenylimidazole		1UE8
152A1	Bacilis subtilis	Palmitoleic acid		1IZO
154A1	Streptomyces coelicolor A3	4-phenylimidazole		1ODO
154C1	Streptomyces coelicolor A3			1GWI
158A2	Streptomyces coelicolor A3	4-phenylimidazole		1S1F
175A1	Thermus thermophilus (Hb8)			1N97
EpoK	Sorangium cellulosum	Epothilone B and D		1WIY 1Q5E
OxyB	Amycolatopsis orientalis			1LFK
OxyC	Amycolatopsis orientalis			1UED
51	Mycobacterium tuberculosis	4-phenylimidazole, fluconazole, estriol	C37L/C151T/ C442A	1H5Z
55A1	Fusarium oxysporum	*N*-butyl isocyanide	T243A, T243N, T243V, S286V, S286T, S73G/S75G	1JFB
121	Mycobacterium tuberculosis	Iodopyrazole	[a]	1N4O
2B4	Oryctolagus cuniculus (rabbit)	4-(4-chlorophenyl)-imidazole	[a]	1PO5
2C5/3	Oryctolagus cuniculus (rabbit)	Diclofenac, 4-methyl-*N*-methyl-*N*-(2-phenyl-2H-pyrazol-3-yl)-benzenesulfonamide	[a]	1DT6
2A6	Homo sapiens	Coumarin, methoxsalen	[a]	1Z10
2C8	Homo sapiens	Palmitic acid	[a]	1PQ2
2C9	Homo sapiens	*S*-warfarin, *S*-flurbiprofen	[a]	1R9O
3A4	Homo sapiens	Progesterone, metyrapone	[a]	1TQN
2D6	Homo sapiens			2F9Q

[a] *all mammalian CYPs contain non-active site mutations to improve the crystallization. The PDB codes of the highest resolution ligand-free structures are given.*

X-ray diffraction

The common way of obtaining three-dimensional structural information is by using X-ray diffraction on crystallized molecules. The bacterial CYPs 101 and 102 are soluble, relatively easily expressed and purified, hence these were the first to be crystallized [82, 86, 129]. In the absence of crystallized mammalian CYPs, initially the bacterial CYP X-ray structures were used as templates for computer homology models of mammalian CYPs (*vide supra*). Later other bacterial and fungal CYPs [130-132], and recently also mammalian CYPs were crystallized [112, 133]. To make crystallization of mammalian CYPs possible, the membrane-anchoring N-termini had to be removed and other residues were mutated too. It still needs to be determined whether these modifications influence the overall structure. Substrate free rabbit CYP2B4 crystallized as a dimer, with H226 of the one monomer attached to the heme iron atom of the second. This can be an artifact of the crystallization instead of a functional conformation, which would implicate large conformational changes upon substrate binding [134]. Recently, the human CYPs 2C9, 3A4 and 2A6 were crystallized with and without substrates [46, 135, 136]. Nevertheless, some skepticism about the resemblance of the crystallized protein to the wild-type membrane bound protein still exists, because the mutated crystallized CYP2C9 for example, although still active, displayed different kinetic behavior compared to the wild-type enzyme [135]. An overview of the currently crystallized CYPs is presented in Table 5.

Electronic absorption spectroscopy

CYPs are brown-red colored enzymes, because of the typical light absorbance of their heme prosthetic group [8, 137]. Because of the heme porphyrin and the exceptional 5^{th} ligand being a cysteine sulfur atom, CYPs display an absorption spectrum with an intense Soret band at about 418 nm, a δ-band at 385 nm and two Q-bands at about 535 and 560 nm (Figure 6) [8]. CYPs can bind CO instead of O_2 when the iron is in the ferrous state. This is not uncommon for heme proteins but due to the cysteine ligand, axial CO binding yields a typical absorbance maximum around 450 nm. This characteristic was used to name the enzymes, and can also be used to quantify them, as the extinction coefficient was determined [8, 138]. Other features that can be obtained from the Soret maximum in the absorbance spectrum are the oxidation state and the spin state of the heme iron atom. The latter feature can be used to quantify saturation of ligand binding when this competes with the binding of the water molecule which is present in the resting state. Thus, dissociation constants can be estimated [116].

The optical spectra of CYPs are very sensitive to heme ligation, so UV-vis spectroscopy is also an ideal technique to study the oxidized heme intermediates of the catalytic cycle (Figure 2). Because these species are very short-lived (microseconds), stop-flow or freeze-quenching techniques need to be combined with spectroscopy to detect the intermediates [139]. This way the primary reduced oxy-P450 species in CYP101 was identified at 77 K as a superoxo- or hydroperoxo-Fe^{3+} heme complex. The primary intermediate, a hydroperoxo species, was stable below 180 K and converted smoothly to the product complex at approximately 195 K. In the course of the thermal annealing, no spectral changes indicating the presence of an oxoferryl species (compound I) were observed [117]. Later the oxoferryl species was detected, when iron-oxo intermediates of substrate free CYP101 were formed using peracids [120, 140]. But these studies were contradictory in whether a porphyrin π-cation radical system was formed or a tyrosine radical. Formation of either of these two radicals was found to be pH dependent [141]. Furthermore, the structures of the camphor analog substrates could influence the physical (spectroscopic) properties of the heme dioxygen complex and could also affect its reactivity. This indicated that the ability of

substrates to modulate the reactivity of oxygen intermediates could be a relevant factor in explaining the remarkable diversity of reactions catalyzed by the enzyme [142]. So far the application of the stop-flow and freeze-quenching techniques combined with electronic absorption spectroscopy has been limited to bacterial CYPs.
Another tool used in combination with absorbance spectroscopy to examine the conformation of CYP active sites, is laser driven photodissociation (flash photolysis) of heme-bound CO. For instance, this technique was applied to study human CYP2E1. It was found that ethanol decreased the rate of CO binding in CYP2E1 whereas arachidonic acid completely abolished the photodissociation of CO, confirming the modeled hydrophobic substrate binding pocket of the enzyme [143].

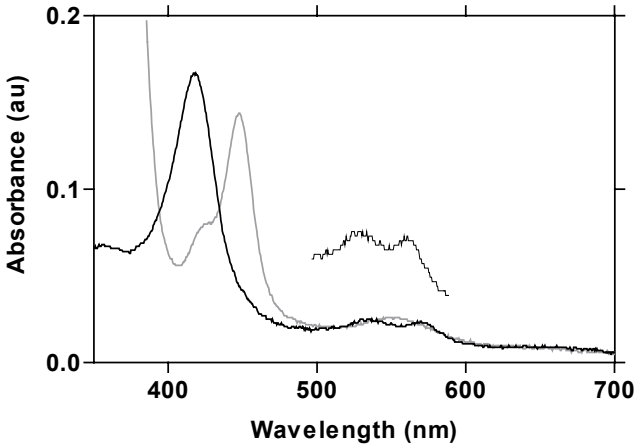

Figure 6: Absolute absorbance spectra of ferric (black) and ferrous CO-bound (gray) CYP2D6. An enlarged 500-600 nm region of the ferric enzyme is inserted to show the Q-bands.

Vibration spectroscopy
The two forms of vibration spectroscopy, infrared (IR) and Raman spectroscopy, have been used to study CYPs. Although both methods are relatively insensitive, the high light absorbance of the heme makes resonance Raman spectroscopy a useful tool to study CYPs [118, 144-148]. From Raman spectra information on heme iron spin state, oxidation state and coordination number can be obtained. Furthermore, vibrations of the porphyrin vinyl and propionate side chains, and heme bound CO are sensitive to active site conformations.
A resonance Raman spectroscopy study on rabbit CYP2B4 and CYP1A2 revealed that while in CYP2B4 the six-coordinated low-spin configuration is predominantly occupied, in CYP1A2 it is the five-coordinated high-spin form [118, 145]. This was attributed to the structures of the active sites. In the low-spin form of CYP2B4 the protein matrix forces the heme into a more rigid conformation than in CYP1A2. The vibrational modes of the vinyl groups were found to be characteristic markers for the specific structures of the heme pockets in both isoforms as they responded sensitively to substrate binding. The resonance Raman technique can make structural changes visible which are induced by substrate binding in addition and independent of the changes associated with the shift of the spin state equilibrium: the high-spin states in the substrate-bound and substrate-free enzyme were found to be structurally different. The formation of the inactive form, P420, involves a

severe structural rearrangement in the heme-binding pocket leading to drastic changes of the vinyl group conformations. The conformational differences of the active sites in CYPs 1A2 and 2B4, indicate a structural basis accounting for the substrate specificity of CYPs. An advantage of using Raman spectroscopy is the ability to calculate and predict Raman frequencies [149, 150], which has not yet been described for the electronic absorption spectroscopy.
Fourier transform IR spectroscopy (FTIR) was applied to CYP101 to study the binding of O_2 by using the model ligands CO and NO [119, 151]. Thus it was found that sterical hindrance, substrate mobility, and protein flexibility determine the position and width of the CO-stretching mode signals. The technique is much more insensitive (mM protein needed) than resonance Raman scattering and the examination of model ligand vibrations can in general not be performed in water as this is IR active. Nevertheless, it could also be used to estimate reduction rates following photoinduced electron transfer from covalently linked $Ru(bpy)_3^{2+}$ to CYP101 [152].

Mössbauer spectroscopy
The iron isotope ^{57}Fe can sensitively absorb gamma-radiation by the so-called Mössbauer effect. The transmission spectrum obtained can be used to determine the iron electronic structure of a CYP which is changing through the catalytic cycle [153]. Mössbauer spectroscopy was used to study CYP101 already in 1973 [154], and it has recently gained new interests, as a tool to study the heme iron electronic structure in CYPs since fast freeze-quenching techniques have become available [120, 155]. Thus it was found that approximately 10% of freeze quenched ^{57}Fe labeled CYP101 is a Fe^{IV} species with a tyrosine radical (active site Y96 in the wild-type and Y75 in the Y96F mutant) after 8 ms reaction time in presence of peroxy acetic acid, as assigned by its Mössbauer signature [156]. The long measuring time to obtain Mössbauer spectra however (up to three weeks) probably makes this technique unsuitable for studying mammalian CYPs.

Nuclear magnetic resonance (NMR)
The heme iron atom of a CYP is paramagnetic when in oxidized state. This is an experimentally useful characteristic, which can be used to measure orientations of substrates bound in the active site of the enzyme by measuring spin lattice relaxation NMR [88, 121, 157, 158]. Hydrogen atoms in a magnetic field will re-align in the direction of this field after their orientation has been flipped with a radio-frequency pulse. The velocity of this re-alignment, or relaxation back in the lattice, is dependent on the local strength of the magnetic field in the direct proximity of the hydrogen atom. So a substrate hydrogen atom close to the heme in the active site of a CYP, will relax faster due to the magnetic moment of the heme iron atom. The relationship between the iron atom to hydrogen atom distance, and the rate of relaxation has been established by Solomon and Bloembergen [159], and can be used to measure substrate orientations in CYP active sites (example of caffeine in CYP1A2 is shown in Figure 7). A disadvantage of the technique is that high concentrations of ligands (mM) need to be present to measure NMR spectra and this can be a problem with poorly soluble compounds. Furthermore, average substrate active site orientations do not always match the metabolic profile [158]. An overview of reported spin lattice relaxation studies using CYPs is given in Table 6. In most of the cases the catalytic site of the substrate was found closest to the heme iron atom, but in many occasions the range of distances is not as large as the substrate itself.
NMR methods (^1H-^{15}N correlations) have also been used to solve the solution 3D structure of CYP101. Furthermore, the effects of interactions of CYP101 with its protein partner

putidaredoxin [122], and also with substrates [160] were studied using NMR methods. A clear advantage of this technique to solve 3D structures is that no crystals are needed and that solution structures are probably a better model for physiological conditions. However, a disadvantage for using this technique in the study of mammalian CYPs is the millimolar concentrations of soluble protein that are required.

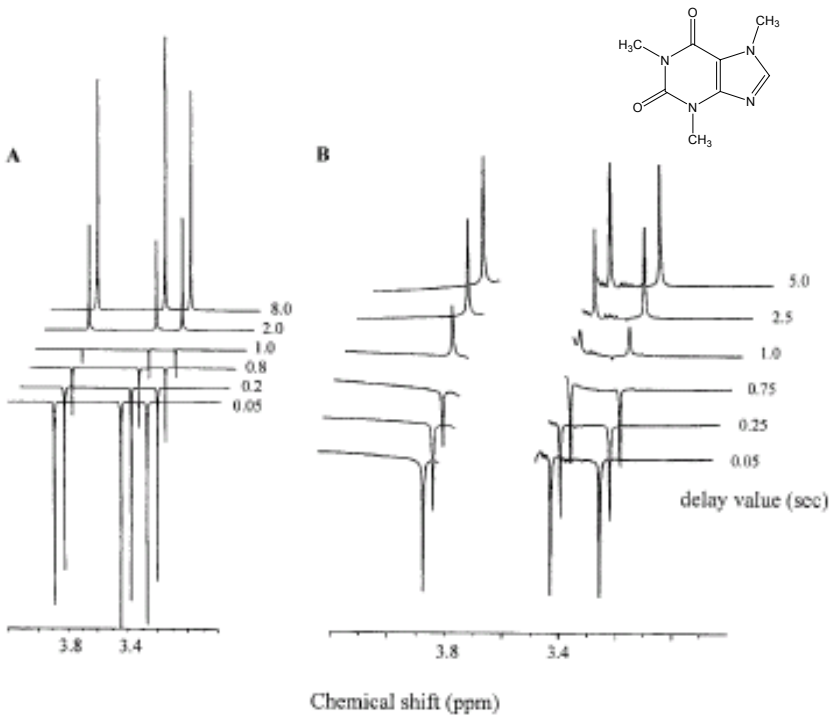

Figure 7: NMR inversion recovery spectra of 25 mM caffeine in the absence (A) or presence (B) of 3.5 μM CYP1A2. The glycerol, HDO and C8 hydrogen signals have been deleted. Taken from [158].

Table 6: Spin lattice relaxation NMR studies used to determine active site ligand orientations in CYPs.

CYP	Ligand	Distances (Å)*	Major reaction	Reference
102	12-Br-lauric acid	7.8 (C1H)-16.3 (C12H)	*C*2-OH	[161]
1A	Paracetamol	5.9 (phenylH)-6.7 (methylH)	Benzoquinone formation	[121]
1A2	Caffeine	6.5 (N1-methylH)-6.7 (N3 and N7 methylH)	*N*1-demethylation	[158]
2B	Paracetamol	5.8 (methylH)-6.3 (phenylH)	Inactive	[121]
2C9	Tienilic acid, Lauric acid, Diclofenac,	5.4 (C5H of thiophene)-7.1 (phenylH) 6.0 (C4-11H)-6.6 (C2H and C12H) 6.0 (C4'H)- 6.9 (phenylacetateH)	Thiophene-OH ω-1-OH 4'-OH	[157]
2D6	Codeine, MPTP Testosterone[1], MDMA	3.1 (OCH_3)-12.1 (NCH_3) 3.4 (NCH_3)- 11.9 (C9H) 3.6 (15β)- 9.2 (2α and 2β) 6.3 (methylene)-7.2 (NCH_3)	*O*-demethylation *N*-demethylation 15-OH *O*-demethylenation	[88], [162] [111] (this thesis)

**The minimal and maximal hydrogen atoms to heme iron atom measured are given. [1]Measured in the F483I mutant of CYP2D6, the wild-type is inactive towards testosterone.*

Electron magnetic resonance (EMR)
Electron magnetic resonance (EMR) is the generic name for magnetic resonance spectroscopy involving free or unpaired electrons, and includes electronic paramagnetic resonance (EPR), electron spin resonance (ESR) and electron nuclear double resonance (ENDOR). These techniques are successfully applied to CYPs to measure the heme iron spin state and ligation [163, 164]. Because the rhombicity of the EPR signal is dependent on the ligation of the heme iron, thiolate ligation could be distinguished from thiolate combined with distal glutamate ligation in the A264E mutant of CYP102 [147].
EPR/ENDOR studies have also been carried out on oxyferrous wild-type and the T252A mutant of CYP101, after one-electron cryoreduction by gamma-irradiation at 77 K in the absence of substrate and in the presence of a variety of substrates. The properties and reactivity of the oxyheme were modulated by the bound substrates. The presence of a substrate increased the lifetime of a hydroperoxo iron species in CYP101 about 20-fold. Thus these observations showed that substrates influence the properties of the iron-bound oxygen intermediates. Furthermore, because of the observed differences between the T252A and the wild-type enzyme, also the proton-delivery network to the heme appeared to be disrupted substrate dependent [41].

Fluorescence spectroscopy
Inter- and intra-protein distances in CYPs have been measured by using various fluorescence spectroscopy techniques. First of all, fluorescent probes can be (covalently) attached to a CYP, thus using the fluorescence intensity as a measure for distances from the probe to the quenching heme or to interacting proteins. Thus, by labeling the CPR with a coumarin based fluorophore, the interactions of the CPR with CYP2B4 were studied [165]. In another study, after labeling of a single lysine residue with a fluorescein isothiocyanate fluorophore, Förster resonance energy transfer (FRET) quenching was measured in CYP11A1, enabling to estimate the distance between K338 and the heme group as well as the changes in this distance upon substrate binding and interactions with other proteins and phospholipids [166]. Also fluorescent ruthenium probes have been attached through a linker to a substrate in CYP101, allowing to measure distances, probe-protein interactions and heme photo-reduction rates (nanoseconds) [167, 168].
An elegant way in which the protein itself is not modified is by measuring the fluorescence of endogenous tryptophan residues. This way, distances of different parts of the protein to the quenching heme center have been measured of wild-type and Y96A mutant CYP101 in absence and presence of various substrates, leading to insights in the dynamics of the enzymes [124, 169]. Furthermore, accessibilities of the tryptophan residues by quenchers gave information about their positions in the protein during the binding of a substrate.

Atomic force/scanning tunneling microscopy
The structure of mammalian CYPs in their native environment of the phospholipid bilayer is critical for understanding their activity. Therefore solubilized purified CYP2B4 was incorporated into phospholipid bilayer nanostructures (nanodiscs) and oriented on a surface for visualization by atomic force microscopy (AFM) [125]. Individual CYP molecules were shown to be protruding 3.5 nanometers from the bilayer surface, indicating that the enzymes are buried deep into the membrane and not only attached through their membrane anchor.
Scanning tunneling microscopy (STM) was used to study the complexes of the K344C mutant of CYP101 and putidaredoxin on a gold surface. STM imaging of a 1:1 mixture of the two proteins showed a regular array of pairs of different-sized proteins 20-25 Å apart

arranged in rows across the gold surface, which could be attributed to the formation of a complex. The redox centers of the two proteins were approximately 20 Å apart, too far for rapid intracomplex electron transfer, so whether the observed complex is competent for electron transfer or physiologically relevant remains to be elucidated [170].

Mass spectrometry

Mass spectrometry (MS), was successfully employed to study covalent interactions between reactive intermediates and the CYP that formed them [126, 171]. Analysis of the tienilic acid adducts to CYP2C9 after irreversible inhibition with this compound, revealed the active site residues to which these adducts bound [126].

Rabbit CYP2E1 is irreversibly inhibited by tert-butyl acetylene (tBA), which forms heme-adducts as observed from the fragmentation patterns in the MS spectrum. The T303A mutant of the enzyme however, was only reversibly inactivated by tBA, unless the samples were pre-acidified, then also the same fragmentation patterns were detected. These results suggested a role for the highly conserved threonine 303 residue in proton donation to the CYP2E1 active site and thereby stabilizing a reactive intermediate during substrate metabolism by CYP2E1 [171].

Potentiometry and voltammetry

Substrate binding is thought to trigger electron transfer in CYPs 101 and 102 by inducing a shift from a low- to high-spin ferric heme and increasing the heme reduction potential [115, 172]. Whether the combination of change in reduction potential and the change in iron spin state is the trigger to start the catalytic cycle, or if either of the two is sufficient, is still under debate [30, 31, 173, 174]. Therefore, the changes in reduction potential of CYPs have been measured in defined parts of the catalytic cycle, upon substrate binding or after mutagenesis [147]. It was found that by mutating F393, the reduction potential of CYP102 could be modulated, depending on the residue introduced [172]. The potential of the wild-type enzyme appeared to be optimal for a maximal overall turnover rate. Later it was shown by Raman spectroscopy that the size of residue 393 also influences the porphyrin vinyl and propionate conformations, which might subsequently influence the heme redox potential [175].

In some studies CYPs have been immobilized on electrodes to study their redox properties. For instance, CYP102 could be studied when immobilized in a didodecyldimethylammonium bromide film cast on an edge-plane graphite electrode [176]. In a setting like this it may also be possible to donate electrons to the CYP without the requirement of coenzymes and cofactors, which would be beneficial in the development of a CYP based bioreactor [176]. Using CYP2B4 immobilized on clay-modified glassy carbon electrodes in the presence of the nonionic detergent Tween 80, it was possible to metabolize several substrates such as aminopyrine and benzphetamine [177]. However the turnover rates were slow (aminopyrine *N*-demethylation: 0.04 min^{-1}) and high concentrations (mM) of substrates were needed to measure activity.

Cyclic voltammetry has also been used to study the iron electronic structure of the human CYP2C family members in presence of various substrates. The electrochemistry of human CYP2C9 was influenced by both pH and ionic strength and a substrate dependent anodic shift in the reduction potential was observed. These results suggest alternative mechanisms by which CYP2C9 (and by inference other P450 enzymes) may alter the reduction potential to facilitate electron delivery from physiological donors [127, 178].

Chemical probes
Diazene-containing probes have been used to sample active site cavities of CYPs [106, 128]. These probes will label porphyrin nitrogen atoms on the positions where they sense the least sterical hindrance from active site residues and can thus be used to give information on the topology of the CYP active site. In this way, the role of D301 in CYP2D6 was examined, and the modeled prediction of charge pairing with the substrate positive charge was validated [106].
In another study, the active site topology of CYP3A4 was examined using phenyldiazene. After incubation all the four potential *N*-phenylprotoporphyrin regioisomers were formed. Further study using active site mutants, showed that substitution of residues close to the heme, caused large changes in regioisomer formation, which reflected the location of these amino acid residues in a CYP3A4 homology model. Regioisomer formation was also compared in the absence and in the presence of CPR, cytochrome b5, or both. Formation of all four regioisomers in CYP3A4 was reduced in the presence of both CPR and cytochrome b_5, mutation dependent, suggesting that conformational changes occur due to protein-protein interactions between CYP3A4, the CPR, and cytochrome b5 [50].

Scope and objectives of this thesis

As outlined above, CYP2D6 is one of the most important enzymes in human drug metabolism. It is involved in the oxidative metabolism of a large number of clinically relevant drugs and furthermore there is a wide variability of the enzyme activity in different human populations [64, 76, 179]. It would be a great advantage if the metabolism of new chemical entities and drug-candidates could be rationalized and predicted in the early stages of drug discovery and development. Therefore increasing the understanding of the structure, dynamics and functioning of CYP2D6 has been the major objective of this thesis. This goal was approached, by studying the major factors that may determine the substrate binding, the activity, and the regio- and stereoselectivity of CYP2D6. The impact of these factors on the functioning of CYP2D6 will subsequently be addressed in this thesis:

(i) First of all, the active site topology may dictate substrate binding and conversion by specific interactions with the compound, or by steric restriction. By studying binding and metabolism of series of compounds [180], by performing site-directed mutagenesis [99], and by computer modeling of the CYPs [95], critical interaction points in the active site CYPs will be determined.
(ii) At second, the nature of oxygenating species can determine CYP activity and regioselectivity. In studies using artificial oxidants to activate CYPs [32], and in studies using active site threonine mutants of CYPs [37], the existence of multiple oxygenating species has been evaluated before. In these studies it was found that regioselectivity in catalysis could be manipulated, apparently by changing the balance of the reactive oxygen species.
(iii) At third, based on previous studies on other CYPs it is thought that the heme configuration can also influence the activity. Originally, changes in the heme iron spin state were related to substrate binding [30], later it was found that also other porphyrin characteristics, like sidechain conformations are influenced by the binding of substrates and by mutation of active site residues [172, 175].
(iv) Finally, the overall (changes in) conformation of the CYP during the catalytic cycle may allow for substrates to enter the active site and substrate active site mobility may determine the regioselectivity. Large conformational changes have been proposed for CYP2C9 upon

substrate binding, based on its crystallized structures in the presence and absence of substrates [135]. For CYP101, fluorescence spectroscopy was employed to determine conformational changes upon substrate binding [124], indicating that conformational changes can be measured, and crystallization of CYPs is not necessary to predict enzyme dynamics.
These four factors (i-iv) will be addressed in the following chapters.

Ad i: At the start of this study in 2001, a new homology model of CYP2D6 was being developed [95]. This model had good predictive qualities concerning the active site orientations of substrates and also predicted positions of residues in the active site. According to the model, two active site phenylalanine residues were proposed to play an important role in substrate interaction in CYP2D6. Therefore, in **Chapters 2** and **3** the active site residues F120 and F483 are experimentally studied by site-directed mutagenesis. Their individual roles in interaction with typical substrates are described in these chapters and a comparison between the two is made in **Chapter 4**. In this chapter, also additional active site residues involved in substrate interaction are predicted based upon experimental data and computational predictions. The first practical objective for these studies was the recombinant expression and subsequent purification of CYP2D6. The human CYP1A2 was already expressed in *E coli* [181], but without the CPR needed to measure activity, nor without an affinity tag to ease purification. It was reported that CYP2D6 could be expressed and purified in high amounts via a histidine tag [88, 182], and it was also co-expressed with CPR [101], but these two aspects were not combined before in a single expression system. This is also described in chapters 2,3 and 4.
Besides determining substrate affinity, the active site topology also influences the orientation of the substrate, thereby determining regio- and stereoselectivity. Therefore spin lattice relaxation NMR was employed to study active site substrate orientations in CYP2D6, in **Chapter 6**. Spin lattice relaxation NMR was used before to measure differences in the active site orientation of paracetamol in rat CYPs 1A and 2B [121]. In this study, the active site orientations of the enantiomers of 3,4-methylenedioxymethylamphetamine (MDMA) in the active sites of wild-type and F120A mutant CYP2D6 were determined and compared to automated docking and molecular dynamics simulations of MDMA in the CYP2D6 homology model. The experimental data are used to validate computational predictions and to study the role of residue F120 in substrate binding.

Ad ii: CYP2D6 can catalyze several types of reactions; even from one single substrate different products can be formed that are apparently formed through different mechanisms [33, 183]. Besides the active site topology, determining the substrate orientation, an additional explanation for this may be the involvement of different oxygenating species in the enzyme. In other CYPs multiple oxygenating species have been suggested, each responsible for certain reactions. A conserved active site threonine residue was identified in rabbit CYPs 2B4 and 2E1 that could influence the balance of these oxygenating species [39]. In **Chapter 5** the homologous threonine residue, T309, is studied in relation to the mechanism of oxidation by CYP2D6 by performing site-directed mutagenesis studies.

Ad iii: The heme configuration of CYP2D6 was studied in **Chapter 7** using resonance Raman spectroscopy. This technique is used to measure the heme iron spin state, coordination number, and oxidation state, information that is complementary to that obtained from homology modeling. Furthermore, vinyl and propionate vibrations can be used to yield information on the active site topology. A resonance Raman microscope was

build and used to measure anionic dyes [184] and by adapting the instrumental setup and the sample presentation it could be used to study CYPs. Notably the influence of the T309V mutation on the resonance Raman spectrum of CYP2D6 is studied, in order to rationalize the effects of the mutation on the CYP2D6 activity.

Ad iv: In **Chapter 8** conformational changes of CYP2D6 upon binding of the model substrate 7-methoxy-4-(aminomethyl)-coumarin (MAMC) are examined using fluorescence spectroscopy. The emission lifetimes of fluorescent endogenous tryptophan residues can be used to study conformational changes in proteins [185, 186]. External quenching with KI or acrylamide can add to the information on relative positions of the tryptophan residues. The examination of possible FRET pathways enables to study distances between tryptophan residues, the (fluorescent) substrate and the heme prosthetic group. Furthermore, by measuring the anisotropy of MAMC, its active site mobility is examined. The data obtained from all these fluorescence spectroscopy approaches can together, in combination with computational studies, be used to study CYP2D6 conformational changes upon substrate binding.
With the site directed mutations (**Part I**), and the used spectroscopic techniques (**Part II**), substrate binding and metabolism has been studied in relation to the conformation of the prosthetic group and holoenzyme of wild-type and mutants of CYP2D6. Furthermore, the active site orientation and mobility of the substrates was examined. All together, by using these approaches in combination with molecular modeling, more insights in the functioning of CYP2D6 have been gained, which was the aim of this thesis-project.

Chemistry of complex molecules
At the start of the study described in this thesis in 2001, at the Vrije Universiteit the 'Chemistry of Complex Molecules' (CCM) program was launched (www.chem.vu.nl/ccm). This program constituted a collaboration of the departments Biochemistry, Analytical Chemistry and Applied Spectroscopy, Organic Chemistry, and LACDR-Pharmacochemistry. The CCM program focused on the integration of a number of chemical disciplines in order to gain novel insights into how complex macromolecular systems, like proteins, function in space and time. The structure, the dynamics and the functioning of cytochromes P450 was chosen as one of the main subjects in the CCM program. The work described in this thesis was performed within the CCM program.

References

1. Vermeulen NPE, Role of metabolism in chemical toxicity. In: *Cytochromes P450 metabolic and toxicological aspects* (Ed. Ioannides), pp. 29-53. CRC Press, New York, 1996.
2. van Bladeren PJ, Glutathione conjugation as a bioactivation reaction. *Chem Biol Interact* **129:** 61-76, 2000.
3. Klaassen CD, *Casarett and Doull's toxicology: the basic science of poisons*. McGraw-Hill, New York, 2001.
4. Verkade PE, Elzas M, van der Lee J, de Wolff HH, Verkade-Sandbergen A and van der Sande D, Untersuchen uber den fettstoffwechsel. *Proc K Ned Akad Wet* **35:** 251-66, 1932.
5. Coon MJ, Cytochrome P450: Nature's most versatile biological catalyst. *Annu Rev Pharmacol Toxicol* **45:** 1-25, 2005.
6. Den H, The biological oxidation of 2,2-dimethyloctanoic acid. *Biochim Biophys Acta* **98:** 462-9, 1965.
7. Lu AY and Coon MJ, Role of hemoprotein P-450 in fatty acid omega-hydroxylation in a soluble enzyme system from liver microsomes. *J Biol Chem* **243:** 1331-2, 1968.

8. Omura T and Sato R, The carbon monoxide-binding pigment of liver microsomes. I. Evidence for its hemoprotein nature. *J Biol Chem* **239:** 2370-8, 1964.
9. Garfinkel D, Studies on pig liver microsomes. I. Enzymatic and pigment composition of different microsomal fractions. *Arch Biochem Biophys* **77:** 493-509, 1958.
10. Omura T, Sato R, Cooper DY, Rosenthal O and Estabrook RW, Function of cytochrome P-450 of micosomes. *Fed Proc* **24:** 1181-9, 1965.
11. Ortiz de Montellano PR, *Cytochromes P450: structure, mechanism, and biochemistry*. Kluwer Academic, New York, 2005.
12. Nelson DR, Kamataki T, Waxman DJ, Guengerich FP, Estabrook RW, Feyereisen R, Gonzalez FJ, Coon MJ, Gunsalus IC, Gotoh O and et al., The P450 superfamily: update on new sequences, gene mapping, accession numbers, early trivial names of enzymes, and nomenclature. *DNA Cell Biol* **12:** 1-51, 1993.
13. Nelson DR, Koymans L, Kamataki T, Stegeman JJ, Feyereisen R, Waxman DJ, Waterman MR, Gotoh O, Coon MJ, Estabrook RW, Gunsalus IC and Nebert DW, P450 superfamily: update on new sequences, gene mapping, accession numbers and nomenclature. *Pharmacogenetics* **6:** 1-42, 1996.
14. Oscarson M and Ingelman-Sundberg M, CYPalleles: a web page for nomenclature of human cytochrome P450 alleles. *Drug Metab Pharmacokinet* **17:** 491-5, 2002.
15. Nelson DR, Zeldin DC, Hoffman SM, Maltais LJ, Wain HM and Nebert DW, Comparison of cytochrome P450 (CYP) genes from the mouse and human genomes, including nomenclature recommendations for genes, pseudogenes and alternative-splice variants. *Pharmacogenetics* **14:** 1-18, 2004.
16. de la Torre R, Farre M, Ortuno J, Mas M, Brenneisen R, Roset PN, Segura J and Cami J, Non-linear pharmacokinetics of MDMA ('ecstacy') in humans. *Br J Clin Pharmacol* **49:** 104-109, 2000.
17. Venkatakrishnan K, von Moltke LL and Greenblatt DJ, Human drug metabolism and the cytochromes P450: application and relevance of in vitro models. *J Clin Pharmacol* **41:** 1149-79, 2001.
18. Kemp CA, Marechal JD and Sutcliffe MJ, Progress in cytochrome P450 active site modeling. *Arch Biochem Biophys* **433:** 361-68, 2005.
19. Shimada T, Yamazaki H, Mimura M, Inui Y and Guengerich FP, Interindividual variations in human liver cytochrome P450 enzymes involved in the oxidation of drugs, carcinogens and toxic chemicals: studies with liver microsomes of 30 Japanese and 30 Caucasians. *J Pharmacol Exp Ther* **270:** 414-23, 1994.
20. Jones BC, Tyman CA and Smith DA, Identification of the cytochrome P450 isoforms involved in the O-demethylation of 4-nitroanisole in human liver microsomes. *Xenobiotica* **27:** 1025-37, 1997.
21. Bertilsson L, Dahl ML, Dalen P and Al-Shurbaji A, Molecular genetics of CYP2D6: clinical relevance with focus on psychotropic drugs. *Br J Clin Pharmacol* **53:** 111-22, 2002.
22. Evans WE and Relling MV, Pharmacogenomics: translating functional genomics into rational therapeutics. *Science* **286:** 487-91, 1999.
23. Wormhoudt LW, Commandeur JN and Vermeulen NP, Genetic polymorphisms of human N-acetyltransferase, cytochrome P450, glutathione-S-transferase, and epoxide hydrolase enzymes: relevance to xenobiotic metabolism and toxicity. *Crit Rev Toxicol* **29:** 59-124, 1999.
24. Ingelman-Sundberg M, Pharmacogenetics of cytochrome P450 and its applications in drug therapy: the past, present and future. *Trends Pharmacol Sci* **25:** 193-200, 2004.
25. White RE and Coon MJ, Oxygen activation by cytochrome P-450. *Annu Rev Biochem* **49:** 315-56, 1980.
26. Guengerich FP, Common and uncommon cytochrome P450 reactions related to metabolism and chemical toxicity. *Chem Res Toxicol* **14:** 611-646, 2001.
27. Groenhof AR, Swart M, Ehlers AW and Lammertsma K, Electronic ground states of iron porphyrin and of the first species in the catalytic reaction cycle of cytochrome P450s. *J Phys Chem A* **109:** 3411-3417, 2005.
28. Lange R, Hui Bon Hoa G, Debey P and Gunsalus IC, A thermodynamic-kinetic analysis of the cytochrome P-450 heme pocket. *Acta Biol Med Ger* **38:** 143-52, 1979.

29. Ortiz de Montellano PR and De Voss JJ, Substrate oxidation by cytochrome P450 enzymes. In: *Cytochrome P450 structure, mechanism, and biochemistry* (Ed. Ortiz de Montellano PR). Kluwer Academic, New York, 2005.
30. Sligar SG, Coupling of spin, substrate, and redox equilibria in cytochrome P450. *Biochemistry* **15:** 5399-406, 1976.
31. Lawson RJ, Leys D, Sutcliffe MJ, Kemp CA, Cheesman MR, Smith SJ, Clarkson J, Smith WE, Haq I, Perkins JB and Munro AW, Thermodynamic and biophysical characterization of cytochrome P450 BioI from Bacillus subtilis. *Biochemistry* **43:** 12410-26, 2004.
32. Guengerich FP, Vaz AD, Raner GM, Pernecky SJ and Coon MJ, Evidence for a role of a perferryl-oxygen complex, FeO3+, in the N-oxygenation of amines by cytochrome P450 enzymes. *Mol Pharmacol* **51:** 147-151, 1997.
33. Hutzler JM, Powers FJ, Wynalda MA and Wienkers LC, Effect of carbonate anion on cytochrome P450 2D6-mediated metabolism in vitro: the potential role of multiple oxygenating species. *Arch Biochem Biophys* **417:** 165-175, 2003.
34. Sligar SG, Lipscomb JD, Debrunner PG and Gunsalus IC, Superoxide anion production by the autoxidation of cytochrome P450cam. *Biochem Biophys Res Commun* **61:** 290-6, 1974.
35. Goeptar AR, Scheerens H and Vermeulen NPE, Oxygen and xenobiotic reductase activities of cytochrome P450. *Crit Rev Toxicol* **25:** 25-65, 1995.
36. Raag R, Martinis SA, Sligar SG and Poulos TL, Crystal structure of the cytochrome P-450CAM active site mutant Thr252Ala. *Biochemistry* **30:** 11420-9, 1991.
37. Vaz AD, Pernecky SJ, Raner GM and Coon MJ, Peroxo-iron and oxenoid-iron species as alternative oxygenating agents in cytochrome P450-catalyzed reactions: switching by threonine-302 to alanine mutagenesis of cytochrome P450 2B4. *Proc Natl Acad Sci U S A* **93:** 4644-8, 1996.
38. Vaz AD, McGinnity DF and Coon MJ, Epoxidation of olefins by cytochrome P450: evidence from site-specific mutagenesis for hydroperoxo-iron as an electrophilic oxidant. *Proc Natl Acad Sci U S A* **95:** 3555-60, 1998.
39. Coon MJ, Vaz AD, McGinnity DF and Peng HM, Multiple activated oxygen species in P450 catalysis: contributions To specificity in drug metabolism. *Drug Metab Dispos* **26:** 1190-3, 1998.
40. Chandrasena RE, Vatsis KP, Coon MJ, Hollenberg PF and Newcomb M, Hydroxylation by the hydroperoxy-iron species in cytochrome P450 enzymes. *J Am Chem Soc* **126:** 115-26, 2004.
41. Davydov R, Perera R, Jin S, Yang TC, Bryson TA, Sono M, Dawson JH and Hoffman BM, Substrate modulation of the properties and reactivity of the oxy-ferrous and hydroperoxo-ferric intermediates of cytochrome P450cam as shown by cryoreduction-EPR/ENDOR spectroscopy. *J Am Chem Soc* **127:** 1403-13, 2005.
42. Newcomb M, Hollenberg PF and Coon MJ, Multiple mechanisms and multiple oxidants in P450-catalyzed hydroxylations. *Arch Biochem Biophys* **409:** 72-9, 2003.
43. Shaik S, Kumar D, de Visser SP, Altun A and Thiel W, Theoretical perspective on the structure and mechanism of cytochrome P450 enzymes. *Chem Rev* **105**, 2005.
44. Shaik S, de Visser SP and Kumar D, One oxidant, many pathways: a theoretical perspective of monooxygenation mechanisms by cytochrome P450 enzymes. *J Biol Inorg Chem* **9:** 661-8, 2004.
45. Wade RC, Winn PJ, Schlichting I and Sudarko, A survey of active site access channels in cytochromes P450. *J Inorg Biochem* **98:** 1175-82, 2004.
46. Williams PA, Cosme J, Vinkovic DM, Ward A, Angove HC, Day PJ, Vonrhein C, Tickle IJ and Jhoti H, Crystal structures of human cytochrome P450 3A4 bound to metyrapone and progesterone. *Science* **305:** 683-6, 2004.
47. Ludemann SK, Lounnas V and Wade RC, How do substrates enter and products exit the buried active site of cytochrome P450cam? 1. Random expulsion molecular dynamics investigation of ligand access channels and mechanisms. *Journal of Molecular Biology* **303:** 797-811, 2000.
48. Kelley RW, Reed JR and Backes WL, Effects of ionic strength on the functional interactions between CYP2B4 and CYP1A2. *Biochemistry* **44:** 2632-41, 2005.

49. Backes WL and Kelley RW, Organization of multiple cytochrome P450s with NADPH-cytochrome P450 reductase in membranes. *Pharmacol Ther* **98:** 221-33, 2003.
50. Yamaguchi Y, Khan KK, He YA, He YQ and Halpert JR, Topological changes in the CYP3A4 active site probed with phenyldiazene: effect of interaction with NADPH-cytochrome P450 reductase and cytochrome b5 and of site-directed mutagenesis. *Drug Metab Dispos* **32:** 155-61, 2004.
51. Guengerich FP, Cytochrome P450: what have we learned and what are the future issues? *Drug Metab Rev* **36:** 159-97, 2004.
52. Allen JG, East PB, Francis RJ and Haigh JL, Metabolism of debrisoquine sulfate. Identification of some urinary metabolites in rat and man. *Drug Metab Dispos* **3:** 332-7, 1975.
53. Mahgoub A, Idle JR, Dring LG, Lancaster R and Smith RL, Polymorphic hydroxylation of Debrisoquine in man. *Lancet* **2:** 584-6, 1977.
54. Tucker GT, Silas JH, Iyun AO, Lennard MS and Smith AJ, Polymorphic hydroxylation of debrisoquine. *Lancet* **2:** 718, 1977.
55. Boobis AR, Murray S, Kahn GC, Roberts GM and Davies DS, Substrate specificity of the form of cytochrome P-450 catalyzing the 4-hydroxylation of debrisoquine in man. *Mol Pharmacol* **23:** 474-81, 1983.
56. Larrey D, Distlerath LM, Wilkinson GR and Guengerich FP, Purification and characterization of the rat liver microsomal cytochrome P-450 involved in the 4-hydroxylation of debrisoquine, a prototype for genetic variation in oxidative drug metabolism. *Biochemistry* **23:** 2787-95, 1984.
57. Distlerath LM, Reilly PE, Martin MV, Davis GG, Wilkinson GR and Guengerich FP, Purification and characterization of the human liver cytochromes P-450 involved in debrisoquine 4-hydroxylation and phenacetin O-deethylation, two prototypes for genetic polymorphism in oxidative drug metabolism. *J Biol Chem* **260:** 9057-67, 1985.
58. Eichelbaum M, Baur MP, Dengler HJ, Osikowska-Evers BO, Tieves G, Zekorn C and Rittner C, Chromosomal assignment of human cytochrome P-450 (debrisoquine/sparteine type) to chromosome 22. *Br J Clin Pharmacol* **23:** 455-8, 1987.
59. Gonzalez FJ, Matsunaga T, Nagata K, Meyer UA, Nebert DW, Pastewska J, Kozak CA, Gillette J, Gelboin HV and Hardwick JP, Debrisoquine 4-hydroxylase: characterization of a new P450 gene subfamily, regulation, chromosomal mapping, and molecular analysis of the DA rat polymorphism. *DNA* **6:** 149-61, 1987.
60. Gonzalez FJ, Vilbois F, Hardwick JP, McBride OW, Nebert DW, Gelboin HV and Meyer UA, Human debrisoquine 4-hydroxylase (P450IID1): cDNA and deduced amino acid sequence and assignment of the CYP2D locus to chromosome 22. *Genomics* **2:** 174-9, 1988.
61. Skoda RC, Gonzalez FJ, Demierre A and Meyer UA, Two mutant alleles of the human cytochrome P-450db1 gene (P450C2D1) associated with genetically deficient metabolism of debrisoquine and other drugs. *Proc Natl Acad Sci U S A* **85:** 5240-3, 1988.
62. Kimura S, Umeno M, Skoda RC, Meyer UA and Gonzalez FJ, The human debrisoquine 4-hydroxylase (CYP2D) locus: sequence and identification of the polymorphic CYP2D6 gene, a related gene, and a pseudogene. *Am J Hum Genet* **45:** 889-904, 1989.
63. Løvlie R, Daly AK, Matre GE, Molven A and Steen VM, Polymorphisms in CYP2D6 duplication-negative individuals with the ultrarapid metabolizer phenotype: a role for the CYP2D6*35 allele in ultrarapid metabolism? *Pharmacogenetics* **11:** 45-55, 2001.
64. Zanger UM, Raimundo S and Eichelbaum M, Cytochrome P450 2D6: overview and update on pharmacology, genetics, biochemistry. *Naunyn Schmiedebergs Arch Pharmacol* **369:** 23-37, 2004.
65. Rendic S, Summary of information on human CYP enzymes: human P450 metabolism data. *Drug Metab Rev* **34:** 83-448, 2002.
66. Pirmohamed M and Park BK, Genetic susceptibility to adverse drug reactions. *Trends Pharmacol Sci* **22:** 298-305, 2001.
67. Phillips KA, Veenstra DL, Oren E, Lee JK and Sadee W, Potential role of pharmacogenomics in reducing adverse drug reactions: a systematic review. *Jama* **286:** 2270-9, 2001.
68. Du L, Hoffman SM and Keeney DS, Epidermal CYP2 family cytochromes P450. *Toxicol Appl Pharmacol* **195:** 278-87, 2004.

69. Siegle I, Fritz P, Eckhardt K, Zanger UM and Eichelbaum M, Cellular localization and regional distribution of CYP2D6 mRNA and protein expression in human brain. *Pharmacogenetics* **11:** 237-45, 2001.
70. Pai HV, Komaddi RP, Chinta SJ, Mori T, Boyd MR and Ravindranath V, A frameshift mutation and alternate splicing in human brain generate a functional form of the pseudogene cytochrome P4502D7 that demethylates codeine to morphine. *J Biol Chem* **279:** 27383-9, 2004.
71. Yu A, Idle JR, Byrd LG, Krausz KW, Kupfer A and Gonzalez FJ, Regeneration of serotonin from 5-methoxytrypamine by polymorphic human CYP2D6. *Pharmacogenetics* **13:** 173-181, 2003.
72. Yu A, Idle JR, Herraiz T, Kupfer A and Gonzalez FJ, Screening for endogenous substrates reveals that CYP2D6 is a 5-methoxyindolethylamine O-demethylase. *Pharmacogenetics* **13:** 307-319, 2003.
73. Yu AM, Idle JR and Gonzalez FJ, Polymorphic cytochrome P450 2D6: humanized mouse model and endogenous substrates. *Drug Metab Rev* **36:** 243-77, 2004.
74. Kawanishi C, Lundgren S, Agren H and Bertilsson L, Increased incidence of CYP2D6 gene duplication in patients with persistent mood disorders: ultrarapid metabolism of antidepressants as a cause of nonresponse. A pilot study. *Eur J Clin Pharmacol* **59:** 803-7, 2004.
75. de Graaf C, Vermeulen NPE and Feenstra KA, Cytochrome P450 in silico: an integrative modeling approach. *J Med Chem* **48:** 2725-55, 2005.
76. Vermeulen NPE, Prediction of drug metabolism: the case of cytochrome P450 2D6. *Curr Top Med Chem* **3:** 1227-39, 2003.
77. Wolff T, Distlerath LM, Worthington MT, Groopman JD, Hammons GJ, Kadlubar FF, Prough RA, Martin MV and P. GF, Substrate specificity of human liver cytochrome P-450 debrisoquine 4-hydroxylase probed using immunochemical inhibition and chemical modeling. *Cancer Res* **45:** 2116-2122, 1985.
78. Meyer UA, Gut J, Kronbach T, Skoda C and Meier UT, The molecular mechanisms of two common polymorphisms of drug oxidation-evidence for functional changes in cytochrome P-450 isozymes catalysing bufuralol and mephenytoin oxidation. *Xenobiotica* **16:** 449-464, 1986.
79. Koymans L, Vermeulen NP, van Acker SA, te Koppele JM, Heykants JJ, Lavrijsen K, Meuldermans W and Donne-Op den Kelder GM, A predictive model for substrates of cytochrome P450-debrisoquine (2D6). *Chem Res Toxicol* **5:** 211-9, 1992.
80. de Groot MJ, Bijloo GJ, Hansen KT and Vermeulen NPE, Computer prediction and experimental validation of cytochrome P450-2D6 dependent oxidation of GBR 12909 (1-[2-[bis(4-fluorophenyl)methoxy]ethyl]-4-(3-phenylpropyl)piperazine). *Drug Metab Dispos* **23:** 667-669, 1995.
81. de Groot MJ, Bijloo GJ, Martens BJ, van Acker FA and Vermeulen NP, A refined substrate model for human cytochrome P450 2D6. *Chem Res Toxicol* **10:** 41-8, 1997.
82. Poulos TL, Finzel BC and Howard AJ, High-resolution crystal structure of cytochrome P450cam. *J Mol Biol* **195:** 687-700, 1987.
83. Poulos TL and Howard AJ, Crystal structures of metyrapone- and phenylimidazole-inhibited complexes of cytochrome P-450cam. *Biochemistry* **26:** 8165-74, 1987.
84. Raag R and Poulos TL, Crystal structure of the carbon monoxide-substrate-cytochrome P-450CAM ternary complex. *Biochemistry* **28:** 7586-92, 1989.
85. Koymans LM, Vermeulen NP, Baarslag A and Donne-Op den Kelder GM, A preliminary 3D model for cytochrome P450 2D6 constructed by homology model building. *J Comput Aided Mol Des* **7:** 281-9, 1993.
86. Ravichandran KG, Boddupalli SS, Hasermann CA, Peterson JA and Deisenhofer J, Crystal structure of hemoprotein domain of P450BM-3, a prototype for microsomal P450's. *Science* **261:** 731-6, 1993.
87. Yeom H, Sligar SG, Li H, Poulos TL and Fulco AJ, The role of Thr268 in oxygen activation of cytochrome P450BM-3. *Biochemistry* **34:** 14733-40, 1995.

88. Modi S, Paine MJ, Sutcliffe MJ, Lian LY, Primrose WU, Wolf CR and Roberts GC, A model for human cytochrome P450 2D6 based on homology modeling and NMR studies of substrate binding. *Biochemistry* **35:** 4540-50, 1996.
89. Lewis DF, Eddershaw PJ, Goldfarb PS and Tarbit MH, Molecular modelling of cytochrome P4502D6 (CYP2D6) based on an alignment with CYP102: structural studies on specific CYP2D6 substrate metabolism. *Xenobiotica* **27:** 319-39, 1997.
90. de Groot MJ, Vermeulen NP, Kramer JD, van Acker FA and Donne-Op den Kelder GM, A three-dimensional protein model for human cytochrome P450 2D6 based on the crystal structures of P450 101, P450 102, and P450 108. *Chem Res Toxicol* **9:** 1079-91, 1996.
91. de Groot MJ, Ackland MJ, Horne VA, Alex AA and Jones BC, A novel approach to predicting P450-mediated drug metabolism: Development of a combined protein and pharmacophore model for CYP2D6. *J Med Chem* **42:** 1515-1524, 1999.
92. De Rienzo F, Fanelli F, Menziani MC and De Benedetti PG, Theoretical investigation of substrate specificity for cytochromes P450 IA2, P450 IID6 and P450 IIIA4. *J Comput Aided Mol Des* **14:** 93-116, 2000.
93. de Groot MJ, Ackland MJ, Horne VA, Alex AA and Jones BC, A novel approach to predicting P450 mediated drug metabolism. CYP2D6 catalyzed N-dealkylation reactions and qualitative metabolite predictions using a combined protein and pharmacophore model for CYP2D6. *J Med Chem* **42:** 4062-4070, 1999.
94. Ekins S, de Groot MJ and Jones JP, Pharmacophore and three-dimensional quantitative structure activity relationship methods for modeling cytochrome P450 active sites. *Drug Metab Dispos* **29:** 936-44, 2001.
95. Venhorst J, ter Laak AM, Commandeur JNM, Funae Y, Hiroi T and Vermeulen NPE, Homology modeling of rat and human cytochrome P450 2D (CYP2D) isoforms and computational rationalization of experimental ligand-binding specificities. *J Med Chem* **46:** 74-86, 2003.
96. Williams PA, Cosme J, Sridhar V, Johnson EF and McRee DE, Microsomal cytochrome P450 2C5: comparison to microbial P450s and unique features. *J Inorg Biochem* **81:** 183-90, 2000.
97. Kirton SB, Kemp CA, Tomkinson NP, St-Gallay S and Sutcliffe MJ, Impact of incorporating the 2C5 crystal structure into comparative models of cytochrome P450 2D6. *Proteins* **49:** 216-31, 2002.
98. Gotoh O, Substrate recognition sites in cytochrome P450 family 2 (CYP2) proteins inferred from comparative analyses of amino acid and coding nucleotide sequences. *J Biol Chem* **267:** 83-90, 1992.
99. Ellis SW, Hayhurst GP, Smith G, Lightfoot T, Wong MM, Simula AP, Ackland MJ, Sternberg MJ, Lennard MS and Tucker GT, Evidence that aspartic acid 301 is a critical substrate-contact residue in the active site of cytochrome P450 2D6. *J Biol Chem* **270:** 29055-8, 1995.
100. Hanna IH, Kim MS and Guengerich FP, Heterologous expression of cytochrome P450 2D6 mutants, electron transfer, and catalysis of bufuralol hydroxylation: the role of aspartate 301 in structural integrity. *Arch Biochem Biophys* **393:** 255-61, 2001.
101. Paine MJ, McLaughlin LA, Flanagan JU, Kemp CA, Sutcliffe MJ, Roberts GC and Wolf CR, Residues glutamate 216 and aspartate 301 are key determinants of substrate specificity and product regioselectivity in cytochrome P450 2D6. *J Biol Chem* **278:** 4021-7, 2003.
102. Guengerich FP, Hanna IH, Martin MV and Gillam EM, Role of glutamic acid 216 in cytochrome P450 2D6 substrate binding and catalysis. *Biochemistry* **42:** 1245-53, 2003.
103. Flanagan JU, Marechal JD, Ward R, Kemp CA, McLaughlin LA, Sutcliffe MJ, Roberts GC, Paine MJ and Wolf CR, Phe120 contributes to the regiospecificity of cytochrome P450 2D6: mutation leads to the formation of a novel dextromethorphan metabolite. *Biochem J* **380:** 353-60, 2004.
104. Masuda K, Tamagake K, Okuda Y, Torigoe F, Tsuzuki D, Isobe T, Hichiya H, Hanioka N, Yamamoto S and Narimatsu S, Change in enantioselectivity in bufuralol 1''-hydroxylation by the substitution of phenylalanine-120 by alanine in cytochrome P450 2D6. *Chirality* **17:** 37-43, 2005.
105. Tsuzuki D, Hichiya H, Okuda Y, Yamamoto S, Tamagake K, Shinoda S and Narimatsu S, Alteration in catalytic properties of human CYP2D6 caused by substitution of glycine-42 with arginine, lysine and glutamic acid. *Drug Metab Pharmacokin* **18:** 79-85, 2003.

106. Mackman R, Tschirret-Guth RA, Smith G, Hayhurst GP, Ellis SW, Lennard MS, Tucker GT, Wolf CR and Ortiz de Montellano PR, Active-site topologies of human CYP2D6 and its aspartate-301 --> glutamate, asparagine, and glycine mutants. *Arch Biochem Biophys* **331:** 134-40, 1996.
107. Guengerich FP, Miller GP, Hanna IH, Martin MV, Leger S, Black C, Chauret N, Silva JM, Trimble LA, Yergey JA and Nicoll-Griffith DA, Diversity in the oxidation of substrates by cytochrome P450 2D6: lack of an obligatory role of aspartate 301-substrate electrostatic bonding. *Biochemistry* **41:** 11025-34, 2002.
108. Ellis SW, Hayhurst GP, Lightfoot T, Smith G, Harlow J, Rowland-Yeo K, Larsson C, Mahling J, Lim CK, Wolf CR, Blackburn GM, Lennard MS and Tucker GT, Evidence that serine 304 is not a key ligand-binding residue in the active site of cytochrome P450 2D6. *Biochem J* **345:** 565-71, 2000.
109. Ellis SW, Rowland K, Ackland MJ, Rekka E, Simula AP, Lennard MS, Wolf CR and Tucker GT, Influence of amino acid residue 374 of cytochrome P-450 2D6 (CYP2D6) on the regio- and enantio-selective metabolism of metoprolol. *Biochem J* **316:** 647-54, 1996.
110. Hayhurst GP, Harlow J, Chowdry J, Gross E, Hilton E, Lennard MS, Tucker GT and Ellis SW, Influence of phenylalanine-481 substitutions on the catalytic activity of cytochrome P450 2D6. *Biochem J* **355:** 373-9, 2001.
111. Smith G, Modi S, Pillai I, Lian LY, Sutcliffe MJ, Pritchard MP, Friedberg T, Roberts GC and Wolf CR, Determinants of the substrate specificity of human cytochrome P-450 CYP2D6: design and construction of a mutant with testosterone hydroxylase activity. *Biochem J* **331:** 783-92, 1998.
112. Wester MR, Johnson EF, Marques-Soares C, Dansette PM, Mansuy D and Stout CD, Structure of a substrate complex of mammalian cytochrome P450 2C5 at 2.3 A resolution: evidence for multiple substrate binding modes. *Biochemistry* **42:** 6370-9, 2003.
113. Wester MR, Johnson EF, Marques-Soares C, Dijols S, Dansette PM, Mansuy D and Stout CD, Structure of mammalian cytochrome P450 2C5 complexed with diclofenac at 2.1 A resolution: evidence for an induced fit model of substrate binding. *Biochemistry* **42:** 9335-45, 2003.
114. Kemp CA, Flanagan JU, van Eldik AJ, Marechal JD, Wolf CR, Roberts GC, Paine MJ and Sutcliffe MJ, Validation of model of cytochrome P450 2D6: an in silico tool for predicting metabolism and inhibition. *J Med Chem* **47:** 5340-6, 2004.
115. Raag R and Poulos TL, The structural basis for substrate-induced changes in redox potential and spin equilibrium in cytochrome P-450CAM. *Biochemistry* **28:** 917-22, 1989.
116. Jefcoate CR, Measurement of substrate and inhibitor binding to microsomal cytochrome P450 by optical-difference spectroscopy. *Methods Enzymol* **52:** 258-79, 1978.
117. Denisov IG, Makris TM and Sligar SG, Cryotrapped reaction intermediates of cytochrome p450 studied by radiolytic reduction with phosphorus-32. *J Biol Chem* **276:** 11648-52, 2001.
118. Hildebrandt P, Garda H, Stier A, Stockburger M and Van Dyke RA, Resonance Raman study of the cytochrome P-450 LM2-halothane intermediate complex. *FEBS Lett* **237:** 15-20, 1988.
119. Jung C, Hoa GH, Schroder KL, Simon M and Doucet JP, Substrate analogue induced changes of the CO-stretching mode in the cytochrome P450cam-carbon monoxide complex. *Biochemistry* **31:** 12855-62, 1992.
120. Schunemann V, Jung C, Terner J, Trautwein AX and Weiss R, Spectroscopic studies of peroxyacetic acid reaction intermediates of cytochrome P450cam and chloroperoxidase. *J Inorg Biochem* **91:** 586-96, 2002.
121. van de Straat R, de Vries J, de Boer HJ, Vromans RM and Vermeulen NPE, Relationship between paracetamol binding to and its oxidation by two cytochromes P-450 isozymes--a proton nuclear magnetic resonance and spectrophotometric study. *Xenobiotica* **17:** 1-9, 1987.
122. Pochapsky TC, Lyons TA, Kazanis S, Arakaki T and Ratnaswamy G, A structure-based model for cytochrome P450cam-putidaredoxin interactions. *Biochimie* **78:** 723-33, 1996.
123. Schunemann V, Lendzian F, Jung C, Contzen J, Barra AL, Sligar SG and Trautwein AX, Tyrosine radical formation in the reaction of wild type and mutant cytochrome P450cam with peroxy acids: a multifrequency EPR study of intermediates on the millisecond time scale. *J Biol Chem* **279:** 10919-30, 2004.

124. Prasad S and Mitra S, Role of protein and substrate dynamics in catalysis by Pseudomonas putida cytochrome P450cam. *Biochemistry* **41:** 14499-508, 2002.
125. Bayburt TH and Sligar SG, Single-molecule height measurements on microsomal cytochrome P450 in nanometer-scale phospholipid bilayer disks. *Proc Natl Acad Sci U S A* **99:** 6725-30, 2002.
126. Koenigs LL, Peter RM, Hunter AP, Haining RL, Rettie AE, Friedberg T, Pritchard MP, Shou M, Rushmore TH and Trager WF, Electrospray ionization mass spectrometric analysis of intact cytochrome P450: identification of tienilic acid adducts to P450 2C9. *Biochemistry* **38:** 2312-9, 1999.
127. Johnson DL, Lewis BC, Elliot DJ, Miners JO and Martin LL, Electrochemical characterisation of the human cytochrome P450 CYP2C9. *Biochem Pharmacol* **69:** 1533-41, 2005.
128. Swanson BA, Dutton DR, Lunetta JM, Yang CS and Ortiz de Montellano PR, The active sites of cytochromes P450 IA1, IIB1, IIB2, and IIE1. Topological analysis by in situ rearrangement of phenyl-iron complexes. *J Biol Chem* **266:** 19258-64, 1991.
129. Poulos TL, Perez M and Wagner GC, Preliminary crystallographic data on cytochrome P-450CAM. *J Biol Chem* **257:** 10427-9, 1982.
130. Hasemann CA, Ravichandran KG, Peterson JA and Deisenhofer J, Crystal structure and refinement of cytochrome P450terp at 2.3 A resolution. *J Mol Biol* **236:** 1169-85, 1994.
131. Cupp-Vickery JR, Li H and Poulos TL, Preliminary crystallographic analysis of an enzyme involved in erythromycin biosynthesis: cytochrome P450eryF. *Proteins* **20:** 197-201, 1994.
132. Park SY, Shimizu H, Adachi S, Nakagawa A, Tanaka I, Nakahara K, Shoun H, Obayashi E, Nakamura H, Iizuka T and Shiro Y, Crystal structure of nitric oxide reductase from denitrifying fungus Fusarium oxysporum. *Nat Struct Biol* **4:** 827-32, 1997.
133. Williams PA, Cosme J, Sridhar V, Johnson EF and McRee DE, Mammalian microsomal cytochrome P450 monooxygenase: structural adaptations for membrane binding and functional diversity. *Mol Cell* **5:** 121-31, 2000.
134. Scott E, He Y, Wester MR, White M, Chin C, Halpert J, Johnson EF and Stout CD, An open conformation of mammalian cytochrome P450 2B4 at 1.6-A resolution. *Proc Natl Acad Sci U S A* **100:** 13196-201, 2003.
135. Williams PA, Cosme J, Ward A, Angove HC, Matak Vinkovic D and Jhoti H, Crystal structure of human cytochrome P450 2C9 with bound warfarin. *Nature* **424:** 464-8, 2003.
136. Yano JK, Hsu MH, Griffin KJ, Stout CD and Johnson EF, Structures of human microsomal cytochrome P450 2A6 complexed with coumarin and methoxsalen. *Nat Struct Mol Biol* **12:** 822-3, 2005.
137. Peterson JA and Coon MJ, Enzymatic omega-oxidation. III. Purification and properties of rubredoxin, a component of the omega-hydroxylation system of Pseudomonas oleovorans. *J Biol Chem* **243:** 329-34, 1968.
138. Omura T and Sato R, The carbon monoxide-binding pigment of liver microsomes. II. Solubilization, purification, and properties. *J Biol Chem* **239:** 2379-85, 1964.
139. Schlichting I, Berendzen J, Chu K, Stock AM, Maves SA, Benson DE, Sweet RM, Ringe D, Petsko GA and Sligar SG, The catalytic pathway of cytochrome p450cam at atomic resolution. *Science* **287:** 1615-22, 2000.
140. Egawa T, Shimada H and Ishimura Y, Evidence for comppund I formation in the reaction of cytochrome P450cam with m-chloroperbenzoic acid. *Biochem Biophys Res Commun* **201:** 1464-9, 1994.
141. Spolitak T, Dawson JH and Ballou DP, Reaction of ferric cytochrome P450cam with peracids. *J Biol Chem* **280:** 20300-20309, 2005.
142. Sono M, Perera R, Jin S, Makris TM, Sligar SG, Bryson TA and Dawson JH, The influence of substrate on the spectral properties of oxyferrous wild-type and T252A cytochrome P450-CAM. *Arch Biochem Biophys* **436:** 40-9, 2005.
143. Smith SV, Koley AP, Dai RK, Robinson RC, Leong H, Markowitz A and Friedman FK, Conformational modulation of human cytochrome P450 2E1 by ethanol and other substrates: a CO flash photolysis study. *Biochemistry* **39:** 5731-5737, 2000.

144. Hildebrandt P, Greinert R, Stier A, Stockburger M and Taniguchi H, Surface enhanced resonance Raman study of phenobarbital-induced rabbit liver cytochrome P-450 LM2. *FEBS Lett* **227:** 76-80, 1988.
145. Hildebrandt P, Greinert R, Stier A and Taniguchi H, Resonance Raman study on the structure of the active sites of microsomal cytochrome P-450 isozymes LM2 and LM4. *Eur J Biochem* **186:** 291-302, 1989.
146. Munro AW, Lindsay JG, Coggins JR, MacDonald I, Smith WE and Rospendowski BN, Resonance Raman spectroscopic studies on intact cytochrome P450 BM3. *Biochem Soc Trans* **22:** 54S, 1994.
147. Girvan HM, Marshall KR, Lawson RJ, Leys D, Joyce MG, Clarkson J, Smith WE, Cheesman MR and Munro AW, Flavocytochrome P450 BM3 mutant A264E undergoes substrate-dependent formation of a novel heme iron ligand set. *J Biol Chem* **279:** 23274-86, 2004.
148. Wells AV, Li P, Champion PM, Martinis SA and Sligar SG, Resonance Raman investigations of Escherichia coli-expressed Pseudomonas putida cytochrome P450 and P420. *Biochemistry* **31:** 4384-93, 1992.
149. Ohta T, Matsuura K, Yoshizawa K and Morishima I, The electronic and vibrational structures of iron-oxo porphyrin with a methoxide or cysteinate axial ligand. *J Inorg Biochem* **82:** 141-52, 2000.
150. Linder DP, Rodgers KR, Banister J, Wyllie GR, Ellison MK and Scheidt WR, Five-coordinate Fe(III)NO and Fe(II)CO porphyrinates: where are the electrons and why does it matter? *J Am Chem Soc* **126:** 14136-48, 2004.
151. Jung C and Ghosh DK, High pressure fourier transform infrared (FT-IR) spectroscopic studies on inducible nitric oxide (NO) synthase active site: a comparison to cytochrome p450CAM. *Cell Mol Biol (Noisy-le-grand)* **50:** 335-46, 2004.
152. Contzen J, Kostka S, Kraft R and Jung C, Intermolecular electron transfer in cytochrome P450cam covalently bound with Tris(2,2'-bipyridyl)ruthenium(II): structural changes detected by FTIR spectroscopy. *J Inorg Biochem* **91:** 607-17, 2002.
153. Mössbauer R, Kernresonzfluoreszenz von gammastrahlung in Ir191. *Z Physik* **151:** 124-143, 1958.
154. Sharrock M, Munck E, Debrunner PG, Marshall V, Lipscomb JD and Gunsalus IC, Mossbauer studies of cytochrome P-450 cam. *Biochemistry* **12:** 258-65, 1973.
155. Schoneboom JC, Neese F and Thiel W, Toward identification of the compound I reactive intermediate in cytochrome P450 chemistry: a QM/MM study of its EPR and Mossbauer parameters. *J Am Chem Soc* **127:** 5840-53, 2005.
156. Schunemann V, Jung C, Trautwein AX, Mandon D and Weiss R, Intermediates in the reaction of substrate-free cytochrome P450cam with peroxy acetic acid. *FEBS Lett* **479:** 149-54, 2000.
157. Poli-Scaife S, Attias R, Dansette PM and Mansuy D, The substrate binding site of human liver cytochrome P450 2C9: an NMR study. *Biochemistry* **36:** 12672-82, 1997.
158. Regal KA and Nelson SD, Orientation of caffeine within the active site of human cytochrome P450 1A2 based on NMR longitudinal (T1) relaxation measurements. *Arch Biochem Biophys* **384:** 47-58, 2000.
159. Solomon I and Bloembergen N, Nuclear magnetic interactions in the HF molecule. *J Chem Phys* **25:** 261-266, 1956.
160. Wei JY, Pochapsky TC and Pochapsky SS, Detection of a high barrier conformational change in the active site of cytochrome P450cam upon binding of putidaredoxin. *J Am Chem Soc* **127:** 6974-6, 2005.
161. Modi S, Primrose WU, Boyle JM, Gibson CF, Lian LY and Roberts GC, NMR studies of substrate binding to cytochrome P450 BM3: comparisons to cytochrome P450 cam. *Biochemistry* **34:** 8982-8, 1995.
162. Modi S, Gilham DE, Sutcliffe MJ, Lian LY, Primrose WU, Wolf CR and Roberts GCK, 1-Methyl-4-phenyl-1,2,3,6-tetrahydropyridine as a substrate of cytochrome P450 2D6: allosteric effects of NADPH-cytochrome P450 reductase. *Biochemistry* **36:** 4461-70, 1997.
163. Stern JO, Peisach J, Blumberg WE, Lu AY and Levin W, A low-temperature EPR study of partially purified, soluble ferric cytochromes P-450 and P-448 from rat liver microsomes. *Arch Biochem Biophys* **156:** 404-13, 1973.

164. Dus K, On the structure of putidaredoxin and cytochrome P-450 cam and their mode of interaction. *Adv Exp Med Biol* **58:** 287-309, 1975.
165. Davydov DR, Knyushko TV, Kanaeva IP, Koen YM, Samenkova NF, Archakov AI and Hui Bon Hoa G, Interactions of cytochrome P450 2B4 with NADPH-cytochrome P450 reductase studied by fluorescent probe. *Biochimie* **78:** 734-743, 1996.
166. Lepesheva GI, Strushkevich NV and Usanov SA, Conformational dynamics and molecular interaction reactions of recombinant cytochrome p450scc (CYP11A1) detected by fluorescence energy transfer. *Biochim Biophys Acta* **1434:** 31-43, 1999.
167. Dunn AR, Hays AM, Goodin DB, Stout CD, Chiu R, Winkler JR and Gray HB, Fluorescent probes for cytochrome p450 structural characterization and inhibitor screening. *J Am Chem Soc* **124:** 10254-5, 2002.
168. Dunn AR, Dmochowski IJ, Winkler JR and Gray HB, Nanosecond photoreduction of cytochrome p450cam by channel-specific Ru-diimine electron tunneling wires. *J Am Chem Soc* **125:** 12450-6, 2003.
169. Prasad S, Mazumdar S and Mitra S, Binding of camphor to Pseudomonas putida cytochrome p450(cam): steady-state and picosecond time-resolved fluorescence studies. *FEBS Lett* **477:** 157-60, 2000.
170. Djuricic D, Hill HA, Lo KK and Wong LL, A scanning tunneling microscopy (STM) investigation of complex formation between cytochrome P450(cam) and putidaredoxin. *J Inorg Biochem* **88:** 362-7, 2002.
171. Blobaum AL, Kent UM, Alworth WL and Hollenberg PF, Novel reversible inactivation of P450 2E1 T303A by tert-butyl acetylene: The role of threonine 303 in proton delivery to the active site of cytochrome P450 2E1. *J Pharmacol Exp Ther*, 2004.
172. Ost TW, Clark J, Mowat CG, Miles CS, Walkinshaw MD, Reid GA, Chapman SK and Daff S, Oxygen activation and electron transfer in flavocytochrome P450 BM3. *J Am Chem Soc* **125:** 15010-20, 2003.
173. Sligar SG, Cinti DL, Gibson GG and Schenkman JB, Spin state control of the hepatic cytochrome P450 redox potential. *Biochem Biophys Res Commun* **90:** 925-32, 1979.
174. Munro AW, Leys DG, McLean KJ, Marshall KR, Ost TW, Daff S, Miles CS, Chapman SK, Lysek DA, Moser CC, Page CC and Dutton PL, P450 BM3: the very model of a modern flavocytochrome. *Trends Biochem Sci* **27:** 250-7, 2002.
175. Chen Z, Ost TW and Schelvis JP, Phe393 mutants of cytochrome P450 BM3 with modified heme redox potentials have altered heme vinyl and propionate conformations. *Biochemistry* **43:** 1798-808, 2004.
176. Fleming BD, Tian Y, Bell SG, Wong LL, Urlacher V and Hill HA, Redox properties of cytochrome p450BM3 measured by direct methods. *Eur J Biochem* **270:** 4082-8, 2003.
177. Shumyantseva VV, Ivanov YD, Bistolas N, Scheller FW, Archakov AI and Wollenberger U, Direct electron transfer of cytochrome P450 2B4 at electrodes modified with nonionic detergent and colloidal clay nanoparticles. *Anal Chem* **76:** 6046-52, 2004.
178. Shukla A, Gillam EM, Mitchell DJ and Bernhardt PV, Direct electrochemistry of enzymes from the cytochrome P450 2C family. *Electrochem Comm* **7:** 437-442, 2005.
179. Ingelman-Sundberg M, Genetic polymorphisms of cytochrome P450 2D6 (CYP2D6): clinical consequences, evolutionary aspects and functional diversity. *the Pharmacogenomics Journal* **5:** 6-13, 2005.
180. Venhorst J, Onderwater RC, Meerman JH, Commandeur JNM and Vermeulen NPE, Influence of N-substitution of 7-methoxy-4-(aminomethyl)-coumarin on cytochrome P450 metabolism and selectivity. *Drug Metab Dispos* **28:** 1524-32, 2000.
181. Kranendonk M, Mesquita P, Laires A, Vermeulen NP and Rueff J, Expression of human cytochrome P450 1A2 in Escherichia coli: a system for biotransformation and genotoxicity studies of chemical carcinogens. *Mutagenesis* **13:** 263-9, 1998.
182. Kempf AC, Zanger UM and Meyer UA, Truncated human P450 2D6: expression in Eschirichia coli, Ni(2+)-chelate affinity purification, and characterization of solubility and aggregation. *Arch Biochem Biophys* **321:** 277-88, 1995.
183. Lightfoot T, Ellis SW, Mahling J, Ackland MJ, Blaney FE, Bijloo GJ, De Groot MJ, Vermeulen NP, Blackburn GM, Lennard MS and Tucker GT, Regioselective hydroxylation of debrisoquine

by cytochrome P4502D6: implications for active site modelling. *Xenobiotica* **30:** 219-33, 2000.

184. Seifar RM, Altelaar MA, Dijkstra RJ, Ariese F, Brinkman UA and Gooijer C, Surface-enhanced resonance Raman spectroscopy as an identification tool in column liquid chromatography. *Anal Chem* **72:** 5718-24, 2000.

185. Stortelder A, Buijs JB, Bulthuis J, Gooijer C and van der Zwan G, Fast-gated intensified charge-coupled device camera to record time-resolved fluorescence spectra of tryptophan. *Appl Spectrosc* **58:** 705-10, 2004.

186. Stortelder A, Buijs JB, Bulthuis J, van der Vies SM, Gooijer C and van der Zwan G, Time-resolved fluorescence of the bacteriophage T4 capsid protein gp23. *J Photochem Photobiol B* **78:** 53-60, 2005.

Part I:

Key determinants of CYP2D6 activity

Chapter 2

Influence of phenylalanine 120 on cytochrome P450 2D6 catalytic selectivity and regiospecificity: crucial role in 7-methoxy-4-(aminomethyl)-coumarin metabolism

Peter H.J. Keizers, Barbara M.A. van Vugt-Lussenburg, Chris de Graaf, Letty M. Mentink, Nico P.E. Vermeulen, and Jan N.M. Commandeur

adapted from: Biochemical Pharmacology 2004 **68**:2263-2271

The polymorphic human debrisoquine hydroxylase, cytochrome P450 2D6 (CYP2D6), is one of the most important phase I drug metabolising enzymes. It is responsible for metabolizing a large number of compounds that mostly share similarity in having a basic *N*-atom and an aromatic moiety. In homology modeling studies it has been suggested that in fixation of this aromatic moiety there may be an important role for phenylalanine 120 (F120). In this study, the role of F120 in ligand binding and catalysis was experimentally examined by mutating it into an alanine. Strikingly, this substitution led to a completely abolished 7-methoxy-4-(aminomethyl)-coumarin *O*-demethylating activity of CYP2D6. On the other hand, bufuralol metabolism was hardly affected (K_m 1-hydroxylation mutant: 1.2 μM, wild-type: 2.9 μM, 4-hydroxylation mutant 1.5 μM, wild-type: 3.2 μM) and neither was affected dextromethorphan *O*-demethylation (K_m mutant: 1.2 μM, wild-type: 2 μM, k_{cat} mutant 4.5 min^{-1}, wild-type: 3.3 min^{-1}). However, the F120A mutant also formed 3-hydroxymorphinan, the double demethylated form of dextromethorphan, which was not detected using wild-type CYP2D6. 3,4-Methylenedioxymethamphetamine was demethylenated by both mutant and wild-type CYP2D6 to 3,4-dihydroxymethamphetamine (K_m mutant 55 μM, wild-type: 2 μM). In addition the mutant formed two additional metabolites; 3,4-methylenedioxy-amphetamine and *N*-hydroxy-3,4-methylenedioxymethamphetamine. Inhibition experiments of dextromethorphan *O*-demethylation showed a decreased affinity of the F120A mutant for quinidine (IC_{50} mutant: 240 nM, wild-type 40 nM), while IC_{50}'s for quinine were equal (1 μM). These data indicate the importance of F120 in the selectivity and regiospecificity in substrate binding and catalysis by CYP2D6.

Introduction

Cytochromes P450 (CYPs) are heme containing enzymes capable of oxidizing and reducing a large variety of endogenous and exogenous substrates in virtually all living organisms [1, 2]. In humans one of the most important hepatic phase I drug metabolizing enzymes is CYP2D6. It is involved in the metabolism of about 30% of the currently marketed drugs, including neuroleptics, antidepressants β-blockers, opioids and antiarythmics [3, 4]. The enzyme is known for its genetic polymorphisms, even increasing its clinical relevance [5, 6]. Although some crystal structures of mammalian CYPs have become available in recent years [7, 8], so far no crystal structure of CYP2D6 has been resolved. Structural information on this enzyme still depends on homology modeling and mutagenesis studies.

Recently we have developed a new homology model of CYP2D6 based on the crystal structure of rabbit CYP2C5 [9]. This was the first model of CYP2D6 based on a mammalian CYP template and is therefore considered an improvement over the existing models. This was indicated by the good correlation between experimental data and the modelled protein-substrate interactions. The model identified some active site key residues. First of all E216 has been shown to be a key ligand binding residue involved in hydrogen bonding with a variety of substrates. This residue has been subjected to mutagenesis studies [10, 11], that indicated involvement of this residue in fixation of basic nitrogen atoms present in many CYP2D6 substrates. A second important active site residue in this and other homology models is F483 [12], interacting via van der Waals forces with substrates like codeine. Earlier mutagenesis of this residue to an isoleucine showed effects on testosterone metabolism [13]. However, the anchoring of aromatic moieties present in most CYP2D6 substrates, as predicted in pharmacophore models [14-16], cannot be completely ascribed to this residue. Therefore other phenylalanine residues contributing to aromatic interactions with substrates have to be present in the active site. Mutation of F481 to other non-aromatic residues led to decreased activities towards model substrates [17], although in the model of Venhorst et al. this residue is not considered to be in the active site of CYP2D6.

Even more interesting is the position of a third phenylalanine at position 120 in the active site of CYP2D6 homology models [9, 11, 12]. In these CYP2C5-based models F120 appears to be positioned directly above the porphyrin ring. From docking and molecular dynamics studies this residue seems to be the anchoring residue for the aromatic moiety of ligands like quinidine and sparteine via π-stacking [9]. In the present study the role of F120 in ligand binding and metabolism by CYP2D6 is studied experimentally by mutating this residue into an alanine. According to computational simulations this mutation will create not only more space in the active site, but also eliminates a potentially important aromatic anchoring point. By mutating F120 into alanine we are aiming at the elucidation of the role of this residue in substrate binding and turnover by CYP2D6.

Materials and Methods

Materials

The pSP19T7LT plasmid containing human 2D6 with a C-terminal His_6-tag bicistronically co-expressed with human cytochrome P450 NADPH reductase was kindly provided by Prof. Dr. Ingelman-Sundberg. 7-methoxy-4-(aminomethyl)-coumarin (MAMC), 7-hydroxy-4-(aminomethyl)-coumarin (HAMC), 3,4-methylenedioxymethylamphetamine (MDMA) and 3,4-methylenedioxyamphetamine (MDA) were synthesized as described [18, 19]. Bufuralol hydrochloride was obtained from Gentest. *N*-methylhydroxylamine hydrochloride, Dextromethorphan hydrobromide and dextrorphan tartrate were obtained from Sigma. All other chemicals were of analytical grade and obtained from standard suppliers.

Synthesis of N-hydroxy-3,4-methylenedioxymethylamphetamine
N-hydroxy-3,4-methylenedioxymethylamphetamine (1-(3,4-methylenedioxyphenyl)-*N*-methyl,2-hydroxylaminopropane) was prepared from piperonyl methyl ketone and *N*-methylhydroxylamine by reductive amination with sodium cyanoborohydride [20]. A two-fold surplus of *N*-methylhydroxylamine hydrochloride was stirred with piperonyl methyl ketone in methanol at room temperature, sodium cyanoborohydride was added and stirred for 48 h. After adding water, neutralizing the cyanoborohydride with 6 M HCl and neutralizing the acid with 6 M NaOH, the product was extracted in dichloromethane. ^{1}H NMR (400 Hz, $CDCl_3$): δ 1.00 (d, 3H, CCH_3), 2.38 (dd, 1H, H-1), 2.68 (s, 3H, NCH_3), 2.91 (m, 1H, CHN), 3.10 (dd, 1H, H-1), 5.90 (s, 2H, OCH_2O), 6.63 (dd, 1H, H-6′), 6.70 (d, 1H, H-2′), 6.72 (d, 1H, H-5′). ^{13}C NMR (400 Hz, $CDCl_3$): δ 14.20 (CH_3), 38.82 (CH_2), 43.95 (CH_3N), 65.35 (CH), 72.82, 100.83 (OCH_2O), 108.17 (C-5′), 109.70 (C-2′), 122.13 (C-6′), 133.29 (C-1′), 145.87 (C-4′), 147.59 (C-3′). MS direct injection: *m/z*, $M^{+\cdot}$ 210, MS/MS: 179 (3), 163 (100), 135 (3).

Site-directed mutagenesis
The phenylalanine 120→alanine (F120A) mutation was introduced into pSP19T7LT using the QuickChange XL Site-Directed Mutagenesis kit (Stratagene). The sequences of the forward- and reverse oligonucleotides, respectively, with the mutated residue in *italic*, were as follows: 5′-CGT TCC CAA GGG GTG *GCC* CTG GCG CGC TAT-3′ and 5′-ATA GCG CGC CAG *GGC* CAC CCC TTG GGA ACG-3′. After mutagenesis, the presence of the desired F120A mutation was confirmed by DNA sequencing.

Expression and membrane isolation
Both the F120A mutant and the wild-type CYP2D6 containing pSP19T7LT plasmids were transformed into *Escherichia coli* strain JM109. Expression was carried out in 3L flasks containing 300 ml TB (Terrific Broth) medium with additives (1 mM δ-aminolevulinic acid, 400 μl/L trace elements [21], 1 μg/ml thiamine, 100 μg/ml ampicillin). Cultures were inoculated with 3 ml frozen *E. coli* cells containing the desired plasmid, and induction was initiated by the addition of 2 mM isopropyl β-D-thiogalactoside. Cultures were grown for 48 h at 28 °C and 125 rpm, before they were harvested. CYP contents were determined by CO difference spectra [22].
Harvested cells were pelleted by centrifugation (15 min, 4000 g, 4 °C) and the resulting pellet was resuspended in TSE buffer (50 mM Tris-acetate pH 7.6, 250 mM sucrose, 0.25 mM EDTA), 35 mg wet weight cells/ ml. Spheroblasts were prepared by adding 0.1 mg/ml lysozyme and gently shaking the cells for 30 min on ice. Spheroblasts were pelleted by centrifugation (15 min, 4000 g, 4 °C), and resuspended in KPi-glycerol buffer (100 mM potassium phosphate buffer, pH 7.4, 20% glycerol, 0.1 mM DTT), 0.5 g/ml. The spheroblasts were lysed by passage through a French press followed by sonication (Branson Sonifier 250, 10 x 20 sec, 70% full power), and the membrane fraction was isolated by ultracentrifugation (45 min, 120,000 g, 4 °C). Membranes were resuspended in 0.4% of the original culture volume of TSE buffer and CYP contents were determined with CO difference spectra.

Metabolism and inhibition assays
MAMC *O*-demethylation [23]: Reactions were carried out in duplicate in a 96 wells plate, in a total volume of 200 μl. The reaction mixture consisted of 50 mM potassium phosphate buffer (KPi) pH 7.4, 5 mM $MgCl_2$, 0-500 μM MAMC (10 concentrations used) and *E. coli* membranes corresponding to 40 nM wild-type or F120A mutant CYP2D6. The reactions were initiated by addition of an NADPH regenerating system, resulting in final concentrations of 0.1 mM NADPH, 0.3 mM glucose-6-phosphate, and 0.4 units/ml glucose-6-phosphate dehydrogenase. The reaction was monitored for 40 min at 37 °C on a Victor^2 1420 multilabel counter (Wallac) (λ_{ex}= 405 nm, λ_{em}= 460 nm). The metabolite of MAMC, i.e. HAMC, was identified and quantified using the synthetic reference compound. HPLC analysis of MAMC metabolism was performed as described [18], using a C18 column (Chrompack Chromspher 5, 250 x 4.6 mm) with a flow rate of 0.4 ml/min.
Dextromethorphan *O*-demethylation [10]: Reactions were carried out in 300 μl 50 mM KPi pH 7.4, 5 mM $MgCl_2$ supplemented with 10 concentrations ranging from 0 to 40 μM dextromethorphan and *E. coli* membranes corresponding to 50 nM wild-type or 25 nM F120A mutant CYP2D6. After 5 min of pre-incubation at 37 °C, the reactions were initiated with an NADPH regenerating system as described above. The reaction was allowed to proceed for 5 min before it was stopped by the addition of 15 μl 70% $HClO_4$. After centrifugation (10 min, 6800 g), 30 μl aliquots of the supernatant were analyzed by

HPLC. Metabolites were separated using a C18 column (Chrompack Chromspher 5, 250 x 4.6 mm) with a flow rate of 1 ml/min. The mobile phase consisted of 30% acetonitrile and 1% triethylamine, set to pH 3 with 70% $HClO_4$. Metabolites were detected by fluorescence (λ_{ex}= 280 nm, λ_{em}= 311 nm) and identified by LC-MS. Inhibition of *O*-demethylation by various concentrations of quinidine and quinine was measured under the same conditions using a concentration of 8 μM dextromethorphan.
Bufuralol hydroxylation [10, 24]: Reactions were carried out as described above using 9 concentrations ranging from 0 to 100 μM bufuralol and *E. coli* membranes corresponding to 50 nM wild-type or 25 nM F120A mutant CYP2D6. Metabolites were separated using a C18 column (Chrompack Chromspher 5, 250 x 4.6 mm) with a flow rate of 0.6 ml/min. The mobile phase consisted of 30% acetonitrile and 0.1% triethylamine, set to pH 3 with 70% $HClO_4$. Metabolites were detected by fluorescence (λ_{ex}= 252 nm, λ_{em}= 302 nm). Metabolites of bufuralol were identified by comparison with other studies [24].
MDMA metabolism: Reactions were carried out as described above with 9 concentrations ranging from 0 to 200 μM MDMA and *E. coli* membranes corresponding to 50 nM wild-type or 25 nM F120A mutant CYP2D6. Metabolites were separated using a C18 column (Phenomenex Inertsil ODS 150 x 4.6 mm) with a flow rate of 0.4 ml/min. The mobile phase consisted of 23% acetonitrile and 0.1% triethylamine, set to pH 3 with 70% $HClO_4$. Metabolites were detected by fluorescence (λ_{ex}= 280 nm, λ_{em}= 320 nm) and identified electrochemically (ECD, oxidation mode 0.8 V, for detection of 3,4-OH-MA), by LC-MS (3,4-OH-MA, MDA, *N*-OH-MDMA) and using synthesized reference compounds (MDA, *N*-OH-MDMA). Peak areas of all metabolites were quantified by Shimadzu Class VP 4.3 and analyzed using Graph Pad Prism 4.0.

LC-MS
To identify the metabolites of MDMA, dextromethorphan and dextrorphan, incubations were carried out for 10 min as described above with 100 μM MDMA, 100 μM dextrorphan or 25 μM dextromethorphan respectively and *E. coli* membranes corresponding to 50 nM 2D6 wild-type or 50 nM 2D6 F120A. Volumes of 100 μl supernatant were injected and separated using a phenyl column (Waters Novapak Phenyl 150 x 4.6 mm) with a flow rate of 0.4 ml/min. The metabolites were eluted using a gradient starting with a 1% ACN eluens, supplemented with 10 mM ammonium acetate, increasing linearly to 95% ACN with 10 mM ammoniumacetate in 30 min and analyzed by MS. APCI positive ionisation was used on a LCQ Deca mass spectrometer (Thermo Finnigan), vaporizer temperature 450 °C, N_2 as sheath (40 psi) and auxiliary gas (10 psi), needle voltage 6000 V, heated capillary 150 °C.

Homology Modeling
A protein homology model of CYP2D6 was constructed based on the crystal structures of dimethylsulphophenazole and diclofenac bound rabbit CYP2C5, PDB codes 1N6B and 1NR6 respectively [7, 25]. Homology modeling, model refinement and model validation was performed as described [9]. The final model of wild-type CYP2D6 was used as a template for modeling of the F120A mutant. The F120 residue was mutated to alanine using the homology module of InsightII (Biosym), after which an energy minimization and a one picosecond position restrained molecular dynamics simulation was carried out.

Results

Expression of wild-type and F120A mutant CYP2D6
The F120A mutant had consistently significantly lower expression levels compared to wild-type CYP2D6. An average culture contained about 70 nM of CYP for the mutant versus 200 nM for wild-type after 48 hours induction. In the difference spectrum taken from the culture of the mutant enzyme a high absorbance was measured at 420 nm, showing the presence of large amounts of P420, the inactive form of CYP, indicating that the mutation decreases the stability of the enzyme to some extent.

Metabolism of model compounds
O-demethylation of the CYP2D6 marker substrate MAMC (Figure 1) showed to be linear for over 40 minutes using *E. coli* membranes containing 40 nM of wild-type CYP2D6. Enzyme

kinetics analysis revealed a K_m of 49 μM and a k_{cat} of 3.7 min^{-1} (Table 1). Using the F120A mutant under the same conditions did not lead to detectable HAMC formation. HPLC analysis of these incubations gave the same results and did not show any additional metabolites.

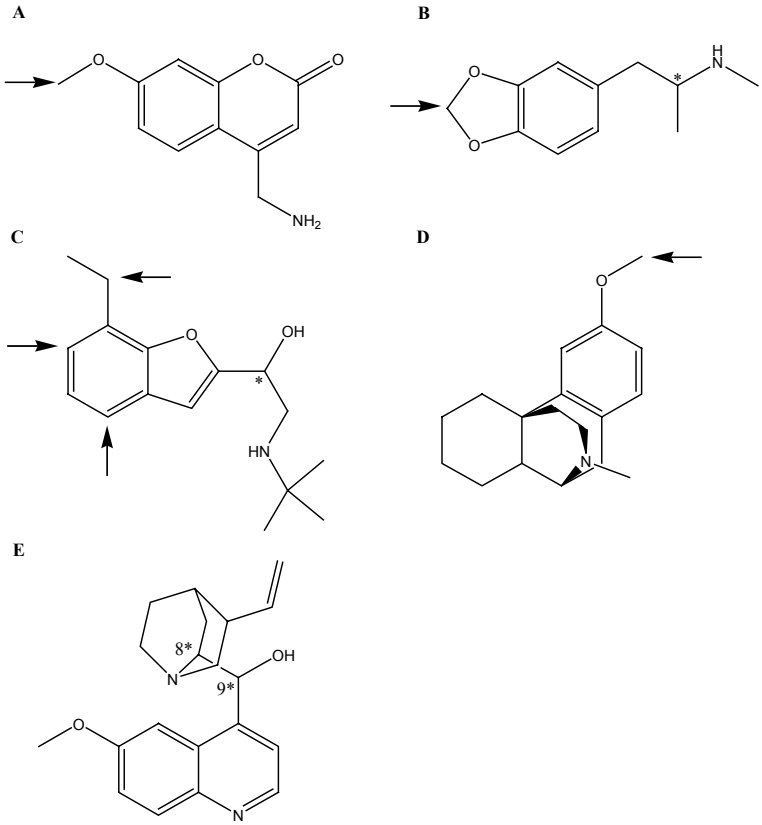

Fig. 1. Structures of the substrates (A: MAMC, B: MDMA, C: bufuralol, D: dextromethorphan) and ligands (E: quinidine (8R, 9S) and quinine (8S, 9R)) used, showing sites of oxidation by wild-type CYP2D6 (↑) and chiral carbon atoms (*).

Dextromethorphan was selectively *O*-demethylated to dextrorphan by wild-type CYP2D6 (K_m 2 μM, k_{cat} 3.3 min^{-1}). The F120A mutant also formed dextrorphan be it with a slightly lower K_m and higher k_{cat} than the wild-type. The formation of dextrorphan showed to be linear for at least 20 minutes, indicating the mutant to be stable enough for studying the metabolism. Dextrorphan and other metabolites were identified by LC-MS. The *N*-demethylated metabolite of dextromethorphan, i.e. 3-methoxymorphinan (*m/z* 258, MS/MS: *m/z* 215), was detected for both the wild-type as for the F120A mutant with a t_R of 36 min. Because of overlap with the peak of dextromethorphan (*m/z* 272, MS/MS: *m/z* 215) at t_R 37 min, *N*-demethylation could not be quantified. Interestingly, also a metabolite with *m/z* 244 (t_R 31.1 min, MS/MS: *m/z* 147) was detected for the F120A mutant, apparently the double *O*- and *N*-demethylated metabolite of dextromethorphan, i.e. 3-hydroxymorphinan. The 3-hydroxymorphinan formation could also not be quantified under the conditions used

because it is a secondary metabolite. When the F120A mutant was incubated with dextrorphan again 3-hydroxymorphinan was formed and two other metabolites with *m/z* 274 were detected (t_R 27.5 min, MS/MS: *m/z* 199 and t_R 30.3 min MS/MS: *m/z* 257 and 201), indicating hydroxylation of dextrorphan. With the wild-type CYP2D6 no metabolites of dextrorphan were detected.

Table 1: Kinetic parameters of wild-type and F120A mutant CYP2D6 towards model substrates.

Substrate	Products	Wild-type		F120A	
		K_m	V_{max}	K_m	V_{max}
MAMC	HAMC	49 ± 2	3.7 ± 0.6 [a]	- [b]	- [b]
dextromethorphan	dextrorphan	2.0 ± 0.2	3.3 ± 0.4 [a]	1.2 ± 0.4	4.5 ± 0.3 [a]
	3-OH-morphinan	- [b]	- [b]	+ [c]	+ [c]
dextrorphan	3-OH-morphinan	- [b]	- [b]	+ [c]	+ [c]
bufuralol	1'-OH	2.9 ± 0.4	54 ± 17 [d]	1.2 ± 0.2	51 ± 11 [d]
	4-OH	3.2 ± 0.5	2.7 ± 0.8 [d]	1.5 ± 0.3	2.7 ± 0.6 [d]
MDMA	3,4-OH-MA	1.9 ± 0.7	3.4 ± 1.0 [d]	55.4 ± 16	4.6 ± 1.1 [d]
	MDA	- [b]	- [b]	9.0 ± 2.5	6.0 ± 3.3 [d]
	N-OH-MDMA	- [b]	- [b]	11.0 ± 2.8	10.9 ± 3.8 [d]

All values are the means of at least three independent experiments ± S.D. as described in the Methods section. K_m expressed in μM, [a] V_{max} expressed in min^{-1}, [b] not detectable, [c] present but not quantifiable, [d] V_{max} expressed in 1 x 10^5 fluorescence units/min/nmol P450.

Upon incubation of bufuralol both with wild-type and F120A mutant CYP2D6 four metabolites were detected; 6-OH bufuralol, 1'-OH bufuralol, 4-OH bufuralol and $\Delta^{1',2'}$ bufuralol, as identified before by others [24]. Under the conditions used only peak areas of the metabolites 1'-OH bufuralol and 4-OH bufuralol could be quantified. For both these metabolites the F120A mutant showed a two times lower K_m than wild-type CYP2D6 with a comparable turnover (Table 1).

Another known CYP2D6 substrate that was subjected to incubations with wild-type and F120A mutant CYP2D6 was MDMA [26]. In the case of wild-type CYP2D6 only O-demethylenenation of MDMA to the catechol 3,4-dihydroxymethylamphetamine (3,4-OH-MA) was observed with a K_m of 2 μM and a V_{max} of 3.4 x 10^5 AU. This metabolite was identified by ECD, LC-MS (measured as the quinone, t_R 21.2 min, *m/z* 180) and it was described before by others [26]. The mutant enzyme also formed this catechol with a similar V_{max}, but with a 30-fold higher K_m (Figure 2). In addition to demethylenenation, MDMA was also *N*-demethylated to MDA by the mutant enzyme, with a K_m of 9 μM and a V_{max} of 6 x 10^5 AU, as identified by LC-MS (t_R 21.4 min, *m/z* 180) and co-elution with the synthetic reference (Figure 2). Furthermore, a third metabolite was formed by the F120A mutant with a K_m of 11 μM, and a V_{max} of 11 x 10^5 AU. This metabolite was also identified by LC-MS. An *m/z* of 210 was observed for this metabolite (t_R 21.9 min), indicating hydroxylation of MDMA (*m/z* 194). MS/MS data showed a mass over charge of 163, suggesting that hydroxylation took place on the nitrogen, as the *m/z* of 163 is the propyl-methylenedioxyphenyl fragment, which is also a common fragment of both MDA and MDMA. In order to confirm the identity of this new metabolite of MDMA, *N*-OH-MDMA was synthesized and showed identical mass spectroscopic behavior. Direct injection of this compound in the MS gave an *m/z* 210, with as the major MS/MS fragment *m/z* 163. In addition, the *N*-OH-MDMA also co-eluted with the

new metabolite on both the C18 as the phenyl reversed phase columns, when spiked in an incubation sample, verifying it to have the same molecular structure.

A

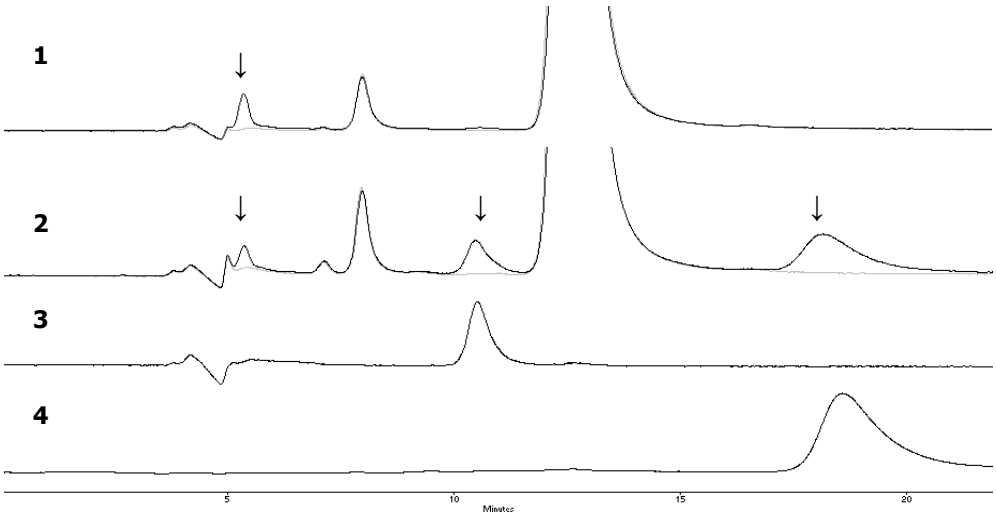

B

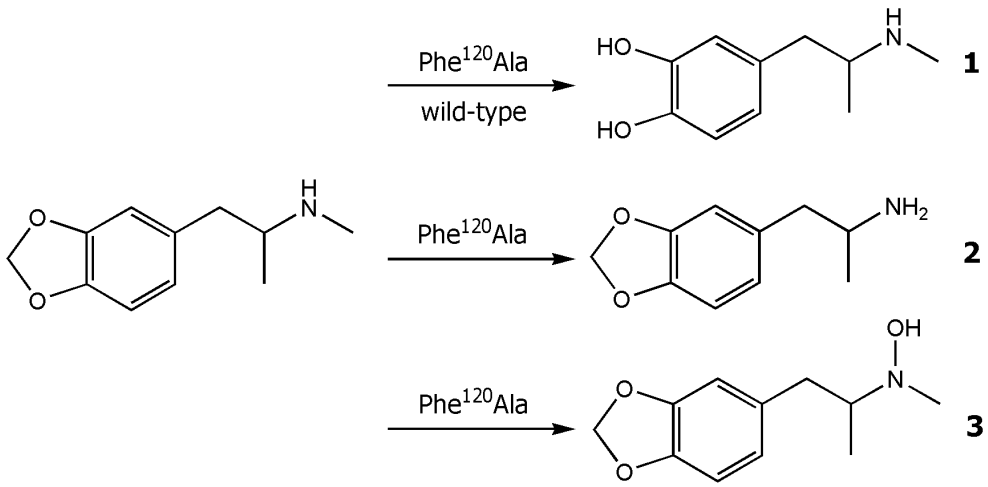

Fig. 2. Chromatograms of 100 μM MDMA incubations with membranes of E. coli cells expressing wild-type (1) and F120A mutant (2) CYP2D6 with (gray), and without (black) 20 μM quinidine (A). Metabolites are indicated (↓) and reference chromatograms of synthesized MDA (3) and synthesized N-OH-MDMA (4) are also shown. t_R of the substrate MDMA is 13.2 min, t_R metabolites: 3,4-OH-MA 5.5 min, MDA 10.9 min, N-OH-MDMA 18.8 min. For conditions used see Methods section. Scheme of MDMA metabolism by wild-type (1) and F120A mutant CYP2D6 into 3,4-OH-MA (1), MDA (2), and N-OH-MDMA (3) is shown (B).

Inhibition of dextromethorphan metabolism

Inhibition of dextromethorphan *O*-demethylation by quinidine and quinine was determined for both F120A and wild-type CYP2D6 (Figure 3). In case of both the enzymes, quinine inhibited dextrorphan formation with an IC_{50} of about 1 μM (Table 2), whereas quinidine was about six-fold less potent in inhibiting the F120A mutant (IC_{50} 200 nM) than the wild-type enzyme (IC_{50} 40 nM).

Table 2

IC_{50} values (μM) of the ligands quinine and quinidine against 8 μM dextromethorphan for wild-type and F120A mutant CYP2D6.

Ligand	IC_{50}	
	Wild-type	F120A
quinidine	0.04 ± 0.01	0.24 ± 0.04
quinine	0.76 ± 0.17	1.3 ± 0.27

All values are the means of at least two independent experiments ± S.D. as described in the Methods section.

Modeling

In a refined homology model of CYP2D6 used in this study, F120, E216, and F483 are positioned at approximately the same location as in the previously reported homology model [9]. D301 however, does not point into the active site, but is oriented such that it stabilizes the B/C-loop by hydrogen bonding to the backbone *N*-atoms of residues V119 and F120. D301 however may also play an electrostatic role in the binding of basic substrates by increasing the net negative charge within the active site [12]. Furthermore, the constructed homology model used in this study has a more 'closed' binding pocket as a result of the fact that the substrate-free CYP2C5 crystal structure template used for the old homology model is lacking the F/G-loop (unpublished data).

Discussion

Recently, computer homology modeling studies suggested F120 to be a CYP2D6 active site residue involved in the binding of substrates via aromatic interactions [9, 11, 12]. The primary aim of this study was to evaluate the role of this residue in the CYP2D6 active site. The results presented in this study show that F120 is very relevant in CYP2D6 ligand binding, substrate selectivity and regiospecificity in catalysis.

The expression levels of the F120A mutant in *E. coli* were found to be lower than the wild-type enzyme, indicating that F120 may have a role in the stability of the enzyme. High levels of P420 were seen in the difference spectra, showing that the expression itself was not hampered, but that a large amount of enzyme formed was not functional as was reported before for several other CYP2D6 mutants [10, 27].

Four typical CYP2D6 substrates were selected to characterize the F120A mutant. Compared to wild-type CYP2D6 large substrate-dependent differences in metabolism were found after introducing a single mutation, not reported before for other CYP2D6 mutants. MAMC was not metabolized by the F120A mutant while bufuralol metabolism by the F120A mutant was similar to the metabolism by the wild-type enzyme. For both dextromethorphan and MDMA there were changes in catalytic regiospecificity after mutating F120 into an alanine. So despite the fact that all four substrates show structural similarity in having a basic *N*-atom at about 7 Å of the site of oxidation and in having an adjacent aromatic moiety [14], still the influence of the mutation differed between these substrates. The only time large substrate

dependent differences were described for a CYP2D6 mutant was with a $Glu^{216}Gln$ mutant, using the substrate spirosulfonamide [11], that lacks a basic *N*-atom and therefore does not fit into the classical pharmacophore model [14-16].

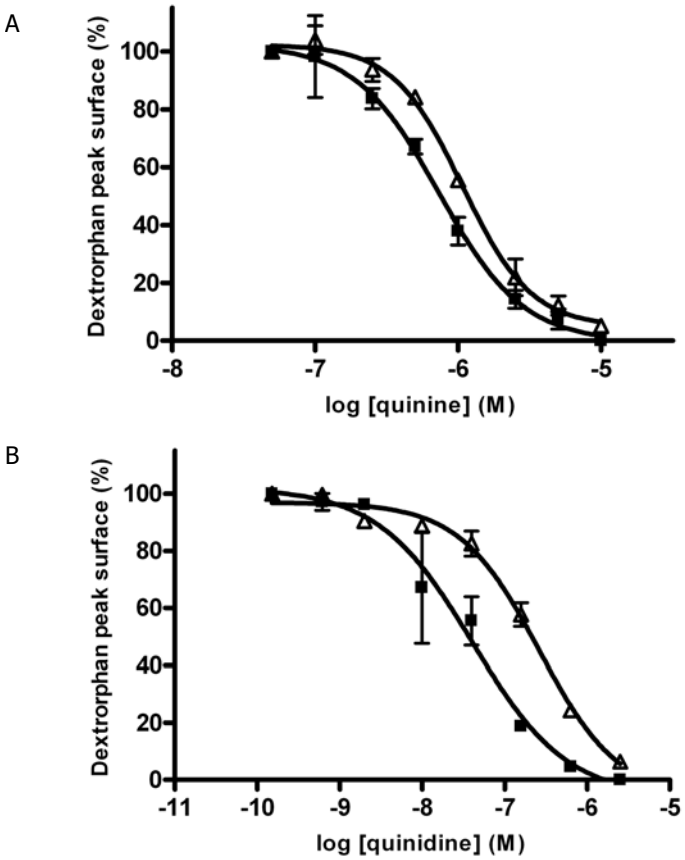

Fig. 3. Relative amounts of dextromethorphan O-demethylation in presence of various amounts of quinine (A) and quinidine (B) by F120A mutant (Δ) and wild-type CYP2D6 (■). Plotted values are the means of at least two independent experiments ± S.D. as described in the Methods section.

Neither HAMC nor other metabolites were detected after incubating MAMC with the F120A mutant so apparently F120 influences either the affinity, or the orientation of this substrate with respect to the heme. More experiments with other coumarin derivatives could give more information about the underlying mechanisms [28].
Bufuralol metabolism by CYP2D6 was studied previously using a series of D301 mutants [24], and also mutants of E216 to non-acidic residues were studied using this model substrate [10, 11]. Large effects were found on affinity and turnover of the mutants for this compound, showing that these acidic residues are more important for bufuralol metabolism than F120 as can be concluded from this study. The role of D301 was postulated also to be fixation of the B-C loop containing residue F120 [10-12] however the present results do not seem to support this role as the F120A mutation hardly shows an effect on bufuralol

metabolism. Consequently, the role of D301 does not seem to be merely the fixation of F120 into the active site [29], but creation of the net negative charge together with E216 may be of bigger importance.

A

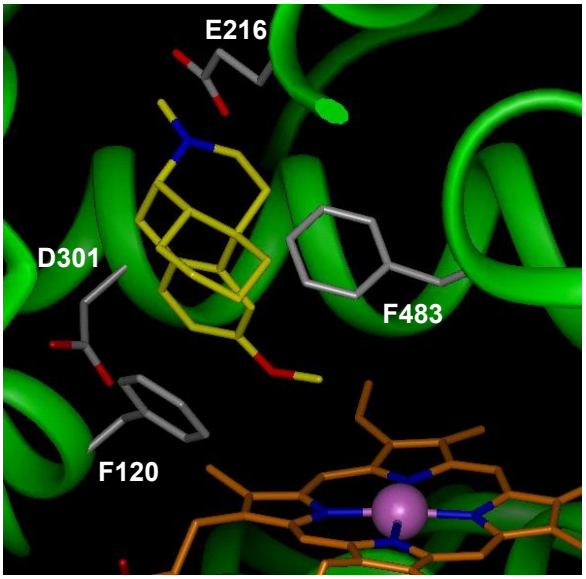

B

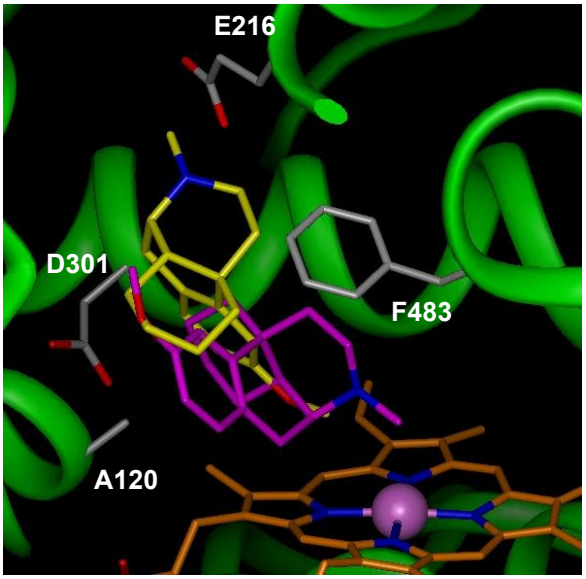

Fig. 4. Binding orientation of dextromethorphan automatically docked in the active site of the homology models of CYP2D6 using Autodock with standard conditions [30]. In wild-type CYP2D6 the orientation of dextromethorphan with its O-methyl pointing towards the heme is favored (A), in the F120A mutant two distinct high ranking orientations were found, supporting both N-demethylation as O-demethylation (B). A colored version of the figure is shown in the Appendix of this thesis.

N-dealkylation of substrates is a possible route in CYP2D6 metabolism and F481 was predicted previously to be an important substrate binding residue involved in these reactions [15]. However mutating the F481 residue into a Gly did not have a large influence on *N*-deisopropylation of metoprolol [17]. Both MDMA and dextrorphan were *N*-demethylated by the F120A mutant implicating a more promiscuous way of orientation of these two substrates in the active site of CYP2D6 and the involvement of the F120 residue in binding substrates undergoing *N*-dealkylation.
Besides *N*-dealkylation of MDMA, also *N*-hydroxylation occurred when MDMA was incubated with the F120A mutant. *N*-OH-MDMA has been described before as a MDMA metabolite in horse urine [31], however from this previous study it remained unclear what enzymes were playing a role in this reaction. Furthermore, aliphatic *N*-hydroxylation has not been described before as a metabolic reaction catalysed by CYP2D6 wild-type or mutants for any substrate. The co-occurrence of both *N*-dealkylation and *N*-hydroxylation of a single substrate has been reported once before for *N*-methylbenzamidine by rabbit CYP2C3 [32]. Additional work should give more insights in the mechanism of these transformations by the F120A CYP2D6 mutant.
The role of F120 in the active site of CYP2D6 seems to be at least two-fold; firstly, the phenyl ring fills the active site cavity causing a reduction of its size and secondly, it may have a function as an aromatic interaction site. The metabolite 3-hydroxymorphinan is detected exclusively in dextromethorphan incubations with the F120A mutant. In Figure 4, it is demonstrated how the mutation of the bulky Phe into a smaller Ala-residue allows the dextromethorphan *N*-demethylation binding mode to be accommodated more easily by creating more space in the CYP2D6 active site. As indicated earlier, F120 is considered important for interacting with quinidine via π-stacking [9]. The six-fold increase in IC_{50}-value as determined for the F120A mutant validates the specific anchoring role of this residue. This role was confirmed by the inability of the F120A mutant to metabolize MAMC. The two roles; space filling and aromatic anchoring however only partly explain the substrate specific influence, as bufuralol, MDMA and MAMC are structurally similar substrates but showed different changes in metabolism when incubated with the F120A mutant.
In the rat isoforms of the CYP2D family, no homologous aromatic residues are present in the B-C loop so the F120 is a human CYP2D6 active site specific residue [9]. The data presented here introduce F120 as the fourth important residue in the binding of ligands to and catalysis by CYP2D6, next to E216, D301 and F483. The effects of removing the F120 phenyl-moiety are on the affinity, turnover and orientation of substrates, but the effects were quite different for structurally similar substrates. To rationalize the large differences found with the four chosen substrates advanced molecular modeling is needed. Combined with molecular dynamics it can give insights where space is a limiting factor or where specific interactions play a role in the CYP2D6 active site.

Acknowledgements
We thank Frans de Kanter for his help with recording and elucidating the NMR spectra and Ed Groot for his help in preparing the *E. coli* membranes.

References

1. Estabrook RW, Cytochromes P450: from a single protein to a family of proteins-with some personal reflections. In: *Cytochromes P450: metabolic and toxicological aspects* (Eds. Ioannides and Costas), pp. 3-28. Crc press inc, New York, 1996.

2. Goeptar AR, Scheerens H and Vermeulen NPE, Oxygen and xenobiotic reductase activities of cytochrome P450. *Crit Rev Toxicol* **25:** 25-65, 1995.
3. Zanger UM, Raimundo S and Eichelbaum M, Cytochrome P450 2D6: overview and update on pharmacology, genetics, biochemistry. *Naunyn Schmiedebergs Arch Pharmacol* **369:** 23-37, 2004.
4. Bertilsson L, Dahl ML, Dalen P and Al-Shurbaji A, Molecular genetics of CYP2D6: clinical relevance with focus on psychotropic drugs. *Br J Clin Pharmacol* **53:** 111-22, 2002.
5. Ingelman-Sundberg M, Oscarson M and McLellan RA, Polymorphic human cytochrome P450 enzymes: an opportunity for individualized drug treatment. *Trends Pharmacol Sci* **20:** 342-9, 1999.
6. Oscarson M, Pharmacogenetics of drug metabolising enzymes: importance for personalised medicine. *Clin Chem Lab Med* **41:** 573-80, 2003.
7. Wester MR, Johnson EF, Marques-Soares C, Dansette PM, Mansuy D and Stout CD, Structure of a substrate complex of mammalian cytochrome P450 2C5 at 2.3 A resolution: evidence for multiple substrate binding modes. *Biochemistry* **42:** 6370-9, 2003.
8. Williams PA, Cosme J, Ward A, Angove HC, Matak Vinkovic D and Jhoti H, Crystal structure of human cytochrome P450 2C9 with bound warfarin. *Nature* **424:** 464-8, 2003.
9. Venhorst J, ter Laak AM, Commandeur JNM, Funae Y, Hiroi T and Vermeulen NPE, Homology modeling of rat and human cytochrome P450 2D (CYP2D) isoforms and computational rationalization of experimental ligand-binding specificities. *J Med Chem* **46:** 74-86, 2003.
10. Paine MJ, McLaughlin LA, Flanagan JU, Kemp CA, Sutcliffe MJ, Roberts GC and Wolf CR, Residues glutamate 216 and aspartate 301 are key determinants of substrate specificity and product regioselectivity in cytochrome P450 2D6. *J Biol Chem* **278:** 4021-7, 2003.
11. Guengerich FP, Hanna IH, Martin MV and Gillam EM, Role of glutamic acid 216 in cytochrome P450 2D6 substrate binding and catalysis. *Biochemistry* **42:** 1245-53, 2003.
12. Kirton SB, Kemp CA, Tomkinson NP, St-Gallay S and Sutcliffe MJ, Impact of incorporating the 2C5 crystal structure into comparative models of cytochrome P450 2D6. *Proteins* **49:** 216-31, 2002.
13. Smith G, Modi S, Pillai I, Lian LY, Sutcliffe MJ, Pritchard MP, Friedberg T, Roberts GC and Wolf CR, Determinants of the substrate specificity of human cytochrome P-450 CYP2D6: design and construction of a mutant with testosterone hydroxylase activity. *Biochem J* **331:** 783-92, 1998.
14. Koymans L, Vermeulen NPE, van Acker SA, te Koppele JM, Heykants JJ, Lavrijsen K, Meuldermans W and Donne-Op den Kelder GM, A predictive model for substrates of cytochrome P450-debrisoquine (2D6). *Chem Res Toxicol* **5:** 211-9, 1992.
15. de Groot MJ, Ackland MJ, Horne VA, Alex AA and Jones BC, A novel approach to predicting P450 mediated drug metabolism. CYP2D6 catalyzed N-dealkylation reactions and qualitative metabolite predictions using a combined protein and pharmacophore model for CYP2D6. *J Med Chem* **42:** 4062-4070, 1999.
16. Vermeulen NPE, Prediction of drug metabolism: the case of cytochrome P450 2D6. *Curr Top Med Chem* **3:** 1227-39, 2003.
17. Hayhurst GP, Harlow J, Chowdry J, Gross E, Hilton E, Lennard MS, Tucker GT and Ellis SW, Influence of phenylalanine-481 substitutions on the catalytic activity of cytochrome P450 2D6. *Biochem J* **355:** 373-9, 2001.
18. Onderwater RC, Venhorst J, Commandeur JNM and Vermeulen NPE, Design, synthesis, and characterization of 7-methoxy-4-(aminomethyl)coumarin as a novel and selective cytochrome P450 2D6 substrate suitable for high-throughput screening. *Chem Res Toxicol* **12:** 555-9, 1999.
19. Braun U, Shulgin AT and Braun G, Centrally active N-substituted analogs of 3,4-methylenedioxyphenylisopropylamine (3,4-methylenedioxyamphetamine). *J Pharm Sci* **69:** 192-5, 1980.
20. de Boer D, Tan LP, Gorter P, van de Wal RM, Kettenes-van den Bosch JJ, de Bruijn EA and Maes RA, Gas chromatographic/mass spectrometric assay for profiling the enantiomers of 3,4-methylenedioxymethamphetamine and its chiral metabolites using positive chemical ionization ion trap mass spectrometry. *J Mass Spectrom.* **32:** 1236-46, 1997.

21. Bauer S and Shiloach J, Maximal exponential growth rate and yield of E. coli obtainable in a bench-scale fermentor. *Biotechnol Bioeng* **16:** 933-41, 1974.
22. Omura T and Sato R, The carbon monoxide-binding pigment of liver microsomes. II. Solubilization, purification, and properties. *J Biol Chem* **239:** 2379-85, 1964.
23. Venhorst J, Onderwater RC, Meerman JH, Vermeulen NPE and Commandeur JNM, Evaluation of a novel high-throughput assay for cytochrome P450 2D6 using 7-methoxy-4-(aminomethyl)-coumarin. *Eur J Pharm Sci* **12:** 151-8, 2000.
24. Hanna IH, Krauser JA, Cai H, Kim MS and Guengerich FP, Diversity in mechanisms of substrate oxidation by cytochrome P450 2D6. Lack of an allosteric role of NADPH-cytochrome P450 reductase in catalytic regioselectivity. *J Biol Chem* **276:** 39553-61, 2001.
25. Wester MR, Johnson EF, Marques-Soares C, Dijols S, Dansette PM, Mansuy D and Stout CD, Structure of mammalian cytochrome P450 2C5 complexed with diclofenac at 2.1 A resolution: evidence for an induced fit model of substrate binding. *Biochemistry* **42:** 9335-45, 2003.
26. Lin LY, Di Stefano EW, Schmitz DA, Hsu L, Ellis SW, Lennard MS, Tucker GT and Cho AK, Oxidation of methamphetamine and methylenedioxymethamphetamine by CYP2D6. *Drug Metab Dispos* **25:** 1059-64, 1997.
27. Hanna IH, Kim MS and Guengerich FP, Heterologous expression of cytochrome P450 2D6 mutants, electron transfer, and catalysis of bufuralol hydroxylation: the role of aspartate 301 in structural integrity. *Arch Biochem Biophys* **393:** 255-61, 2001.
28. Venhorst J, Onderwater RC, Meerman JH, Commandeur JNM and Vermeulen NPE, Influence of N-substitution of 7-methoxy-4-(aminomethyl)-coumarin on cytochrome P450 metabolism and selectivity. *Drug Metab Dispos* **28:** 1524-32, 2000.
29. Guengerich FP, Miller GP, Hanna IH, Martin MV, Leger S, Black C, Chauret N, Silva JM, Trimble LA, Yergey JA and Nicoll-Griffith DA, Diversity in the oxidation of substrates by cytochrome P450 2D6: lack of an obligatory role of aspartate 301-substrate electrostatic bonding. *Biochemistry* **41:** 11025-34, 2002.
30. Morris GM, Goodsell DS, Halliday RS, Huey R, Hart WE, Belew RK and Olson AJ, Automated docking using a Lamarckian genetic algorithm and an empirical binding free energy function. *J Comput Chem* **19:** 1639-1662, 1998.
31. Dumasia MC, Identification of some N-hydroxylated metabolites of (+/-)-3,4-methylenedioxymethamphetamine in horse urine by gas chromatography-mass spectrometry. *Xenobiotica* **33:** 1013-25, 2003.
32. Clement B and Jung F, N-hydroxylation and N-dealkylation by CYP2C3 of N-methylbenzamidine: N-oxygenation and N-oxidative dealkylation of one functional group. *Xenobiotica* **25:** 443-55, 1995.

Chapter 3

The role of phenylalanine 483 in cytochrome P450 2D6 is strongly substrate dependent

Barbara M.A. van Vugt-Lussenburg, Peter H.J. Keizers, Chris de Graaf, Mats Hidestrand, Magnus Ingelman-Sundberg, Nico P.E. Vermeulen, and Jan N.M. Commandeur

adapted from: Biochemical Pharmacology 2005 **70**:1253-61

The polymorphic cytochrome P450 2D6 (CYP2D6) is involved in the metabolism of 30% of the drugs currently prescribed, and is thus clinically relevant. Typical CYP2D6 substrates generally contain a basic nitrogen atom and an aromatic moiety adjacent to the site of metabolism. Recently, we demonstrated the importance of active site residue F120 in substrate binding and catalysis in CYP2D6. On the basis of protein homology models, it is claimed that another active site phenylalanine, F483, may also play an important role in the interaction with the aromatic moiety of CYP2D6 substrates. Experimental data to support this hypothesis, however, is not yet available. In fact, in the only study performed, mutation of F483 to isoleucine or tryptophan did not affect the 1'-hydroxylation of bufuralol at all [1]. In the present study the role of F483 in ligand binding and metabolism by CYP2D6 was examined experimentally using site-directed mutagenesis. Replacement of F483 by alanine resulted in a 30-fold lower V_{max} for bufuralol 1'-hydroxylation, while the K_m was hardly affected. The V_{max} for 3,4-methylenedioxy-methylamphetamine *O*-demethylenation on the other hand decreased only two-fold, whereas the effect on the K_m was much larger. For dextromethorphan, in addition to dextrorphan (*O*-demethylation) and 3-methoxymorphinan (*N*-demethylation), two other metabolites were formed that could not be detected for the wild-type. The substrate 7-methoxy-4-(aminomethyl)-coumarin was not metabolized at all by F483A mutant CYP2D6, a phenomenon that was reported also for F120A mutant CYP2D6. The presented data show that next to F120, residue F483 plays a very important role in the metabolism of typical CYP2D6 substrates. The influence of F483 on metabolism was found to be strongly substrate-dependent.

Introduction

The cytochrome P450 (CYP) superfamily constitutes a large group of oxido-reductases that are responsible for the oxidation and reduction of many endogenous compounds as well as a wide variety of xenobiotics [2-4]. In humans, cytochrome P450 2D6 (CYP2D6) is one of the most important enzymes of this family [5]. Despite its low abundance, CYP2D6 represents only 3% of the total amount of CYP in human liver, it metabolizes ~30% of the drugs currently on the market [6, 7]. Its clinical relevance is even increased by the fact that CYP2D6 is highly polymorphic; 6% of the European population is classified as a poor metabolizer, while another 3% has the ultrarapid metabolizer phenotype [7-10], thus contributing to large interindividual differences in drug metabolism.

The development of accurate models of the active site of CYP2D6 is useful to identify potential drug candidates that interact with the enzyme. Because no crystal structure is yet available for CYP2D6, the structural information required for such models has to be obtained from homology modeling [11, 12] and experimental mutagenesis studies.

Most substrates of CYP2D6 contain a basic nitrogen at a distance of approximately 5 to 7 Å from the site of oxidation, and an adjacent aromatic moiety [13]. Besides the negatively charged active site residues E216 and D301 that have been shown to play a role in fixation of the basic nitrogen atom [14-16], pharmacophore and homology models suggest a role for aromatic residues in the active site to undergo van der Waals interactions with aromatic moieties of the ligands [17]. Three aromatic phenylalanine residues have been proposed as active-site residues, F120, F481 and F483. Recently, it was experimentally underlined that F120 is indeed one of the aromatic active site residues playing an important role in substrate binding and metabolism [18, 19]. In earlier CYP2D6 homology models based on bacterial CYP crystal structure templates it was suggested that another aromatic residue associated with ligand binding is F481 [17, 20, 21]. Substitution of F481 by non-aromatic residues reduced the affinity of several typical CYP2D6 substrates [17]. In more recent homology models based on rabbit CYP2C5, however, F481 is positioned outside the binding pocket, but in close contact with active site residue F483 [1, 15, 22, 23]. Our model (figure 1) [22] and several others [1, 15, 23, 24] suggest that this aromatic active site residue, i.e. F483, is also a potential ligand-contact residue (Figure 1). In a modeling study by Kemp et al. phenylalanines 120 and 483 are referred to as important residues in the active site of CYP2D6, which are involved in the binding of various compounds from the National Cancer Institute database [24]. However, experimental data supporting a role for F483 in binding known CYP2D6 substrates is not yet available. In fact, in the only experimental study on this residue, it was shown that substitution of F483 by isoleucine or tryptophan did not affect the 1'-hydroxylation of the typical CYP2D6 substrate bufuralol [1]. Interestingly, the F483I mutant was able to catalyze the 15α-hydroxylation of testosterone, which is not a substrate for wild-type CYP2D6 [23]. Therefore, it is not yet clear whether this residue plays a role in the binding of typical CYP2D6 substrates. Recently, we demonstrated that the role of another active-site phenylalanine residue, F120, is substrate dependent [18, 19]. The F120A mutant completely lost the ability to metabolize 7-methoxy-4-(aminomethyl)coumarin (MAMC), while no significant effect on bufuralol metabolism was observed. 3,4-Methylenedioxymethamphetamine (MDMA) and dextromethorphan were still metabolized by F120A, but the regiospecificity of metabolism had changed significantly.

The goal of the present study is to investigate whether the role of phenylalanine F483 in the metabolism of typical CYP2D6 substrates is substrate dependent. Using site-directed mutagenesis, this phenylalanine residue was substituted by an alanine (F483A), and the effect of this mutation on the binding and metabolism of four typical CYP2D6 substrates, notably dextromethorphan, bufuralol, MDMA and MAMC, was studied.

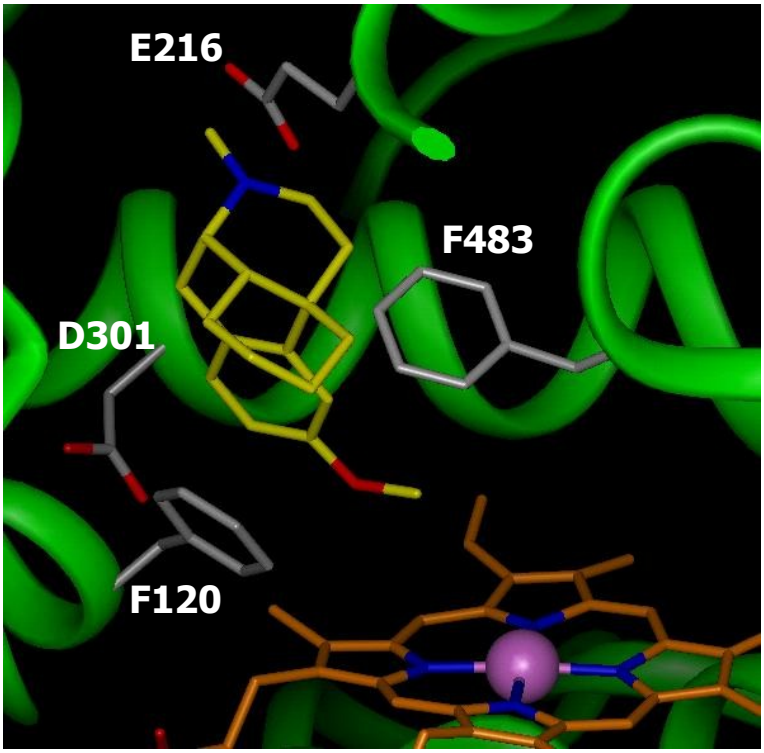

Figure 1. The active site of the homology model of CYP2D6 [18], showing the active site residues F120, E216, D301 and F483. The heme iron atom is shown as a sphere, and the substrate dextromethorphan is depicted. A colored version of the figure is shown in the Appendix of this thesis.

Materials and methods

Materials

7-methoxy-4-(aminomethyl)-coumarin (MAMC), 7-hydroxy-4-(aminomethyl)-coumarin (HAMC), 3,4-methylenedioxymethylamphetamine (MDMA) and 3,4-methylenedioxyamphetamine (MDA) were synthesized as described [25, 26]. Bufuralol hydrochloride was obtained from Gentest. Dextromethorphan hydrobromide and dextrorphan tartrate were obtained from Sigma. All other chemicals were of analytical grade and obtained from standard suppliers.

Plasmid and site-directed mutagenesis

The pSP19T7LT plasmid containing human CYP2D6 with a C-terminal His_6-tag bicistronically co-expressed with human Cytochrome P450 NADPH reductase (CPR) was constructed as follows: the CPR was generated by reverse transcription of human genomic DNA using a reverse transcription kit with oligo dT primers (Clontech, inc, USA). After reverse transcription, the cDNA was amplified with primers creating restriction enzyme sites. Human CYP2D6 was amplified from a cDNA. During amplification additional C-terminal histidine residues as well as sites for restriction enzyme cleavage were introduced. The amplified and digested 2D6 and CPR were subsequently ligated into the expression plasmid pSP19T7LT [27] in tandem, with a short linker region in-between the two genes. The correct gene sequence was verified by sequencing.

The phenylalanine 483 to alanine (F483A) mutation was introduced into pSP19T7LT using the QuikChange XL Site-Directed Mutagenesis kit (Stratagene). The sequences of the forward- and reverse oligonucleotides, respectively, with the altered nucleotides in *italic*, were as follows: 5'-AT-GGT-GTC-

TTT-GCT-*GCC*-CTG-GTG-AGC-CC-3' and 5'-GG-GCT-CAC-CAG-*GGC*-AGC-AAA-GAC-ACC-AT-3'. After mutagenesis, the presence of the desired F483A mutation was confirmed by DNA sequencing.

Expression and membrane isolation

Both the F483A mutant and the wild-type pSP19T7LT plasmids were transformed into *Escherichia coli* strain JM109. Expression was carried out in 3L flasks containing 300 ml TB (Terrific Broth) medium with additives (1 mM δ-aminolevulinic acid, 400 μl/L trace elements [28], 1 μg/ml thiamine, 100 μg/ml ampicillin). Cultures were inoculated with 3 ml frozen *E. coli* cells containing the desired plasmid, and expression of CYP2D6 and CPR was initiated by the addition of 2 mM isopropyl-β-D-thiogalactopyranoside. Cultures were grown for 48 h at 28 °C and 125 rpm, before they were harvested. CYP contents were determined by CO difference spectra [29].

Harvested cells were pelleted by centrifugation (15 min, 4000 g, 4 °C) and the resulting pellet was resuspended in 1/20 original culture volume of Tris-Sucrose-EDTA (TSE) buffer (50 mM Tris-acetate pH 7.6, 250 mM sucrose, 0.25 mM EDTA). After the addition of 0.1 mg/ml lysozyme, the cells were disrupted using a French Press (1000psi, 3 repeats). To remove remaining undisrupted cells, the lysate was centrifuged (15 min, 4000 g, 4 °C) and the resulting pellet was discarded. The cytosolic fraction was separated from the membranous fraction by centrifugation for 45 min at 120,000 g, 4 °C. The membrane pellet was resuspended in 1/75 original culture volume of TSE buffer and CYP contents were determined using CO difference spectra. CPR activity was measured using cytochrome c reduction as described previously [30, 31]. To convert the CPR activities to CPR concentrations, a specific activity of 3200 nmol cytochrome c/min/nmol reductase was used [30, 31].

For determination of dissociation constants of ligands, the CYP was purified from the membranes. Enzymes were solubilized by stirring for 2 hrs at 4°C in KPi-glycerol buffer (50 mM potassium phosphate buffer pH 7.4 with 10% glycerol), supplemented with 0.5% Emulgen 911. Insoluble parts were removed by centrifugation (60 min, 120,000 g, 4 °C). Supernatant was incubated, gently rocking, with Ni-NTA agarose (Qiagen) for 30 min at 4 °C. The column material was retained in a polypropylene tube with porous disc (Pierce), washed with KPi-glycerol buffer containing 2 mM histidine. CYP2D6 was eluted with 0.2 M histidine. After overnight dialysis in KPi-glycerol buffer the sample was concentrated on a Vivaspin 20 filtration tube (10.000 MWCO PES, Sartorius).

Metabolism of model compounds

Before the enzyme kinetic parameters of the four substrates were determined, a series of experiments was performed to determine the linearity of the reactions with time and enzyme concentration. Based on these experiments (data not shown), incubation times and enzyme concentrations were chosen that are within the linear range.

MAMC metabolism [25, 32]: Reactions were carried out in triplicate in a black Costar 96 wells plate, in a total volume of 200 μl. The reaction mixture consisted of 100 mM potassium phosphate buffer pH 7.4 (KPi) containing 5 mM $MgCl_2$ and 2 mM EDTA, and *E. coli* membranes containing 40 nM CYP2D6 (wild-type or F483A mutant CYP2D6), and CPR. 9 Different concentrations of MAMC were used ranging from 0 to 320 μM. The reaction was initiated by addition of an NADPH regenerating system, resulting in final concentrations of 0.1 mM NADPH, 0.3 mM glucose-6-phosphate, and 0.4 units/ml glucose-6-phosphate dehydrogenase. The reaction was monitored for 30 min at 37 °C on a Victor^2 1420 multilabel counter (Wallac) (λ_{ex}= 405 nm, λ_{em}= 460 nm). The metabolite of MAMC, i.e. HAMC, was identified and quantified using the synthetic reference compound. Samples were also analyzed by high-performance liquid chromatography (HPLC) as described previously [25] to determine if other metabolites were formed that could not be detected on the fluorescence microplate reader.

Dextromethorphan metabolism [16]: The reaction mixture was composed as described for MAMC, with *E. coli* membranes containing 25 nM CYP2D6 (wild-type or F483A mutant CYP2D6), and CPR. 10 Different concentrations of dextromethorphan were used ranging from 0 to 80 μM. After 5 min of preincubation at 37 °C, the reaction was initiated by addition of an NADPH regenerating system as described above. The reaction was allowed to take place for 10 min at 37 °C before it was stopped with 1/20 volume of 70% $HClO_4$. Precipitated proteins were removed by centrifugation (10 min, 6800 g), and the supernatant was analyzed by HPLC (injection volume 25 μl). Metabolites were separated using a C18 column (Phenomenex Luna 5μ, 150 x 4.6 mm) with a flow rate of 0.6 ml/min. The mobile phase consisted of 30% acetonitrile (ACN) and 0.1% triethylamine, set to pH 3 with $HClO_4$. Metabolites were

quantified by fluorescence (λ_{ex}= 280 nm, λ_{em}= 311 nm). The metabolite dextrorphan was identified using co-elution with the reference compound; other metabolites were identified by LC-MS.
Bufuralol metabolism [16, 33]: Reactions were carried out as described above for dextromethorphan, with 9 concentrations of bufuralol ranging from 0 to 80 μM. Metabolites were separated using a C18 column (Phenomenex Luna 5μ, 150 x 4.6 mm) with a flow rate of 0.6 ml/min. The mobile phase consisted of 30% ACN and 0.1% triethylamine, set to pH 3 with $HClO_4$. Metabolites were detected by fluorescence (λ_{ex}= 252 nm, λ_{em}= 302 nm). Metabolites of bufuralol were identified by comparison with other studies by comparing retention times and peak areas [33], and 1'-OH bufuralol was identified using co-elution with a reference compound. LC/MS was used to identify $\Delta^{1,2}$-bufuralol (data not shown).
MDMA metabolism [34]: Reactions were carried out as described above with 9 concentrations of MDMA ranging from 0 to 220 μM. Metabolites were separated using a C18 column (Phenomenex Luna 5μ, 150 x 4.6 mm) with a flow rate of 0.6 ml/min. The mobile phase consisted of 22% ACN and 0.1% triethylamine, set to pH 3 with $HClO_4$. Metabolites were detected by fluorescence (λ_{ex}= 280 nm, λ_{em}= 320 nm). MDA was identified using the synthesized reference compound (kind gift of Urs Meyer), and the catechol 3,4-dihydroxy-methylamphetamine (3,4-OH-MA) was identified previously using electrochemical detection [18]. The peak areas of all metabolites were quantified by Shimadzu Class VP 4.3. Reaction rates were calculated and plotted against the substrate concentrations to obtain Michaelis Menten curves, from the 'one site binding hyperbola fitting' module of Graph Pad Prism 4.0, yielding K_m and V_{max} values.

Identification of metabolites using LC-MS
To identify any unknown metabolites of dextromethorphan, LC-MS was used. For LC-MS measurements, incubations were carried out as described above with 40 μM substrate, and *E. coli* membranes containing 25 nM CYP2D6 (wild-type or F483A mutant CYP2D6), and CPR. Volumes of 50 μl supernatant were injected and separated using a phenyl column (Phenomenex Phenyl 150 x 4.6 mm) with a flow rate of 0.6 ml/min. The metabolites were eluted using a gradient starting with a 5% ACN eluens, supplemented with 20 mM ammonium acetate, increasing linearly to 90% ACN with 20 mM ammoniumacetate in 14 min and analyzed by MS. Positive ion Atmospheric Pressure Chemical Ionisation (APCI) was used on a LCQ Deca mass spectrometer (Thermo Finnigan), vaporizer temperature 450 °C, N_2 as sheath (40 psi) and as auxiliary gas (10 psi), needle voltage 6000 V, heated capillary 150 °C. MS/MS was performed with an activation energy of 30%.

Determination of dissociation constants
Dissociation constants were determined for dextromethorphan, bufuralol and MDMA in disposable 1 ml cuvettes. Two cuvettes were prepared containing 1 μM of purified CYP (wild-type or F483A mutant CYP2D6) in a final volume of 500 μl 100 mM potassium phosphate buffer (KPi) pH 7.4. Aliquots of 5 μl of a 1 mM substrate solution in KPi buffer were added to the sample cuvette, while the same amount of KPi buffer was added to the reference cuvette. Difference spectra from 350 to 450 nm were taken after every addition. In total, 11 aliquots were added, which corresponds to a substrate concentration ranging from 10 μM (addition 1) to 104 μM (addition 11). Upon type 1 binding of the substrates, a peak at 390nm and a trough at 420nm appeared. The $\Delta A_{390nm-420nm}$ values were plotted against the substrate concentration, and the 'one site binding hyperbola fitting' module of Graph Pad Prism 4.0 was used to estimate the spectral dissociation constants (K_s).

Results

Expression of wild-type and F483A mutant CYP2D6
Wild-type and F483A mutant CYP2D6 were successfully expressed in *E. coli*. A typical cell culture yielded approximately 400 nM CYP, and the expression levels of CYP were not affected by the F483A mutation (Figure 2). The CYP and CPR concentrations in the membranes were similar for wild-type and F483A mutant CYP2D6 (Table 1). The purified fractions contained 50 ± 5 μM of CYP for wild-type and mutant. The CYP content of wild-type and mutant membranes or purified fractions did not decrease after storage of up to six

months at –80°C and repeated cycles of freeze-thawing, indicating that the stability of the enzyme was not significantly influenced by the mutation.
A substantial amount of P420, the inactive form of CYP, could also be detected in the whole cell fractions and in the membrane factions. The amount of P420 in wild-type and F483A mutant CYP2D6 was similar (Figure 2). In the purified fractions, no P420 could be detected.

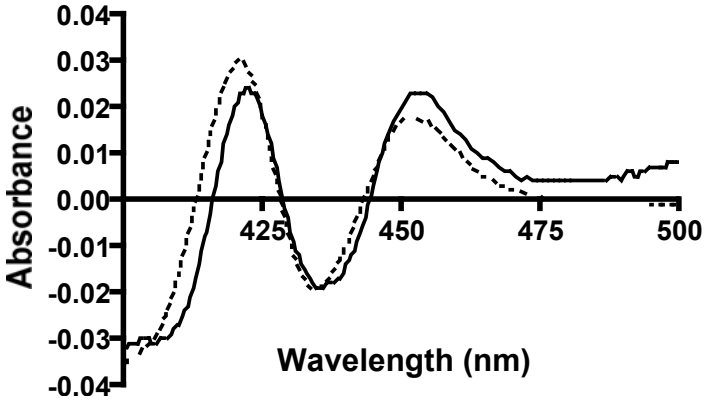

Figure 2. CO-difference spectra of E. coli JM109 cells expressing wild-type and F483A mutant CYP2D6. The cell samples, taken after 48h of expression, were diluted two-fold before the spectra were recorded. Solid line: wild-type CYP2D6; dashed line: F483A mutant CYP2D6. Both spectra correspond to approximately 200 nM CYP.

Table 1. CYP and CPR concentrations in membrane fractions.

	Wild-type	F483A
[CYP] (μM)	8.1 ± 0.8	7.9 ± 0.7
[CPR] (μM)	4.7 ± 0.5	4.0 ± 0.5
[CYP]/[CPR] ratio	1.7 ± 0.3	2.0 ± 0.3

CPR concentrations were calculated from CPR activities of 15 mM Cyt C/minute for CYP2D6 and 12.9 mM Cyt C/minute for F483A mutant CYP2D6.

Metabolism of model compounds

The CYP2D6 marker substrate MAMC was *O*-demethylated by wild-type CYP2D6 with a K_m of 42 μM and a V_{max} of 2.0 min^{-1} (Table 2). In contrast, the F483A mutant CYP2D6 did not form any detectable HAMC; re-analysis of the samples using HPLC also showed no detectable metabolites of MAMC.
The main metabolite formed upon dextromethorphan metabolism by wild-type CYP2D6 was the *O*-demethylated form, dextrorphan (Table 2) (m/z 258 and MS/MS m/z 201). In addition, trace amounts of the *N*-demethylated compound, 3-methoxymorphinan (m/z 258 and MS/MS m/z 215), were detected, but the amounts were too low to determine accurate enzyme kinetic parameters (Figure 3). The F483A mutant also formed dextrorphan, with a 15-fold higher K_m and a two-fold higher V_{max} than the wild-type resulting in a 7.5-fold lower V_{max}/K_m. 3-Methoxymorphinan was formed by F483A mutant CYP2D6 with higher activity than the wild-type, and V_{max} and K_m values could be determined (Table 2). In addition, trace amounts of two other metabolites were observed (Figure 4). LC-MS analysis showed that these were the double (*O*- and *N*-) demethylated 3-hydroxymorphinan (m/z 244 and MS/MS m/z 201), and the monohydroxylated, *O*-demethylated hydroxydextrorphan (m/z 274 and MS/MS m/z 217), respectively.

Bufuralol was metabolized by wild-type CYP2D6 into three detectable metabolites, 1'-OH-bufuralol, 4-OH-bufuralol and $\Delta^{1',2'}$-bufuralol, as described before [18] (Table 2). Although the K_m values of wild-type and F483A mutant CYP2D6 for bufuralol 1'-hydroxylation were very similar, the V_{max} of F483A mutant CYP2D6 was 32-fold lower. Under the conditions applied, only 1'-OH-bufuralol and trace amounts of 4-OH-bufuralol could be detected for F483A mutant CYP2D6 (Table 2).

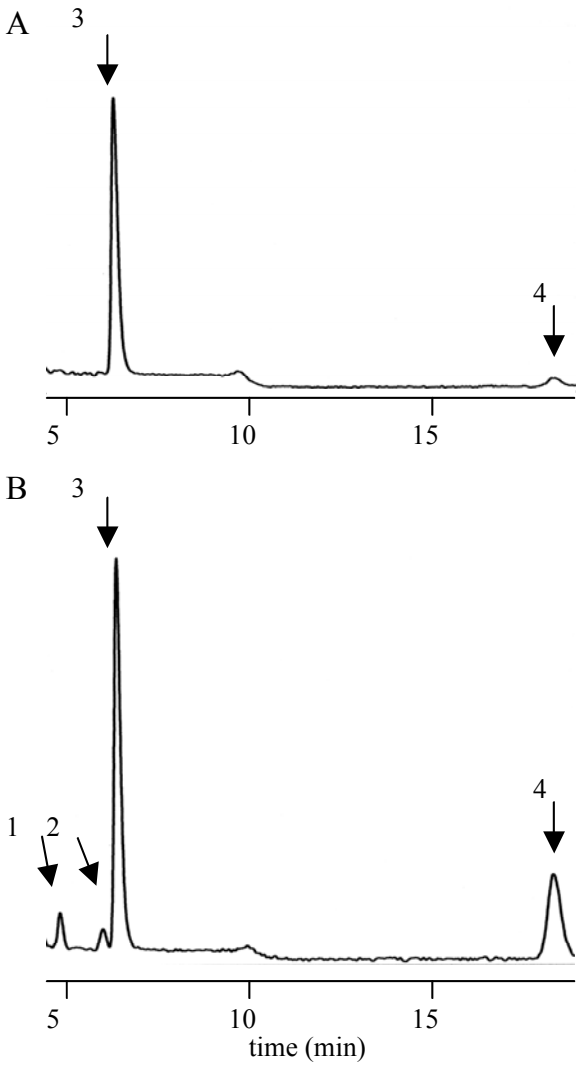

Figure 3. HPLC chromatograms of dextromethorphan incubations with wild-type (A) or F483A mutant (B CYP2D6. Incubations were carried out as described in the Methods section. Metabolites indicated by arrows are 1: hydroxy-dextrorphan; 2: 3-hydroxymorphinan; 3: dextrorphan and 4: 3-methoxymorphinan. The substrate dextromethorphan had a retention time of 24 minutes and is not displayed in these chromatograms.

Table 2. Kinetic parameters of wild-type and F483A mutant CYP2D6.

Substrate	Product	Wild-type			F483A		
		K_m	V_{max}	V_{max}/K_m	K_m	V_{max}	V_{max}/K_m
MAMC	HAMC	42.4 ± 2.6	2.0 ± 0.1[a]	0.050 ± 0.003	-[b]	-[b]	-
dextromethorphan	dextrorphan	1.1 ± 0.1	5.6 ± 0.1[a]	5.1 ± 0.4	17.0 ± 1.3	11.5 ± 0.3[a]	0.68 ± 0.06
	3-MO-morphinan	+[c]	+[c]	-	64.9 ± 5.7	80.0 ± 4.0[d]	1.2 ± 0.1
	3-OH-morphinan	-[b]	-[b]	-	+[c]	+[c]	-
	OH-dextrorphan	-[b]	-[b]	-	+[c]	+[c]	-
bufuralol	1'-OH	5.0 ± 0.1	14.5 ± 2.0[d]	2.9 ± 0.4	4.6 ± 0.4	0.43 ± 0.01[d]	0.09 ± 0.01
	4-OH	5.8 ± 0.1	1.3 ± 0.2[d]	0.2 ± 0.1	+[c]	+[c]	-
	$\Delta^{1',2'}$	23.0 ± 5.4	1.3 ± 0.1[d]	0.06 ± 0.01	-[b]	-[b]	-
MDMA	3,4-OH-MA	2.2 ± 0.3	1.7 ± 0.1[d]	0.8 ± 0.5	28.6 ± 3.9	0.80 ± 0.03[d]	0.030 ± 0.004
	MDA	+[c]	+[c]	-	+[c]	+[c]	-

All values are the means of at least three independent experiments ± S.D as described in the Methods section. K_m values expressed in μM, V_{max} values expressed in [a]min^{-1} or in [d]1 x 10^5 fluorescence units/min/nmol CYP. [b]: not detectable, [c]: present but not quantifiable.

MDMA was converted by wild-type CYP2D6 mainly to the catechol i.e. 3,4-OH-MA, with a K_m of 2.2 μM and a V_{max} of 1.7 x 10^5 fluorescence units min^{-1} $nmol^{-1}$ CYP. Only trace amounts of MDA [34] were detected. F483A mutant CYP2D6 formed 3,4-OH-MA with a 13-fold higher K_m and a 2-fold lower V_{max}, resulting in a 26-fold lower V_{max}/K_m value (Table 2). Like for the wild-type, trace amounts of MDA were also observed for F483A mutant CYP2D6. In contrast to the F120A mutant, no detectable *N*-hydroxylation of MDMA was performed by F483A mutant CYP2D6 [18].

Determination of dissociation constants

The K_s values of dextromethorphan, bufuralol and MDMA were determined for wild-type and F483A mutant CYP2D6 (Table 3). For MAMC, no K_s values could be determined because this ligand has a high absorbance at 350-450 nm that interfered with the binding spectra. Dextromethorphan, bufuralol and MDMA all showed type 1 spectra for wild-type and F483A mutant CYP2D6, indicating that the ligands bind at the substrate binding site. No large differences were found between K_s values for wild-type and F483A mutant CYP2D6. K_s values of dextromethorphan and bufuralol were both in the range of 20–30 μM for wild-type and F483A mutant CYP2D6, while the K_s values of MDMA were higher for both enzymes (50–60 μM).

Table 3. Optical dissociation constants (μM) of substrates for wild-type and F483A mutant CYP2D6.

Substrate	K_s			
	wild-type		F483A	
dextromethorphan	23.9 ± 1.1	21.9± 0.7	29.5± 1.5	38.1 ± 3.5
bufuralol	19.4 ± 2.0	15.4 ± 1.2	18.2 ± 1.4	21.8 ± 1.9
MDMA	34.5 ± 2.1	51.5 ± 3.6	52.4 ± 5.0	60.7 ± 7.1

Optical dissociation constants were determined in two separate experiments as described in the Methods section. Each value represents an independent experiment. The 11 data points were analyzed in Graphpad Prism using the 'one site binding hyperbola fitting' module. The standard errors of the fits are shown in the table.

Discussion

The purpose of this study was to investigate the role of CYP2D6 active site residue F483 in ligand binding and metabolism. Aromatic residues in the CYP2D6 active site cavity are thought to be particularly important, because of their ability to interact with aromatic moieties present in many CYP2D6 substrates [13]. Recently, it has been described that substitution of active site F120 by an alanine has large substrate dependent effects on the binding and metabolism of typical CYP2D6 substrates [18, 19]. Homology modeling studies have also suggested an important role for residue F483 [1, 15, 22-24], but to date experimental evidence supporting this suggestion was not available. The results presented in this study clearly show that substitution of the phenylalanine moiety at position 483 by an alanine (F483A) has marked effects on substrate selectivity and regiospecificity when using four typical CYP2D6 substrates (Figure 4). The observed effects of the F483A mutation were found to be strongly substrate-dependent, as was seen recently for F120A.

F483A mutant CYP2D6 did not metabolize MAMC, in contrast to wild-type CYP2D6. Apparently, residue F483 (this study) and residue F120 [18] are both required for metabolism of this substrate. These residues could either provide steric constraints to keep the substrate in the orientation required for metabolism, or they could function as aromatic anchoring points. A possible explanation is that MAMC is kept into position by both phenylalanines in a 'sandwich' configuration.

Dextromethorphan is believed to bind by electrostatic interactions between its basic nitrogen atom and the acidic residues E216 and D301 [16]. Recently, it has been shown that aromatic residue F120 also plays a role in dextromethorphan metabolism, since substitution of this residue resulted in the formation of two novel metabolites [18, 19]. The present study shows that residue F483 is also involved in metabolism of dextromethorphan. Wild-type CYP2D6 performed mainly *O*-demethylation of dextromethorphan, while F483A also formed substantial amounts of *N*-demethylated product. In addition, two extra metabolites were formed (Figure 4) that could not be detected in wild-type CYP2D6 incubations, but have been described previously for F120A mutant CYP2D6 [18, 19]. The K_s values of dextromethorphan were similar for wild-type and F483A mutant CYP2D6 (table 3), indicating that the binding affinity of dextromethorphan is not greatly affected by the mutation. The observed effects on the metabolic ratio may therefore result from the different orientations that can be adopted by the large, non-flat substrate dextromethorphan in the active site of F483A mutant CYP2D6, as a consequence of the increased available space.

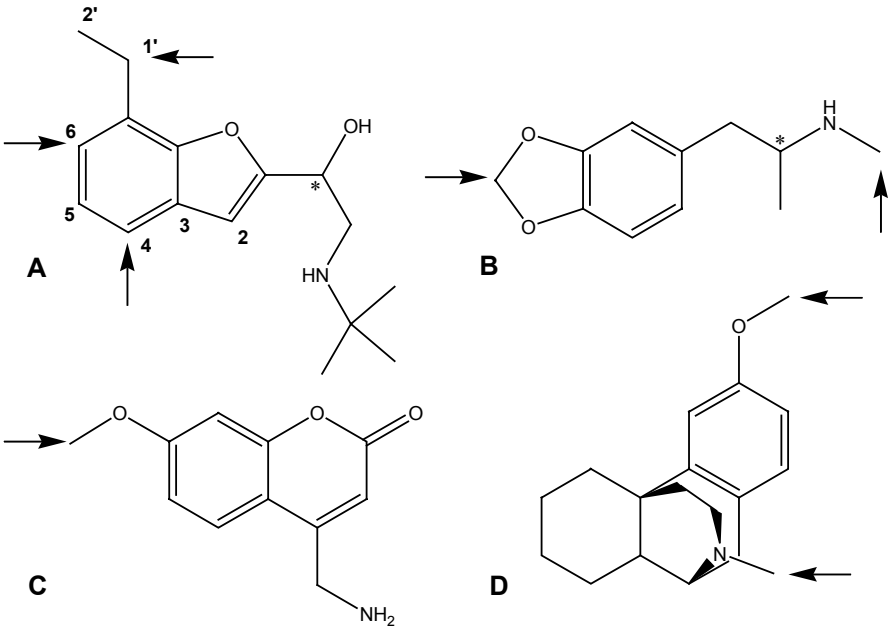

Figure 4. Structures of the used CYP2D6 substrates: (A) bufuralol, (B) MDMA, (C) MAMC, (D) dextromethorphan, Chiral atoms (*), and sites of oxidation by wild-type CYP2D6 are indicated (↑).

For bufuralol metabolism, the acidic residues E216 and D301 have been shown to be important because they are involved in the fixation of the basic nitrogen of bufuralol [15, 16, 33]. Mutagenesis of aromatic residue F120 to alanine, on the other hand, did not significantly affect the metabolism of this substrate [18]. In a previous mutagenesis study, it was found that the substitution of F483 by tryptophan or isoleucine also had no influence bufuralol 1'-hydroxylation [1]. In the present study, however, a significant effect on bufuralol metabolism was observed when F483 was replaced by the smaller alanine. This mutation resulted in a 32-fold lower V_{max} for bufuralol 1'-hydroxylation, while the K_m value was hardly affected. The binding affinity of bufuralol was not significantly influenced by the F483A mutation (Table 3). The fact that the more conservative substitutions of F483 by

tryptophan and isoleucine have no effect on bufuralol metabolism suggests that these amino acid residues can compensate for the loss of the phenylalanine-residue, by aromatic, hydrophobic, and/or steric interaction with bufuralol.
Previous studies with F120A mutant CYP2D6 showed that for this mutant, regioselectivity of MDMA metabolism had changed significantly. The amount of MDA produced by this mutant was greatly increased compared to wild-type CYP2D6. In addition, a novel metabolite was formed which could be identified as *N*-OH-MDMA [18]. In the present study it was shown that the effect of a F483A substitution on MDMA did not influence the metabolic ratio, but only the kinetic parameters of 3,4-OH-MA formation (Table 2). For the formation of the major metabolite 3,4-OH-MA, the K_m value of F483A mutant CYP2D6 was 13-fold higher than the wild-type value, while the V_{max} value decreased only two-fold (Table 2). The K_s value of MDMA was similar for the wild-type and F483A mutant CYP2D6 (Table 3). The fact that the K_m value and the K_s value do not follow the same trend is because K_m and K_s values represent qualitatively different processes. Whereas the K_s value merely reflects the spin shift upon binding of a substrate, the parameter K_m is also influenced by catalytic processes such as product release [35].
Residue F120 was shown to be important for MDMA metabolism, but not for bufuralol metabolism [18], while for F483A both bufuralol and MDMA metabolism are affected by the mutation. For bufuralol, only the V_{max} was altered, while for MDMA O-demethylenation mainly the K_m was influenced by the mutation. These results suggest that these two compounds have different modes of binding, despite their high degree of structural similarity.
In conclusion, the data presented in this study prove that F483 plays an important role in CYP2D6 selectivity and activity. Together with acidic residues E216 and D301 and aromatic residue F120, it defines the ligand binding properties and the regiospecificity of metabolism. However, of the at least 25 residues postulated to form the active site of CYP2D6, only eight have been subjected to experimental studies [36]. Therefore it is possible that in the near future additional residues will be identified that contribute to ligand binding and metabolism. For E216 and D301, it has been shown that they are important for the fixation of the basic nitrogen atom in ligands [14-16]. The strongly substrate dependent effects observed after mutagenesis of the aromatic residues F120 and F483 can be attributed either to the change in the active site topology upon removal of the phenylalanine residues, or can be due to loss of aromatic interaction points.

Acknowledgements
We thank Ed Groot for his help with the expression and purification of wild-type and F483A mutant CYP2D6.

References

1. Smith G, Modi S, Pillai I, Lian LY, Sutcliffe MJ, Pritchard MP, Friedberg T, Roberts GC and Wolf CR, Determinants of the substrate specificity of human cytochrome P-450 CYP2D6: design and construction of a mutant with testosterone hydroxylase activity. *Biochem J* **331:** 783-92, 1998.
2. Evans WE and Relling MV, Pharmacogenomics: translating functional genomics into rational therapeutics. *Science* **286:** 487-91, 1999.
3. Mansuy D, The great diversity of reactions catalyzed by cytochromes P450. *Comp Biochem Physiol C Pharmacol Toxicol Endocrinol* **121:** 5-14, 1998.
4. Goeptar AR, Scheerens H and Vermeulen NPE, Oxygen and xenobiotic reductase activities of cytochrome P450. *Crit Rev Toxicol* **25:** 25-65, 1995.

5. Zanger UM, Raimundo S and Eichelbaum M, Cytochrome P450 2D6: overview and update on pharmacology, genetics, biochemistry. *Naunyn Schmiedebergs Arch Pharmacol* **369:** 23-37, 2004.
6. Anzenbacher P and Anzenbacherova E, Cytochromes P450 and metabolism of xenobiotics. *Cell Mol Life Sci* **58:** 737-47, 2001.
7. Ingelman-Sundberg M, Pharmacogenetics of cytochrome P450 and its applications in drug therapy: the past, present and future. *Trends Pharmacol Sci* **25:** 193-200, 2004.
8. Oscarson M, Pharmacogenetics of drug metabolising enzymes: importance for personalised medicine. *Clin Chem Lab Med* **41:** 573-80, 2003.
9. Ingelman-Sundberg M, Oscarson M and McLellan RA, Polymorphic human cytochrome P450 enzymes: an opportunity for individualized drug treatment. *Trends Pharmacol Sci* **20:** 342-9, 1999.
10. Wormhoudt LW, Commandeur JNM and Vermeulen NPE, Genetic polymorphisms of human N-acetyltransferase, cytochrome P450, glutathione-S-transferase, and epoxide hydrolase enzymes: relevance to xenobiotic metabolism and toxicity. *Crit Rev Toxicol* **29:** 59-124, 1999.
11. Ekins S, de Groot MJ and Jones JP, Pharmacophore and three-dimensional quantitative structure activity relationship methods for modeling cytochrome p450 active sites. *Drug Metab Dispos* **29:** 936-44, 2001.
12. Vermeulen NPE, Prediction of drug metabolism: the case of cytochrome P450 2D6. *Curr Top Med Chem* **3:** 1227-39, 2003.
13. Koymans L, Vermeulen NPE, van Acker SA, te Koppele JM, Heykants JJ, Lavrijsen K, Meuldermans W and Donne-Op den Kelder GM, A predictive model for substrates of cytochrome P450-debrisoquine (2D6). *Chem Res Toxicol* **5:** 211-9, 1992.
14. Ellis SW, Hayhurst GP, Smith G, Lightfoot T, Wong MM, Simula AP, Ackland MJ, Sternberg MJ, Lennard MS and Tucker GT, Evidence that aspartic acid 301 is a critical substrate-contact residue in the active site of cytochrome P450 2D6. *J Biol Chem* **270:** 29055-8, 1995.
15. Guengerich FP, Hanna IH, Martin MV and Gillam EM, Role of glutamic acid 216 in cytochrome P450 2D6 substrate binding and catalysis. *Biochemistry* **42:** 1245-53, 2003.
16. Paine MJ, McLaughlin LA, Flanagan JU, Kemp CA, Sutcliffe MJ, Roberts GC and Wolf CR, Residues glutamate 216 and aspartate 301 are key determinants of substrate specificity and product regioselectivity in cytochrome P450 2D6. *J Biol Chem* **278:** 4021-7, 2003.
17. Hayhurst GP, Harlow J, Chowdry J, Gross E, Hilton E, Lennard MS, Tucker GT and Ellis SW, Influence of phenylalanine-481 substitutions on the catalytic activity of cytochrome P450 2D6. *Biochem J* **355:** 373-9, 2001.
18. Keizers PHJ, Lussenburg BMA, de Graaf C, Mentink LM, Vermeulen NPE and Commandeur JNM, Influence of phenylalanine 120 on cytochrome P450 2D6 catalytic selectivity and regiospecificity: crucial role in 7-methoxy-4-(aminomethyl)-coumarin metabolism. *Biochem Pharmacol* **68:** 2263-2271, 2004.
19. Flanagan JU, Marechal JD, Ward R, Kemp CA, McLaughlin LA, Sutcliffe MJ, Roberts GC, Paine MJ and Wolf CR, Phe120 contributes to the regiospecificity of cytochrome P450 2D6: mutation leads to the formation of a novel dextromethorphan metabolite. *Biochem J* **380:** 353-60, 2004.
20. Ellis SW, Rowland K, Ackland MJ, Rekka E, Simula AP, Lennard MS, Wolf CR and Tucker GT, Influence of amino acid residue 374 of cytochrome P-450 2D6 (CYP2D6) on the regio- and enantio-selective metabolism of metoprolol. *Biochem J* **316 (Pt 2):** 647-54, 1996.
21. de Groot MJ, Ackland MJ, Horne VA, Alex AA and Jones BC, A novel approach to predicting P450 mediated drug metabolism. CYP2D6 catalyzed N-dealkylation reactions and qualitative metabolite predictions using a combined protein and pharmacophore model for CYP2D6. *J Med Chem* **42:** 4062-4070, 1999.
22. Venhorst J, ter Laak AM, Commandeur JNM, Funae Y, Hiroi T and Vermeulen NPE, Homology modeling of rat and human cytochrome P450 2D (CYP2D) isoforms and computational rationalization of experimental ligand-binding specificities. *J Med Chem* **46:** 74-86, 2003.
23. Kirton SB, Kemp CA, Tomkinson NP, St-Gallay S and Sutcliffe MJ, Impact of incorporating the 2C5 crystal structure into comparative models of cytochrome P450 2D6. *Proteins* **49:** 216-31, 2002.

24. Kemp CA, Flanagan JU, van Eldik AJ, Marechal JD, Wolf CR, Roberts GC, Paine MJ and Sutcliffe MJ, Validation of model of cytochrome P450 2D6: an in silico tool for predicting metabolism and inhibition. *J Med Chem* **47:** 5340-6, 2004.
25. Onderwater RC, Venhorst J, Commandeur JNM and Vermeulen NPE, Design, synthesis, and characterization of 7-methoxy-4-(aminomethyl)coumarin as a novel and selective cytochrome P450 2D6 substrate suitable for high-throughput screening. *Chem Res Toxicol* **12:** 555-9, 1999.
26. Braun U, Shulgin AT and Braun G, Centrally active N-substituted analogs of 3,4-methylenedioxyphenylisopropylamine (3,4-methylenedioxyamphetamine). *J Pharm Sci* **69:** 192-5, 1980.
27. Weinander R, Mosialou E, DeJong J, Tu CP, Dypbukt J, Bergman T, Barnes HJ, Hoog JO and Morgenstern R, Heterologous expression of rat liver microsomal glutathione transferase in simian COS cells and Escherichia coli. *Biochem J* **311 (Pt 3):** 861-6, 1995.
28. Bauer S and Shiloach J, Maximal exponential growth rate and yield of E. coli obtainable in a bench-scale fermentor. *Biotechnol Bioeng* **16:** 933-41, 1974.
29. Omura T and Sato R, The carbon monoxide-binding pigment of liver microsomes. II. Solubilization, purification, and properties. *J Biol Chem* **239:** 2379-85, 1964.
30. Kranendonk M, Fisher CW, Roda R, Carreira F, Theisen P, Laires A, Rueff J, Vermeulen NPE and Estabrook RW, Escherichia coli MTC, a NADPH cytochrome P450 reductase competent mutagenicity tester strain for the expression of human cytochrome P450: comparison of three types of expression systems. *Mutat Res* **439:** 287-300, 1999.
31. Yamazaki H, Nakamura M, Komatsu T, Ohyama K, Hatanaka N, Asahi S, Shimada N, Guengerich FP, Shimada T, Nakajima M and Yokoi T, Roles of NADPH-P450 reductase and apo- and holo-cytochrome b5 on xenobiotic oxidations catalyzed by 12 recombinant human cytochrome P450s expressed in membranes of Escherichia coli. *Protein Expr Purif* **24:** 329-37, 2002.
32. Venhorst J, Onderwater RC, Meerman JH, Vermeulen NPE and Commandeur JNM, Evaluation of a novel high-throughput assay for cytochrome P450 2D6 using 7-methoxy-4-(aminomethyl)-coumarin. *Eur J Pharm Sci* **12:** 151-8, 2000.
33. Hanna IH, Krauser JA, Cai H, Kim MS and Guengerich FP, Diversity in mechanisms of substrate oxidation by cytochrome P450 2D6. Lack of an allosteric role of NADPH-cytochrome P450 reductase in catalytic regioselectivity. *J Biol Chem* **276:** 39553-61, 2001.
34. Lin LY, Di Stefano EW, Schmitz DA, Hsu L, Ellis SW, Lennard MS, Tucker GT and Cho AK, Oxidation of methamphetamine and methylenedioxymethamphetamine by CYP2D6. *Drug Metab Dispos* **25:** 1059-64, 1997.
35. Guengerich FP, Miller GP, Hanna IH, Sato H and Martin MV, Oxidation of methoxyphenethylamines by cytochrome P450 2D6. Analysis of rate-limiting steps. *J Biol Chem* **277:** 33711-9, 2002.
36. Guengerich F, Human Cytochrome P450 Enzymes. In: *Cytochrome P450: structure, mechanism, and biochemistry* (Ed. Montellano POd), pp. 417. Kluwer Academic/Plenum Publishers, New York, 2005.

Chapter 4

Metabolism of N-substituted 7-methoxy-4-(aminomethyl)-coumarins by cytochrome P450 2D6 mutants indicates additional substrate interaction points

Peter H.J. Keizers, Ben R. van Dijk, Chris de Graaf, Barbara M.A. van Vugt-Lussenburg, Nico P.E. Vermeulen, and Jan N.M. Commandeur

adapted from: Xenobiotica 2006 in press

Previous studies have shown the critical roles residues F120 and F483 play in the oxidative metabolism of 7-methoxy-4-(aminomethyl)-coumarin by cytochrome P450 2D6 (CYP2D6). In this study, a series of *N*-alkyl-7-methoxy-4-(aminomethyl)-coumarins (MAMC-analogs) were used as substrates for the F120A and F483A mutants in order to further probe the active site of CYP2D6. The F120A and F483A mutants of CYP2D6 displayed significant activity towards the MAMC-analogs. Automated docking studies of the MAMC-analogs in a CYP2D6 homology model suggested a distal hydrophobic active site binding cleft for the substrate *N*-alkyl chains, consisting of the residues L213 and V308.

Introduction

One of the most important drug metabolizing phase I enzymes in humans is cytochrome P450 2D6 (CYP2D6). Although CYP2D6 accounts for just 3% of all hepatic CYP, it is involved in the metabolism of about 30% of currently marketed drugs, and it is well known for its genetic polymorphisms [1]. Structural information on the active site of this enzyme is beneficial for rational drug development [2].

Two active site acidic residues, D301 and E216, have been suggested in computational studies to be involved in fixation of the basic nitrogen-atom that is present in most CYP2D6 substrates [3]. The importance of both residues for CYP2D6 activity was confirmed by site-directed mutagenesis studies [4, 5]. In modeling studies, D301 appeared to be involved in stabilizing the B/C-loop containing F120, rather than binding the substrate [6]. Site-directed mutation studies on F120 itself indicated that this residue indeed determines catalytic selectivity and regioselectivity in CYP2D6 [7, 8]. In addition, F483 was shown to be an important residue in metabolism by CYP2D6 [9]. It was suggested that F120 and F483 anchor the substrates, which are typically aromatic compounds [3], by aromatic interactions and π-stacking. Typically, 7-methoxy-4-(aminomethyl)-coumarin (MAMC) was not metabolized by the F120A mutant, nor by the F483A mutant, although both mutants did metabolize other model CYP2D6 substrates [8, 9]. Apparently, both phenylalanine residues are crucial in facilitating MAMC in a reactive conformation in the CYP2D6 active site.

Previously, a series of MAMC-analogs was evaluated as alternative substrates for CYP2D6 [10]. It was found that by increasing the *N*-alkyl chain length, the affinity for the enzyme increased substantially, suggesting that additional interaction points play a role in binding of the longer *N*-alkyl chain substrates. In the current study, we have examined the oxidative metabolism of this series of MAMC-analogs by the F120A, F483A and D301Q mutants of CYP2D6, in order to verify the existence of distal interaction points. Automated docking of the MAMC-analogs into the CYP2D6 homology model [11], was employed to rationalize the experimental findings and to allocate the distal active site residues involved in substrate interaction.

Materials and Methods

Materials

The pSP19T7LT plasmid containing the cDNAs of human cytochrome P450 2D6 with a C- terminal His_6-tag and human NADPH-cytochrome P450 reductase in tandem was used as described before [9]. *N*-alkyl-7-methoxy-4-(aminomethyl)-coumarins and *N*-alkyl-7-hydroxy-4-(aminomethyl)-coumarins (Figure 1) were synthesized before as described [10, 12] and were higher than 98% chemically pure.

Enzyme production

The D301Q mutation was introduced into pSP19T7LT using the QuickChange XL Site-Directed Mutagenesis kit (Stratagene, La Jolla CA). The sequences of the forward- and reverse oligonucleotides respectively, with the mutated residue in *italic*, were as follows: 5'-ATA GTG GTG GCT *CAG* CTG TTC TCT GCC GG-3' and 5'-CC GGC AGA GAA CAG *CTG* AGC CAC CAC TAT-3'. After mutagenesis, the presence of the mutation was confirmed by DNA sequencing. The F483A and F120A mutants were obtained as previously described [8, 9]. The mutants and wild-type CYP2D6 containing pSP19T7LT plasmids were transformed into *Escherichia coli* strain JM109. Expression and membrane isolation was carried out as previously described [8]. Membranes were resuspended in 0.5% of the original culture volume in a 50 mM potassium phosphate buffer, pH 7.4, containing 10% glycerol, 1 mM EDTA and 1 mM DTT, and P450 contents were determined by CO difference spectra [13]. The expression levels of the D301Q mutant were approximately 200 nM, similar to those of wild-type CYP2D6.

Analysis of oxidative metabolism

O-demethylation of ten concentrations ranging from 0 to 200 μM MAMC and analogs by CYP2D6 was analyzed by plate reader technology as previously described [8], using the synthesized references for quantification. *N*-dealkylation was determined by HPLC. For this, enzyme reactions were carried out in 200 μl potassium phosphate buffer, containing 5 mM $MgCl_2$, supplemented with 10 concentrations ranging from 0 to 200 μM of the MAMC-analogs and *E. coli* membranes corresponding to 40 nM CYP2D6. After 5 min of pre-incubation at 37 °C, the reactions were initiated with an NADPH regenerating system [8]. The reactions were allowed to proceed for 20 min before they were quenched by the addition of 20 μl 23% $HClO_4$. After centrifugation (10 min, 6800 g), 30 μl aliquots of the supernatant were analyzed using a C18 column (Phenomenex Inertsil ODS 150 x 4.6 mm) with a flow rate of 0.6 ml/min. Incubation components were eluted by a linear gradient from 5% acetonitrile in 20 mM ammonium acetate, to 90% acetonitrile in 10 mM ammonium acetate. The products were detected by fluorescence (λ_{ex}= 360 nm, λ_{em}= 460 nm) and identified and quantified using the synthetic references. Metabolite peak areas were quantified using Shimadzu Class VP 4.3. Kinetic parameters were analyzed using non-linear regression in Graph Pad Prism 3.0 (Graph Pad Software Inc. San Diego CA).

Molecular Modeling

A protein homology model of CYP2D6 was constructed, refined and validated as described before [11]. MAMC and analogs were automatically docked in the CYP2D6 homology model, according to the method that was previously found optimal in predicting sites of oxidation of substrates in CYP2D6 [14]. In short, preparation of protein and substrate input structures, defining the binding pocket, and the GRID-based prediction of energetically favorable positions of active site water molecules was performed as previously described [15]. A total of fifty docking poses were generated per substrate using the program GOLD-Chemscore [16], and rescored using the scoring function SCORE [17].

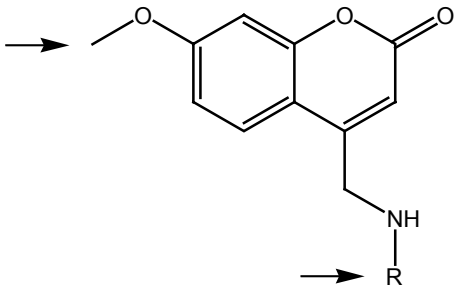

Compound	R
MAMC	H
MMAMC	CH_3
EMAMC	C_2H_5
PMAMC	C_3H_7
BMAMC	C_4H_9

Figure 1: Structure and names of the N-alkyl-7-methoxy-4-(aminomethyl)-coumarins. Sites of oxidation are indicated (→).

Results and discussion

The plate reader and HPLC analyses of the enzyme incubations with the MAMC-analogs (Figure 1) showed that the *O*-demethylated and *N*-dealkylated products were formed linearly for at least 30 minutes. Quantification of *O*-demethylation by HPLC led to similar results as quantification by plate reader analysis.

Wild-type CYP2D6 efficiently *O*-demethylated MAMC and its analogs (Table 1), with K_m-values decreasing with *N*-alkyl chain length, consistent with previous observations [10]. The F120A mutant of CYP2D6, which did not metabolize MAMC at all, as described previously [8], *O*-demethylated all the MAMC-analogs having an alkyl-group on the 4-aminomethyl position. Similarly to the wild-type enzyme, the F120A mutant displayed a decreasing K_m with increasing *N*-alkyl chain length. The V_{max}-values however, were in all occasions far lower than those of the wild-type and were found to substantially increase with *N*-alkyl chain length.

Table 1: O-demethylation (A) and N-dealkylation (B) reactions of MAMC-analogs by CYP2D6.

A *O*-demethylation

Substrate	Wild-type		F120A		F483A		D301Q	
	K_m	V_{max}	K_m	V_{max}	K_m	V_{max}	K_m	V_{max}
MAMC	37 ± 1	6.8 ± 0.5	- [a]	<0.04	- [a]	<0.04	86 ± 7	1.8 ± 0.2
MMAMC	8.6 ± 0.8	3.4 ± 0.7	16 ± 2	0.04 ± 0.01	- [a]	<0.04	110 ± 26	0.13 ± 0.03
EMAMC	3.3 ± 0.6	1.6 ± 0.3	13 ± 1	0.04 ± 0.01	19.4 ± 0.2	0.10 ± 0.02	>200	- [b]
PMAMC	1.2 ± 0.2	2.6 ± 0.3	8.5 ± 0.1	0.8 ± 0.1	10 ± 2	1.7 ± 0.1	63 ± 6	3.7 ± 0.4
BMAMC	1.45 ± 0.01	7.5 ± 1.5	4.7 ± 0.5	1.5 ± 0.1	5.8 ± 0.1	1.9 ± 0.5	23.8 ± 0.6	15 ± 4

B *N*-dealkylation

Substrate	Wild-type		F120A		F483A		D301Q	
	K_m	V_{max}	K_m	V_{max}	K_m	V_{max}	K_m	V_{max}
MMAMC	18.9 ± 0.2	0.072 ± 0.003	>300	- [a]	166 ± 40	0.2 ± 0.1	114 ± 10	2.4 ± 0.5
EMAMC	12 ± 1	0.6 ± 0.1	54 ± 6	1.8 ± 0.3	107 ± 6	0.8 ± 0.2	191 ± 24	24 ± 6
PMAMC	60 ± 14	0.31 ± 0.01	10.1 ± 0.4	1.48 ± 0.02	125 ± 33	0.54 ± 0.02	75 ± 3	4.5 ± 0.3
BMAMC	- [a]	<0.1	5 ± 1	0.78 ± 0.03	157 ± 18	0.3 ± 0.1	15 ± 3	0.45 ± 0.01

All values are the means ± S.D. of at least three independent experiments as described in the Methods section. K_m expressed in μM, V_{max} expressed in pmol product/min/pmol CYP2D6, [a] not detected, [b] detected, not quantified.

The F483A mutant of CYP2D6 also did not metabolize MAMC, as described previously [9]. Furthermore, *O*-demethylation of MMAMC was not observed. *O*-demethylation activities towards the longer chain MAMC-analogs were similar to that by the F120A mutant. Like in the wild-type enzyme, the catalytic efficiency of the F120A and F483A mutants towards the MAMC-analogs increased with the length of the *N*-alkyl chain (Figure 2), suggesting that distal active site residues are involved in substrate binding. To identify these residues, the optimal binding configurations of the MAMC-analogs in CYP2D6 were examined by automated docking in the homology model.

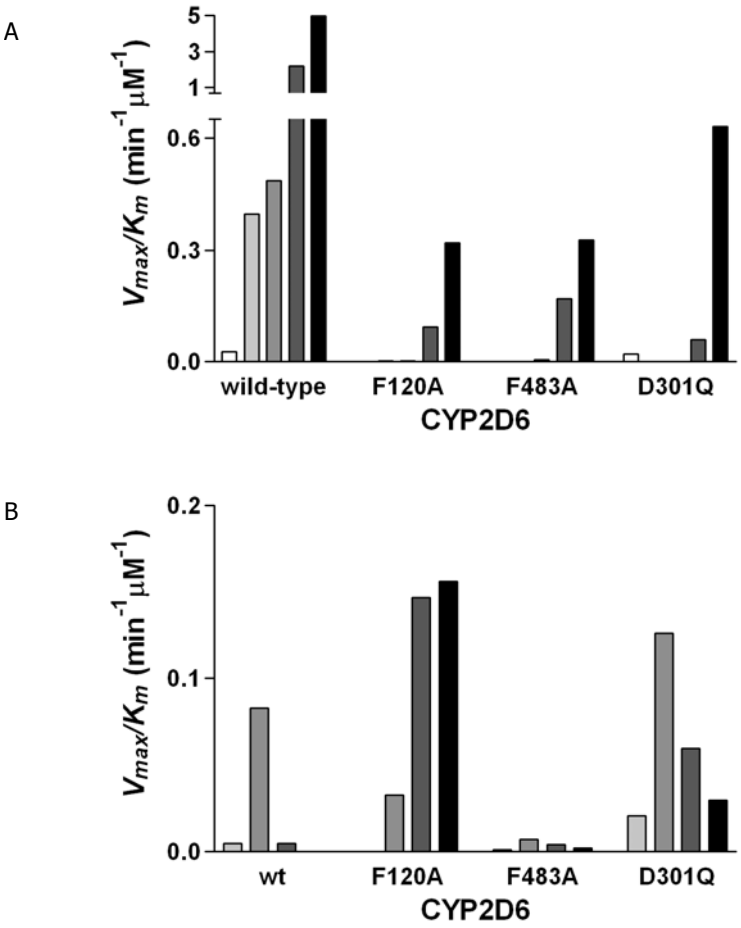

Figure 2: Catalytic efficiencies (V_{max}/K_m) of the wild-type, the F120A, the F483A, and the D301Q mutant of CYP2D6 towards the substrates MAMC, MMAMC, EMAMC, PMAMC and BMAMC (blank, light gray, gray, dark gray and black bars respectively), as described in the Methods section. O-demethylation reactions are depicted in A, N-dealkylation in B. Data represent the average of three determinations

The highest scoring binding modes of MAMC, MMAMC and BMAMC are shown in Figure 3, and the optimal orientations of the coumarin ring systems of EMAMC and PMAMC were very similar to those of MMAMC and BMAMC. The close contacts between MAMC-analogs and

specific CYP2D6 active site residues are summarized in Table 3. MAMC and the analogs have approximately the same binding mode, corresponding to *O*-demethylation, and providing electrostatic interactions between their nitrogen atoms and the E216 carboxylate. With the exception of MAMC, F120 provides π-stacking interactions to the substrates aromatic moiety. An additional difference between the binding modes of the five substrates concerns the conformation of the *N*-alkyl chain. BMAMC and to a lesser extend PMAMC, accommodate their relatively long *N*-alkyl chains in a cleft formed by the apolar sidechains of residues L213, V308, and F483, at the top of the binding pocket, providing additional hydrophobic interactions with the CYP2D6 active site. Very recently, a crystal structure of CYP2D6 was reported [18]. This structure shows high similarity with our homology model, placing F120, F483, D301 and L213 in approximately identical positions, therefore confirming the model, and supporting the findings in the present study.
From the series of MAMC-analogs, MAMC is *O*-demethylated with far the lowest catalytic efficiency by wild-type CYP2D6 (Figure 2). In the automated docking studies, MAMC was found to have an optimal binding conformation different from its analogs. The conformation of the MAMC-analogs, stacked to F120, is apparently beneficial for activity. This could explain why MAMC is a worse substrate than its analogs and also why mutation of F120 to an alanine leads to an enzyme incapable of metabolizing MAMC. Mutating F483 to an alanine might lead to binding of MAMC even further away from the heme, because F483 was found to interact with MAMC by hydrophobic contacts (Table 2). The fact that the F483A mutant does not metabolize MAMC supports this hypothesis.

Table 2: Ionic and hydrophobic interactions between the MAMC-analogs and CYP2D6 active site residues.

Residue	Interaction[a]	SRS [b]	Substrate [c]				
			MAMC	MMAMC	EMAMC	PMAMC	BMAMC
F120	Hydrophobic	1	-	+	+	+	+
L213	Hydrophobic	2	+	-	-	+	+
E216	Ionic	2	+	+	+	+	+
V308	Hydrophobic	4	+	-	-	+	+
V374	Hydrophobic	5	-	+	+	-	+
F483	Hydrophobic	6	+	-	+	+	+

[a] Hydrophobic substrate-protein interactions are defined as the occurrence of at least three close contacts (within 4 Å) between the carbon atoms of the substrate and the (aromatic or aliphatic) carbon atoms of the side chain of a specific amino acid residue. Ionic interactions are defined as at least one close contact (within 3.5 Å) between charged groups in the substrate and charged groups in the amino acid residue. [b] Substrate recognition site (SRS) as defined for the CYP2 family members [19]. [c] + indicates interaction, - indicates no interaction.

It has been hypothesized that F120 and F483 function in concert to maintain substrates in place by hydrophobic interactions and π-stacking, more or less sandwiching the substrate into a reactive conformation [20, 21]. In the current study, similar trends in catalytic efficiency of *O*-demethylation of the MAMC-analogs were observed for the F120A and F483A mutants of CYP2D6, which could suggest a similar role for the two residues. The *N*-dealkylation of the substrates however, was much more significant with the F120A mutant than with the F483A mutant (Table 1, Figure 2). Hence the F120A mutant appears to allow more for variable orientations of the MAMC-analogs than the F483A mutant does. By automated docking of the MAMC-analogs different roles of the two phenylalanine residues could be distinguished; F120 appeared to be more involved in aromatic interaction, whereas F483 more sterically influenced substrate binding (Table 2 and Figure 3).

The D301Q mutant of CYP2D6 displayed the same trend in catalytic efficiency of *O*-demethylation of the MAMC-analogs as the F120A mutant. Furthermore, mutation of D301 also led to a significant increase in *N*-dealkylation of the MAMC-analogs. The correlation between the effects of mutation of F120 and D301 is consistent with the proposed role of D301 in positioning F120 [5, 6]. The differences in reactivity towards the MAMC-analogs that were observed for the two mutants may be explained by the nature of the different mutations, affecting in one case the removal, and in the other case redirection of the phenyl moiety of residue 120, combined with the removal of part of the active site negative charge [6].

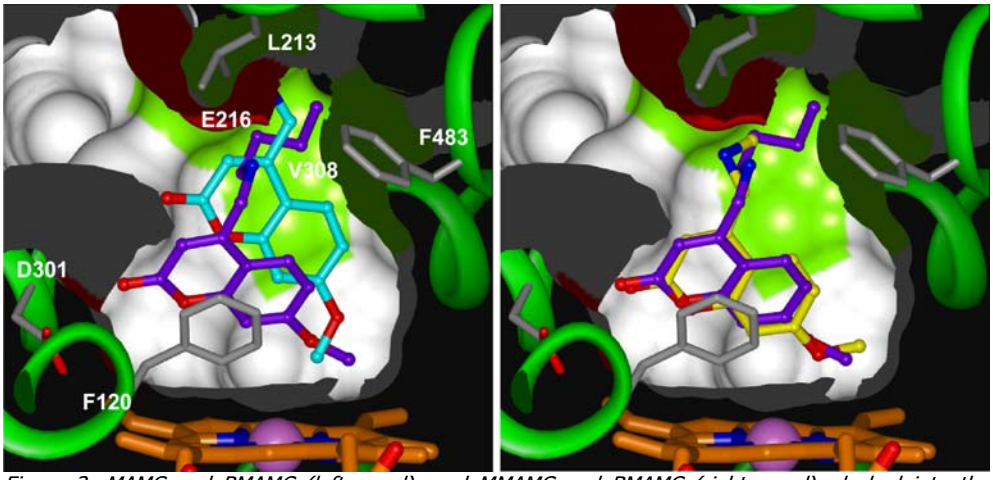

Figure 3: MAMC and BMAMC (left panel), and MMAMC and BMAMC (right panel), docked into the CYP2D6 homology model as described in the Methods section. The molecular Connoly surface of the active site of CYP2D6 is depicted; the surfaces of carboxyl oxygen atoms of D301 and E216, and the apolar sidechain atoms of L213, V308, and F483 are shown. Amino acid side chains involved in substrate binding are shown as sticks. For reasons of clarity, only the locations of E216 and V308 are indicated. A colored version of the figure is shown in the Appendix of this thesis.

In conclusion, the addition and elongation of an *N*-alkyl chain in the MAMC-analogs restored the ability of the F120A and F483A mutants of CYP2D6 to catalyze MAMC. Based upon automated docking studies a distal hydrophobic active site binding cleft for the *N*-alkyl chains is suggested, consisting of L213 and V308, which appear to be as important for activity as the two phenylalanine residues.

Acknowledgements
We thank Ed Groot for technical assistance.

References

1. Zanger UM, Raimundo S and Eichelbaum M, Cytochrome P450 2D6: overview and update on pharmacology, genetics, biochemistry. *Naunyn Schmiedebergs Arch Pharmacol* **369:** 23-37, 2004.
2. Vermeulen NPE, Prediction of drug metabolism: the case of cytochrome P450 2D6. *Curr Top Med Chem* **3:** 1227-39, 2003.
3. de Groot MJ, Bijloo GJ, Martens BJ, van Acker FA and Vermeulen NP, A refined substrate model for human cytochrome P450 2D6. *Chem Res Toxicol* **10:** 41-8, 1997.

4. Paine MJ, McLaughlin LA, Flanagan JU, Kemp CA, Sutcliffe MJ, Roberts GC and Wolf CR, Residues glutamate 216 and aspartate 301 are key determinants of substrate specificity and product regioselectivity in cytochrome P450 2D6. *J Biol Chem* **278:** 4021-7, 2003.
5. Guengerich FP, Hanna IH, Martin MV and Gillam EM, Role of glutamic acid 216 in cytochrome P450 2D6 substrate binding and catalysis. *Biochemistry* **42:** 1245-53, 2003.
6. Venhorst J, ter Laak AM, Commandeur JNM, Funae Y, Hiroi T and Vermeulen NPE, Homology modeling of rat and human cytochrome P450 2D (CYP2D) isoforms and computational rationalization of experimental ligand-binding specificities. *J Med Chem* **46:** 74-86, 2003.
7. Flanagan JU, Marechal JD, Ward R, Kemp CA, McLaughlin LA, Sutcliffe MJ, Roberts GC, Paine MJ and Wolf CR, Phe120 contributes to the regiospecificity of cytochrome P450 2D6: mutation leads to the formation of a novel dextromethorphan metabolite. *Biochem J* **380:** 353-60, 2004.
8. Keizers PHJ, Lussenburg BMA, de Graaf C, Mentink LM, Vermeulen NPE and Commandeur JNM, Influence of phenylalanine 120 on cytochrome P450 2D6 catalytic selectivity and regiospecificity: crucial role in 7-methoxy-4-(aminomethyl)-coumarin metabolism. *Biochem Pharmacol* **68:** 2263-2271, 2004.
9. Lussenburg BMA, Keizers PHJ, de Graaf C, Hidestrand M, Ingelman-Sundberg M, Vermeulen NPE and Commandeur JNM, The role of phenylalanine 483 in cytochrome P450 2D6 is strongly substrate dependent. *Biochem Pharmacol* **70:** 1253-61, 2005.
10. Venhorst J, Onderwater RC, Meerman JH, Commandeur JNM and Vermeulen NPE, Influence of N-substitution of 7-methoxy-4-(aminomethyl)-coumarin on cytochrome P450 metabolism and selectivity. *Drug Metab Dispos* **28:** 1524-32, 2000.
11. Keizers PHJ, de Graaf C, de Kanter FJJ, Oostenbrink C, Feenstra KA, Commandeur JNM and Vermeulen NPE, Metabolic regio- and stereoselectivity of cytochrome P450 2D6 towards 3,4-methylenedioxy-N-alkyl-amphetamines: in silico predictions and experimental validation. *J Med Chem* **48:** 6117-6127, 2005.
12. Onderwater RC, Venhorst J, Commandeur JNM and Vermeulen NPE, Design, synthesis, and characterization of 7-methoxy-4-(aminomethyl)coumarin as a novel and selective cytochrome P450 2D6 substrate suitable for high-throughput screening. *Chem Res Toxicol* **12:** 555-9, 1999.
13. Omura T and Sato R, The carbon monoxide-binding pigment of liver microsomes. I. Evidence for its hemoprotein nature. *J Biol Chem* **239:** 2370-8, 1964.
14. de Graaf C, Oostenbrink C, Keizers PHJ, van der Wijst T, Jongejan A and Vermeulen NPE, Catalytic site prediction and virtual screening of cytochrome P450 2D6 substrates by consideration of water and rescoring in automated docking. *J Med Chem* **49:** 2417-2430, 2006.
15. de Graaf C, Pospisil P, Pos W, Folkers G and Vermeulen NPE, Binding mode prediction of cytochrome P450 and thymidine kinase protein-ligand complexes by consideration of water and rescoring in automated docking. *J Med Chem* **7:** 2308-2318, 2005.
16. Verdonk ML, Cole JC, Hartshorn MJ, Murray CW and Taylor RD, Improved protein-ligand docking using Gold. *Proteins* **52:** 609-23, 2003.
17. Wang RX, Liu L, Lai LH and Tang YQ, SCORE: A new empirical method for estimating the binding affinity of a protein-ligand complex. *J Mol Model* **4:** 379-394, 1998.
18. Rowland P, Blaney FE, Smyth MG, Jones JJ, Leydon VR, Oxbrow AK, Lewis CJ, Tennant MG, Modi S, Eggleston DS, Chenery RJ and Bridges AM, Crystal structure of human cytochrome P450 2D6. *J Biol Chem* **in press**, 2005.
19. Gotoh O, Substrate recognition sites in cytochrome P450 family 2 (CYP2) proteins inferred from comparative analyses of amino acid and coding nucleotide sequences. *J Biol Chem* **267:** 83-90, 1992.
20. Kemp CA, Flanagan JU, van Eldik AJ, Marechal JD, Wolf CR, Roberts GC, Paine MJ and Sutcliffe MJ, Validation of model of cytochrome P450 2D6: an in silico tool for predicting metabolism and inhibition. *J Med Chem* **47:** 5340-6, 2004.
21. Vaz RJ, Nayeem A, Santone K, Chandrasena G and Gavai AV, A 3D-QSAR model for CYP2D6 inhibition in the aryloxypropanolamine series. *Bioorg Med Chem Lett* **15:** 3816-20, 2005.

Chapter 5

Role of the conserved threonine 309 in mechanism of oxidation by cytochrome P450 2D6

Peter H.J. Keizers, Loek H.M. Schraven, Chris de Graaf, Mats Hidestrand, Magnus Ingelman-Sundberg, Ben R. van Dijk, Nico P.E. Vermeulen, and Jan N. M. Commandeur

adapted from: Biochemical and Biophysical Research Communications 2005 **338**: 1065-74

Based on sequence alignments and homology modeling, threonine 309 in cytochrome P450 2D6 (CYP2D6) is proposed to be the conserved I-helix threonine, which is supposed to be involved in dioxygen activation by CYPs. The T309V mutant of CYP2D6 displayed a strong shift from *O*-dealkylation to *N*-dealkylation reactions in oxidation of dextromethorphan and 3,4-methylenedioxymethylamphetamine (MDMA). This may be explained by an elevated ratio of hydroperoxo-iron to oxenoid-iron of the oxygenating species. In consistence, using cumene hydroperoxide, which directly forms the oxenoid-iron, the T309V mutant again selectively catalysed the *O*-dealkylation reactions. The changed ratio of oxygenating species can also explain the decreased activity and changed regioselectivity that was observed in 7-methoxy-4-(aminomethyl)-coumarin (MAMC) and bufuralol oxidation respectively by the T309V mutant. Interestingly, the T309V mutant always showed a significantly increased, up to 75-fold, higher activity compared to the wild-type when using cumene hydroperoxide. These results indicate that T309 in CYP2D6 is involved in maintaining the balance of multiple oxygenating species and thus influences substrate and regioselectivity.

Introduction

Cytochromes P450 (CYPs) are enzymes responsible for the oxidative biotransformation of a large variety of endogenous and exogenous substrates, like steroids, carcinogens and also drugs, and can be found in virtually all organisms [1]. In humans, one of the most important CYPs is CYP2D6. This hepatic drug metabolizing enzyme is involved in the phase I metabolism of about 30% of the currently marketed drugs, including neuroleptics, antidepressants, β-blockers, opioids and antiarythmics [2]. The enzyme is known for its genetic polymorphisms and gene multiplicities, even increasing its clinical relevance [3]. Clearly there is a need for structural data on this enzyme, to understand and predict the oxidative metabolism of known and new (drug-like) compounds [4-6].

So far, little is known about amino acid residues involved in the mechanism of oxygen activation by CYP2D6. In several other CYPs a highly conserved threonine residue in the I-helix was experimentally shown to have a role in fixation and activation of the heme bound oxygen [7-9]. In CYP101 (*cam*), the heme bound oxygen is activated by proton delivery mediated by threonine 252 and aspartic acid 251. The latter is forming hydrogen bonds to charged residues at the surface, thereby serving as a bridge between solvent trapped in the groove of the I-helix and bulk solvent [10]. The threonine 252 hydroxyl group subsequently forms a hydrogen bond to a catalytic water molecule which is the ultimate proton donor [11, 12]. In CYP102 (*BM3*), a similar proton delivery system is proposed via threonine 268, glutamic acid 267, and a catalytic water molecule [13, 14]. It is suggested that in both CYP101 and CYP102, dioxygen to heme binding triggers conformational changes in the I-helix, controlled by the highly conserved threonine residue and its neighboring acidic residue, which together enable the transport of a catalytic water molecule into the active site [12, 14]. In CYP107A (*EryF*), which is lacking the conserved threonine, the natural substrate 6-deoxyerythronolide itself is involved in proton delivery by forming a hydrogen bond with the catalytic water molecule [15], or directly with the oxygen [16], and in CYP55A (*nor*), which does not have the conserved acidic residue in close proximity to the threonine, an alternate proton delivery pathway has been proposed [17]. Obviously, the role of threonine residues can vary between the CYP isoenzymes [13].

The overall amino acid sequence and structure of the I-helix is highly conserved among CYPs in general and the mammalian CYP2 family more specifically [18, 19]. The crystal structures of CYPs 2B4, 2C5, 2C8 and 2C9 show a cluster of four conserved threonine residues in the I-helix above the porphyrin plane [20]. An identical cluster is found in the sequence of CYP2D6. According to amino acid sequence alignments and based upon protein homology modeling [6, 21], T309 is expected to be the conserved threonine involved in proton delivery to the catalytic water (Figure 1). The role of the other conserved threonine residues in the mammalian CYPs is as yet unknown; they might also have a role in the proton delivery network.

In this study we have experimentally examined the roles of T309 and T312 by mutating these to a valine. These mutations do not significantly alter the size of the residue whereas the putative proton delivering hydroxyl moiety is removed. T309 was selected because it is expected to be the ultimate proton donor to the oxygen, T312 because it is one turn of the I-helix away but still pointing with its hydroxy-moiety towards the porphyrin plane. The oxidation of model substrates by the two mutants was examined and compared to that by wild-type CYP2D6. Furthermore, the binding of substrates to and the formation of uncoupling products by the T309V mutant have been measured. In addition, the oxene donor cumene hydroperoxide (CuOOH) was used in the substrate oxidation reactions by wild-type and the T309V mutant, to distinguish oxidizing species used by the enzymes. It has been shown before that by using the oxygen donor CuOOH, formation of the oxenoid-

iron is mimicked, whereas the other reactive oxygenating species are not formed [22, 23]. Our data reveal the crucial role of T309 in the catalytic activity of CYP2D6 by facilitating oxenoid-iron formation.

A

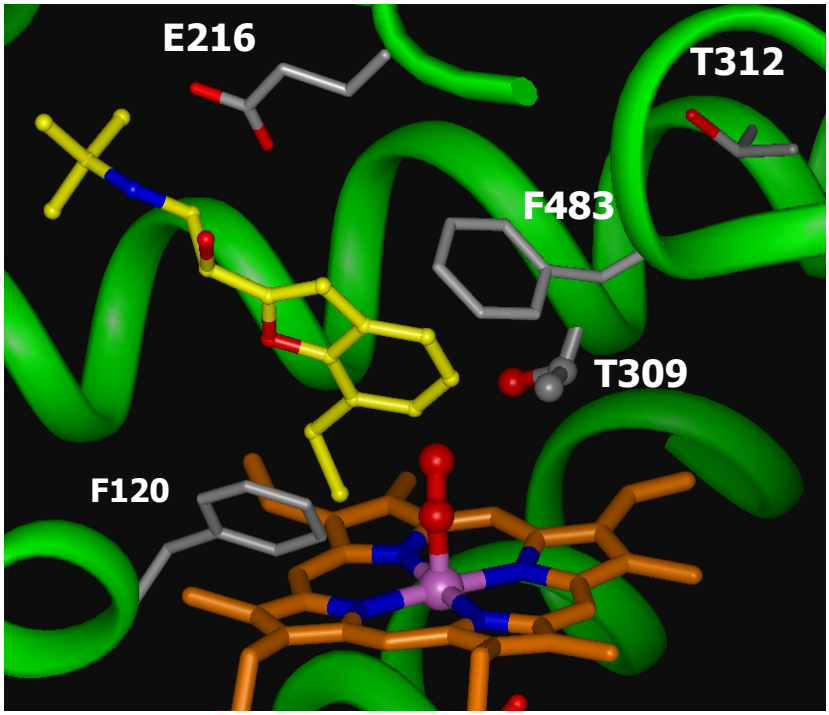

B

CYP	Species	I-helix sequence	Last residue
101	*P. putida*	SDEAKRMCGLLLVGGLD**T**VVNFLSFSMEFLAKSP	268
102A1	*B. megaterium*	DENIRYQIITFLIAGHE**T**TSGLLSFALYFLVKNP	284
107A	*S. erythraea*	ADELTSIALVLLLAGFE**A**SVSLIGIGTYLLLTHP	261
55A1	*F. oxysporum*	KSDAVQIAFLLLVAGNA**T**MVNMIALGVATLAQHP	258
1A2	*Rat*	QEKIVNIVNDIFGAGFE**T**VTTAIFWSILLLVTEP	335
2B4	*Rabbit*	HQNLILTVLSLFFAGTE**T**TSTTLRYGFLLMLKYP	318
2E1	*Rabbit*	LENIAVTVADMFFAGTE**T**TSTTLRYGLLILLKHP	319
2C5	*Rabbit*	LESLVIAVSDLFGAGTE**T**TSTTLRYSLLLLLKHP	314
2D6	*Human*	DENLRIVVADLFSAGMV**T**TSTTLAWGLLLMILHP	325

Figure 1: Protein model displaying the active site of CYP2D6 with dioxygen and S-bufuralol bound, showing the positions of the substrate interacting residues F120, F483 and E216, the conserved putative oxygen activating T309, and conserved T312 (A). A colored version of the figure is shown in the Appendix of this thesis. Alignment of the I-helix protein sequences (drnelson.utmem.edu/ CytochromesP450.html) showing the conserved threonine residue (in bold) of CYPs of which this residue was experimentally shown to be involved in oxygen activation (B). The threonine mutants of the bacterial CYPs 101, 102A1 and fungal CYP55A1 were crystallized [10, 13, 17] and so are mammalian CYPs 2B4 [24] and 2C5 [25], the latter structure was used to build the CYP2D6 model. In CYP107A, the A245T mutant was shown to oxidize alternative substrates [26], and in CYPs 1A2, 2B4 and 2E1 the conserved threonine residues were also subjected to mutagenesis studies [7, 27, 28].

Materials and Methods

Materials

Escherichia coli JM109 were obtained from DSMZ. 7-methoxy-4-(aminomethyl)-coumarin (MAMC), 7-hydroxy-4-(aminomethyl)-coumarin (HAMC), 3,4-methylenedioxymethylamphetamine (MDMA) and 3,4-methylenedioxyamphetamine (MDA) were synthesized before as described [29, 30]. Bufuralol hydrochloride was obtained from Gentest, dextromethorphan hydrobromide and dextrorphan tartrate were obtained from Sigma, cumene hydroperoxide was obtained from Aldrich, Emulgen 911 was obtained from Kao chemicals. All other chemicals were of analytical grade and obtained from standard suppliers.

Construction of plasmid for bicistronic expression of CYP2D6 and reductase

The cDNA of human NADPH-cytochrome P450 reductase was generated by reverse transcription of human genomic DNA using a reverse transcription kit with oligo dT primers (Clontech). After reverse transcription, the cDNA was amplified with primers creating restriction enzyme cleavage sites. Human CYP2D6 was amplified from a cDNA. During amplification additional C-terminal histidines as well as sites for restriction enzyme cleavage were introduced. The amplified and digested products were subsequently ligated into the expression plasmid pSP19T7LT [31] in tandem, with a short linker region in-between the two genes. The correct gene sequence was verified by DNA sequencing.

Site-directed mutagenesis

The threonine 309 → valine (T309V) and threonine 312 → valine (T312V) mutations were introduced into pSP19T7LT containing CYP2D6 using the QuickChange XL Site-Directed Mutagenesis kit (Stratagene). The sequences of the forward- and reverse oligonucleotides, respectively, with the mutated residuein *italic*, were as follows: 5′-T GCC GGG ATG GTG *GTC* ACC TCG ACC ACG C-3′ and 5′-A CGG CCC TAC CAC *CAG* TGG AGC TGG TGC G-3′ for T309V, and 5′-G GTG ACC ACC TCG *GTC* ACG CTG GCC TGC G-3′ and 5′-C CAC TGG TGG AGC *CAG* TGC GAC CGG ACC C-3′ for T312V. After mutagenesis, the presence of the desired mutation was confirmed by DNA sequencing.

Expression and Purification of CYP2D6

The pSP19T7LT plasmids containing wild-type and mutants of CYP2D6 cDNAs were transformed into *Escherichia coli* strain JM109. Expression and membrane isolation was carried out as described [32]. Membranes were resuspended in 0.5% of the original culture volume of KPi-glycerol buffer (50 mM potassium phosphate buffer, pH 7.4, 10% glycerol) and stored at –80° C after determining CYP contents by CO difference spectra [33]. The enzymes were purified, first by solubilization from the membranes by stirring in KPi-glycerol supplemented with 0.5% Emulgen 911 for 2 hrs at 4°C. Insoluble parts were removed by centrifugation (60 min, 120,000 g at 4 °C). Supernatant (100 ml) was incubated, gently rocking, with 4 ml Ni-NTA agarose slurry for 60 min at 4 °C. The Ni-NTA agarose was transferred into a 15 ml polypropylene tube with porous disc (Pierce), and washed with 3 volumes of KPi-glycerol buffer containing 2 mM histidine. Subsequently, CYP2D6 was eluted with 8 ml 0.2 M histidine. After overnight dialysis in KPi-glycerol buffer, the sample was concentrated to 2 ml in a Vivaspin 20 filtration tube (10.000 MWCO PES, Sartorius). The purity of the enzymes was checked by SDS polyacrylamide gelelectrophoresis, yielding single bands at approximately 55 kD after Coomassie staining.

Metabolism assays

Oxidative metabolism of model substrates by mutants and wild-type CYP2D6 were performed as described previously [32]. Shortly, MAMC *O*-demethylation reactions were carried out in duplicate in a 96 wells plate, in a total volume of 200 μl. The reaction mixture consisted of 5 mM $MgCl_2$ in KPi buffer, 0-200 μM MAMC and *E. coli* membranes corresponding to 40 nM wild-type or mutant CYP2D6. The reactions were initiated by the addition of an NADPH regenerating system, resulting in final concentrations of 0.1 mM NADPH, 0.3 mM glucose-6-phosphate, and 0.4 units/ml glucose-6-phosphate dehydrogenase. The reaction was monitored for 30 min at 37°C on a Victor^2 1420 multilabel counter (Wallac) using λ_{ex}= 405nm, λ_{em}= 460nm. The product of MAMC, i.e. HAMC, was quantified using the synthetic reference.

Dextromethorphan *O*-demethylation reactions were carried out in 200 μl KPi buffer containing 5 mM $MgCl_2$, with 0-100 μM dextromethorphan and *E. coli* membranes corresponding to 25 nM wild-type or mutant CYP2D6. After 5 min of pre-incubation at 37°C, the reactions were initiated with an NADPH regenerating system as described above. The reaction was allowed to proceed for 10 min before it was stopped by the addition of 20 μl 23% $HClO_4$. After centrifugation (10 min, 6800xg), 30 μl aliquots of the supernatant were analyzed by HPLC, using a C18 column (Phenomenex Inertsil ODS 150x4.6mm) with a flow rate of 1 ml/min. The mobile phase consisted of 30% acetonitrile and 0.1% triethylamine, set to pH 3 with 70% $HClO_4$. Products were detected by fluorescence at λ_{ex}= 280nm, λ_{em}= 311nm and dextrorphan was quantified using a calibration curve of the commercial reference.
Bufuralol oxidation reactions were carried out as described above with 0-100 μM bufuralol and *E. coli* membranes corresponding to 25 nM wild-type or mutant CYP2D6. Analytes were separated using a C18 column (Phenomenex Inertsil ODS 150x4.6mm) with a flow rate of 0.6 ml/min. The mobile phase consisted of 30% acetonitrile and 0.1% triethylamine, set to pH 3 with 70% $HClO_4$. Products were detected by fluorescence at λ_{ex}=252nm, λ_{em}=302nm and identified by comparison to a standard in the case of 1′-OH-bufuralol (kind gift of Dr. Urs Meyer), and previous studies [34]. The product masses were verified by LC-MS, using the same conditions as described before [6]. 6-OH-bufuralol eluted at 17.3 min, m/z 278, fragmenting to 260, 242 (100%), 204 and 186. 1′-OH-bufuralol eluted at 18.0 min, m/z 278, fragmenting to 260 (100%), 221 and 203. 4-OH-bufuralol eluted at 18.2 min, m/z 278, fragmenting to 260 (100%) and 204. $\Delta^{1'-2'}$-bufuralol eluted at 19.6 min, m/z 260, fragmenting to 242 (100%) and 186.
MDMA oxidation reactions were carried out as described above with 0-200 μM MDMA and *E. coli* membranes corresponding to 25 nM wild-type or mutant CYP2D6. Analytes were separated using a C18 column (Phenomenex Inertsil ODS 150x4.6mm) with a flow rate of 0.4 ml/min. The mobile phase consisted of 23% acetonitrile and 0.1% triethylamine, set to pH 3 with 70% $HClO_4$. Products were detected by fluorescence at λ_{ex}= 280nm, λ_{em}= 320nm, MDA was quantified using a calibration curve of the synthetic reference.
The oxidation reactions supported by CuOOH were in presence of 100 μM of substrate and initiated by the addition of 500 μM CuOOH. For MAMC oxidation, 25 nM of enzyme was added to the incubation and the reaction was monitored for 15 min, for the other substrates 2.5 nM of enzyme was added and the reactions were allowed to proceed for 5 min. Peak areas of all products were quantified by Shimadzu Class VP 4.3 and analyzed using Graph Pad Prism 3.0 software (GraphPad Software Inc.).

Optical Titrations
Dissociation constants of the substrates to the enzymes were determined by spectral titration, according to the method of Jefcoate [6, 35]. Spectra were taken at room temperature on a Pharmacia Ultrospec 2000 spectrometer. In short, 1 ml of 0.5 μM purified enzyme in KPi-glycerol buffer was divided over two cuvettes, to the first 5 μl of a 1 mM solution of compound in the same buffer was added, to the second the same volume of just buffer. Difference spectra from 350 to 450 nm were taken before, and after each addition of compound. The substrates themselves did not show absorbance in this spectral range at the concentrations used. The difference between the absorbance at 390 nm and 425 nm was plotted against the substrate concentration to estimate the dissociation constant (K_s) using Equation 1 in Graph Pad Prism 3.0 software, where B is the absorbance difference (390-425) and B_{max} is the maximal absorbance difference.

$$B = \frac{B_{max}[S]}{K_s + [S]} \quad (1)$$

Uncoupling of substrate monooxygenation activity
To determine uncoupling of activity, incubation reactions were carried out as described above in KPi buffer with 5 mM $MgCl_2$, which was treated with Chelex 100 beads (Biorad) and supplemented with 0.2 mM DETAPAC to remove traces of iron. Substrates (100 μM) and *E. coli* membranes corresponding to 25 nM wild-type or mutant CYP2D6 were added to a total reaction volume of 200 μl. To measure the total amount of formed hydrogen peroxide and superoxide anion radical, 1870 units of superoxide dismutase and 40 units of horseradish peroxidase were added together with 3.6 mM para-hydroxy-

phenyl-acetic acid [36]. Reactions were initiated by adding the NADPH regenerating system described above and terminated after 10 min by adding 3% $HClO_4$. After centrifugation (10 min, 6800xg), 30 μl aliquots of the supernatant were analyzed by HPLC, using a C18 column (Phenomenex Inertsil ODS 150x4.6mm) with a flow rate of 0.6 ml/min. Analytes were eluted by a gradient: 5 min of A (20 mM ammonium acetate containing 5% acetonitrile) followed by an increase to B (10 mM ammonium acetate containing 90% acetonitrile) over 5 min. After running in B for 5 min the gradient returned to starting conditions in 1 min and equilibrated for another 10 min. The product 2,2'-dihydroxybiphenyl-5,5'-diacetate eluted at 4.6 min and was detected by fluorescence (λ_{ex}= 323 nm, λ_{em}= 400 nm). H_2O_2 was quantified by a calibration curve made by adding various concentrations of 0 to 1 μM of H_2O_2 to incubations without substrate.

Results

Expression and spectroscopy of wild-type and mutants of CYP2D6

The expression levels of T309V, T312V and wild-type CYP2D6 were approximately 200 nM, the same as described before for the wild-type [32]. In the case of T309V, significant amounts of P420 (inactive enzyme, observed as an absorbance band at 420 nm in the CO-difference spectrum) were present in the cells and in the membrane fraction. After purification no significant P420 was detected in the CO-difference spectra of the enzymes.

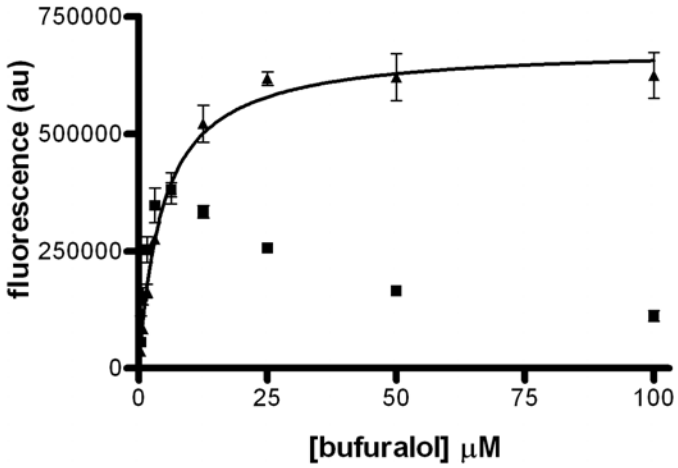

Figure 2: Substrate-velocity plots for 4-hydroxylation (▲) and 6-hydroxylation (■) of bufuralol by wild-type CYP2D6. Shown are the averages ± S.D. of two independent experiments as described in the Methods section.

Oxidation reactions supported by NADPH

MAMC was linearly *O*-demethylated by the T309V and T312V mutants for at least 30 minutes, indicating that the enzymes were stable for at least that time at 37° C. The T312V mutant showed an activity approximately equal to that of wild-type CYP2D6 (Table 1). The T309V mutant showed a similar K_m as the wild-type enzyme and a 20-fold decreased turnover rate.

Bufuralol was oxidized by the T312V mutant similar as by the wild-type, only minor changes, up to two-fold, in turnover rates were found. Interestingly, concentration dependence of 6-hydroxylation of bufuralol by the wild-type and the T312V mutant showed substrate inhibition at concentrations above 20 μM (Figure 2).

Table 1: Oxidative metabolism of various substrates by wild-type, T309V and T312V mutants CYP2D6 supported by NADPH.

Substrate	Product	Wild-type		T309V		T312V	
		K_m	V_{max}	K_m	V_{max}	K_m	V_{max}
MAMC	HAMC	22 ± 1	3.7± 0.04[a]	12 ± 7	0.17 ± 0.01 [a]	18 ± 3	2.3 ± 0.5
bufuralol	1'-OH	3.7 ± 0.2	6.7 ± 0.2[b]	3.6 ± 0.2	0.47 ± 0.02 [b]	4.7 ± 1.6	3.7 ± 0.8 [b]
	4-OH	4.3 ± 0.3	0.7 ± 0.1 [b]	4.1 ± 0.6	0.55 ± 0.02 [b]	5.5 ± 1.6	0.7 ± 0.2 [b]
	6-OH	1.9 ± 0.5	0.5 ± 0.03 [b]	-[d]	-[d]	0.9 ± 0.1	0.21 ± 0.05 [b]
	$\Delta^{1',2'}$	28 ± 2	0.8 ± 0.03 [b]	-[d]	-[d]	24 ± 7	0.46 ± 0.17 [b]
MDMA	3,4-OH-MA[2]	3.3 ± 0.4	3.4 ± 0.4 [b]	1.9 ± 0.9	0.25 ± 0.13 [b]	1.9 ± 0.2	7.1 ± 0.1 [b]
	MDA	>100	+ [c]	0.6 ± 0.0	1 ± 0.1 [a]	>100	+ [c]
dextromethorphan	dextrorphan	1.0 ± 0.1	5.5 ± 0.4[a]	2.1 ± 0.2	2.9 ± 0.1 [a]	1.4 ± 0.2	8.2 ± 0.8
	3-MOmorphinan[1]	>200	+ [c]	>200	+ [c]	>200	+ [c]

All values are the means ± S.D. of at least three independent experiments as described in the Methods section. [1] 3-methoxymorphinan, [2] 3,4-dihydroxymethylamphetamine. K_m expressed in μM, V_{max} expressed in [a] pmol product/min/pmol CYP2D6, [b] 1 x 10^6 fluorescence counts/min/nmole CYP, [c] detected, not quantified, [d] not detected.

The turnover rate and K_m were estimated from the initial part of the substrate-velocity plots. For the 1'-hydroxylation of bufuralol the T309V mutant displayed a K_m equal to that of wild-type CYP2D6, with a turnover rate about 10-fold lower. However, for 4-hydroxylation of bufuralol both K_m and turnover rates were equal for mutant and wild-type. The other products of bufuralol formed by wild-type CYP2D6, 6-OH-bufuralol and $\Delta^{1',2'}$bufuralol, were not detected in incubations with the T309V mutant, indicating that the product ratio of bufuralol oxidation by the T309V mutant is significantly different to that by wild-type CYP2D6.

A

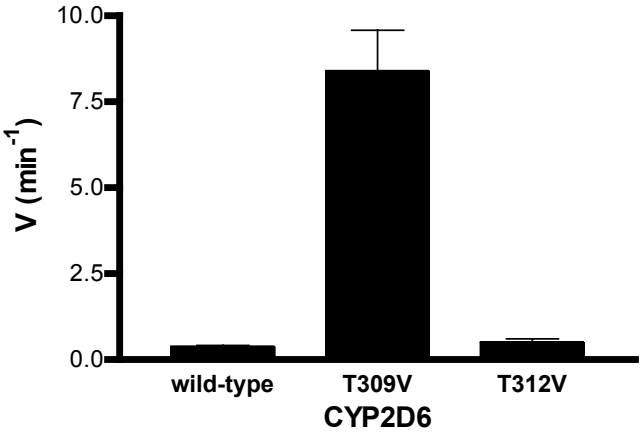

B

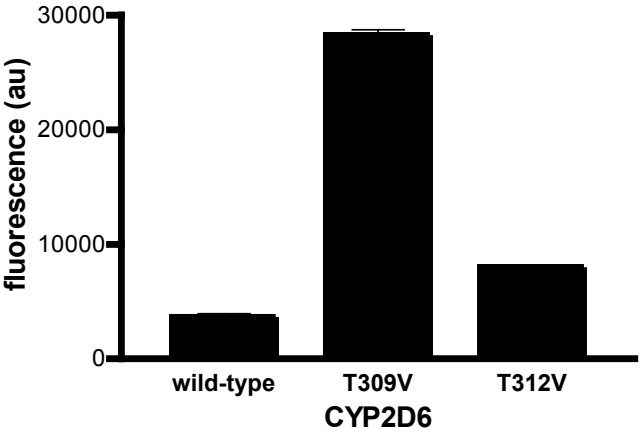

Figure 3: Product formation through N-demethylation of 100 μM MDMA (A) and 100 μM dextromethorphan (B) by wild-type, T309V and T312V mutants CYP2D6. Shown are the averages ± S.D. of three independent HPLC experiments as described in the Methods section.

Similar results were obtained when studying MDMA oxidation. Incubations with the T312V mutant yielded only up to two-fold changes in K_m and V_{max} compared to the wild-type, whereas the T309V mutant *O*-demethylenated MDMA with a 14-fold lower turnover rate. Interestingly the T309V mutant also significantly *N*-dealkylated MDMA, whereas for the wild-type and the T312V mutant *N*-dealkylation was a minor pathway (Figure 3).
Dextromethorphan was efficiently *O*-demethylated by both the mutants, the T309V displayed only a two-fold lower turnover rate and the T312V mutant a two-fold higher turnover rate, all with similar K_m. However, a clear difference was seen in *N*-demethylation of dextromethorphan. Although the turnover rates and K_m were not quantified, 3-methoxy-morphinan was formed from 100 μM dextromethorphan in 8-fold higher amounts by the T309V mutant than by wild-type CYP2D6 (Figure 3). So in both cases significantly more *N*-demethylation of MDMA and dextromethorphan was observed with the T309V mutant over T312V and wild-type CYP2D6.

Substrate binding
To study the influence of the T309V mutation on substrate binding affinity, the dissociation constants of the used substrates to wild-type and T309V mutant CYP2D6 were determined by optical titration (Table 2). Solutions of purified enzymes had to be used, because the crude membrane fractions were too turbid for these experiments, due to the relatively low expression levels. The addition of bufuralol, MDMA and dextromethorphan to wild-type and T309V mutant CYP2D6 all led to a type I change in the absorbance spectrum of both of the enzymes, as indicated by an increase of the absorbance at 390 nm and a decrease at 425 nm. It was found that the affinity of the T309V mutant for MDMA was decreased two-fold and the affinity for dextromethorphan was increased by 30%. The estimated K_s for bufuralol did not change compared to the wild-type enzyme. Binding of MAMC to the enzymes could not be measured this way because the absorbance of this substrate was too high in this spectral range.

Table 2: K_s values (μM) of the substrates for wild-type and T309V mutant CYP2D6.

Substrate	K_s	
	Wild-type	T309V
Bufuralol	26 ± 12	21 ± 4
MDMA	28 ± 3	47 ± 1
Dextromethorphan	33 ± 5	20 ± 1

All values are the means ± S.D. of at least two independent experiments as described in the Methods section.

Uncoupling of substrate monooxygenation activity
To investigate whether the loss in turnover of the substrates by the T309V mutant was caused by a higher degree of uncoupling of the monooxygenase activity, the formation of uncoupling products H_2O_2 and $O_2^{-\cdot}$ was determined in the incubations. Because of the turbidity of the membrane fractions, the amount of 2,2′-dihydroxybiphenyl-5,5′-diacetate formed was analyzed by HPLC. The incubations were performed with 100 μM of substrate, a concentration high enough to reach V_{max} conditions for the oxidation of MAMC, bufuralol, MDMA and dextromethorphan by wild-type and T309V mutant CYP2D6. Only low amounts of uncoupling products were formed by wild-type CYP2D6 when metabolizing MAMC, bufuralol, MDMA or dextromethorphan (Table 3). The rate of formation of uncoupling products is the highest when MAMC is present, i.e. up to 0.5 pmol H_2O_2/min/pmol CYP, compared to a rate of HAMC formation of 3.7 pmol/min/pmol CYP. Similar rates were found

when the T309V mutant was used in the incubations, suggesting that decreased product formation was not due to increased uncoupling of activity.

Table 3: Formation of uncoupling products by wild-type and T309V mutant CYP2D6.

Substrate	Reaction rate	
	Wild-type	T309V
MAMC	0.50 ± 0.19	0.39 ± 0.22
Bufuralol	0.24 ± 0.06	0.07 ± 0.04
MDMA	0.03 ± 0.01	0.03 ± 0.02
Dextromethorphan	0.03 ± 0.01	0.03 ± 0.03

All values are the means ± S.D. of at least three independent experiments as described in the Methods section, reaction rates are expressed in pmol H_2O_2/min/pmol CYP2D6.

Table 4: Metabolic oxidation rates of various substrates (100 μM) by wild-type and T309V mutant CYP2D6 supported by CuOOH.

Substrate	Product	Wild-type	T309V
MAMC	HAMC	5.1 ± 0.2	16.5 ± 0.2
Bufuralol	1'-OH	15.6 ± 2.0	60 ± 7
	4-OH	0.5 ± 0.3	37 ± 10
	6-OH	0.5 ± 0.1	4.8 ± 0.5
	$\Delta^{1',2'}$	2.6 ± 0.5	12.4 ± 0.8
MDMA	3,4-OH-MA	2.2 ± 0.7	5.2 ± 1.1
Dextromethorphan	dextrorphan	122 ± 14	414 ± 70
	3-MOH-Mor	- [a]	0.04 ± 0.01
	3-OH-Mor	- [a]	0.22 ± 0.01

All values are the means ± S.D. of at least three experiments as described in the Methods section. Rates of HAMC and dextrorphan formation are in pmol product/min/pmol CYP2D6, other products in 1 x 10^6 fluorescence counts/min/pmol CYP2D6, [a] not detected.

Oxidation reactions supported by CuOOH

To further investigate the mechanism of oxidation by the T309V mutant of CYP2D6, incubations were also performed with the oxene donor CuOOH, which directly forms the oxenoid-iron in CYPs [23]. MAMC was *O*-demethylated by both the wild-type and T309V mutant CYP2D6 when supported by CuOOH. The reaction rates were linear for at least 15 min and the turnover rate of the T309V mutant was found to be 3-fold higher than that of the wild-type (Table 4). Bufuralol was oxidized by wild-type CYP2D6 to the same products supported by CuOOH as by O_2/NADPH. However, 1'-hydroxylation and Δ1'-2' desaturation took place with a 2 to 3-fold higher turnover rate when compared to the incubations supported by NADPH, whereas the aromatic hydroxylations rates did not change. The same observation was described before by others [34]. The T309V mutant formed the same four products as wild-type CYP2D6, all of them with a higher turnover rate. The rate of aromatic 4-hydroxylation was even 70-fold higher, leading to a completely different product ratio than wild-type CYP2D6.

O-demethylenation of MDMA was supported by CuOOH in the case of both wild-type and T309V mutant CYP2D6. The turnover rate of the T309V mutant was two-fold higher than that of the wild-type enzyme. *N*-dealkylation of MDMA was not detected.

Dextromethorphan was *O*-demethylated by both enzymes, with a 3-fold higher rate by the T309V mutant compared to wild-type cyp2d6. Furthermore, low levels of 3-methoxymorphinan and significant amounts of 3-hydroxymorphinan were formed by the mutant, indicating that some *N*-dealkylation was still taking place.

Interestingly, the T309V mutant displayed higher turnover rates than wild-type CYP2D6 in all reactions supported by CuOOH, ranging from two-fold for MDMA *O*-demethylenation to 70-fold for bufuralol 4-hydroxylation.

Discussion

CYPs are enzymes capable of oxidizing and reducing a vast amount of chemically different substrates by using two electrons donated by NADPH-cytochrome P450 reductase and activating molecular oxygen. To bind molecular oxygen CYPs are equipped with an iron containing porphyrin ring and the protein surroundings of this heme group are thought to activate the iron bound oxygen by delivering protons as well as to stabilize it to avoid unwanted side-reactions. A conserved threonine residue in the I-helix overlaying the porphyrin is involved in this process, as shown in various mutagenesis and X-ray diffraction studies of several CYPs [7, 9-13, 27, 28]. From amino acid sequence alignments and protein homology modeling we propose T309 to fulfill this role in CYP2D6.

The results of the present study show that the catalytic behavior of the T309V mutant is clearly different from that of wild-type CYP2D6, with significantly decreased turnover rates of MAMC, bufuralol and MDMA (Table 1). The mutation hardly had an effect on substrate affinity, as bufuralol, MDMA and dextromethorphan still bound equally well to the enzyme after mutation (Table 2). Besides changing the substrate affinity, an active site mutation can lead to alternative orientations of bound substrates [32, 37]. However, because this threonine residue is so highly conserved in CYPs with completely different substrate preferences, it is unlikely to determine substrate selectivity or metabolic regioselectivity by substrate binding. Furthermore, modeling studies did not show involvement of active site threonine residues in CYP2D6 substrate interaction [4, 6, 38].

As an explanation for the diminished product formation from MAMC, bufuralol and MDMA by the T309V mutant, a higher degree of uncoupling was considered because H_2O_2 formation was previously shown to be increased in the oxidative metabolism by other CYPs of which this conserved threonine was mutated [13, 27, 28]. However, in this study this was not the case (Table 3). An explanation for the lack of increased hydrogen peroxide formation by the T309V mutant may be found in the alignment of CYPs (Figure 1). The alignment of the I-helix of CYPs of which the role of the conserved threonine was studied experimentally, shows homology in the conserved threonine residue but also in a highly conserved acidic residue preceding the threonine. This acidic residue is believed to be of crucial importance in the proton delivery to the reactive oxygen species [10, 14]. For CYP55A, which is lacking the conserved acidic residue, alternate proton delivery pathways have been proposed based on its crystal structure [17]. In CYP2D6 there is a valine at position 308 preceding T309 so protons are likely to be shuttled different then in CYPs 101, 102, 1A2, 2B4 and 2E1. A different proton shuttling mechanism will probably change the ease of uncoupling in T309V mutant CYP2D6.

The T309V mutant displayed significantly altered product ratio's of bufuralol, MDMA and dextromethorphan metabolism compared to wild-type CYP2D6 (Table 1, Figure 3). Changes in preference of certain types of reactions like these were observed before for other conserved threonine residue mutants of CYPs. For example, the T302A mutant of CYP2B4 showed a decreased cyclohexane hydroxylation but an increased deformylation of cyclohexane carboxaldeyde [27]. The T303A mutant of CYP2E1 showed a reduced epoxidation of several model substrates but an enhanced epoxidation of olefins [28]. It was hypothesized that CYPs can deploy three different oxygenating species in oxidation reactions, namely a peroxo, a hydroperoxo and an oxenoid-iron (shown in Figure 4). These species have different oxidative properties and therefore prefer certain types of reactions,

which can in specific cases each lead to formation of one product [9, 28]. The abundance and reactivity of these different oxygenating species would thus determine the amount of product formed. The conserved threonine is thought to be involved in proton delivery to the oxygen species and thus a mutation would shift the distribution of these three species. In this study, the turnover rates of the *N*-demethylation reactions of dextromethorphan and MDMA by the T309V mutant were strongly increased compared to wild-type (Figure 3). Previously, *N*-dealkylation reactions were proposed to be mediated predominantly by the (hydro)peroxo-iron, whereas *O*-dealkylation reactions were proposed to be mediated by the oxenoid-iron in CYP2D6 [23]. Our observation that the T309V mutant *N*-dealkylates rather than to *O*-demethylates or *O*-demethylenates dextromethorphan and MDMA respectively, might therefore be explained by an increased ratio of (hydro)peroxo-iron to oxenoid-iron. To test this hypothesis, we used CuOOH to support the T309V mutant CYP2D6 mediated reactions, instead of NADPH with molecular oxygen. CuOOH is a model oxidant, known to short-circuit the catalytic cycle of CYP and directly form the oxenoid-iron [22, 23, 34, 39]. Indeed, in presence of CuOOH the T309V mutant was again well capable to *O*-demethylate MAMC and dextromethorphan and to *O*-demethylenate MDMA (Table 4). This suggests that the changed regioselectivity of the T309V mutant may be caused by its incapability to form the oxenoid-iron. Consistent with these findings it was recently proposed, based upon crystallographic data of the dioxygen complex of the T252A mutant of CYP101, that T252 accepts a hydrogen bond from the hydroperoxo-iron promoting the second protonation leading to O-O cleavage and oxenoid-iron formation [40].

Bufuralol is widely used as a CYP2D6 model substrate [34, 41], however, several interesting changes were observed in CYP2D6 mediated bufuralol oxidative metabolism in this study. The formation of 1'-OH-bufuralol and $\Delta^{1',2'}$bufuralol by the T309V mutant was decreased supported by NADPH and O_2 compared to wild-type CYP2D6. Like the *O*-demethylation reactions these activities could be restored with CuOOH, suggesting that also the aliphatic hydroxylation and the desaturation reaction are predominantly mediated through the oxenoid-iron. The fact that both these activities were also relatively increased by the wild-type when supported by CuOOH strengthens this hypothesis. The active oxygen species involved in aromatic hydroxylations of bufuralol are more difficult to assign. The aromatic hydroxylations of debrisoquine by CYP2D6 were previously suggested to be determined by the mechanism of oxidation rather then the orientation of the substrate in the active site [42]. Several mechanisms have been proposed for aromatic hydroxylation reactions by CYPs. Firstly, epoxidation may occur, followed by spontaneous rearrangement restoring aromaticity. Secondly, aromatic hydroxylation may result from initial electron abstraction, yielding the hydroxylated product via a radical cation intermediate. Finally, in case a benzylic hydrogen atom is present this can be abstracted, followed by spin-delocalization, and then via oxygen rebound leading to the hydroxylated product [43-45]. The T309V mutant displayed equal 4-hydroxylation and decreased 6-hydroxylation of bufuralol compared to the wild-type when supported by NADPH and O_2, whereas when supported by CuOOH the mutant displayed highly increased aromatic hydroxylations compared to the wild-type (Tables 1 and 4). This suggests the oxenoid-iron has a part in the aromatic hydroxylations, probably as the electrophilic oxidant, abstracting the electron, or inserting the O-atom in the epoxidation reaction. However, the high turnover of 4-OH-bufuralol by the T309V mutant supported by NADPH and O_2, implies that also the (hydro)peroxo-iron may be involved in aromatic hydroxylation of bufuralol. The currently general accepted idea is that the hydroperoxo-iron effects oxidation by insertion of OH^+ into a C-H bond [46-48]. The mechanism of aromatic hydroxylation of bufuralol by the hydroperoxo-iron would be via epoxidation, as the hydroperoxo-iron is an effective electrophilic epoxidizing agent [49]. The

reaction types determined in this study and the oxygenating species suggested to be involved are summarized in Table 5.

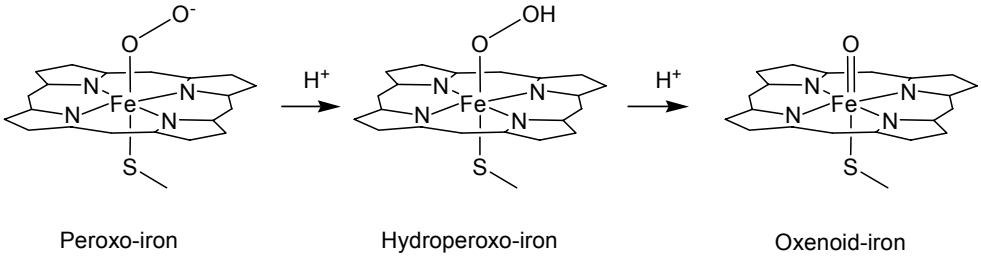

Figure 4: Schematic showing the oxygenating species in CYP, adapted from Vaz et al. [28].

Table 5: Involvement of oxygenating species (shown in Figure 4) in reactions catalyzed by CYP2D6 measured in this study.

Oxygenating species	(Hydro)peroxo-iron	Oxenoid-iron
Reactions	N-dealkylation	O-dealkylation
	Aromatic hydroxylation[1]	Aromatic Hydroxylation[2]
		Desaturation
		O-demethylenation
		Aliphatic hydroxylation

In the current study peroxo-iron and hydroperoxo-iron were not distinguished. The aromatic hydroylation occurs via [1]epoxidation or via [2]epoxidation, electron abstraction or proton abstraction.

The reason that the T309V mutant formed more 4- then 6-OH-bufuralol, might have to do with sterical hindrance of the 1'-ethyl. A striking observation was the fact that 4- and 6-hydroxylation of bufuralol by the T309V mutant supported by CuOOH are respectively 75- and 10-fold higher than the turnover rates by the wild-type enzyme. Although CuOOH has been used to support reactions by conserved threonine mutants of CYPs, to study mechanism based inactivation [50, 51], such strong increases in product formation have not been described yet. Apparently, the T309 hydroxy moiety has a negative influence on the mechanism leading to aromatic hydroxylations of bufuralol. Possible explanations for this might be hydrogen bond interactions of the threonine hydroxy moiety with the CuOOH, leading to less oxenoid-iron formation, or destabilization by the threonine hydroxy moiety of the bufuralol radical cation intermediate after electron abstraction.
The formation of 6-OH-bufuralol displayed substrate inhibition, while formation of the other three bufuralol products displayed Michaelis-Menten kinetics (Figure 2). Atypical kinetics of only one of several products of a substrate have been described before for the metabolism of midazolam and verapamil by CYP3A4 [52, 53]. These effects were explained by steric interaction of substrates in a two binding-site model. Several recent observations suggest that also CYP2D6 may contain two substrate binding sites. Potentiation of MAMC *O*-demethylation by sparteine and phenformine was observed previously [21], biphasic kinetics were observed in MDMA *O*-demethylenation by the polymorphic variant CYP2D6*17 [54], and an additional binding site for MAMC was observed in wild-type CYP2D6 [55].
Besides T309 (Figure 1A), three other threonine residues are present in the I-helix at positions 310, 312 and 313 (Figure 1B). The latter three threonine residues are also highly conserved in mammalian CYPs but with unknown function. In the homology model of CYP2D6, T312 is one turn of the I-helix further away from the heme and seems to be

stabilizing a distortion in the I-helix by providing hydrogen bonds to the carbonyl group of V308. Mutating T312 to a valine in this study however, did not result in changes in expression levels, nor in the metabolic activity towards MAMC, bufuralol, MDMA or dextromethorphan, suggesting that the role of T312 in the oxidative metabolism by CYP2D6 is limited.
In summary, the present study suggests T309 in CYP2D6 to be the conserved I-helix threonine involved in oxygen activation. Retrieving the lost activities of the T309V mutant with CuOOH, indicated that T309 is a key determinant in maintaining the balance of reactive oxygen species. Interestingly, supported by CuOOH the T309V mutant displayed even higher activities than wild-type CYP2D6 of which the mechanism remains to be resolved. Furthermore, atypical enzyme kinetics in the metabolism of bufuralol by wild-type CYP2D6 was observed, which might indicate a second substrate binding place in CYP2D6.

Acknowledgements
We thank André Groenhof for the valuable discussions about the mechanisms of bufuralol oxidation, and Ed Groot for his help in preparing the *E Coli* membranes and purifying the enzymes.

References

1. Ortiz de Montellano PR, *Cytochromes P450: structure, mechanism, and biochemistry*. Kluwer Academic, New York, 2005.
2. Zanger UM, Raimundo S and Eichelbaum M, Cytochrome P450 2D6: overview and update on pharmacology, genetics, biochemistry. *Naunyn Schmiedebergs Arch Pharmacol* **369:** 23-37, 2004.
3. Ingelman-Sundberg M, Genetic polymorphisms of cytochrome P450 2D6 (CYP2D6): clinical consequences, evolutionary aspects and functional diversity. *the Pharmacogenomics Journal* **5:** 6-13, 2005.
4. Kemp CA, Marechal JD and Sutcliffe MJ, Progress in cytochrome P450 active site modeling. *Arch Biochem Biophys* **433:** 361-68, 2005.
5. Vermeulen NPE, Prediction of drug metabolism: the case of cytochrome P450 2D6. *Curr Top Med Chem* **3:** 1227-39, 2003.
6. Keizers PHJ, de Graaf C, de Kanter FJJ, Oostenbrink C, Feenstra KA, Commandeur JNM and Vermeulen NPE, Metabolic regio- and stereoselectivity of cytochrome P450 2D6 towards 3,4-methylenedioxy-N-alkyl-amphetamines: in silico predictions and experimental validation. *J Med Chem* **48:** 6117-6127, 2005.
7. Furuya H, Shimizu T, Hirano K, Hatano M, Fujii-Kuriyama Y, Raag R and Poulos TL, Site-directed mutagenesis of rat liver cytochrome P-450d: catalytic activities toward benzphetamine and 7-ethoxycoumarin. *Biochemistry* **28:** 6848-57, 1989.
8. Imai M, Shimada H, Watanabe Y, Matsushima-Hibiya Y, Makino R, Koga H, Horiuchi T and Ishimura Y, Uncoupling of the cytochrome P-450cam monooxygenase reaction by a single mutation, threonine-252 to alanine or valine: possible role of the hydroxy amino acid in oxygen activation. *Proc Natl Acad Sci U S A* **86:** 7823-7, 1989.
9. Coon MJ, Vaz AD, McGinnity DF and Peng HM, Multiple activated oxygen species in P450 catalysis: contributions To specificity in drug metabolism. *Drug Metab Dispos* **26:** 1190-3, 1998.
10. Raag R, Martinis SA, Sligar SG and Poulos TL, Crystal structure of the cytochrome P-450CAM active site mutant Thr252Ala. *Biochemistry* **30:** 11420-9, 1991.
11. Kimata Y, Shimada H, Hirose T and Ishimura Y, Role of Thr-252 in cytochrome P450cam: a study with unnatural amino acid mutagenesis. *Biochem Biophys Res Commun* **208:** 96-102, 1995.

12. Schlichting I, Berendzen J, Chu K, Stock AM, Maves SA, Benson DE, Sweet RM, Ringe D, Petsko GA and Sligar SG, The catalytic pathway of cytochrome p450cam at atomic resolution. *Science* **287:** 1615-22, 2000.
13. Yeom H, Sligar SG, Li H, Poulos TL and Fulco AJ, The role of Thr268 in oxygen activation of cytochrome P450BM-3. *Biochemistry* **34:** 14733-40, 1995.
14. Haines DC, Tomchick DR, Machius M and Peterson JA, Pivotal role of water in the mechanism of P450BM-3. *Biochemistry* **40:** 13456-65, 2001.
15. Cupp-Vickery JR, Han O, Hutchinson CR and Poulos TL, Substrate-assisted catalysis in cytochrome P450eryF. *Nat Struct Biol* **3:** 632-7, 1996.
16. Nagano S, Cupp-Vickery JR and Poulos TL, Crystal structures of the ferrous dioxygen complex of wild-type cytochrome P450eryF and its mutants, A245S and A245T: investigation of the proton transfer system in P450eryF. *J Biol Chem* **280:** 22102-7, 2005.
17. Park SY, Shimizu H, Adachi S, Nakagawa A, Tanaka I, Nakahara K, Shoun H, Obayashi E, Nakamura H, Iizuka T and Shiro Y, Crystal structure of nitric oxide reductase from denitrifying fungus Fusarium oxysporum. *Nat Struct Biol* **4:** 827-32, 1997.
18. Gotoh O, Substrate recognition sites in cytochrome P450 family 2 (CYP2) proteins inferred from comparative analyses of amino acid and coding nucleotide sequences. *J Biol Chem* **267:** 83-90, 1992.
19. Hasemann CA, Kurumbail RG, Boddupalli SS, Peterson JA and Deisenhofer J, Structure and function of cytochromes P450: a comparative analysis of three crystal structures. *Structure* **3:** 41-62, 1995.
20. Mestres J, Structure conservation in cytochrome P450. *Proteins* **58:** 596-609, 2005.
21. Venhorst J, ter Laak AM, Commandeur JNM, Funae Y, Hiroi T and Vermeulen NPE, Homology modeling of rat and human cytochrome P450 2D (CYP2D) isoforms and computational rationalization of experimental ligand-binding specificities. *J Med Chem* **46:** 74-86, 2003.
22. Guengerich FP, Vaz AD, Raner GM, Pernecky SJ and Coon MJ, Evidence for a role of a perferryl-oxygen complex, FeO3+, in the N-oxygenation of amines by cytochrome P450 enzymes. *Mol Pharmacol* **51:** 147-151, 1997.
23. Hutzler JM, Powers FJ, Wynalda MA and Wienkers LC, Effect of carbonate anion on cytochrome P450 2D6-mediated metabolism in vitro: the potential role of multiple oxygenating species. *Arch Biochem Biophys* **417:** 165-175, 2003.
24. Scott E, He Y, Wester MR, White M, Chin C, Halpert J, Johnson EF and Stout CD, An open conformation of mammalian cytochrome P450 2B4 at 1.6-A resolution. *Proc Natl Acad Sci U S A* **100:** 13196-201, 2003.
25. Williams PA, Cosme J, Sridhar V, Johnson EF and McRee DE, Mammalian microsomal cytochrome P450 monooxygenase: structural adaptations for membrane binding and functional diversity. *Mol Cell* **5:** 121-31, 2000.
26. Xiang H, Tschirret-Guth RA and Ortiz de Montellano PR, An A245T mutation conveys on cytochrome P450eryF the ability to oxidizs alternative substrates. *J Biol Chem* **275:** 35999-6006, 2000.
27. Vaz AD, Pernecky SJ, Raner GM and Coon MJ, Peroxo-iron and oxenoid-iron species as alternative oxygenating agents in cytochrome P450-catalyzed reactions: switching by threonine-302 to alanine mutagenesis of cytochrome P450 2B4. *Proc Natl Acad Sci U S A* **93:** 4644-8, 1996.
28. Vaz AD, McGinnity DF and Coon MJ, Epoxidation of olefins by cytochrome P450: evidence from site-specific mutagenesis for hydroperoxo-iron as an electrophilic oxidant. *Proc Natl Acad Sci U S A* **95:** 3555-60, 1998.
29. Braun U, Shulgin AT and Braun G, Centrally active N-substituted analogs of 3,4-methylenedioxyphenylisopropylamine (3,4-methylenedioxyamphetamine). *J Pharm Sci* **69:** 192-5, 1980.
30. Onderwater RC, Venhorst J, Commandeur JNM and Vermeulen NPE, Design, synthesis, and characterization of 7-methoxy-4-(aminomethyl)coumarin as a novel and selective cytochrome P450 2D6 substrate suitable for high-throughput screening. *Chem Res Toxicol* **12:** 555-9, 1999.

31. Weinander R, Mosialou E, de Jong J, Tu CP, Dypbukt J, Bergman T, Barnes HJ, Hoog JO and Morgenstern R, Heterologous expression of rat liver microsomal glutathione transferase in simian COS cells and Eschirichia coli. *Biochem J.* **311:** 861-6, 1995.
32. Keizers PHJ, Lussenburg BMA, de Graaf C, Mentink LM, Vermeulen NPE and Commandeur JNM, Influence of phenylalanine 120 on cytochrome P450 2D6 catalytic selectivity and regiospecificity: crucial role in 7-methoxy-4-(aminomethyl)-coumarin metabolism. *Biochem Pharmacol* **68:** 2263-2271, 2004.
33. Omura T and Sato R, The carbon monoxide-binding pigment of liver microsomes. II. Solubilization, purification, and properties. *J Biol Chem* **239:** 2379-85, 1964.
34. Hanna IH, Krauser JA, Cai H, Kim MS and Guengerich FP, Diversity in mechanisms of substrate oxidation by cytochrome P450 2D6. Lack of an allosteric role of NADPH-cytochrome P450 reductase in catalytic regioselectivity. *J Biol Chem* **276:** 39553-61, 2001.
35. Jefcoate CR, Measurement of substrate and inhibitor binding to microsomal cytochrome P450 by optical-difference spectroscopy. *Methods Enzymol* **52:** 258-79, 1978.
36. Rooseboom M, Vermeulen NPE, van Hemert N and Commandeur JNM, Bioactivation of chemopreventive selenocysteine Se-conjugates and related amino acids by amino acid oxidases novel route of metabolism of selenoamino acids. *Chem Res Toxicol* **14:** 996-1005, 2001.
37. Lussenburg BMA, Keizers PHJ, de Graaf C, Hidestrand M, Ingelman-Sundberg M, Vermeulen NPE and Commandeur JNM, The role of phenylalanine 483 in cytochrome P450 2D6 is strongly substrate dependent. *Biochem Pharmacol* **70:** 1253-61, 2005.
38. de Groot MJ, Ackland MJ, Horne VA, Alex AA and Jones BC, A novel approach to predicting P450-mediated drug metabolism: Development of a combined protein and pharmacophore model for CYP2D6. *J Med Chem* **42:** 1515-1524, 1999.
39. Ortiz de Montellano PR and De Voss JJ, Substrate oxidation by cytochrome P450 enzymes. In: *Cytochrome P450 structure, mechanism, and biochemistry* (Ed. Ortiz de Montellano PR). Kluwer Academic, New York, 2005.
40. Nagano S and Poulos TL, Crystallographic study on the dioxygen complex of wild-type and mutant cytochrome P450cam. Implications for the dioxygen activation mechanism. *J Biol Chem* **280:** 31659-63, 2005.
41. Paine MJ, McLaughlin LA, Flanagan JU, Kemp CA, Sutcliffe MJ, Roberts GC and Wolf CR, Residues glutamate 216 and aspartate 301 are key determinants of substrate specificity and product regioselectivity in cytochrome P450 2D6. *J Biol Chem* **278:** 4021-7, 2003.
42. Lightfoot T, Ellis SW, Mahling J, Ackland MJ, Blaney FE, Bijloo GJ, De Groot MJ, Vermeulen NP, Blackburn GM, Lennard MS and Tucker GT, Regioselective hydroxylation of debrisoquine by cytochrome P4502D6: implications for active site modelling. *Xenobiotica* **30:** 219-33, 2000.
43. de Visser SP and Shaik S, A proton-shuttle mechanism mediated by the porphyrin in benzene hydroxylation by cytochrome P450 enzymes. *J Am Chem Soc* **125:** 7413-24, 2003.
44. Mueller EJ, Loida PJ and Sligar SG, Twenty-five years of P450cam research: mechanistic insigths into catalysis. In: *Cytochrome P450- Structure, mechanism, and biochemistry.* (Ed. Ortiz de Montellano PR), pp. 83-124. Plenum, New York, 1996.
45. de Groot MJ, Donne-Op den Kelder GM, Commandeur JNM, van Lenthe JH and Vermeulen NPE, Metabolite predictions for para-substituted anisoles based on ab initio complete active space self-consistent field calculations. *Chem Res Toxicol* **8:** 437-43, 1995.
46. Hlavica P, Models and mechanisms of O-O bond activation by cytochrome P450. A critical assessment of the potential role of multiple active intermediates in oxidative catalysis. *Eur J Biochem* **271:** 4335-4360, 2004.
47. Chandrasena REP, Vatsis KP, Coon MJ, Hollenberg PF and Newcomb M, Hydroxylation bvy the hydroperoxy-iron species in cytochrome P450 enzymes. *J Am Chem Soc* **126:** 115-126, 2004.
48. Coon MJ, Cytochrome P450: Nature's most versatile biological catalyst. *Annu Rev Pharmacol Toxicol* **45:** 1-25, 2005.
49. Newcomb M, Hollenberg PF and Coon MJ, Multiple mechanisms and multiple oxidants in P450-catalyzed hydroxylations. *Arch Biochem Biophys* **409:** 72-79, 2003.

50. Roberts ES, Pernecky SJ, Alworth WL and Hollenberg PF, A role for threonine 302 in the mechanism-based inactivation of P450 2B4 by 2-ethynylnaphthalene. *Arch Biochem Biophys* **331:** 170-6, 1996.
51. Blobaum AL, Lu Y, Kent UM, Wang S and Hollenberg PF, Formation of a novel reversible cytochrome P450 spectral intermediate: role of threonine 303 in P450 2E1 inactivation. *Biochemistry* **43:** 11942-52, 2004.
52. Wang RW, Newton DJ, Liu N, Atkins WM and Lu AY, Human cytochrome P-450 3A4: in vitro drug-drug interaction patterns are substrate dependent. *Drug Metab Dispos* **28:** 360-6, 2000.
53. Shen L, Fitzloff JF and Cook CS, Differential enantioselectivity and product-dependent activation and inhibition in metabolism of verapimil by human CYP3As. *Drug Metab Dispos* **32:** 186-196, 2004.
54. Ramamoorthy Y, Yu A, Suh N, Haining RL, Tyndale RF and Sellers EM, Reduced (±)-3,4-methylenedioxymethamphetamine ("ecstacy") metabolism with cytochrome P450 2D6 inhibitors and pharmacogenic variants in vitro. *Biochem Pharmacol* **63:** 2111-9, 2002.
55. Stortelder A, Keizers PHJ, Oostenbrink C, de Graaf C, de Kruijf P, Vermeulen NPE, Gooijer C, Commandeur JNM and van der Zwan G, Binding of 7-methoxy-4-(aminomethyl)-coumarin to wild-type and W128F mutant cytochrome P450 2D6 studied by time resolved fluorescence spectroscopy. *Biochem J* **393:** 635-643, 2006.

Part II:

Spectroscopy and modeling of CYP2D6

Chapter 6

Metabolic regio- and stereoselectivity of cytochrome P450 2D6 towards 3,4-methylenedioxy-N-alkyl-amphetamines: in silico predictions and experimental validation

Peter H.J. Keizers*, Chris de Graaf*, Frans J.J. de Kanter, Chris Oostenbrink, K. Anton Feenstra, Jan N.M. Commandeur, and Nico P.E. Vermeulen *contributed equally

adapted from: The Journal of Medicinal Chemistry 2005 **48**: 6117-27

A series of 3,4-methylenedioxy-N-alkylamphetamines (MDAAs) were automatically docked and subjected to molecular dynamics (MD) simulations in a cytochrome P450 2D6 (CYP2D6) protein model. The predicted substrate binding orientations, sites of oxidation, and relative reactivities were compared to experimental data of wild-type and F120A mutant CYP2D6. Automated docking results were not sufficient to accurately rationalize experimental binding orientations of 3,4-methylenedioxy-N-methylamphetamine (MDMA) in the two enzymes as measured with spin lattice relaxation NMR. Nevertheless, the docking results could be used as starting structures for MD simulations. Predicted binding orientations of MDMA and sites of oxidation of the MDAAs derived from MD simulations matched well with the experimental data. It appeared the experimental results were best described in MD simulations considering the nitrogen-atoms of the MDAAs in neutral form. Differences in regioselectivity and stereoselectivity in the oxidative metabolism of the MDAAs by the F120A mutant CYP2D6 were correctly predicted and the effects of the F120A mutation could be rationalized as well.

Introduction

Cytochromes P450 (CYPs) are heme containing enzymes which can be found in virtually all organisms. This large family of enzymes is capable of oxidizing and reducing a broad range of endogenous and exogenous substrates, such as steroids, carcinogens and drugs [1, 2]. In humans one of the most relevant drug metabolizing CYPs is CYP2D6. Although the expression levels of CYP2D6 are only 3% of all hepatic CYPs, following CYP3A4, it is the second most important drug metabolizing enzyme, involved in the metabolism of about 30% of the currently marketed drugs, including β-blockers, neuroleptics, antidepressants and antiarythmics [3-5]. Large interindividual differences exist in CYP2D6 activity, due to gene multiplicity and polymorphisms, thus further increasing its clinical importance [6, 7]. The rationalization and prediction of potential CYP2D6 substrates is therefore advantageous in the discovery and development of new drugs. Nowadays the first crystal structures of mammalian CYPs are becoming available [8-10]. However, so far a crystal structure of CYP2D6 remains to be resolved and any structural information on this enzyme still depends on homology modeling, mutagenesis and spectroscopic studies.

CYP2D6 is one of the CYP isoforms studied most extensively using molecular modeling [11]. Several homology model structures of CYP2D6 have been built, refined and validated experimentally. The homology models of CYP2D6 suggest substrates to interact with two or three aromatic/hydrophobic residues, F120 and F483 and a carboxylic acid residue, E216 or D301 [12, 13]. The relevance of these residues was supported by site-directed mutagenesis studies [14-18]. These interactions are consistent as well with those derived from pharmacophore models of inhibitors and substrates [19, 20]. Molecular modeling can provide information on active site characteristics and the importance of specific amino acid residues in enzyme-substrate interactions, but it can also be used to rationalize and predict regio- and stereoselectivity in metabolism by CYPs. It has recently also been shown that automated docking can successfully be applied to predict sites of oxidation in substrates using CYP crystal structures [21]. Molecular Dynamics (MD) simulations in addition can account for distributions of multiple binding conformations and thus give a more comprehensive description of multiple sites of oxidation in substrates catalyzed by CYPs [22-25].

In this study a molecular modeling approach has been used to study the binding orientation and the sites of oxidation of a series of 3,4-methylenedioxy-N-alkylamphetamines (MDAAs), or XTC analogues, by CYP2D6. The primary aim was to evaluate an integrated molecular modeling approach to rationalize and predict substrate binding and metabolism by CYP2D6. When regioselectivity and stereoselectivity in drug metabolism, and the effect of active site mutations can be rationalized for a series of closely related compounds, such an approach can be considered as accurate and reliable. The molecular modeling predictions were based on a homology model of CYP2D6. Reactive substrate poses were generated using automated docking and were obtained from MD simulations of wild-type and mutant CYP2D6 protein containing all three MDAAs. Two different protonation states of the basic nitrogen-atom were studied, as it is known that this can drastically influence the oxidation by CYP2D6 [26]. These computational predictions were validated experimentally. The effects of mutating F120 into alanine on the binding modes and metabolic products were studied for five MDAAs, i.e. 3,4-methylenedioxy-N-methylamphetamine (MDMA) and its stereoisomers, 3,4-methylenedioxy-N-ethylamphetamine (MDEA) and 3,4-methylenedioxy-N-propylamphetamine (MDPA). For the recently described F120A mutant large effects on the regioselective oxidation of MDMA were demonstrated [16]. Dissociation constants for the three MDAAs were determined by spectral titration. The metabolic products were analyzed and furthermore, the binding orientations of MDMA in the wild-type and mutant

active sites were explored experimentally by NMR spin lattice relaxation rate measurements, a technique previously used to determine hydrogen atom to heme distances in CYPs [27-30].

Materials and Methods

Materials

The pSP19T7LT plasmid containing human 2D6 with a C- terminal His_6-tag bicistronically co-expressed with human NADPH-cytochrome P450 reductase was kindly provided by Prof. Dr. Ingelman-Sundberg. 3,4-methylenedioxy- N-alkylamphetamines (MDAAs) were synthesized as described before [31, 32]. *S*- and *R*-MDMA.HCl were obtained from the division of Neurioscience and Behavioral Research of the National Institute on Drug Abuse (Bethesda, MD USA). Emulgen 911 was obtained from KAO Chemicals (Tokyo, Japan). Ni-NTA-agarose was from Qiagen (Westburg, Leusden, The Netherlands). All other chemicals were of analytical grade and obtained from standard suppliers.

Expression and purification of CYP2D6

Both the F120A mutant and the wild-type pSP19T7LT plasmids were transformed into *Escherichia coli,* strain JM109. Expression and membrane isolation was carried out as described [16]. Membranes were resuspended in 0.4% of the original culture volume of KPi-glycerol buffer (50 mM potassium phosphate buffer, pH 7.4, 10% glycerol) and CYP contents were determined by CO difference spectra [33]. Enzymes were solubilized from membranes by stirring in KPi-glycerol supplemented with 0.5% Emulgen 911 for 2 h at 4°C. Insoluble parts were removed by centrifugation (60 min, 120,000 g at 4 °C). The supernatant was incubated, gently rocking, with Ni-NTA agarose for 30 min at 4 °C. The Ni-NTA agarose was retained in a polypropylene tube with porous disc (Pierce, Perbio Science, Ettenleur, The Netherlands), washed with KPi-glycerol buffer containing 2 mM histidine. CYP2D6 was eluted with 0.2 M histidine. After overnight dialysis in KPi-glycerol buffer the sample was concentrated on a Vivaspin 20 filtration tube (10.000 MWCO PES, Sartorius, Nieuwegein, The Netherlands). For NMR spin lattice relaxation rate measurements the buffer was exchanged for deuterated KPi-glycerol buffer by repeated rounds of adding a larger volume of deuterated buffer and concentrating. Deuterated KPi-glycerol buffer was made by repeated rounds of evaporating water or D_2O from a KPi buffer and dissolving the residue again in D_2O. Then 5% of glycerol was added and traces of iron were removed with Chelex 100 (Biorad, Richmond CA).

Optical titrations

Dissociation constants of substrates to the enzymes were determined by spectral titration, according to the method of Jefcoate [34, 35]. Spectra were taken at room temperature on a Pharmacia Ultrospec 2000 spectrometer. In short, 1 ml of 0.5 μM purified enzyme in KPi-glycerol buffer was divided over two cuvettes, to the first 5 μl of a 1 mM solution of compound in the same buffer was added, to the second the same volume of just buffer. Difference spectra from 350 to 450 nm were taken before, and after each addition of compound. The difference in absorbance at 390 and 425 was plotted against the substrate concentration to estimate the dissociation constant (K_s) using Equation (1) in Graph Pad Prism 4.0 software, where B is the absorbance difference (390-425), B_{max} is the absorbance difference when [S] = ∞.

$$B = \frac{B_{max}[S]}{K_s + [S]} \qquad (1)$$

Metabolism of MDAAs

Metabolic reactions were carried out in 200 μl 50 mM KPi pH 7.4, 5 mM $MgCl_2$ supplemented with 10 concentrations ranging from 0 to 200 μM of one of the MDAAs and *E. coli* membranes corresponding to 25 nM wild-type or F120A mutant CYP2D6. After 5 min of pre-incubation at 37 °C, the reactions were initiated with an NADPH regenerating system, resulting in final concentrations of 0.2 mM NADPH, 0.3 mM glucose-6-phosphate, and 0.4 units/ml glucose-6-phosphate dehydrogenase. The reaction was allowed to proceed for 10 min before it was stopped by the addition of 20 μl 23% $HClO_4$. After centrifugation (10 min, 6800 g), 30 μl aliquots of the supernatant were analyzed by HPLC. To measure

O-demethylenation, analytes were separated isocratically using a C18 column (Phenomenex Luna 5u 150 x 4.6) with a mobile phase consisting of 22% acetonitrile (ACN) and 0.1% triethylamine, set to pH 3 with $HClO_4$ at a flow rate of 0.6 ml/min. Other oxidation products were found using the same column with a gradient (A: 5% ACN with 20 mM ammonium acetate, B: 90% ACN with 10 mM ammonium acetate). All oxidation products were detected by fluorescence (λ_{ex}= 280 nm, λ_{em}= 320 nm) and identified by LC-MS. Peak areas of all products were quantified by Shimadzu Class VP 4.3 software and analyzed using non linear regression with one site binding in Graph Pad Prism 3.0.

LC-MS
To identify the metabolic products of the MDAAs, incubations were carried out for 15 min as described above with 100 μM of MDMA, MDEA or MDPA and *E. coli* membranes corresponding to 50 nM wild-type or F120A CYP2D6. Volumes of 100 μl supernatant were injected and separated using a C18 column (Phenomenex Luna 5u 150 x 4.6) with a flow rate of 0.6 ml/min and analyzed by MS. The analytes were eluted using a gradient starting with a 5% ACN eluens, supplemented with 20 mM ammonium acetate for 7 min, then increasing linearly to 90% ACN with 10 mM ammonium acetate in 14 min and kept there for 5 min. APCI positive ionization was used on a LCQ Deca mass spectrometer (Thermo Finnigan, Breda, The Netherlands), vaporizer temperature 450 °C, N_2 as sheath (40 psi) and auxiliary gas (10 psi), needle voltage 6000 V, heated capillary 150 °C.
Products of MDMA metabolism: 3,4-OH-MA (t_R: 9.5 min., *m/z* 182, MS/MS: *m/z* 151), MDA (t_R: 17.0 min., *m/z* 180, MS/MS: *m/z* 163) and N-OH-MDMA (t_R: 20.4 min., *m/z* 210, MS/MS: *m/z* 163). Products of MDEA metabolism: 3,4-OH-EA (t_R: 13.0 min., *m/z* 196, MS/MS: *m/z* 151), MDA (t_R: 17.0 min., *m/z* 180, MS/MS: *m/z* 163) N-OH-MDEA (t_R: 21.6 min., *m/z* 224, MS/MS: *m/z* 163) a fourth product was detected for the mutant (t_R 18.5 min., *m/z* 222, MS/MS: *m/z* 163). Products of MDPA metabolism: 3,4-OH-PA (t_R: 16.0 min., *m/z* 210, MS/MS: *m/z* 151), MDA (t_R: 17.0 min., *m/z* 180, MS/MS: *m/z* 163), N-OH-MDPA (t_R: 23.4 min., *m/z* 238, MS/MS: *m/z* 163) a fourth product was detected for the mutant (t_R: 19.2 min *m/z* 254, no fragmentation observed).

NMR spin lattice relaxation rate measurements
Distances from substrate hydrogen atoms to the enzyme heme iron atom were calculated from their longitudinal relaxation rates determined using ^{1}H NMR [27-30]. ^{1}H NMR measurements were performed on a Bruker Avance 400 MHz spectrometer, signals were referenced to HDO at 4.75 ppm. Longitudinal relaxation times (T_1) of substrate hydrogen atoms were measured with a standard inversion recovery sequence of 180°-τ-90°. The spectra were recorded with 20 values of τ, ranging from 0.1 to 12.5 s and a relaxation delay of 5-10 x T_1. The temperature was kept at 300 K, except for the variable temperature experiments. T_1 was determined by plotting peak areas against delay times τ and exponential fitting (I_t = A +$Be^{-\tau/T_1}$) with Bruker XWINNMR software. The measured T_1 was transformed into the longitudinal paramagnetic relaxation rate (R_{1P}) according to equation 2.

$$R_{1P} = (T_{1,Fe^{3+}})^{-1} - (T_{1,Fe^{2+}+CO})^{-1} \quad (2)$$

Where $T_{1,Fe^{3+}}$ is the relaxation time of substrate hydrogen atoms in the presence of ferric enzyme, and $T_{1,Fe^{2+}+CO}$ is the relaxation time in the presence of ferrous CO-bound enzyme. The hydrogen atoms to iron atom distance, r^{NMR} can be calculated from R_{1P} using the simplified Solomon and Bloembergen equation [27, 36] (Equation 3).

$$r^{NMR} = C(\alpha R_{1P} F(\tau_c))^{1/6} \quad (3)$$

Where C is a constant taking into account the spin state as well as other nuclear and electronic factors, with a value of 813 for high spin CYP, [30] α is the fraction of enzyme bound substrate, determined as the ratio of the concentration of enzyme and the sum of the substrate concentration and its spectral dissociation constant (K_s). F(τ_c) is a function of the correlation time τ_c, for which the value of $3x10^{-10}$ s is taken, as determined for CYP2D6 by others [28]. In the calculations of hydrogen atoms to heme distances, according to eqs. 2 and 3, the assumption has been made that on the NMR time-scale there

is a fast exchange between substrate molecules in solution and in the enzyme active site. This was verified by measuring the temperature dependence of $1/T_1$, which should show a linear increase with the reciprocal value of the temperature [29, 30].
In a typical experiment 5 μM of enzyme and 20 mM of substrate was used in a volume of 500 μl. Recording the spectra for relaxation times determination with oxidized enzyme took about an hour, then sodium dithionite was added and the sample was treated for 30 sec with CO to do the measurements with the reduced CO-bound enzyme.

Homology modeling
A protein homology model of CYP2D6 was constructed based on the crystal structures of dimethylsulphophenazole derivative and diclofenac bound rabbit CYP2C5 (PDB codes 1N6B and 1NR6, respectively) [37, 38]. Homology modeling, model refinement and model validation was performed according to the approach described previously [12]. In short, a hundred CYP2D6 models were generated with the restraint-based comparative modeling program Modeller [39], using the same amino acid alignment as before [12]. Subsequently, three models were selected with the best loop conformations as determined by visual inspection, stereochemical parameters using PROCHECK [40], and side-chain environment using Errat [41], and Verify3D [42]. Homology models had approximately the same protein quality check scores as the crystal structure templates. Finally, one single model was selected which could accommodate codeine best in the experimental binding orientation [28]. This final model was validated on its ability to reproduce substrate binding orientations corresponding to metabolic profiles with AutoDock [43], FlexX [44], and GOLD [45] automated docking studies (de Graaf, unpublished results). The final model of wild-type CYP2D6 was used as a template for modeling of the F120A mutant. The Phe residue at position 120 was mutated to Ala using the homology module of Insight II (Biosym. San Diego, USA), after which an energy minimization and a 1 ps MD simulation with position restraints on the protein backbone was carried out as described under *"MD Simulations"*.

Automated docking studies
The *R-*, and *S-*enantiomers of MDMA, MDEA and MDPA in their neutral (basic) and charged (acidic) forms were docked into the active site of the CYP2D6 homology model using AutoDock and GOLD. Active site water molecules, predicted using a protocol based on the program GRID [46], and a ligand-based cut off were included. The preparation of enzyme and substrate structures in the automated docking studies were performed using default settings and predicted water molecules as described before [21]. For each substrate, 50 independent AutoDock and GOLD docking runs were performed using default parameter values. Docking poses generated by both docking algorithms were clustered (maximum root-mean square differences between members of the cluster of 1 Å) and re-scored with the SCORE scoring function [47]. The three energetically most favorable, distinct docking poses of each MDAA species were selected as starting structures for MD calculations, yielding in total 12 (3 docking poses times 2 enatiomers, times 2 protonation states) simulations for each substrate in both wild-type and F120A mutant CYP2D6.

MD simulations
Substrate conformations selected from the automated docking studies were used as starting structures for MD simulations, using the GROMACS molecular simulation package [48] and the GROMOS-96 force field, parameter set 43A1 [49, 50]. Heme parameters were taken from this parameter set, and additionally, a covalent bond was defined between the heme iron atom and the sulfur atom of C443 with an ideal bond distance of 0.240 nm. The enzyme including substrate and heme, was energy minimized in vacuum using the steepest descent method, first with harmonic position restraints using a force constant of 1000 kJ mol^{-1} nm^{-2} on all non-hydrogen atoms, then without position restraints. Subsequently, pre-equilibrated water was added in a dodecahedral box with a minimum distance of 1 nm between the enzyme and box edges, followed by minimization. The water was allowed to relax for 1 ps, while the whole enzyme was position restrained. Then, first only the side chains of the residues not involved in substrate binding were released for 1 ps, next also the backbone of these residues for 10 ps. Finally, only the backbone of the binding residues were restrained for 100 ps. The equilibration scheme was followed by an unrestrained 10 ns MD production run. MD simulations were carried out with a time step of 2 fs, a twin range cut-off of 0.8/1.4 nm and a relative dielectric constant of 1.0. The

LINCS algorithm was used to constrain the length of all covalent bonds [51]. Pressure was maintained at 1 bar and temperature at 300° K by weak coupling to an external bath [52], with relaxation times of 0.1 and 1.0 ps respectively. Coordinates were saved at a 1.0 ps interval for subsequent analysis. Enzyme-substrate interactions were estimated using the SCORE scoring function and averaged over the trajectories.

Analysis of MD simulations
Hydrogen atoms to iron atom distances r^{MD} for different protonation states of the MDAA enantiomers were derived from MD simulations by averaging distances (r) observed in the three independent simulations with different starting positions as:

$$r^{MD} = (\langle r^{-6} \rangle)^{-1/6} \quad (4)$$

These distances could directly be compared to the experimentally obtained distances r^{NMR}, (Equation 3). Sites of oxidation were predicted based on enzyme-substrate conformations generated by automated docking and MD simulations. Distances of 6.0 Å or less between the heme iron and an atom in the substrate (e.g. corresponding to O-demethylenation, N-dealkylation, N-hydroxylation, or ω-hydroxylation) were considered as reactive in the sense that activation of the C-H bond by the heme-Fe-O moiety is possible [53]. Site of oxidation predictions were performed to determine both substrate reactivity (expressed in the number of reactive MD configurations out of the total) and regioselectivity. The catalytic regioselectivity was calculated by determining which site of oxidation was closest to the heme iron atom for each reactive docking pose or MD configuration. Enzyme-substrate interactions during the MD simulations were monitored in terms of the occurrence of atom-atom distances of 3.5 Å or less between the F/A120 side-chain and the MDAA ring system (representing aromatic/van der Waals interactions) and hydrogen bonds between the E216 carboxylate oxygen atoms and the MDAA N-atom. Substrate reactivity, regioselectivity and enzyme substrate interactions were calculated for any given protonation state, stereo- and regio-isomer, as a Boltzmann weighted average over the three independent MD simulations with different substrate starting orientations. The average of an individual simulation i was weighted by a relative probability p_i, which was calculated from the average enzyme substrate interaction estimates as obtained from the program SCORE (E^i_{SCORE}). In this equation, k_B is the Boltzmann constant (8,3441 kJ mol^{-1} K^{-1}) and T is the temperature (300 K).

$$p_i = (e^{-\Delta E^i_{SCORE}/k_B T}) / (\sum_i e^{-\Delta E^i_{SCORE}/k_B T}) \quad (5)$$

Results

Expression and purification of wild-type and F120A mutant CYP2D6
The expression levels of both wild-type and F120A mutant CYP2D6 were similar as described previously [16]. The enzymes which contained a C-terminal 6 x histidine tag were purified using Ni-NTA-agarose. Eluting the enzymes from the Ni-NTA-agarose using imidazole led to a shift of the Soret absorbance band to 422 nm, apparently due to heme ligation of the imidazole. Even after overnight dialysis, the Soret peak remained shifted to the red. Therefore 0,2 mM *L*-histidine was preferred as eluting agent over imidazole, because it did not cause a change in spin state after dialysis, yielding pure enzymes which were stable for at least four hours at 24° C in the presence of 5% glycerol and 100 μM of substrate as assessed by CO-difference spectroscopy. Hardly any P420 (i.e. inactive CYP detected as an absorbance maximum at 420 nm in the CO-difference spectrum) was present in the batches of purified enzyme.

Spectral titration of substrates to the enzymes
The addition of all MDAAs to purified wild-type or F120A mutant CYP2D6 led to a type I change in the visible absorbance spectrum. By titration of the compounds to the solutions of enzyme the spectral dissociation constants K_s could be estimated (using Equation 1, data

shown in Table 1). While there were minor differences in affinity between the wild-type and the mutant, for both enzymes a slightly lower K_s was found for MDEA and MDPA than for MDMA. The enantiomers of MDMA had about equal affinity for the wild-type, but a slight preference towards *S*-MDMA was observed for the mutant enzyme.

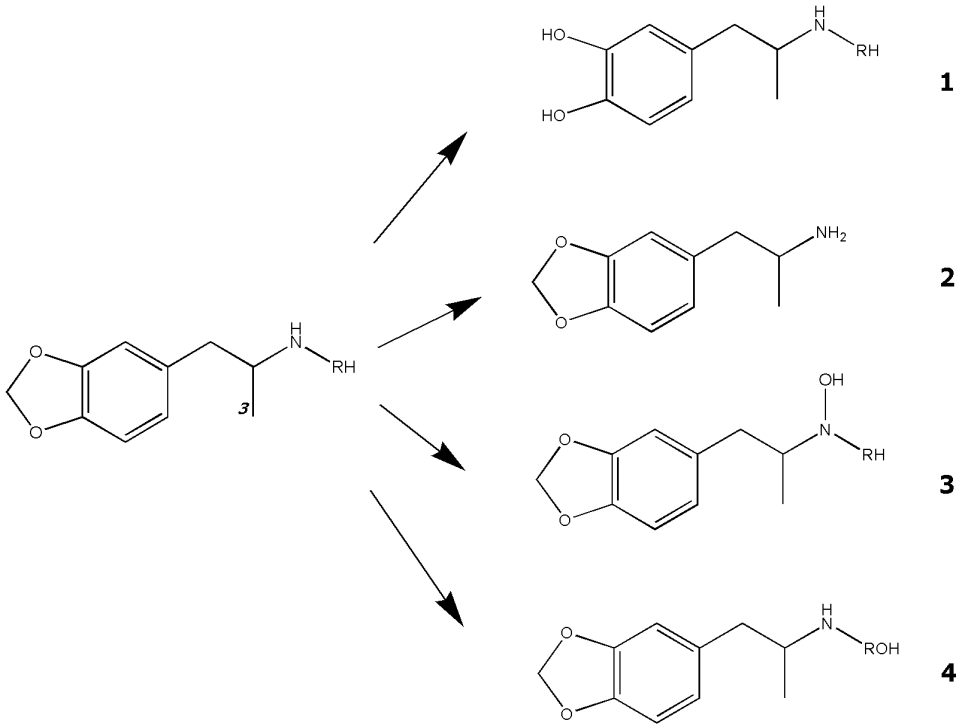

Figure 1: Scheme of 3,4-methylenedioxy-N-alkylamphetamines (MDAAs) oxidation by F120A mutant CYP2D6. The MDAAs are O-demethylenated to 3,4,-dihydroxy-N-alkylamphetamine (1), N-dealkylated to 3,4-methylenedioxyamphetamine (2), N-hydroxylated to 3,4-methylenedioxy-N-hydroxy-N-alkylamphetamine (3) or ω/ω-1-hydroxylated to 3,4-methylenedioxy-ω/ω-1-hydroxy-N-alkyl-amphetamine (4). The C3 methyl is indicated, R is methyl, ethyl and propyl for MDMA, MDEA and MDPA respectively.

Table 1: Estimated dissociation constants, K_s, (μM) of the substrates for wild-type and F120A mutant CYP2D6.

Substrate	K_s	
	Wild-type	F120A
R/S-MDMA	28 ± 3	28 ± 2
R-MDMA	43 ± 6	53 ± 2
S-MDMA	40 ± 5	38 ± 4
MDEA	19 ± 2	15 ± 4
MDPA	18 ± 1	12 ± 2

All values are the means ± S.D. of at least two independent experiments as described in the Methods section. R/S-MDMA refers to the racemic mixture of 3,4-methylenedioxy-N-methylamphetamine (MDMA), R-MDMA and S-MDMA to the pure R- and S-isomer of MDMA respectively. For the corresponding N-ethyl and N-propyl amphetamines (MDEA and MDPA) racemic mixtures were used.

Metabolism of MDAAs

As reported previously [16], MDMA is oxidized by the F120A mutant to MDA and N-OH-MDMA, in addition to 3,4-OH-MA, the only product formed by the wild-type enzyme (Figure 1). Elongation of the N-methyl chain to an ethyl or propyl yielded the corresponding products after incubation with both enzymes. MDEA was O-demethylenated by wild-type and mutant CYP2D6 and additionally the mutant N-dealkylated and N-hydroxylated MDEA. A fourth oxidation product of MDEA by the mutant was detected at t_R 18.5 min, with a *m/z* of 222, fragmenting to *m/z* 163. This product could be the aldehyde- or keto-form of ω- or ω-1-hydroxylation respectively.

Table 2: Product formation of MDAAs oxidation by wild-type and F120A mutant CYP2D6.

Substrate	Product	Structure	Wild-type		F120A	
			K_m	V_{max}	K_m	V_{max}
R/S-MDMA	3,4-OH-MA	1	1.9 ± 0.5	1.2 ± 0.4[a]	11.8 ± 3.8	2.2 ± 0.0[a]
	MDA	2	- [c]	- [c]	14.5 ± 2.4	3.5 ± 0.1[b]
	N-OH-MDMA	3	- [c]	- [c]	11.2 ± 1.4	7.1 ± 0.5[a]
R-MDMA	3,4-OH-MA	1	2.7 ± 0.4	1.2 ± 0.2[a]	13.2 ± 0.6	2.4 ± 0.1[a]
	MDA	2	- [c]	- [c]	26.1 ± 3.3	5.9 ± 0.7[b]
	N-OH-MDMA	3	- [c]	- [c]	20.6 ± 2.5	10.7 ± 1.3[a]
S-MDMA	3,4-OH-MA	1	3.3 ± 0.5	1.2 ± 0.0[a]	4.9 ± 0.1	2.4 ± 0.0[a]
	MDA	2	- [c]	- [c]	10.3 ± 0.6	3.8 ± 0.1[b]
	N-OH-MDMA	3	- [c]	- [c]	6.9 ± 0.6	8.4 ± 0.4[a]
MDEA	3,4-OH-EA	1	1.1 ± 0.1	1.2 ± 0.2[a]	3.3 ± 0.0	2.9 ± 0.2[a]
	MDA	2	- [c]	- [c]	4.5 ± 0.8	4.2 ± 0.1[b]
	N-OH-MDEA	3	- [c]	- [c]	5.7 ± 0.3	1.4 ± 0.1[a]
MDPA	3,4-OH-PA	1	1.0 ± 0.1	1.3 ± 0.1[a]	5.2 ± 0.6	7.5 ± 0.6[a]
	MDA	2	- [c]	- [c]	9.1 ± 0.5	7.3 ± 1.8[b]
	N-OH-MDPA	3	- [c]	- [c]	28.0 ± 6.5	3.0 ± 0.2[a]

All values are the means of at least two independent experiments ± S.D. as described in the Methods section. Structure numbers refer to products drawn in Figure 1, K_m expressed in μM, [a] V_{max} expressed in 1 x 10^6 fluorescence units/min/nmol CYP, [b] V_{max} expressed in min^{-1}, [c] not observed.

MDPA was O-demethylenated by wild-type and the mutant CYP2D6, the latter enzyme also N-dealkylated and N-hydroxylated this substrate. A peak with *m/z* of 254 was found at 19.2 min with the mutant, indicating a double hydroxylation. No fragmentation took place so the positions of the hydroxyl groups remain unknown.

Product formation from all substrates was linear for at least 10 min for both enzymes under the conditions used, and the kinetic parameters were determined for the major products (Table 2). The overall rate of oxidation by the F120A mutant was higher than that of wild-type CYP2D6 for all MDAAs. The rates for O-demethylenation were two to five-fold higher for the mutant and the fact that more products are formed indicate an even higher increase in oxidation rates. To quantify the turnover rates, synthetic reference compound was only available for MDA, for the other products turnover rates were only compared in relative terms.

Because the fluorescence peak areas of equal concentrations of MDA, MDMA, MDEA and MDPA are equal, it is likely that the N-alkyl chain has no influence on the fluorescence yield of the compounds, and therefore it is reasonable this holds true for the O-demethylenated and N-hydroxylated products of the MDAAs as well.
The turnover rates of MDMA, MDEA and MDPA were equal for wild-type CYP2D6 (Table 2). The catalytic efficiency (V_{max}/ K_m) indicated that MDPA is oxidized most efficient and MDMA the least efficient (Figure 2A). The mutant showed a higher catalytic efficiency in O-demethylenating MDPA over MDMA and MDEA, while the efficiency in N-hydroxylation was the highest for MDMA (Figure 2B-D). MDEA and MDPA were N-dealkylated more efficiently than MDMA. So elongation of the N-alkyl chain leads to an altered catalytic regioselectivity by the mutant enzyme.
Stereoselectivity in MDMA oxidation by wild-type CYP2D6 was hardly found (Figure 3). However, the mutant enzyme showed at least two-fold lower K_m values for all three products of *S*-MDMA when compared to *R*-MDMA, while the V_{max} values for the products of both enantiomers did not differ (Table 2). Eventually these changes lead to a different product ratio for the enantiomers: O-demethylenation is more prominent for *S*-MDMA then for *R*-MDMA, followed by N-hydroxylation and N-dealkylation (Figure 3).

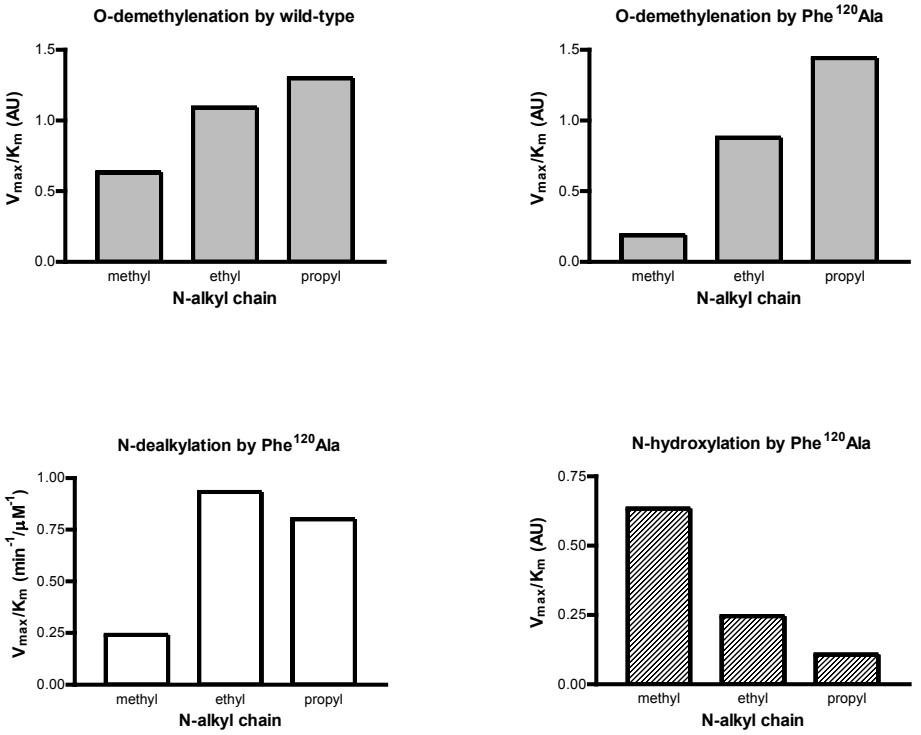

Figure 2: V_{max} / K_m product ratio's ($min^{-1} \cdot \mu M^{-1}$ for N-dealkylation, AU for the other products) for the O-demethylenation by wild-type (grey left), and O-demethylenation (grey right), N-dealkylation (blank) and N-hydroxylation (diagonal stripe) by F120A mutant CYP2D6 of the different MDAAs.

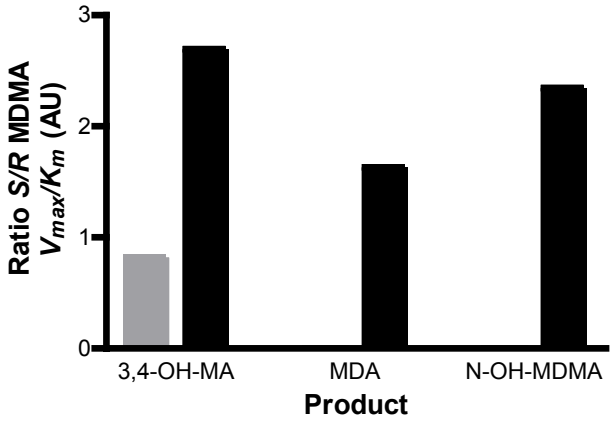

Figure 3: Ratio's of S-MDMA catalytic efficiency (V_{max} / K_m) over R-MDMA catalytic efficiency (V_{max} / K_m) by wild-type (in gray), and by F120A mutant CYP2D6 (in black) for the products 3,4,-dihydroxy-N-alkylamphetamine (3,4-OH MA), 3,4-methylenedioxyamphetamine (MDA) and 3,4-methylenedioxy-N-hydroxy-N-alkylamphetamine (N-OH-MDMA).

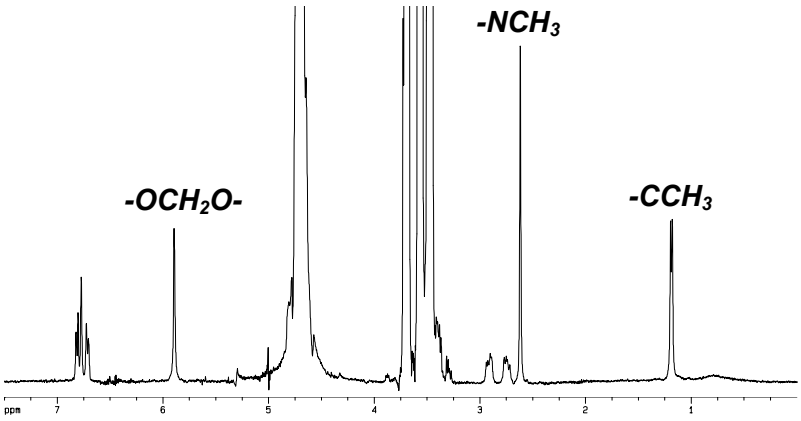

Figure 4: ^{1}H NMR spectrum of 20 mM R-MDMA in deuterated Kpi-glycerol in presence of 5 µM F120A mutant CYP2D6 showing the resonance assignments.

NMR spin lattice relaxation rate measurements

Enzyme bound MDMA hydrogen atom to heme iron distances were determined by spin lattice relaxation NMR to validate the computationally predicted distances. The ^{1}H-NMR spectrum of MDMA in presence of glycerol and each of the two enzyme was well resolved, all signals of the different hydrogen atoms were clearly visible (Figure 4). Because the doublet of the *C3* methyl (δ 1.18 ppm), and the singlets of the N-methyl (δ 2.61 ppm), and methylene (δ 5.89 ppm) hydrogen atoms could be best quantified and are the most distal groups in MDMA, these were used to determine the substrate orientation in the active site

of the two enzymes. An increase in T_1 of the MDMA hydrogen atoms was found after reducing the enzymes with dithionite, indicating that the paramagnetic effect of the enzymes was diminished. From the T_1 the distances from the methylene, *C3* and N-methyl hydrogen atoms to the heme iron atom were calculated (using Equation 2) and tabulated (in Table 3). The fast exchange condition (see Methods section) was validated, by measuring the temperature dependence of R_{1P} from 281° K to 307° K (Figure 5). For the three groups of hydrogen atoms studied, there was a linear increase of R_{1P} with the reciprocal temperature (1/T), showing that the exchange between substrate molecules in the enzyme active site and in solution is fast on the NMR timescale. Only minor differences were observed for the hydrogen atoms to iron distances, between the enantiomers of MDMA and each of the two enzymes. The measured hydrogen atoms to iron distances indicate that the methylene moiety is closest to the heme iron, at about 6.4 Å, the N-methyl is the most distal to the heme at about 7.3 Å and the *C3* hydrogen atoms are at a distance of about 6.7 Å.

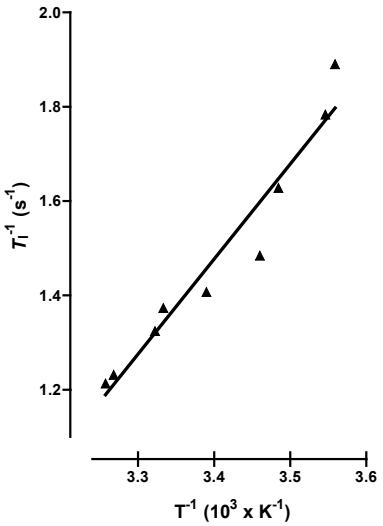

Figure 5: Temperature dependence of T_1 relaxation rates for the hydrogen atoms of N-methyl (δ 2.61) of +/- MDMA in wild-type CYP2D6. The positive slope indicates that the fast exchange condition is satisfied.

Automated docking studies

All automatically docked poses of the MDAAs, in two protonation states and in both enzymes were found to be predominantly within a reactive distance of 6 Å from the heme iron atom (69% and higher, Table 4A). Of these reactive poses, the large majority corresponded to O-demethylenation (62-100%). The relative occurrence of docking poses corresponding to N-dealkylation (0-38%) and N-hydroxylation (0-13%) of the MDAAs was found to be enzyme, stereoisomer, and protonation state dependent. In both enzymes, the neutral forms of the compounds showed the widest range of reactive substrate orientations, whereas the wild-type allowed for more diversity. This observation is in contrast with the experimental finding that wild-type CYP2D6 only catalyzes O-demethylenation, while the F120A mutant allows for alternative product formation.

Three distinct, energetically most favorable automatically docked poses were selected of all MDAAs as starting conformations for MD calculations, an example of charged *R*-MDMA being shown (Figure 6). These three distinct docked poses could be generally described as one binding orientation corresponding to O-demethylenation, with the substrate nitrogen atom in close contact with E216 (pose 1, generated by AutoDock), another corresponding to O-demethylenation, with the substrate nitrogen atom placed between E216 and D301 (pose 2, generated by GOLD) and one corresponding to N-dealkylation or N-hydroxylation (pose 3, generated by AutoDock). In cases where pose 3 was not observed for the substrate in the charged form (see Table 4A), the corresponding pose of the neutral state was protonated and taken as starting conformation for MD simulations.

Table 3: Hydrogen atom to heme iron distances (Å) of the MDMA enantiomers to wild-type and F120A mutant CYP2D6 as determined by NMR spin lattice relaxation rate measurements and by molecular dynamics (MD) simulations of neutral and charged MDMA.

Position		wild-type		F120A	
		R-MDMA	*S*-MDMA	*R*-MDMA	*S*-MDMA
Methylene	NMR	6.4	6.3	6.4	6.5
(δ 5.89 ppm)	MD (charged)	3.5	3.6	4.6	3.1
	MD (neutral)	4.3	4.5	5.0	5.5
N-methyl	NMR	7.3	7.2	7.5	7.2
(δ 2.61 ppm)	MD (charged)	11.0	10.1	10.1	9.4
	MD (neutral)	5.9	6.5	8.4	6.0
C3	NMR	6.9	6.7	6.6	6.7
(δ 1.18 ppm)	MD (charged)	11.8	11.0	8.7	11.5
	MD (neutral)	5.3	6.6	6.9	6.5

NMR derived values are the means of at least two independent measurements with S.D. less then 5%, as described in the Materials and Methods. MD simulations derived values are averaged over time and for three individual runs, starting from different docking poses, according to equation 4.

MD simulations

Simulations of the enzymes with substrates bound in the active site, starting from the three different automatically docked poses, remained stable during 10 ns unrestraint MD at 300° K, with final atom-positional root-mean-square deviation values of 1.3 to 3.8 Å. Throughout the simulations structure determining hydrogen-bonds were observed and the majority of the orientations of the substrates in the enzymes were within a reactive distance to the iron atom (74% and higher, Table 4B). The substrates appeared to have considerable freedom within the binding site. Complete reorientation from the initial coordinates was frequently observed, indicating that the unrestrained MD simulations sampled the substrate conformational space sufficiently. The distances between substrate hydrogen atoms and the heme iron atom of wild-type and F120A mutant CYP2D6 were derived for the two different protonation states of the MDMA enantiomers, by averaging the distances over the three simulations (using Equation 4) and these were subsequently compared to experimentally determined distances (Table 3). Relatively large differences in averaged hydrogen atom to iron distances were found within individual MD simulations starting from different substrate docking poses. However, averaged distances of individual MD simulations of the same protonation state and starting from the same docking pose, were approximately equal.

Table 4: Distributions of substrate orientations corresponding to specific sites of oxidation (in %), according to automated docking studies (A) and MD simulations (B).

A

Substrate			wild-type					F120A				
			reactive	ODM	NDM	NOH	ωOH	reactive	ODM	NDM	NOH	ωOH
MDMA	*R*	H^+	100	100	0	0	-	100	100	0	0	-
		n	88	86	10	4	-	93	90	3	7	-
	S	H^+	92	100	0	0	-	100	100	0	0	-
		n	99	73	14	13	-	80	99	0	1	-
MDEA	*R*	H^+	91	99	1	0	0	100	99	1	0	0
		n	100	91	9	0	0	100	98	2	0	0
	S	H^+	69	99	1	0	0	100	99	1	0	0
		n	99	78	22	0	0	100	93	7	0	0
MDPA	*R*	H^+	70	79	21	0	0	99	99	1	0	0
		n	92	62	38	0	0	100	97	3	0	0
	S	H^+	74	100	0	0	0	95	62	38	0	0
		n	82	99	1	0	0	100	73	27	0	0

B

Substrate			wild-type					F120A				
			reactive	ODM	NDM	NOH	ωOH	reactive	ODM	NDM	NOH	ωOH
MDMA	*R*	H^+	97	100	0	0	-	89	100	0	0	-
		n	77	83	3	12	-	96	69	3	28	-
	S	H^+	99	100	0	0	-	100	100	0	0	-
		n	80	88	1	11	-	92	64	23	13	-
MDEA	*R*	H^+	74	99	0	0	1	64	99	0	0	1
		n	95	85	2	2	11	93	71	18	9	2
	S	H^+	100	100	0	0	0	76	100	0	0	0
		n	82	92	2	6	0	79	61	32	5	2
MDPA	*R*	H^+	97	100	0	0	0	99	100	0	0	0
		n	97	100	0	0	0	100	58	22	1	20
	S	H^+	100	100	0	0	0	98	100	0	0	0
		n	100	100	0	0	0	98	99	1	0	0

The columns 'reactive' indicate the percentage of all binding orientations that displayed a site of oxidation within 6 Å of the heme iron. The subsequent columns show the distribution of the reactive conformations for the different sites of oxidation, corresponding to O-demethylenation (ODM), N-demethylation (NDM), N-hydroxylation (NOH), and 'omega-hydroxylation' (ωOH). The automated docking studies are based on 50 independent AutoDock and GOLD docking runs, the MD simulations are Boltzmann weighted averages over three independent simulations, starting from three different docking poses. Substrates were simulated in neutral (n) and charged (H^+) form.

An exception was the difference in averaged distance of the methylenedioxy hydrogen atoms of both neutral MDMA enantiomers in simulations starting from pose 3 (corresponding to N-demethylation/hydroxylation) in wild-type CYP2D6 (~ 7.5 Å) compared to the F120A mutant (~ 11.0 Å). Also the averaged distances derived from all three simulations of individual protonation states were approximately the same for the different MDMA enantiomers in wild-type and F120A mutant CYP2D6. The averaged hydrogen atom to heme iron distances of the neutral MDMA enantiomers agreed well with the distances determined by NMR spin lattice relaxation rate measurements. Apparently, considering the substrates to be neutral describes the experimental situation best. With the exception of the N-methyl and *C3* hydrogen atoms of *R*-MDMA in the F120A mutant, all hydrogen atom to heme iron distances calculated from MD simulations of neutral MDMA enantiomers were shorter than the experimentally derived distances. The methylenedioxy hydrogen atom to heme iron distances were slightly lower than those of the N-methyl and *C3* hydrogen atoms. In contrast, the averaged N-methyl and *C3* hydrogen atom to heme iron distances of the charged MDMA enantiomers violated the experimental distances consistently.
For all MDAAs, differences between the averaged enzyme-substrate interaction energies calculated using SCORE, were within 3 kJ/mol (~kT) for all three MD simulations of the same protonation states and within 5 kJ/mol for all six MD simulations. The relative weights of the MD simulations of the three starting orientations used in the Boltzmann averaging (Equation 5, see Methods section) over the simulations ranged between 0.11 and 0.54.
Already during the equilibration time, or soon after the start of the MD simulations with charged MDAAs, reorientation of pose 3 (corresponding to N-demethylation) into pose 1 (corresponding to O-demethylenation) occurred. In the case of MDEA, this led to non-reactive binding orientations outside of the binding pocket, forming a hydrogen bond between its protonated nitrogen and the carboxylate group of E216 (Table 4B and Figure 6). Relatively high probabilities of O-demethylenation poses were found for neutral MDAAs (>58%), although orientations corresponding to N-demethylation/hydroxylation were also observed, except for MDPA in wild-type CYP2D6. N-demethylation or N-hydroxylation of neutral MDAAs had significant higher probabilities in the F120A mutant than in wild-type CYP2D6. Furthermore, substrate dependent catalytic regioselectivity was observed for the mutant: elongation of the N-alkyl chain led to a decreased N-hydroxylation efficiency with an optimal N-dealkylation efficiency for MDEA (Table 4B). These trends were equal to those found experimentally and became even more pronounced when the MDAAs were averaged over enantiomers, over protonation states and Boltzmann weighted (Figure 7).
Significant stereoselective differences in the probabilities of O-demethylenation vs. N-demethylation/hydroxylation were not observed for wild-type CYP2D6. The F120A mutant however, did in all cases discriminate the enantiomers of the neutral MDAAs. Differences between the probabilities of N-demethylation and N-hydroxylation of MDMA enantiomers were found and *R*-MDPA was found in orientations leading to N-demethylation and ω-hydroxylation more often than *S*-MDPA (Table 4B).
Enzyme-substrate interactions observed in the MD simulations of neutral MDAAs showed a significant decrease in van der Waals / aromatic interactions with residue 120 in the F120A mutant compared to wild-type CYP2D6 (Table 5). Furthermore, a small decrease in hydrogen-bond interactions with the carboxylic acid of E216 was observed for the F120A mutant as a direct result of the relatively high probability of binding orientations corresponding to N-dealkylation or N-hydroxylation. In both wild-type and F120A mutant CYP2D6 however, hydrogen-bond interactions were found to be significantly decreased for neutral MDAAs (up to 23% on average for each enantiomer) when compared to charged MDAAs (up to 92% on average for each enantiomer). During the MD-simulations, water

molecules were primarily observed to fill the part of the active site which is connected with a so called "water channel" [54], which was already partially occupied by predicted water molecules in the automated docking starting structures (Figure 6). These water molecules were found to form H-bonds with the substrate. At most, one water molecule was observed in other regions of the active site.

A

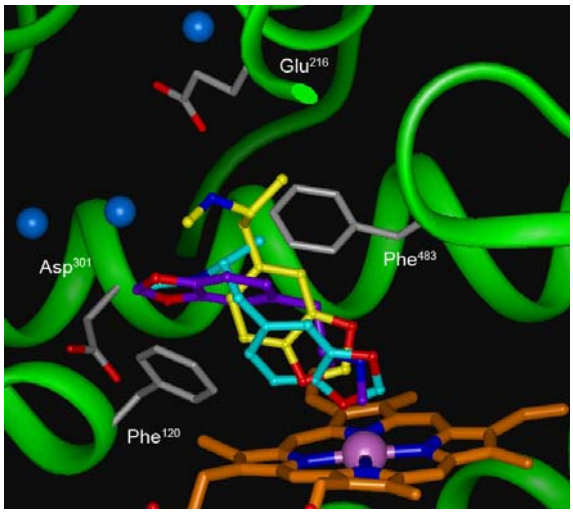

B

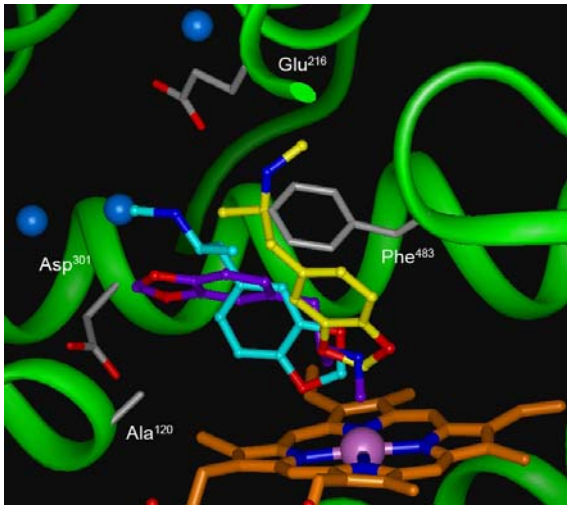

Figure 6: Molecular dynamics (MD) simulations starting orientations of charged R-MDMA, generated by automated docking studies in wild-type (A) and F120A mutant (B) CYP2D6 homology models. Two orientations are corresponding to O-demethylenation, with the substrate nitrogen-atom either in close contact with E216 (pose 1) or placed between E216 and D301 (pose 2). A third orientation is corresponding to N-demethylation or N-hydroxylation (pose 3). Water oxygen atoms, as predicted by GRID (see Materials and Methods section), are depicted as spheres. A colored version of the figure is shown in the Appendix of this thesis.

Table 5: Enzyme-substrate interactions (%) during MD simulations.

Substrate		Wild-type		F120A	
		VdW/arom. F120	H-bond E216	VdW/arom. A120	H-bond E216
MDMA	*R*	81	65	12	54
	S	80	69	23	47
MDEA	*R*	55	51	2	46
	S	66	70	1	57
MDPA	*R*	71	74	5	52
	S	81	52	7	61

Enzyme-substrate interactions during the MD simulations were monitored in terms of the occurrence of atom-atom distances of 3.5 Å or less between the F/A120 side-chain and the MDAA ring system, representing aromatic/van der Waals interactions and hydrogen bonds between the E216 carboxylate oxygen atoms and the MDAA nitrogen-atom. Values of neutral and charged substrates were averaged.

Discussion

The primary aim of this study was to develop an integrated molecular modeling approach to analyze substrate oxidation by CYP2D6. When regioselectivity and stereoselectivity in metabolic oxidation and the effect of enzyme active site mutations can be visualized and quantified using a series of related compounds, such an approach could be a useful tool in the rationalization and prediction of metabolism. Using this approach the experimentally determined binding modes and the product formation of a series of MDAAs by wild-type and F120A mutant CYP2D6 could be rationalized.

Substrate binding orientations

In the present study, molecular modeling was used to explain the apparent discrepancy between experimentally observed differences in regioselective oxidation and the stereoselective preference by the F120A mutant towards MDMA (Figure 1) and the average substrate orientation in the mutant and wild-type active sites as determined by NMR spin lattice relaxation rate measurements (Table 3). The average hydrogen atom to iron distances calculated from the T_1 of the MDMA enantiomers in both enzymes were equal, with the methylene moiety in both cases closest to the heme iron atom. Although the distances between the hydrogen atoms at potential sites of oxidation in MDMA and the heme iron atom were somewhat larger than comparable distances found in CYP X-ray structures (4-6 Å) they were within the ranges of distances determined in other NMR studies [27-30]. This difference can be explained by the fact that experimentally determined distances are averages of all possible substrate orientations during access to, residence in and exit from the active site. As a result they contain more information then just that of a reactive substrate orientation. NMR spin lattice relaxation rate measurements have been used before to determine the orientation of codeine in CYP2D6, where the measured hydrogen atoms to iron atom matched the orientation expected from codeine's metabolic profile [28]. Codeine is a more rigid and bulky substrate than MDMA, which may explain the good match. Caffeine, a small and low affinity substrate of CYP1A2 was also subject of NMR spin lattice relaxation rate measurements, but the orientation found of caffeine did not match the metabolic profile [30]. From other experimental studies it is known that substrates can be quite mobile in CYP active sites [55], and the existence of multiple substrate binding modes and substrate mobility in CYP2D6 is clearly supported by our molecular modeling studies. Averaged distances derived from the present studies, considering three distinct

automatically docked substrate binding modes of the MDAAs in combination with long MD simulations, were in good agreement with the experimentally determined metabolic profiles when considering the MDAAs to be in their neutral form (Table 3). Still, this does not explain the experimentally observed change in regioselective oxidation and stereoselective preference of the F120A mutant towards MDMA compared to wild-type. So it is likely that a small substrate like MDMA is very mobile in the CYP2D6 active site and that the reactivity of possible sites of oxidation determines also which products are being formed.

A

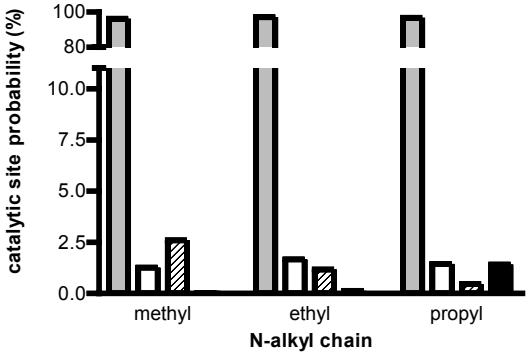

B

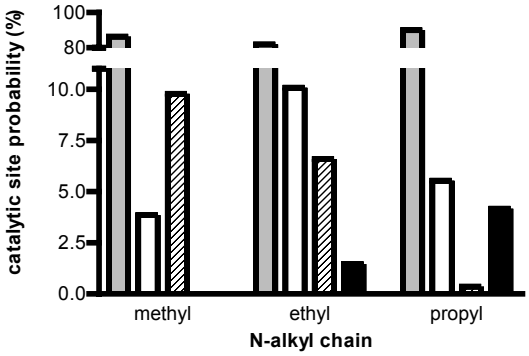

Figure 7: Probabilities (%) of reactive binding orientations corresponding to O-demethylenation (grey), N-dealkylation (blank), N-hydroxylation (diagonal stripe), and ω-hydroxylation (black), of the MDAAs in wild-type (A) and in F120A mutant (B) CYP2D6, as derived from 12 MD simulations. Shown are the Boltzmann weighted averages of two different protonation states and three different docking poses (examples in Figure 6), and assuming a 1:1 ratio between R- and S-enantiomers.

Regioselectivity and stereoselectivity in oxidation

Experimentally observed trends in regioselectivity in the oxidation of the MDAAs by wild-type and F120A mutant CYP2D6 (Table 2) were in good agreement with the relative probabilities of different binding modes of the MDAAs observed in the MD simulations (Table 4B). In the wild-type enzyme, only O-demethylenation was observed experimentally, while

in the F120A mutant also N-demethylation and N-hydroxylation occurred. The molecular modeling studies showed that N-demethylation/hydroxylation probabilities for neutral MDAAs were significantly higher in F120A mutant than in the wild-type enzyme (Table 4B). Both the experimental and modeling studies showed a decreased N-hydroxylation efficiency with elongation of the N-alkyl chain and the highest MDA formation efficiency for MDEA. Stereoselectivity in oxidation of MDMA by wild-type CYP2D6 was hardly found experimentally neither predicted by molecular modeling. However, the experimentally observed preference for *S*-MDMA by the F120A mutant could not be rationalized by molecular modeling. This may be due to the fact that the stereoselectivity is predominantly caused by a difference in K_m and not in V_{max}, while affinities of the substrates to the enzymes were not predicted in a rigorous manner in this study. On the other hand, the small violations of the calculated to the experimentally determined hydrogen atom to iron distances for neutral *R*-MDMA bound to the F120A mutant do indicate that this enantiomer experiences more difficulties to find its optimum orientation in the binding pocket.

Influence of F120A mutation on oxidation reactions

By removing the phenyl ring of F120 more space is created in the active site of CYP2D6 and a specific aromatic interaction point is eliminated [16]. From the MD simulations it became clear that this space was not occupied by the MDAAs or by water molecules, but that critical substrate interactions were lost after mutating F120 into an alanine (Table 5). This observation and the fact that the stereo- and regioselectivity of the mutant enzyme differed from wild-type shows that F120 is important for specific interactions with the MDAAs in CYP2D6. There is not sufficient space in the active sites of wild-type or the F120A mutant CYP2D6 to accommodate two molecules of the MDAAs at the same time. However, it could be possible that two substrate molecules bind simultaneously to different parts of the protein e.g. in the active site and in substrate access channels [54], or in a peripheral binding site [9].

Combination of automated docking and MD simulations

In earlier studies it was shown that automated docking can successfully be applied to predict sites of oxidation by CYPs. [21] In contrast, the current study shows that automated docking alone is not suitable for accurate determination of relative probabilities of different substrate binding modes and for discrimination between substrates and enzymes of high similarity, such as regio/stereoisomers and mutants of enzymes. In order to reproduce the experimental data, which are an average over many different substrate and enzyme orientations in time, a dynamic treatment of both substrate and enzyme is required. Only when averaging over different positions and orientations was taken into account, experimentally determined substrate hydrogen atoms to heme iron atom distances could be reproduced accurately. The experimentally observed differences in substrate oxidation by wild-type and F120A mutant CYP2D6 could only be explained from the different binding modes observed in the MD simulations. Multiple and extensive MD simulations are needed to catch these subtle differences between substrates, enzyme structures and their dynamics.

Substrate protonation states

The molecular modeling was performed with neutral and charged substrates because this markedly influenced the binding and mobility of the MDAAs in the active site of the two enzymes. Even though the MDAAs in physiological solution will occur predominantly in their charged form, the preferred protonation state within the binding pocket can differ significantly, thus reductions of apparent pK_a values for substrates upon binding to CYP2D6

of up to 2 pH units have been reported [26]. From a direct comparison between the experimentally derived hydrogen atom to heme iron distances and the computationally determined values it became clear that the MD simulations reproduced the experimental data best when the MDAAs were represented in their neutral form.

Conclusions

The approach of combining automated docking and MD simulations in a protein model was a successful way to rationalize the oxidative metabolism of a series of 3,4-methylenedioxy-N-alkylamphetamines (MDAAs) by CYP2D6. Differences in oxidative metabolism of these closely related substrates could be predicted in details like regioselectivity and stereoselectivity. Furthermore, the effects of the active site F120A mutation on the substrate selectivity could be rationalized. The presented integrated modeling method is a promising tool in the prediction of the metabolic properties of new (drug-like) compounds by CYP2D6 and might be applicable for other drug metabolizing enzymes as well.

Acknowledgements

We thank Magnus Ingelman-Sundberg and Mats Hidestrand for providing the pSP19T7LT plasmid containing CYP2D6 and the human NADPH-CYP reductase. We thank Hari Sing from the NIDA-NIH for providing the MDMA enantiomers. We thank Ed Groot and Jon de Vlieger for technical assistance.

References

1. Goeptar AR, Scheerens H and Vermeulen NPE, Oxygen and xenobiotic reductase activities of cytochrome P450. *Crit Rev Toxicol* **25:** 25-65, 1995.
2. Guengerich FP, Cytochrome P450: what have we learned and what are the future issues? *Drug Metab Rev* **36:** 159-97, 2004.
3. Zanger UM, Raimundo S and Eichelbaum M, Cytochrome P450 2D6: overview and update on pharmacology, genetics, biochemistry. *Naunyn Schmiedebergs Arch Pharmacol* **369:** 23-37, 2004.
4. Bertilsson L, Dahl ML, Dalen P and Al-Shurbaji A, Molecular genetics of CYP2D6: clinical relevance with focus on psychotropic drugs. *Br J Clin Pharmacol* **53:** 111-22, 2002.
5. Shimada T, Yamazaki H, Mimura M, Inui Y and Guengerich FP, Interindividual variations in human liver cytochrome P450 enzymes involved in the oxidation of drugs, carcinogens and toxic chemicals: studies with liver microsomes of 30 Japanese and 30 Caucasians. *J Pharmacol Exp Ther* **270:** 414-23, 1994.
6. Oscarson M, Pharmacogenetics of drug metabolising enzymes: importance for personalised medicine. *Clin Chem Lab Med* **41:** 573-80, 2003.
7. Ingelman-Sundberg M, Pharmacogenetics of cytochrome P450 and its applications in drug therapy: the past, present and future. *Trends Pharmacol Sci* **25:** 193-200, 2004.
8. Williams PA, Cosme J, Ward A, Angove HC, Matak Vinkovic D and Jhoti H, Crystal structure of human cytochrome P450 2C9 with bound warfarin. *Nature* **424:** 464-8, 2003.
9. Williams PA, Cosme J, Vinkovic DM, Ward A, Angove HC, Day PJ, Vonrhein C, Tickle IJ and Jhoti H, Crystal structures of human cytochrome P450 3A4 bound to metyrapone and progesterone. *Science* **305:** 683-6, 2004.
10. Williams PA, Cosme J, Sridhar V, Johnson EF and McRee DE, Mammalian microsomal cytochrome P450 monooxygenase: structural adaptations for membrane binding and functional diversity. *Mol Cell* **5:** 121-31, 2000.
11. de Graaf C, Vermeulen NPE and Feenstra KA, Cytochrome P450 in silico: an integrative modeling approach. *J Med Chem* **48:** 2725-55, 2005.
12. Venhorst J, ter Laak AM, Commandeur JN, Funae Y, Hiroi T and Vermeulen NP, Homology modeling of rat and human cytochrome P450 2D (CYP2D) isoforms and computational rationalization of experimental ligand-binding specificities. *J Med Chem* **46:** 74-86, 2003.

13. Kemp CA, Flanagan JU, van Eldik AJ, Marechal JD, Wolf CR, Roberts GC, Paine MJ and Sutcliffe MJ, Validation of model of cytochrome P450 2D6: an in silico tool for predicting metabolism and inhibition. *J Med Chem* **47:** 5340-6, 2004.
14. Ellis SW, Hayhurst GP, Smith G, Lightfoot T, Wong MM, Simula AP, Ackland MJ, Sternberg MJ, Lennard MS, Tucker GT and et al., Evidence that aspartic acid 301 is a critical substrate-contact residue in the active site of cytochrome P450 2D6. *J Biol Chem* **270:** 29055-8, 1995.
15. Guengerich FP, Hanna IH, Martin MV and Gillam EMJ, Role of glutamic acid 216 in cytochrome P450 2D6 substrate binding and catalysis. *Biochemistry* **42:** 1245-1253, 2003.
16. Keizers PHJ, Lussenburg BMA, de Graaf C, Mentink LM, Vermeulen NPE and Commandeur JNM, Influence of phenylalanine 120 on cytochrome P450 2D6 catalytic selectivity and regiospecificity: crucial role in 7-methoxy-4-(aminomethyl)-coumarin metabolism. *Biochem Pharmacol* **68:** 2263-2271, 2004.
17. Flanagan JU, Marechal JD, Ward R, Kemp CA, McLaughlin LA, Sutcliffe MJ, Roberts GC, Paine MJ and Wolf CR, Phe120 contributes to the regiospecificity of cytochrome P450 2D6: mutation leads to the formation of a novel dextromethorphan metabolite. *Biochem J* **380:** 353-60, 2004.
18. Paine MJ, McLaughlin LA, Flanagan JU, Kemp CA, Sutcliffe MJ, Roberts GC and Wolf CR, Residues glutamate 216 and aspartate 301 are key determinants of substrate specificity and product regioselectivity in cytochrome P450 2D6. *J Biol Chem* **278:** 4021-7, 2003.
19. Vermeulen NPE, Prediction of drug metabolism: the case of cytochrome P450 2D6. *Curr Top Med Chem* **3:** 1227-39, 2003.
20. Ekins S, de Groot MJ and Jones JP, Pharmacophore and three-dimensional quantitative structure activity relationship methods for modeling cytochrome P450 active sites. *Drug Metab Dispos* **29:** 936-44, 2001.
21. de Graaf C, Pospisil P, Pos W, Folkers G and Vermeulen NPE, Binding mode prediction of cytochrome P450 and thymidine kinase protein-ligand complexes by consideration of water and rescoring in automated docking. *J Med Chem* **7:** 2308-2318, 2005.
22. Harris D and Loew G, Prediction of regiospecific hydroxylation of camphor analogs by cytochrome-P450(Cam). *J Am Chem Soc* **117:** 2738-2746, 1995.
23. Keseru GM, Kolossvary I and Bertok B, Cytochrome P-450 catalyzed insecticide metabolism. Prediction of regio- and stereoselectivity in the primer metabolism of carbofuran: A theoretical study. *J Am Chem Soc* **119:** 5126-5131, 1997.
24. Harris DL and Loew GH, Investigation of the proton-assisted pathway to formation of the catalytically active, ferryl species of P450s by molecular dynamics studies of P450eryF. *J Am Chem Soc* **118:** 6377-87, 1996.
25. Park JY and Harris D, Construction and assessment of models of CYP2E1: Predictions of metabolism from docking, molecular dynamics, and density functional theoretical calculations. *J Med Chem* **46:** 1645-1660, 2003.
26. Miller GP, Hanna IH, Nishimura Y and Guengerich FP, Oxidation of phenethylamine derivatives by cytochrome P450 2D6: the issue of substrate protonation in binding and catalysis. *Biochemistry* **40:** 14215-23, 2001.
27. van de Straat R, de Vries J, de Boer HJ, Vromans RM and Vermeulen NPE, Relationship between paracetamol binding to and its oxidation by two cytochromes P-450 isozymes--a proton nuclear magnetic resonance and spectrophotometric study. *Xenobiotica* **17:** 1-9, 1987.
28. Modi S, Paine MJ, Sutcliffe MJ, Lian LY, Primrose WU, Wolf CR and Roberts GC, A model for human cytochrome P450 2D6 based on homology modeling and NMR studies of substrate binding. *Biochemistry* **35:** 4540-50, 1996.
29. Poli-Scaife S, Attias R, Dansette PM and Mansuy D, The substrate binding site of human liver cytochrome P450 2C9: an NMR study. *Biochemistry* **36:** 12672-82, 1997.
30. Regal KA and Nelson SD, Orientation of caffeine within the active site of human cytochrome P450 1A2 based on NMR longitudinal (T1) relaxation measurements. *Arch Biochem Biophys* **384:** 47-58, 2000.
31. Onderwater RC, Venhorst J, Commandeur JNM and Vermeulen NPE, Design, synthesis, and characterization of 7-methoxy-4-(aminomethyl)coumarin as a novel and selective cytochrome

P450 2D6 substrate suitable for high-throughput screening. *Chem Res Toxicol* **12:** 555-9, 1999.
32. Braun U, Shulgin AT and Braun G, Centrally active N-substituted analogs of 3,4-methylenedioxyphenylisopropylamine (3,4-methylenedioxyamphetamine). *J Pharm Sci* **69:** 192-5, 1980.
33. Omura T and Sato R, The carbon monoxide-binding pigment of liver microsomes. II. Solubilization, purification, and properties. *J Biol Chem* **239:** 2379-85, 1964.
34. Jefcoate CR, Measurement of substrate and inhibitor binding to microsomal cytochrome P450 by optical-difference spectroscopy. *Methods Enzymol* **52:** 258-79, 1978.
35. Hanna IH, Krauser JA, Cai H, Kim MS and Guengerich FP, Diversity in mechanisms of substrate oxidation by cytochrome P450 2D6. Lack of an allosteric role of NADPH-cytochrome P450 reductase in catalytic regioselectivity. *J Biol Chem* **276:** 39553-61, 2001.
36. Solomon I and Bloembergen N, Nuclear magnetic interactions in the HF molecule. *J Chem Phys* **25:** 261-266, 1956.
37. Wester MR, Johnson EF, Marques-Soares C, Dansette PM, Mansuy D and Stout CD, Structure of a substrate complex of mammalian cytochrome P450 2C5 at 2.3 A resolution: evidence for multiple substrate binding modes. *Biochemistry* **42:** 6370-9, 2003.
38. Wester MR, Johnson EF, Marques-Soares C, Dijols S, Dansette PM, Mansuy D and Stout CD, Structure of mammalian cytochrome P450 2C5 complexed with diclofenac at 2.1 A resolution: evidence for an induced fit model of substrate binding. *Biochemistry* **42:** 9335-45, 2003.
39. Sali A and Blundell TL, Comparative protein modelling by satisfaction of spatial restraints. *J Mol Biol* **234:** 779-815, 1993.
40. Laskowski RA, Macarthur MW, Moss DS and Thornton JM, Procheck - a program to check the stereochemical quality of protein structures. *J Appl Cryst* **26:** 283-291, 1993.
41. Colovos C and Yeates TO, Verification of protein structures - patterns of nonbonded atomic interactions. *Protein Science* **2:** 1511-1519, 1993.
42. Luthy R, Bowie JU and Eisenberg D, Assessment of protein models with 3-dimensional profiles. *Nature* **356:** 83-85, 1992.
43. Morris GM, Goodsell DS, Halliday RS, Huey R, Hart WE, Belew RK and Olson AJ, Automated docking using a Lamarckian genetic algorithm and an empirical binding free energy function. *J Comput Chem* **19:** 1639-1662, 1998.
44. Rarey M, Kramer B, Lengauer T and Klebe G, A fast flexible docking method using an incremental construction algorithm. *J Mol Biol* **261:** 470-489, 1996.
45. Jones G, Willett P, Glen RC, Leach AR and Taylor R, Development and validation of a genetic algorithm for flexible docking. *J Mol Biol* **267:** 727-48, 1997.
46. Goodford PJ, A computational procedure for determining energetically favorable binding sites on biologically important macromolecules. *J Med Chem* **28:** 849-57, 1985.
47. Wang RX, Liu L, Lai LH and Tang YQ, SCORE: A new empirical method for estimating the binding affinity of a protein-ligand complex. *J Mol Model* **4:** 379-394, 1998.
48. Lindahl E, Hess B and van der Spoel D, GROMACS 3.0: a package for molecular simulation and trajectory analysis. *J Mol Model* **7:** 306-317, 2001.
49. Daura X, Mark AE and van Gunsteren WF, Parametrization of aliphatic CHn united atoms of GROMOS96 force field. *J Comput Chem* **19:** 535-547, 1998.
50. Scott WRP, Hunenberger PH, Tironi IG, Mark AE, Billeter SR, Fennen J, Torda AE, Huber T, Kruger P and van Gunsteren WF, The GROMOS biomolecular simulation program package. *J Phys Chem A* **103:** 3596-3607, 1999.
51. Hess B, Bekker H, Berendsen HJC and Fraaije JGEM, LINCS: A linear constraint solver for molecular simulations. *J Comput Chem* **18:** 1463-1472, 1997.
52. Berendsen HJC, Postma JPM, Gunsteren WFv, DiNola A and Haak JR, Molecular dynamics with coupling to an external bath. *J. Chem. Phys.* **81:** 3684--3690, 1984.
53. Meunier B, de Visser SP and Shaik S, Mechanism of oxidation reactions catalyzed by cytochrome p450 enzymes. *Chem Rev* **104:** 3947-80, 2004.
54. Wade RC, Winn PJ, Schlichting I and Sudarko, A survey of active site access channels in cytochromes P450. *J Inorg Biochem* **98:** 1175-82, 2004.

55. Prasad S and Mitra S, Role of protein and substrate dynamics in catalysis by Pseudomonas putida cytochrome P450cam. *Biochemistry* **41:** 14499-508, 2002.

Chapter 7

The conserved threonine 309 influences spin state equilibrium in cytochrome P450 2D6: a resonance Raman scattering study

Peter H.J. Keizers, Alois Bonifacio, Gert van der Zwan, Cees Gooijer, Nico P.E. Vermeulen, and Jan N. M. Commandeur

---

The polymorphic cytochrome P450 2D6 (CYP2D6) is one of the major drug metabolizing enzymes in humans. Its active site residue T309 was shown to be of crucial importance for the enzyme activity, probably by determining the ratio of multiple oxygenating species [1]. In this study, the heme prosthetic group, and its environment, of wild-type and the T309V mutant of CYP2D6 have been studied using resonance Raman spectroscopy. It was found that T309 is involved in maintaining a 5-coordinated high spin species in presence and absence of substrates. Binding of dextromethorphan to wild-type CYP2D6 led to a change in the polarity of the heme environment, as observed by a shift of the Fe-CO stretching frequency, whereas in the T309V mutant this effect was less apparent. Dextromethorphan binds similar to the mutant as to the wild-type and the T309V mutation has no direct effect on the polarity of the heme environment. These data suggest that T309 is involved in the hydrogen-bonds network in the active site of CYP2D6, but the residue is too far from the heme to be directly interacting with iron-bound water or molecular oxygen. The observed effects of the T309V mutation on the heme and its environment can be an additional explanation for the changed reactivity of the mutant, besides its effect on the balance of oxygenating species.

Introduction

Cytochromes P450 (CYPs) are enzymes responsible for the oxidative biotransformation of a large variety of endogenous and exogenous substrates, like steroids, carcinogens and drugs, and can be found in virtually all organisms [2]. In human drug metabolism, one of the most important CYP isoforms is CYP2D6. This hepatic enzyme is involved in the phase I oxidative metabolism of about 30% of the currently marketed drugs, including much prescribed antidepressants, β-blockers, opioids and antiarythmics [3]. The enzyme is known for its genetic polymorphisms and gene multiplicities, even increasing its clinical relevance [4]. Structural studies on CYP2D6 are of crucial importance to understand the functioning of the enzyme and to be able to predict the metabolism of new (drug-like) compounds [5].

Previously, we demonstrated the critical role of residue T309 in the mechanism of oxidation by CYP2D6 [1]. The T309V mutant displayed a decreased *O*-dealkylation activity towards model substrates and when possible, *N*-dealkylation reactions were preferred. These observations were explained by a decreased ability to form the oxenoid-iron species (compound I), the presumed dominant oxygenating species involved in *O*-dealkylation reactions [6]. This was confirmed by the fact that by using cumene hydroperoxide as oxygen donor, the *O*-dealkylating activities were restored. Cumene hydroperoxide is known to short-circuit the catalytic cycle and directly forms the oxenoid iron [7]. Apparently, without T309 the oxygenating species preceding the oxenoid iron in the catalytic cycle, the hydroperoxo-iron accumulates, leading to a changed reactivity pattern of the enzyme. Similar results were found after mutation of the homologous threonine residues in other CYP isoforms, like T302 and T303 in rabbit CYP2B4 and CYP2E1 respectively [8, 9]. The I-helix threonine is highly conserved in CYPs and seems to be involved in proton donation to the heme bound oxygen [10]. Based on crystal structures of the ferrous dioxygen complex of the wild-type and the T252A mutant of CYP101, it was proposed that T252 accepts a hydrogen bond from the hydroperoxo-iron intermediate, thereby promoting the second protonation on the distal oxygen atom, which leads to *O-O* bond cleavage and compound I formation [11]. Resonance Raman (RR) spectroscopy can be used to obtain information about several properties of the heme prosthetic group. The iron oxidation state, the spin state, the coordination number, and also conformational changes of the vinyl and propionate side chains of the heme can be studied [12]. Furthermore, the Fe-CO stretching mode is sensitive to the polarity of the heme environment [13, 14]. By choosing the excitation wavelength in resonance with the Soret absorbance band, RR is a sensitive spectroscopic technique to study CYPs [15]. Most bands in RR spectra of CYPs have been assigned to heme vibrational modes and are in many cases well resolved [12]. The technique offers great selectivity and can thus be more sensitive for small changes in the heme than UV-visible absorbance spectroscopy. RR was successfully employed before to study the effects of active site mutations in CYPs [16-18], including those of the conserved I-helix threonine [19, 20]. In this study, we have chosen RR spectroscopy to probe the heme characteristics of wild-type and the T309V mutant of CYP2D6 in order to find out whether the mutation influences the heme properties, correlated with the altered catalytic activity of the mutant.

Materials and Methods

Materials

The pSP19T7LT plasmid containing in tandem the cDNAs of human CYP2D6 with a C- terminal His_6-tag and the human NADPH-cytochrome P450 reductase, was used as described before [1]. *Escherichia coli* JM109 were obtained from DSMZ (Braunschweig, Germany). Dextromethorphan hydrobromide was obtained from Sigma (Sigma, St Louis MO). All other chemicals were of analytical grade and obtained from standard suppliers.

Expression and purification of the enzymes
The pSP19T7LT plasmids containing wild-type or the T309V mutant of CYP2D6 cDNA were transformed into *E. coli* strain JM109. Expression and membrane isolation was carried out as described [1]. Membranes were resuspended in 0.5% of the original culture volume of KPi-glycerol buffer (50 mM potassium phosphate buffer, pH 7.4, 10% glycerol) and the enzymes were purified, using nickel affinity chromatography as described [21]. CYP concentrations were determined by CO-difference absorption spectra on a Pharmacia Ultrospec 2000 spectrometer, using ε= 91 $cm^{-1}mM^{-1}$ according to Omura and Sato [22].

Resonance Raman spectroscopy
Spectroscopic measurements were conducted using a home-built Raman microscope in a backscattering configuration. A Zeiss microscope (D-7082 with 40x objective, NA 0.85, working distance 0.3 mm) was coupled to a single monochromator (Instruments SA Inc., Metuchen, NJ) with a mounted 2400 g/mm grating and a CCD camera (Andor Technologies DV-420OE, Belfast, N.Ireland). The 413.1 nm line of a continuous wave Kr ion laser (Coherent Innova 300c, Coherent Inc., Santa Clara CA) and the 457.9 nm of a continuous wave Ar ion laser (Spectra Physics 2000-336, Newport corp., Mountain View CA) were used for excitation and the Rayleigh scattered light was removed using 3rd Millenium edge long pass filters (Omega Optical, Bratleboro, VT). Laser powers of 10-15 mW (at 413.1 nm) and 1 mW (at 457.9 nm) were used on the sample throughout the experiments. The sloping background of the spectra was subtracted using a baseline fitted to the experimental data with the Andor CCD camera software. The fitting of experimental data with Lorentzian functions was performed with PeakFit 4.12 (SeaSolve Software Inc., Richmond CA). For RR measurements, a 1 mm-diameter glass capillary was filled with 10 µl of varying concentrations (1-50 µM) CYP2D6 in KPi-glycerol buffer and put in a spinning capillary holder under the microscope objective. To measure substrate binding, substrate concentrations of 5-10 mM were used, leading to a 500-1000 fold excess of substrate with respect to the enzyme (saturating conditions, as indicated by the K_s reported for the substrates [1]). No further spectral changes were detected upon increasing substrate concentration, indicating that all the CYP2D6 in the sample was bound to the substrate [23]. To obtain the ferrous CO-complexes, oxygen was removed from the CYP2D6 samples (with or without substrate) by stirring under a nitrogen atmosphere, reduced by adding 5 µl of a 25 mg/ml sodium dithionite in KPi-glycerol buffer, to 20 µl of enzyme in the same buffer, and exposed to CO for 2-3 minutes while stirring. During all measurements the capillary containing the sample was kept spinning to minimize local heating and photodissociation of the iron bound CO. Before and after every RR measurement, CYP integrity was monitored by CO difference absorption spectroscopy.

Results

Expression and purification of the enzymes
Recombinant expression followed by affinity chromatography purification yielded approximately 60 nmoles CYP2D6 per liter of cultured *E coli*, in case of the wild-type and the T309V mutant of CYP2D6. The enzymes were pure, as judged by the observation of a single band of 55 kD on a Coomassie brilliant blue stained SDS-polyacrylamide gel. The absolute absorbance spectra of oxidized, and reduced CO-bound, wild-type CYP2D6 are shown in Figure 1. There were no significant differences between the spectra of the wild-type and the T309V mutant of CYP2D6. A small amount of P420 (inactive CYP, observed as a shoulder at 420 nm in the CO-difference spectrum) was present in the both the wild-type and T309V mutant samples.

Resonance Raman spectroscopy
The low- and high-frequency regions in the RR spectra of the wild-type and T309V mutant of CYP2D6 in the resting state (i.e. without substrate), are at first sight rather similar (Figure 2). In both cases, the most intense band at 1372 cm^{-1} is attributed to the ν_4 vibrational mode, indicative for an oxidized heme iron atom, and the band at 675 cm^{-1} is attributed to the ν_7 vibrational mode [12].

The wild-type enzyme high-frequency region spectrum (Figure 3a), is indicative for a predominantly six-coordinated low-spin (6cLS) oxidized heme. The bands at 1501, 1582 and 1637 cm^{-1} are attributed to the ν_3, ν_2 and ν_{10} vibrational modes for a 6cLS heme respectively [12]. However, a weak shoulder of ν_3 suggests the presence of another band at lower wavenumbers, characteristic of a five-coordinated high-spin (5cHS). In consistence, a better fit of the spectral data for wild-type CYP2D6 was obtained when including bands at 1486, 1567 and 1623 cm^{-1}, for respectively the ν_3, ν_2 and ν_{10} vibrational modes of a 5cHS heme species in addition to the 6cLS bands (Figure 3a).

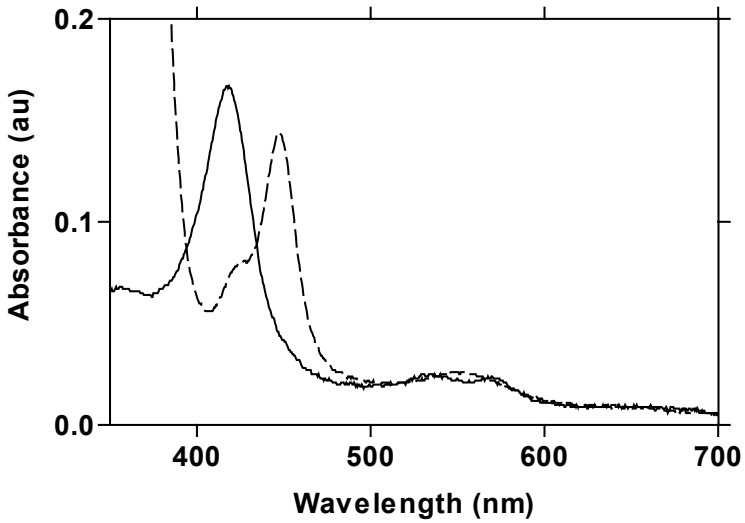

Figure 1: Absolute absorbance spectra of 1 μM purified wild-type CYP2D6 before, and after addition of sodium dithionite and CO (dashed line).

Although the high-frequency region RR spectrum of the T309V mutant seemed similar to that of the wild-type, the difference spectrum of the two enzymes (Figure 3), shows an intensity increase for the bands characteristic of a 6cLS species, and a concomitant decrease of the ν_3, ν_2 and ν_{10} vibrational modes, typical for a 5cHS heme. Therefore, in the T309V mutant the content of 5cHS is decreased compared to the wild-type, with a concomitant increase of the 6cLS fraction.

In the presence of saturating amounts of the substrate dextromethorphan, the bands distinctive of the 5cHS species (ν_3 and ν_2 at 1486 cm^{-1} and 1567 cm^{-1} respectively) increased in intensity, whereas the intensity of the corresponding bands for the 6cLS species (ν_3 and ν_2 at 1501 and 1582 cm^{-1} respectively) diminished, for both the wild-type and the T309V mutant of CYP2D6 (Figures 3 and 4). A difference between the two enzymes was found in the intensity ratio between the 6cLS/5cHS ν_3 bands (at 1501 and 1486 cm^{-1} respectively), which was higher in the T309V mutant than in wild-type CYP2D6 (Figure 3).

The Fe-CO stretching ($\nu_{Fe\text{-}CO}$) frequency is known to decrease with increasing polarity of the heme environment [13, 24]. In both the CO-bound wild-type and T309V mutant CYP2D6, the band attributed to $\nu_{Fe\text{-}CO}$ was observed at 476 cm^{-1}. In the RR spectrum of wild-type

CYP2D6 in the presence of saturating amounts of dextromethorphan, the ν_{Fe-CO} was increased by 5 cm^{-1}. In the spectrum of the CO-bound T309V mutant in the presence of saturating amounts of dextromethorphan, the shift of ν_{Fe-CO} was less evident, although the band broadened towards higher wavenumbers (Figure 5).

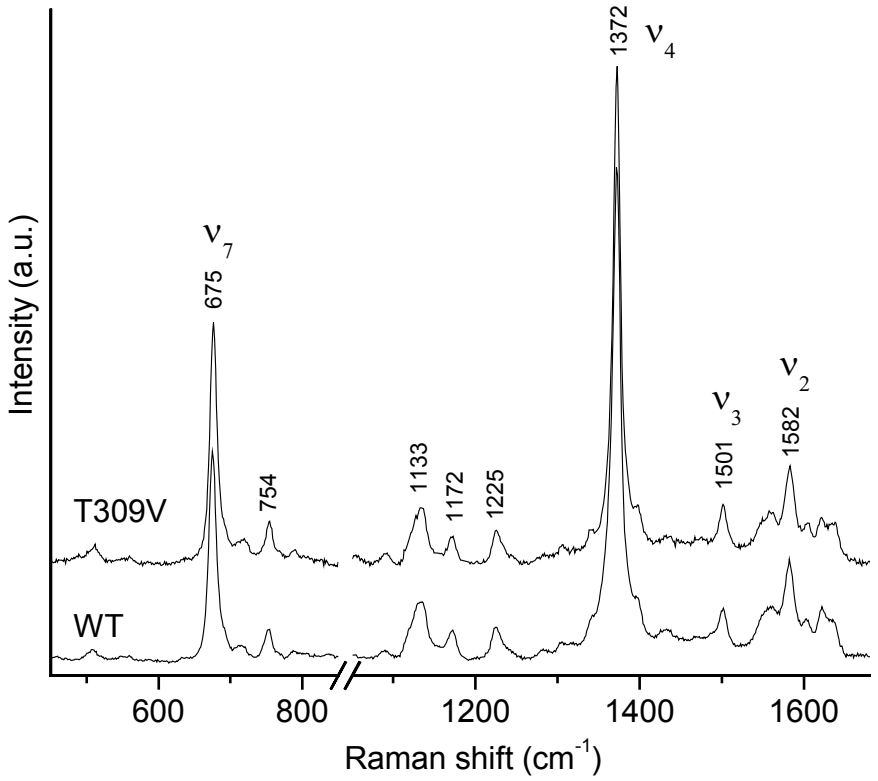

Figure 2. High- and low-frequency RR spectra of wild-type and T309V mutant CYP2D6. Spectra were taken as described in the Methods section, the vibrational modes are assigned to the most intense bands according to Hildebrandt [12]. Excitation wavelength 413.1 nm, power 10 mW, accumulation time 600 s.

Discussion

Conserved I-helix threonines in CYPs play an important role in the mechanism of oxidation by these enzymes. Apparently, these residues are involved in the process of proton donation to the heme-bound molecular oxygen, thereby activating it to the ultimate oxygenating species. Recently, T309 was shown to fulfill this role in CYP2D6. In this study we have employed resonance Raman (RR) spectroscopy to examine the impact of the T309V mutation on the porphyrin prosthetic group properties, and the polarity of its environment.

In the absence of a substrate, the CYP heme iron atom is generally observed as oxidized (Fe^{3+}), and mainly in the 6cLS state with a water molecule (or hydroxyl ion) as the sixth distal ligand trans to the endogenous cysteinate ligand [25]. In this study, the 6cLS state was indeed found predominant for wild-type CYP2D6. In addition, a minor presence of the

5cHS state was observed (Figure 3). The presence of the 5cHS species in the resting state RR spectrum has been reported for other CYPs as well; a mixed spin state with a 5cHS ν_3 mode at 1488 cm^{-1} and a 6cLS ν_3 mode at 1502 cm^{-1} was observed for substrate free rabbit CYP1A2 [26], while for substrate free human CYP1A2 only one ν_3 band at 1487 cm^{-1} was reported, indicating the exclusive presence of an HS resting state [27]. Also in the cases of bacterial CYP121 and CYP152, mixed LS/HS spin states have been reported in the absence of substrates [28, 29].

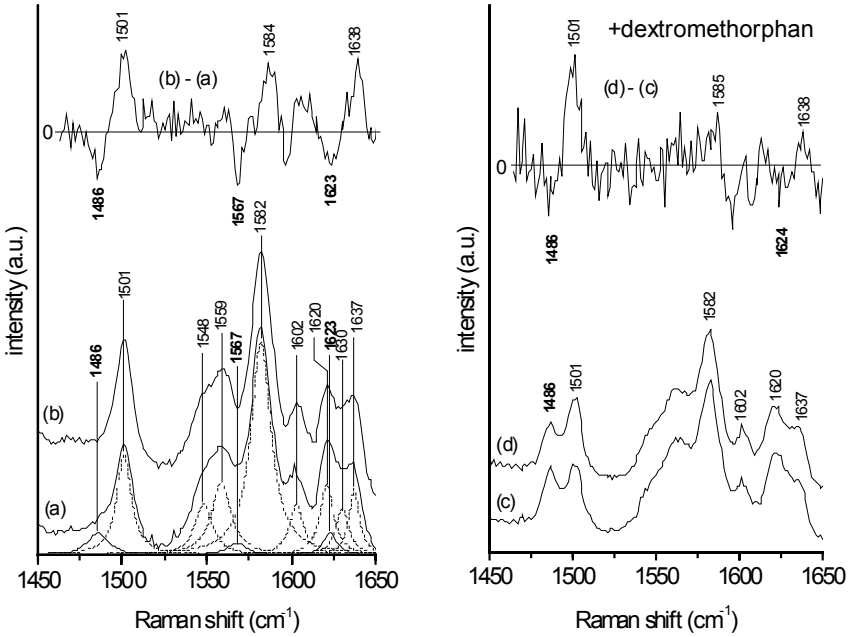

Figure 3. Spin-marker bands region of the RR spectra of 30μM CYP2D6 wild-type (a), T309V mutant (b) and their difference spectrum (b)-(a) are shown in the left panel. Spin-marker bands region of the RR spectra of CYP2D6 wild-type (c), and T309V mutant (d) in presence of dextromethorphan and their difference spectrum (d)-(c) are shown in the right panel. Excitation wavelength 413.1 nm, power 10 mW, accumulation time 600 s. The Lorentzian functions used to fit the spectrum (a) (see Methods section) are represented as solid (high-spin marker bands) or dotted (low-spin marker bands) peaks. Frequencies of high-spin marker bands are reported in bold.

The apparent equilibrium of spin states may be disturbed by active site conformational changes. In the 5cHS state, the heme is no longer ligated to an axial water molecule. This is often observed when a substrate is present in the heme-pocket, perturbing the iron bound water molecule directly, or through inducing conformational changes in the enzyme. In the presence of dextromethorphan, the 5cHS content of CYP2D6 was found significantly increased (Figures 3 and 4). In recent studies on synthesized CYP heme mimetic models [30] and QM/MM calculations on CYP101 [31, 32], it was suggested that the axial water ligand is involved in a hydrogen-bonds network due to a cluster of water molecules in the binding pocket. Changes in this network will directly modulate the properties of the distal water-ligand and thus the relative stability of the 6cLS versus the 5cHS state. In the resting

state of the T309V mutant of CYP2D6 the 5cHS content is decreased, with a concomitant increase of the 6cLS content. This higher stability of the 6cLS in the T309V mutant with respect to wild-type CYP2D6 is preserved in the presence of dextromethorphan (Figures 3 and 4). The substrate itself perturbs the wild-type and mutant spin-equilibria to the same extent (Figure 4). This strongly suggests that the difference in the 6cLS/5cHS ratio between the substrate-bound wild-type and mutant enzyme is not due to different binding modes of dextromethorphan, but rather to a difference caused by the T309V mutation. Apparently the T309 residue is involved in the hydrogen-bonds network involving the cluster of active site water molecules.

To further investigate the role of T309 in CYP2D6, the spectra of the reduced CO-bound wild-type and T309V mutant enzymes were analyzed (Figure 5). The ferrous CO-heme complex has an electronic structure similar to the oxygenated complex but it is stable, and therefore a convenient model to mimic the Fe-O_2-complex [12, 33]. Moreover, CO can be used as a vibrational probe of the heme pocket polarity, since changes in the water content of the pocket cause a variation of the local electromagnetic field and induce a shift in the Fe-CO vibrational frequencies [13, 14, 24].

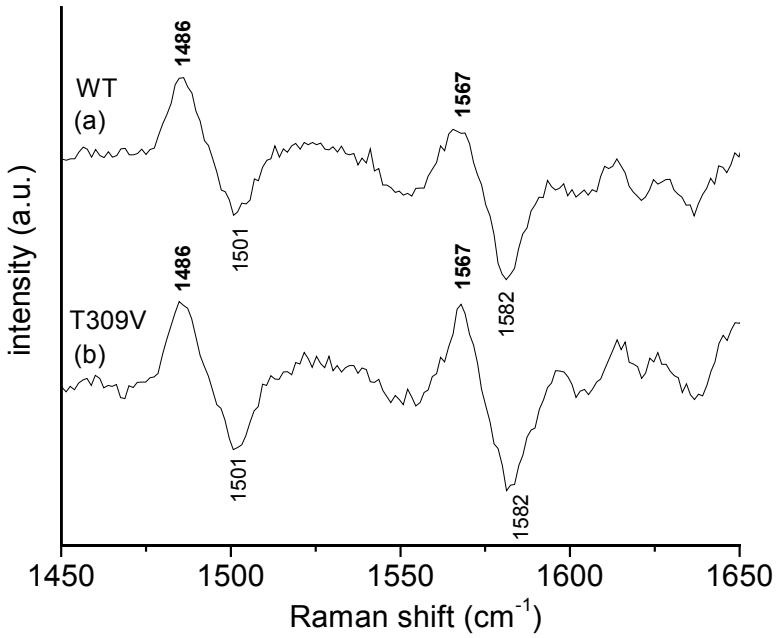

Figure 4. The difference spectra between the dextromethorphan bound and the substrate-free enzyme (Figure 3), for the wild-type (a) and the T309V mutant (b) of CYP2D6. Excitation 413.1 nm, power 10 mW, accumulation time 600 s. Frequencies of high-spin marker bands are reported in bold.

In the absence of substrate no differences were detected between the wild-type and the T309V mutant CYP2D6 $\nu_{Fe\text{-}CO}$ frequencies, suggesting that T309 does not interact directly with CO and has no relevant effect on the polarity of the binding pocket localized directly above the heme. This observation is consistent with RR data from CO-adducts of the T252A mutant of CYP101 [20], and the T243V mutant of CYP55A [34], whereas the T301V mutant

of rabbit CYP4A6 displayed a 3cm^{-1} increase of the $\nu_{Fe\text{-}CO}$ compared to the wild-type [19]. On the other hand, binding of dextromethorphan caused a 5 cm^{-1} increase of $\nu_{Fe\text{-}CO}$ in wild-type CYP2D6, indicating a diminution in local polarity due to a decrease of water content in the binding pocket [13, 24]. A similar but smaller effect is observed for the T309V mutant, showing a broadening of the $\nu_{Fe\text{-}CO}$ peak towards higher wavenumbers, which indicates that the electrostatic field variation caused by dextromethorphan in the two enzymes do not differ substantially. The affinity of the two enzymes for dextromethorphan is similar as well, as was judged from optical titration experiments, which yielded type I binding spectra with spectroscopic dissociation constants (K_s) of 33 and 20 μM for wild-type and mutant respectively [1].

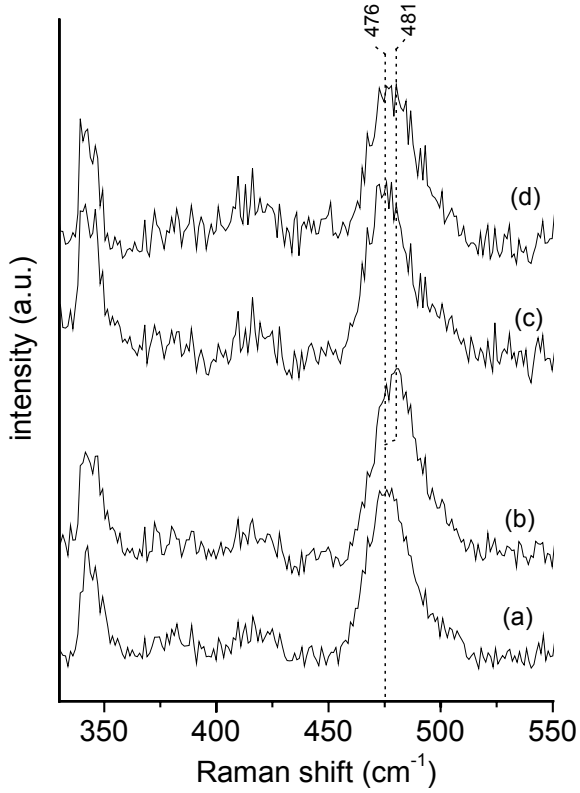

Figure 5. Low-frequency RR spectra of CO-bound CYP2D6 wild-type (a,b) and T309V mutant (c,d), in absence (a,c) and in presence (b,d) of dextromethorphan. Excitation 457.9 nm, power 1 mW, accumulation time 600 s.

Also, modeling studies do not indicate T309 to be involved in substrate binding in CYP2D6 [35]. To summarize, there is no direct effect of T309 on the hydrophobicity of the heme-bound CO environment and the residue does not significantly influence the effects of dextromethorphan binding in the active site. According to our CYP2D6 homology model [36], the T309 hydroxy moiety is at approximately 5 Å from the heme iron atom, depending

on its rotameric state (Figure 6). This distance is too large for T309 to be directly involved in hydrogen bonding with a heme-bound water molecule or with iron-oxygen species, unlike T252 in CYP101, where the distance from the heme iron atom to the T252 hydroxy moiety is 3.5 Å [11]. Therefore, T309 in CYP2D6 is believed to have an indirect influence on the heme bound axial ligand, via hydrogen bonding with other active site water molecules. In a previous study we have shown that T309 affects the proton delivery to the heme-bound oxygen [1], while the present investigations indicate that T309 is involved in the network of hydrogen-bonds in the active site. It is arguable whether there is a relation between a change in spin state and the activity of a CYP, because upon mutation of W97 in CYP102 the spin state also changed, while mutant activities remained high [37]. But the loss of the T309 hydroxy moiety in CYP2D6 does change the active site conformation of the water cluster to some extent, in addition to its role in activating heme-bound oxygen.

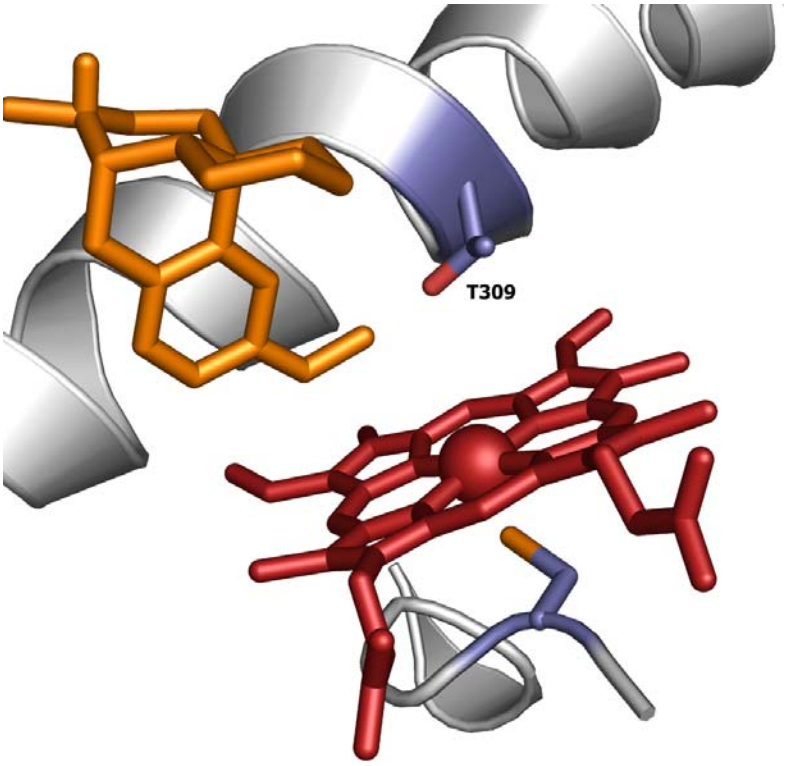

Figure 6: Protein model displaying the active site of CYP2D6 with dextromethorphan bound [36]. The porphyrin is shown with Fe as a sphere, the Fe coordinating C443 is shown and the putative oxygen activating T309. A colored version of the figure is shown in the Appendix of this thesis.

Acknowledgements
We thank Ed Groot for his help in producing the enzymes.

References

1. Keizers PHJ, Schraven LHM, de Graaf C, Hidestrand M, Ingelman-Sundberg M, van Dijk BR,

Vermeulen NPE and Commandeur JNM, Role of the conserved threonine 309 in mechanism of oxidation by cytochrome P450 2D6. *Biochem Biophys Res Commun* **338:** 1065-74, 2005.
2. Ortiz de Montellano PR, *Cytochromes P450: structure, mechanism, and biochemistry*. Kluwer Academic, New York, 2005.
3. Zanger UM, Raimundo S and Eichelbaum M, Cytochrome P450 2D6: overview and update on pharmacology, genetics, biochemistry. *Naunyn Schmiedebergs Arch Pharmacol* **369:** 23-37, 2004.
4. Ingelman-Sundberg M, Genetic polymorphisms of cytochrome P450 2D6 (CYP2D6): clinical consequences, evolutionary aspects and functional diversity. *the Pharmacogenomics Journal* **5:** 6-13, 2005.
5. Vermeulen NPE, Prediction of drug metabolism: the case of cytochrome P450 2D6. *Curr Top Med Chem* **3:** 1227-39, 2003.
6. Hutzler JM, Powers FJ, Wynalda MA and Wienkers LC, Effect of carbonate anion on cytochrome P450 2D6-mediated metabolism in vitro: the potential role of multiple oxygenating species. *Arch Biochem Biophys* **417:** 165-175, 2003.
7. Guengerich FP, Vaz AD, Raner GM, Pernecky SJ and Coon MJ, Evidence for a role of a perferryl-oxygen complex, FeO3+, in the N-oxygenation of amines by cytochrome P450 enzymes. *Mol Pharmacol* **51:** 147-151, 1997.
8. Vaz AD, Pernecky SJ, Raner GM and Coon MJ, Peroxo-iron and oxenoid-iron species as alternative oxygenating agents in cytochrome P450-catalyzed reactions: switching by threonine-302 to alanine mutagenesis of cytochrome P450 2B4. *Proc Natl Acad Sci U S A* **93:** 4644-8, 1996.
9. Vaz AD, McGinnity DF and Coon MJ, Epoxidation of olefins by cytochrome P450: evidence from site-specific mutagenesis for hydroperoxo-iron as an electrophilic oxidant. *Proc Natl Acad Sci U S A* **95:** 3555-60, 1998.
10. Blobaum AL, Kent UM, Alworth WL and Hollenberg PF, Novel reversible inactivation of P450 2E1 T303A by tert-butyl acetylene: The role of threonine 303 in proton delivery to the active site of cytochrome P450 2E1. *J Pharmacol Exp Ther*, 2004.
11. Nagano S and Poulos TL, Crystallographic study on the dioxygen complex of wild-type and mutant cytochrome P450cam. Implications for the dioxygen activation mechanism. *J Biol Chem* **280:** 31659-63, 2005.
12. Hildebrandt P, Resonance Raman spectroscopy of cytochrome P450. In: *Frontiers in biotransformation*, Vol. 7 (Eds. Ruckpaul K and Rein H), pp. 16-215. Akademie-Verlag/VCH, Berlin, 1992.
13. Spiro TG and Wasbotten IH, CO as a vibrational probe of heme protein active sites. *J Inorg Biochem* **99:** 34-44, 2005.
14. Jung C, Hoa GH, Schroder KL, Simon M and Doucet JP, Substrate analogue induced changes of the CO-stretching mode in the cytochrome P450cam-carbon monoxide complex. *Biochemistry* **31:** 12855-62, 1992.
15. Smith SJ, Munro AW and Smith WE, Resonance Raman scattering of cytochrome P450 BM3 and effect of imidazole inhibitors. *Biopolymers* **70:** 620-7, 2003.
16. Yoshioka S, Tosha T, Takahashi S, Ishimori K, Hori H and Morishima I, Roles of the proximal hydrogen bonding network in cytochrome P450cam-catalyzed oxygenation. *J Am Chem Soc* **124:** 14571-9, 2002.
17. Chen Z, Ost TW and Schelvis JP, Phe393 mutants of cytochrome P450 BM3 with modified heme redox potentials have altered heme vinyl and propionate conformations. *Biochemistry* **43:** 1798-808, 2004.
18. Niaura G, Reipa V, Mayhew MP, Holden M and Vilker VL, Structural alterations of the heme environment of cytochrome P450cam and the Y96F mutant as deduced by resonance Raman spectroscopy. *Arch Biochem Biophys* **409:** 102-112, 2003.
19. Egawa T, Imai Y, Ogura T and Kitagawa T, Resonance Raman-Study on Mutant Cytochrome-P-450 Obtained by Site-Directed Mutagenesis. *Biochim Biophys Acta* **1040:** 211-216, 1990.
20. Deng T, Macdonald ID, Simianu MC, Sykora M, Kincaid JR and Sligar SG, Hydrogen-bonding interactions in the active sites of cytochrome P450cam and its site-directed mutants. *J Am Chem Soc* **123:** 269-78, 2001.

21. Stortelder A, Keizers PHJ, Oostenbrink C, de Graaf C, de Kruijf P, Vermeulen NPE, Gooijer C, Commandeur JNM and van der Zwan G, Binding of 7-methoxy-4-(aminomethyl)-coumarin to wild-type and W128F mutant cytochrome P450 2D6 studied by time resolved fluorescence spectroscopy. *Biochem J* **393:** 635-643, 2006.
22. Omura T and Sato R, The carbon monoxide-binding pigment of liver microsomes. II. Solubilization, purification, and properties. *J Biol Chem* **239:** 2379-85, 1964.
23. Deng TJ, Proniewicz LM, Kincaid JR, Yeom H, Macdonald ID and Sligar SG, Resonance Raman studies of cytochrome P450BM3 and its complexes with exogenous ligands. *Biochemistry* **38:** 13699-706, 1999.
24. Jung C, Schulze H and Deprez E, Role of the polarity of the heme environment for the CO stretch modes in cytochrome P-450cam-CO. *Biochemistry* **35:** 15088-94, 1996.
25. Denisov IG, Makris TM, Sligar SG and Schlichting I, Structure and chemistry of cytochrome P450. *Chem Rev* **105:** 2253-77, 2005.
26. Hildebrandt P, Greinert R, Stier A and Taniguchi H, Resonance Raman study on the structure of the active sites of microsomal cytochrome P-450 isozymes LM2 and LM4. *Eur J Biochem* **186:** 291-302, 1989.
27. Hudecek J, Anzenbacherova E, Anzenbacher P, Munro AW and Hildebrandt P, Structural similarities and differences of the heme pockets of various P450 isoforms as revealed by resonance Raman spectroscopy. *Arch Biochem Biophys* **383:** 70-8, 2000.
28. McLean KJ, Cheesman MR, Rivers SL, Richmond A, Leys D, Chapman SK, Reid GA, Price NC, Kelly SM, Clarkson J, Smith WE and Munro AW, Expression, purification and spectroscopic characterization of the cytochrome P450 CYP121 from Mycobacterium tuberculosis. *J Inorg Biochem* **91:** 527-41, 2002.
29. Green AJ, Rivers SL, Cheesman M, Reid GA, Quaroni LG, Macdonald IDG, Chapman SK and Munro AW, Expression, purification and characterization of cytochrome P450 Biol: a novel P450 involved in biotin synthesis in Bacillus subtilis. *J Biol Inorg Chem* **6:** 523-533, 2001.
30. Lochner M, Mu LJ and Woggon WD, Remote effects modulating the spin equilibrium of the resting state of cytochrome P450(cam) - An investigation using active site analogues. *Advanced Synthesis & Catalysis* **345:** 743-765, 2003.
31. Schoneboom JC and Thiel W, The resting state of p450(cam): A QM/MM study. *Journal of Physical Chemistry B* **108:** 7468-7478, 2004.
32. Groenhof AR, Swart M, Ehlers AW and Lammertsma K, Electronic ground states of iron porphyrin and of the first species in the catalytic reaction cycle of cytochrome P450s. *J Phys Chem A* **109:** 3411-3417, 2005.
33. Spiro TG and Li X, Biological applications of Raman spectroscopy. Vol. 3 (Ed. Spiro TG), pp. 1-38. Wiley, New York, 1987.
34. Obayashi E, Shimizu H, Park SY, Shoun H and Shiro Y, Mutation effects of a conserved threonine (Thr243) of cytochrome P450nor on its structure and function. *J Inorg Biochem* **82:** 103-11, 2000.
35. de Groot MJ, Ackland MJ, Horne VA, Alex AA and Jones BC, A novel approach to predicting P450-mediated drug metabolism: Development of a combined protein and pharmacophore model for CYP2D6. *J Med Chem* **42:** 1515-1524, 1999.
36. Keizers PHJ, de Graaf C, de Kanter FJJ, Oostenbrink C, Feenstra KA, Commandeur JNM and Vermeulen NPE, Metabolic regio- and stereoselectivity of cytochrome P450 2D6 towards 3,4-methylenedioxy-N-alkyl-amphetamines: in silico predictions and experimental validation. *J Med Chem* **48:** 6117-6127, 2005.
37. Munro AW, Malarkey K, McKnight J, Thomson AJ, Kelly SM, Price NC, Lindsay JG, Coggins JR and Miles JS, The role of tryptophan 97 of cytochrome P450 BM3 from Bacillus megaterium in catalytic function. Evidence against the 'covalent switching' hypothesis of P-450 electron transfer. *Biochem J* **303 (Pt 2):** 423-8, 1994.

Chapter 8

Binding of 7-methoxy-4-(aminomethyl)-coumarin to wild-type and W128F mutant cytochrome P450 2D6 studied by time-resolved fluorescence spectroscopy

Peter H.J. Keizers*, Aike Stortelder*, Chris Oostenbrink, Chris de Graaf, Petra de Kruijf, Nico P.E. Vermeulen, Cees Gooijer, Jan N.M. Commandeur, and Gert van der Zwan **contributed equally*

adapted from: The Biochemical Journal 2006 **393**: 635-43

Enzyme structure and dynamics may play a main role in substrate binding and the subsequent steps in the cytochrome P450 catalytic cycle. In the present study, changes in the structure of human cytochrome P450 2D6 (CYP2D6) upon binding of the substrate are studied using steady-state and time-resolved fluorescence methods, focusing not only on the emission of the tryptophan residues, but also on emission of the substrate. As a substrate 7-methoxy-4-(aminomethyl)-coumarin (MAMC) was selected, a compound exhibiting native fluorescence. Next to the wild-type enzyme the W128F mutant of CYP2D6 was studied. After binding, a variety of energy transfer possibilities exist, therefore molecular dynamics simulations were performed to calculate distances and relative orientations of donors and acceptors. Energy transfer from W128 to heme appeared to be important, its emission was related to the shortest of the three average tryptophan fluorescence lifetimes observed for CYP2D6. MAMC to heme energy transfer was very efficient as well: when bound in the active site, the emission of MAMC was fully quenched. Steady-state anisotropy revealed that besides the MAMC in the active site, another 2.4% of MAMC was bound outside of the active site to wild-type CYP2D6. The tryptophan residues in CYP2D6 appeared to be less accessible for the external quenchers iodide and acrylamide in presence of MAMC, indicating a tightening of the enzyme structure upon substrate binding. However, the changes in the overall enzyme structure were not very large, since the emission characteristics of the enzyme were not very different in the presence of MAMC.

Introduction

Among the large variety of cytochromes P450 (CYPs), one of the most important phase I drug metabolizing enzymes in humans is CYP2D6. Although the hepatic expression levels are low - about 3% of the total amount of CYP - it is involved in the oxidative metabolism of about 30% of the currently marketed drugs, including β-blockers, neuroleptics, antidepressants and antiarythmics [1, 2]. In addition, this enzyme is clinically relevant because of the large interindividual differences that exist in CYP2D6 activity, due to gene multiplicity and polymorphisms [3]. The scientific challenge is to rationalize why and how substrates are metabolized and to predict the metabolism of newly found or synthesized (drug-like) compounds. For this purpose, detailed structural information on CYP2D6 is essential, but so far no crystal structure of CYP2D6 has been resolved and any structural information on this enzyme still depends on homology modeling.

This paper focuses on some structural features of the enzyme, in particular the conformational changes induced by binding of the substrate. Since homology models as such cannot be used for this purpose, we will make use of molecular dynamics and docking studies, as has been successfully employed for other CYPs [4]. Furthermore, both time-resolved and steady-state fluorescence spectroscopy will be used, as has been applied before to CYP101 [5, 6]. In these studies by Prasad et al. on the dynamics of substrate binding to CYP101, the attention was focused on the emission of the five available tryptophan residues. Tryptophan residues are good endogenous probes since both lifetimes and emission wavelengths may be influenced when the conformation of (parts of) the protein changes [7-9]. Analysis of the tryptophan fluorescence lifetimes data for CYP101 indicated substrate dependent dynamic behavior of W42 in the wild-type and Y96A mutant enzymes. CYP2D6 contains seven tryptophan residues. Based on the homology model, the fluorescence of W128 in CYP2D6 is expected to be sensitive to substrate binding as well. Although it is not located close to the substrate access channel – like W42 in CYP101 – it is close to the heme group. Moreover, it is thought to be bound to the propionate of pyrrole ring D of the porphyrin via hydrogen bonds, as are the homologous tryptophan residues in the crystal structures of mammalian CYPs 2C5, 2C9, 2B4 and 3A4 (PDB codes 1N6B, 1OG2, 1PO5 and 1TQN respectively) [10-13].

A useful feature of tryptophan fluorescence in heme proteins is resonance energy transfer to the heme prophyrin ring [14, 15], which generally leads to a low tryptophan fluorescence quantum yield [16]. In the presence of substrates, other possible energy transfer pathways need consideration as well, i.e. from tryptophan to substrate and from substrate to heme. The CYP2D6 substrate 7-methoxy-4-(aminomethyl)-coumarin (MAMC) is a fluorescing, moderate affinity substrate [17, 18]. Its long-wavelength absorption band overlaps with the tryptophan emission, so when bound to CYP2D6 energy transfer is expected. Furthermore, it can also be excited selectively, allowing for investigation of its properties even when bound to CYP2D6.

In this study, the binding of MAMC to CYP2D6 was studied by steady-state and time-resolved fluorescence experiments on the tryptophan residues and MAMC, both for wild-type and W128F mutant CYP2D6. Quenching experiments with acrylamide and potassium iodide (KI) provide information about the accessibility of the tryptophan residues and the dynamics of the protein structure [19-21]. Experimental results will be compared to molecular dynamics (MD) simulations that are performed on a homology model [22]. The relative locations and orientations of the tryptophan residues, the heme group and MAMC during the simulations can be related to the Förster resonance energy transfer (FRET) efficiency between the individual pairs of FRET partners and are used to support the interpretation of the intricate fluorescence signals.

Materials and Methods

Materials

The pSP19T7LT plasmid containing human C- terminal His_6-tagged CYP2D6 bicistronically together with human NADPH-cytochrome P450 reductase was kindly provided by Prof. Dr. Ingelman-Sundberg. 7-methoxy-4-(aminomethyl)-coumarin (MAMC) and 7-hydroxy-4-(aminomethyl)-coumarin (HAMC) were synthesized as described before [17]. Emulgen 911 was obtained from KAO Chemicals (Tokyo, Japan). Ni-NTA-agarose was from Qiagen (Westburg, Leusden, The Netherlands). All other chemicals were of analytical grade and obtained from standard suppliers.

Mutagenesis and expression

The tryptophan 128→phenylalanine (W128F) mutation was introduced into pSP19T7LT using the QuickChange XL Site-Directed Mutagenesis kit (Stratagene). The sequences of the forward- and reverse oligonucleotides, respectively, with the mutated residue in *italic*, were as follows: 5'-C TAT GGG CCC GCG *TTT* CGC GAG CAG AGG C-3' and 5'-G ATA CCC GGG CGC *AAA* GCG CTC GTC TCC G-3'. After mutagenesis, the presence of the desired W128F mutation was confirmed by DNA sequencing. Both the W128F mutant and the wild-type pSP19T7LT_2D6 plasmids were transformed into *Escherichia coli,* strain JM109. Expression and membrane isolation was carried out as described [23].

Enzyme purification and sample preparation

Enzymes were purified as described before [22]. Shortly, membranes were resuspended in KPi-glycerol buffer (50 mM potassium phosphate buffer, pH 7.4, 10% glycerol). Enzymes were solubilized by stirring in KPi-glycerol supplemented with 0.5% Emulgen 911 for 2 hrs at 4°C. Insoluble parts were removed by centrifugation (60 min, 120,000 g at 4 °C). The supernatant was incubated, gently rocking, with Ni-NTA agarose for 60 min at 4 °C. The column material was filtered out and washed with 10 volumes of KPi-glycerol buffer containing 2 mM histidine. CYP2D6 was eluted with 0.2 M histidine. After overnight dialysis in KPi-glycerol buffer the sample was concentrated on a Vivaspin 20 filtration tube (10.000 MWCO PES, Sartorius, Nieuwegein, The Netherlands). The amount of CYP was quantified by taking CO-difference absorbance spectra [24]. Samples of 1 µM purified enzyme were used for fluorescence measurements. MAMC concentration was 2 µM; at this concentration the emission intensities of CYP2D6 and MAMC were almost equal, the one signal did not overwhelm the other. For the quenching experiments, KI was added to obtain final concentrations in the range from 0 M to 0.5 M. To avoid formation of I_2, 10 mM $Na_2S_2O_3$ was added, the ionic strength was kept constant by addition of KCl.

Enzyme activity

MAMC O-demethylation reactions were carried out in duplicate in a 96 wells plate, in a total volume of 200 µl as described before [23]. The reaction mixture consisted of 50 mM KPi buffer containing 5 mM $MgCl_2$, 0-200 µM MAMC and *E. coli* membranes corresponding to 40 nM wild-type or W128F mutant CYP2D6. The reactions were initiated by addition of an NADPH regenerating system, resulting in final concentrations of 0.1 mM NADPH, 0.3 mM glucose-6-phosphate, and 0.4 units/ml glucose-6-phosphate dehydrogenase. The reaction was monitored for 30 min at 37°C on a Victor^2 1420 multilabel counter (Wallac Oy Finland) (λ_{ex}=405nm, λ_{em}=460nm). The metabolite of MAMC, i.e. HAMC, was quantified using the synthetic reference compound.

Fluorescence instrumentation

Time-resolved fluorescence experiments were performed using a laser system combined with time-resolved photon counting detection. The laser system used was a Mira 900-P laser (Coherent, Santa Clara CA, USA), emitting 3 ps pulses at a repetition rate of 76 MHz, pumped by a Verdi-8 diode laser (Coherent). The Mira 900-P is a mode-locked titanium-sapphire laser, tunable from approximately 700 to 1000 nm. The laser emission was led through a pulse picker (Coherent), which reduced the repetition rate to 4.75 MHz in order to avoid double excitation of molecules. The output wavelength of 290 nm was generated by means of a frequency tripler (Coherent). This light was used to excite the protein sample in a cell with 1 cm pathlength (type 104F, Hellma GmbH &Co KG, Müllheim, Germany). For the time-correlated single-photon counting (TCSPC), a SPC-630 (Becker &Hickl GmbH, Berlin, Germany) system with a time-resolution of about 15 ps was used. A laser pulse focused on a photodiode provided the synchronization signal. Fluorescence emission was collected at 90º, dispersed by a monochromator

(TVC JarrellAsh Monospec 18, Grand Junction CO, USA) and detected by a photomultiplier tube. Decays were recorded at wavelengths between 330 and 440 nm in 10 nm steps. Quenching experiments were performed using TCSPC detection at two wavelengths, 340 and 430 nm. Steady-state fluorescence emission and excitation spectra were recorded on a LS-50B instrument (PerkinElmer Inc., Wellesley, MA, USA). Steady-state anisotropy measurements were conducted using a Fluorolog-tau2 system (HORIBA Jobin Yvon Inc., Edison, NJ, USA).

Data analysis
Fluorescence decay curves were analyzed using a fit procedure based on the Levenberg-Marquardt algorithm. This procedure uses the instrument response signal (obtained by recording scattered laser-light) for deconvolution of the recorded decays and determination of lifetimes and wavelength dependent amplitudes. Each decay-curve is fitted by mono- or multi-exponential curves (eq. 1):

$$I(t) = \sum_i A_i e^{\frac{-t}{\tau_i}} \qquad (1)$$

The quality of the fit ("goodness of fit") was assessed on the basis of χ^2, the covariance matrix and the distribution of residuals. The set of time-constants was kept as low as possible; normally not more than three constants were needed to obtain a fit of sufficient quality. For measurements at a series of detection wavelengths, a global fit procedure was used, based on the method described above. Lifetimes are assumed to be constant for the decays included, while the amplitudes were varied. This assumption is correct for proteins in many cases [25].
Decay-associated spectra (DAS) provide information on the fluorescence emission per lifetime component. DAS are constructed by distributing the total intensity per decay-curve over the lifetimes that make up the total intensity according to their ratio (amplitudes are obtained by global fit). The relative fluorescence intensity of lifetime component τ_j, at wavelength $\lambda_{..}$ with amplitude *A*, can be expressed by the following equation:

$$I_{\tau_j}(\lambda) = \frac{A_j \tau_j}{\sum_i A_i \tau_i} \qquad (2)$$

Förster resonance energy transfer (FRET)
FRET is radiationless transfer of excitation energy from a donor to an acceptor chromophore, controlled by long range dipole-dipole interactions [26, 27]. It can be used for estimation of intermolecular distances, because the efficiency of energy transfer (Φ_T) is dependent on the distance *r* between a donor with lifetime τ_D, and an acceptor, as expressed in equation 3:

$$\Phi_T = \frac{k_T^{dd}}{k_D + k_T^{dd}} = \frac{1}{1 + (r/R_0)^6} = 1 - \frac{\tau_D}{\tau_D^0} \qquad (3)$$

where k_T^{dd} is the energy transfer rate, defined as $k_T^{dd} = k_D \left[\frac{R_0}{r}\right]^6 = \frac{1}{\tau_D^0}\left[\frac{R_0}{r}\right]^6$, k_D is the emission rate constant of the donor and τ^0_D its lifetime in the absence of energy transfer; R_0 is the Förster radius, the distance at which transfer and spontaneous decay of the donor are equally probable. R_0 can be determined experimentally and is given by equation 4:

$$R_0^6 = \frac{9000(\ln 10)\kappa^2 \Phi_D^0}{128\pi^5 N_A n^4} \int_0^\infty I_D(\lambda)\varepsilon_A(\lambda)\lambda^4 \, d\lambda \qquad (4)$$

where κ^2 is the orientation factor of the donor and acceptor transition dipole moments, Φ^0_D the fluorescence quantum yield of the donor in absence of energy transfer, N_A Avogadro's number, n the average refractive index of the medium, and $\int_0^\infty I_D(\lambda)\varepsilon_A(\lambda)\lambda^4\, d\lambda$ the overlap integral of the (normalized) donor emission ($I_D(\lambda)$) and acceptor absorption spectra ($\varepsilon_A(\lambda)$).

The distance dependence of energy transfer makes FRET useful to study structural changes. A complicating feature is the dependency of the FRET efficiency on the orientation of donor and acceptor transition dipoles via κ^2. This orientation factor varies between 0 and 4, and can be calculated from atomic coordinates. Because of the dynamics of the protein, the exact orientations of the dipole transition moments are not constant, and values of κ^2 (and also the distance r) will fluctuate in time.

Anisotropy

Steady-state anisotropy experiments were performed on a Fluorolog FL3-11-Tau3 system (Jobin-Yvon Horiba, Edison NJ, USA). Anisotropy is defined as

$$r = \frac{I_{vv} - I_{vh}}{I_{vv} + 2I_{vh}} = \frac{2\cos^2\theta}{3 + 2\cos^2\theta} \qquad (5)$$

in which I_{vv} and I_{vh} are the intensities of the vertically and horizontally polarized components of the fluorophore emission, respectively, and θ is the angle between absorption and emission transition dipole moment. Equation 5 can be adapted to an equation giving the ratio of concentrations of unbound, [S], to bound, [PS], substrate:

$$r = \frac{2\cos^2\theta_1}{3\left(1 + \frac{[S]}{[PS]}\right) + 2\cos^2\theta_1} \qquad (6)$$

the (measured) anisotropy for the unbound substrate being 0. A solution of 50 μM MAMC in glycerol was used to determine the limiting anisotropy r_0.

Computer simulations

The substrate MAMC was docked into the active site of the homology model with the programs Autodock and GOLD [28, 29]. Five molecular dynamics simulations were performed in explicit Simple Point Charge water [30]: four with different initial orientations of the substrate and one with the wild-type CYP2D6 protein without substrate. Interatomic interactions were calculated from the GROMOS force field parameter set 43A2 [31-33]. All five simulations were performed for ten nanoseconds using the GROMACS simulation package [34]. Simulation parameter settings were chosen as described before [22].

The value of κ^2/r^6 for individual pairs of fluorescent groups is directly proportional to the FRET efficiency of the pair (eq. 3 and 4). In order to relate the structural dynamics to the FRET efficiency, dipole transition moments were chosen as follows. For tryptophan the transition moment ^1L_a lies in the plane of the indole ring at an angle of -46 degrees with respect to the indole molecular frame [35]. Only the ^1L_a transition dipole moment of tryptophan was included, since it is the only emitting state (internal conversion from ^1L_b is on a much faster timescale than fluorescence). For the heme moiety, two degenerate dipole transition moments in the plane of the heme were considered, one pointing from N_1 to N_3 and another perpendicular to this [15]. For the substrate MAMC a transition dipole moment was estimated in analogy to previous studies on coumarin-type compounds point from atom 3 to atom 7 (Figure 1) [36]. κ^2/r^6 was calculated for every pair of trp-heme, trp-MAMC and MAMC-heme transition moments and averaged over the simulations.

Solvent accessible surface areas of all tryptophan residues have been calculated from the MD simulation data according to the algorithm of Lee and Richards [37], for all tryptophan residues, using a probe size of 0.14 nm.

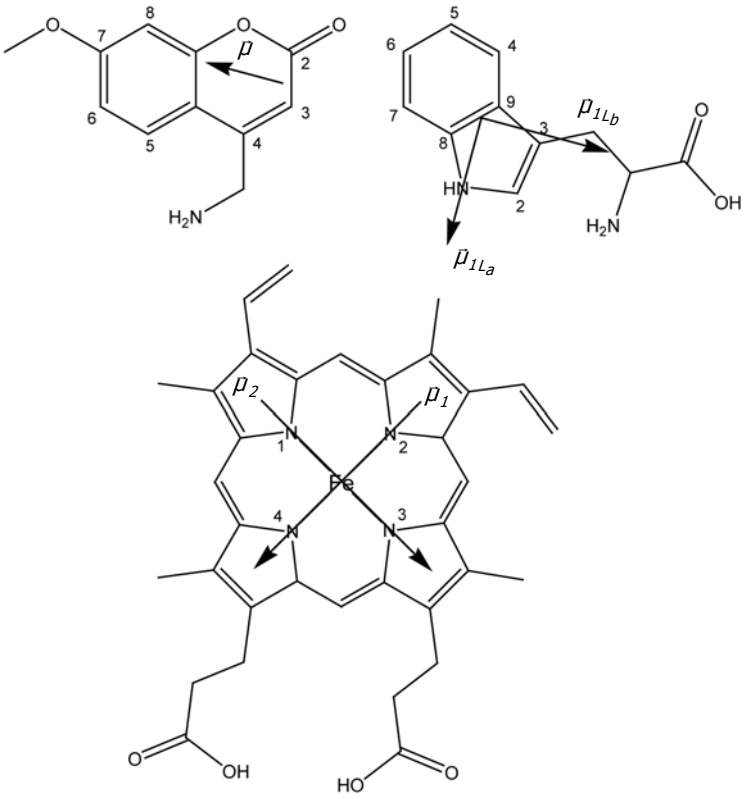

Figure 1: Structures of 7-methoxy-4-(aminomethyl)-coumarin (MAMC), tryptophan and the heme group in CYP 2D6. $\vec{\mu}_{1L_a}$ *indicates the transition dipole moment; for tryptophan and heme two transitions are possible, as indicated.*

Results and discussion

Expression, purification and activity of mutant W128F

The expression levels of the W128F mutant CYP2D6 were about 200 nM in an average culture, which is equal to those of the wild-type enzyme. P420 (inactive form of P450, determined as a peak at 420 nm in CO-difference spectrum) was present in the crude membranes but was lost during the purification of the W128F mutant. The turnover rate of MAMC O-demethylation by the W128F mutant is about two-fold lower than that of wild-type CYP2D6, V_{max} 3.5 ± 0.7 vs. 6.7 ± 0.1 min^{-1}, whereas the K_m remained constant, K_m 29.8 ± 0.1 vs. 30 ± 1 μM for mutant and wild-type respectively. From these similar kinetic parameters W128 does not appear to be crucial for MAMC O-demethylating activity, nor for the CYP2D6 stability. This is in agreement with MD simulations, showing that W128 is not the only residue forming hydrogen bonds to the propionate of pyrrole ring D of the porphyrin; R101 forms H-bonds to the same atoms.

Fluorescence properties of CYP2D6 and MAMC

The fluorescence emission spectra of wild-type and W128F CYP2D6 in the presence and absence of MAMC, as well as for MAMC alone, are depicted in Figure 2. The corresponding excitation and emission maxima together with the fluorescence lifetimes are listed in Table 1.

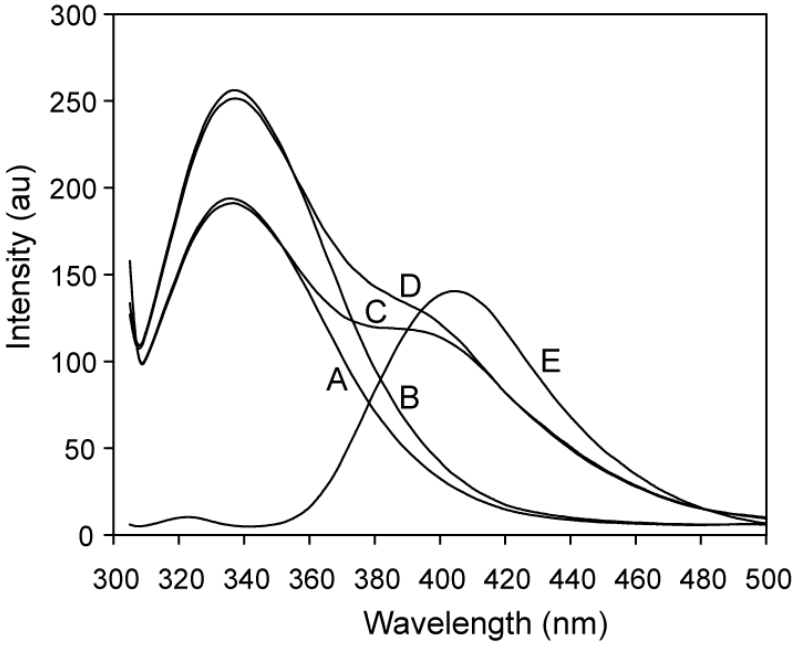

Figure 2: Emission spectra of 1 μM of the W128F mutant (A) and of wild-type CYP2D6 (B), and mixtures of W128F mutant and wild-type CYP2D6 with 2 μM MAMC (C and D, respectively). Also the emission of 2 μM of MAMC is shown (E).

The emission maximum at 335-340 nm indicate moderately buried tryptophan residues [38]. The emission spectrum of the W128F mutant is 2 nm red-shifted compared to wild-type CYP2D6 and is about 22% lower in intensity. In the presence of MAMC, excitation- and emission maxima of wild-type and W128F mutant CYP2D6 do not shift, indicating that no large conformational change of the enzyme is needed to accommodate the substrate, but their intensities decrease about 6%. A notable decrease in the MAMC emission intensity is seen in the presence of enzyme, which is the same for the mutant W128F (35%) and for wild-type CYP2D6 (35%), indicative of some form of energy transfer or quenching. Also, in presence of both CYP2D6 enzymes a blue shift in MAMC emission of about 6 nm is observed. This shift is most likely the result of a smaller Stokes-shift (the excitation spectrum does not change), and indicates a less polar environment for MAMC in presence of CYP2D6 than for pure MAMC in aqueous solution, which is of course expected.

Fitting of the fluorescence intensity decay curves yielded three tryptophan lifetimes for wild-type and W128F mutant CYP2D6 and two for MAMC, as shown in Table 1. The origin of this double exponential decay of MAMC fluorescence is not trivial; it may be caused by a charge transfer state, as described for coumarin-type molecules [26, 39]. The fluorescence lifetimes

of both wild-type and W128F mutant CYP2D6 do not change dramatically upon addition of MAMC. The tryptophan DAS of wild-type CYP2D6 and W128F mutant are shown in Figure 3.

Table 1: Fluorescence maxima (nm), relative intensities (peak area, AU) and emission lifetimes (ns) for wild-type and W128F mutant CYP2D6 and MAMC. For the lifetimes the relative contributions to the total signal are indicated between parentheses (%).

Analytes	λ_{ex}	λ_{em}	I_{em}	τ_1	τ_2	τ_3
WT	278	336	1.38 ± 0.003	0.13 ± 0.05 (80)	1.06 ± 0.03 (17)	3.81 ± 0.08 (3)
WT + MAMC	278	335	1.28 ± 0.006	0.12 ± 0.06 (83)	1.30 ± 0.27 (14)	4.00 ± 0.17 (3)
W128F	280	338	1.07 ± 0.002	0.07 ± 0.02 (84)	1.09 ± 0.06 (13)	4.17 ± 0.06 (3)
W128F + MAMC	280	333	0.99 ± 0.004	0.14 ± 0.04 (81)	1.40 ± 0.24 (16)	3.96 ± 0.30 (3)
MAMC	328	406	0.56 ± 0.018	0.75 ± 0.12 (52)	2.53 ± 0.06 (48)	
MAMC + WT	328	400	0.36 ± 0.006	0.68 ± 0.07 (56)	2.62 ± 0.11 (44)	
MAMC + W128F	327	400	0.36 ± 0.006	0.71 ± 0.16 (50)	2.77 ± 0.17 (50)	

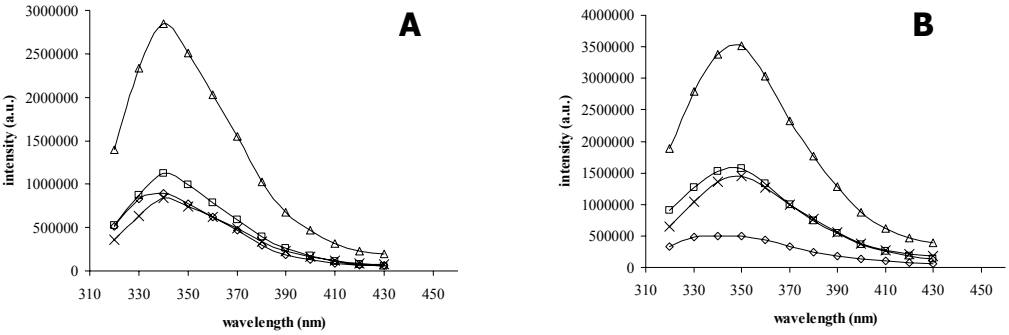

Figure 3: Decay-associated spectra of wild-type CYP2D6 (A) and W128F (B) and the corresponding lifetimes (△total spectrum, ◇ τ_1,□ τ_2, x τ_3).

For the wild-type enzyme all three components have similar relative intensities and their emission maxima are close as well. Interestingly, the spectrum associated with τ1 of the W128F mutant has a three-fold lower intensity than that of τ2 and τ3. This suggests that W128 contributes predominantly to the shortest lifetime (of 130 ps) component of the overall tryptophan emission. This tryptophan residue was expected to have such a short fluorescence lifetime, since its location at position 128 is close to the heme and its emission will therefore be quenched (by a FRET mechanism) more strongly than the other residues. On the other hand, the remaining signal indicates that the shortest lifetime is not solely due to W128 and in fact is even shorter than in wild-type CYP2D6. The shorter τ1 for W128F compared to wild-type CYP2D6 was unexpected: the tryptophan closest to heme is removed, so at first sight the residual lifetime should be longer. However, in view of the

large number of possible relaxation times of the six tryptophan residuess in W128F, this seemingly shortened lifetime may be the result of a shift in the distribution of all tryptophan lifetimes over the three lifetimes obtained from the fit of the data. In addition, lifetimes shorter than 100 ps are not uncommon in proteins, even in cases when no heme or other energy transfer mechanism is present [40, 41], and may be caused by close-lying quenching amino acids such as tyrosine, cysteine or histidine [42]. The decay times of MAMC do not change significantly when either wild-type CYP2D6 or W128F mutant is present. Although a change would be expected due to interactions with the protein, it seems that these interactions do not influence the lifetimes or that the changes are too small to be observed in the overwhelming emission of the unbound MAMC. A more feasible explanation may be that the fluorescence quantum yield of bound MAMC is negligible due to quenching by the close-lying heme. To assess the latter explanation, the FRET "network" in the CYP2D6/MAMC system was evaluated, which will be discussed later.

Quenching experiments

The accessibility of the tryptophan residues was studied using acrylamide and iodide as dynamic quenchers. In both cases quenching only takes place if the quencher and the fluorescing tryptophan residue are in physical contact; long range quenching does not occur. Acrylamide is a small and uncharged molecule that can diffuse into the protein; its quenching behaviour provides information on the overall accessibility of the tryptophan residues in the protein [19]. Iodide is a charged ion, which cannot enter the protein interior, and will quench only exposed tryptophan residues on the periphery of the protein [21]. The fluorescence intensity quenching experiments using acrylamide yielded linear Stern-Volmer curves for both wild-type and W128F CYP2D6. Apparently, static quenching in ground-state tryptophan-acrylamide complexes is negligible. Using iodide as a quencher, slightly downward curved Stern-Volmer curves were obtained, indicating that some tryptophans are unattainable to iodide [19]. For MAMC emission, upward curving Stern-Volmer graphs are observed in the case of iodide quenching, indicating a static component. However, analysis of the data using a modified version of the Stern-Volmer equation which allows for the separation of the static and dynamic part of the observed quenching, showed that quenching in this case is not caused by ground-state complexes, but rather by close proximity of quencher and fluorophore, resulting in almost 100% quenching probability [20], presumably caused by iodide being attracted to the positive charge of the substrate. The quenching constants for all compounds are collected in Table 2.

The acrylamide quenching constants for tryptophan are similar for the two enzymes, so no large differences in permeability exist between wild-type and W128F CYP2D6. In both cases, the quenching rates are somewhat smaller in the presence of MAMC (12.5 and 13.0 vs. 9.7 and 10.5 $M^{-1}ns^{-1}$), indicating a slightly more compact structure. The structure of CYP2D6 is less compact compared to CYP101, which quenching constant is three times lower (4.5 and 1.45 M^{-1}, respectively) [6]. The accessible fraction of tryptophan emission for quenching by acrylamide is, as expected, around 100%. The smaller accessible fraction of wild-type CYP2D6 in the presence of MAMC – some 20% lower - might be caused by MAMC blocking the pathway for acrylamide in the substrate access channel, in line with the somewhat decreased quenching constant found in this case. This effect was not observed for the W128F mutant, which indicates that indeed the access channel to the active site is blocked: apparently it is W128, which lies in the active site, that cannot be reached anymore by acrylamide when MAMC is present.

As expected, the tryptophan residues in both W128F and wild-type CYP2D6 are less easily accessible to iodide than to acrylamide, and the fraction of the total emission accessible to

quenching is accordingly smaller (30-40%). This is somewhat higher than for, for example, the 16% accessible for substrate-free CYP101 [6], but also the quenching constants for CYP2D6 are about five times larger, indicating a higher degree of exposure of the tryptophan residues in CYP2D6 than in CYP101. The quenching constant of W128F is slightly higher than that of wild-type CYP2D6 (0.9 vs. 0.7 M^{-1}). Its structure may be different, and/or the remaining tryptophan residues are relatively more exposed, resulting in a somewhat higher accessible fraction (0.4 instead of 0.3). In the presence of MAMC, the quenching rate is slightly lower, as was the case with acrylamide. This supports the explanation that the substrate-bound enzyme has a less accessible structure. Calculation of the solvent accessible surface areas (SASA) revealed that W152, W262 and especially W75 were accessible to bulk solvent, while W128, W316 and W409 were not found to interact strongly with water. Consequently, we expect the iodide quenching to be mostly acting on W75. Therefore, it is not surprising that the accessible fraction of emission of W128F found with the quenching experiments is not much different from the wild-type. In the presence of the substrate MAMC the SASA do not change much, confirming the fluorescence quenching results. Also in that case, W75 is the most accessible residue and the accessibilities of the other residues are maximally 10%. As acrylamide is much smaller and may penetrate the protein, it is likely to interact with all tryptophan residues and calculations of the SASA will not yield useful results for this probe.

Table 2: Fluorescence quenching parameters (K_{sv} in M^{-1}, k_q in $10^9 \cdot M^{-1}s^{-1}$, τ_{av} in ns) of wild-type CYP2D6, W128F mutant CYP2D6, MAMC and MAMC in presence of the enzymes, obtained from (linear) Stern-Volmer plots.

Analytes	Acrylamide				Iodide			
	K_{SV}	k_q	τ_{av}	f_a	K_{SV}	k_q	τ_{av}	f_a
WT	4.5	12.5	0.36	1.1	0.7	1.8	0.40	0.3
WT+MAMC	3.8	9.7	0.39	0.8	0.6	1.5	0.40	0.3
W128F	3.9	13.0	0.30	1.1	0.9	3.0	0.30	0.4
W128F+MAMC	4.1	10.5	0.39	1.0	0.8	2.1	0.39	0.3
MAMC	2.7	1.5	1.76	0.9	14.1	17.2	0.82	1.1
MAMC+WT	3.1	1.9	1.55	0.8	15.2	10.3	1.47	1.1
MAMC+W128F	2.9	1.8	1.59	0.9	18.4	11.6	1.59	1.1

FRET efficiencies

In CYP2D6 three chromophoric groups are present; the porphyrin, the tryptophan residues and the coumarin substrate, all are absorbing, and the coumarin and tryptophan residues also emitting, in generally the same spectral range. The spectral overlap may give rise to energy transfer pathways, in particular of the Förster-type. The location and orientation of MAMC in the active site of CYP2D6, corresponding to one of the initial structures of the simulations, is illustrated in Figure 5. Three FRET pathways are possible when MAMC is in close proximity of CYP2D6: (a) from the tryptophan residues to heme, a well-known and efficient energy transfer route in heme-proteins [14], (b) from the tryptophan residues to MAMC and (c) from MAMC to the heme-moiety. Over the course of the 10 ns MD simulations the overall structure of the protein was well maintained. Atom-positional root-mean-square deviations (rmsd) from the initial homology model leveled of to approximately 0.3 - 0.4 nm, important secondary structure elements and hydrogen bonds were maintained throughout the simulations. The molecular dynamics simulations to determine the κ^2/r^6 factor of FRET yielded slightly different values for the starting configurations from the two docking algorithms used (Autodock and GOLD), but the trends were identical.

Table 3: Orientation factors (κ^2/r^6 values in nm^{-6}) of the tryptophans to the heme, the tryptophans to MAMC, and of MAMC to the heme, obtained from MD simulations using the CYP2D6 homology model.

	Heme[a] (MAMC present)		Heme[a] (no MAMC present)		MAMC	
	Average	rmsd	Average	rmsd	Average	rmsd
W75	0.007	0.004	0.022	0.011	0.005	0.005
W128	0.330	0.192	0.362	0.145	0.079	0.048
W152	0.048	0.025	0.036	0.016	0.002	0.002
W262	0.002	0.002	0.003	0.003	0.001	0.000
W316	0.069	0.022	0.083	0.019	0.009	0.006
W409	0.017	0.013	0.029	0.011	0.003	0.003
MAMC	7.289	6.365				

[a] *both dipole directions added*

(a) *Tryptophan to heme*. Apart from spectral overlap, the FRET efficiencies for the different residues will not only depend on their distance to the heme group but also on the relative orientation of the donor and acceptor transition dipoles, expressed in κ^2. The value of κ^2/r^6 was calculated from MD simulations for six of the tryptophans to the porphyrin ring in CYP2D6. The data of W29 could not be calculated, since its position is in the membrane anchoring α-helix, which is not included in the homology model. The κ^2/r^6 factors thus obtained differ several orders of magnitude for the tryptophan residues concerned (Table 3). The tryptophan-to-heme κ^2/r^6 factor was found to be much higher for W128 than for the other tryptophan residues. This supports the suggestion that W128 contributes mainly to the shortest fluorescence lifetime, although it should be realized, that energy transfer to the heme may not be the only cause of lifetime-shortening, as mentioned above. The energy transfer from the other tryptophan residues to the heme does not seem to be important: the quantum yield of CYP2D6 as a whole is not extremely low (6% for wild-type CYP2D6, 4% for W128F), and the lifetimes are mostly in the nanosecond range.

(b) *Tryptophan to MAMC*. The spectral overlap of the tryptophan emission and the MAMC absorption is very large. However, as can be seen from Table 1, the fluorescence lifetimes of CYP2D6 are not shorter in the presence of MAMC, while furthermore a negative exponent (indicating an increase of intensity) is not needed to make a good fit of the MAMC intensity decay. Still, the tryptophan emission spectrum in the presence of MAMC decreases about 6%, but also the intensity of the MAMC spectrum itself decreases (Figure 2). Calculations of the κ^2/r^6 value between the various tryptophan residues and MAMC from the MD simulations show no significant changes for most tryptophan residues, and indicate only a possibility for W128 to transfer its energy to MAMC. However, in that case no decrease in emission intensity would be expected for the W128F mutant, in contrast to the results. On the other hand, because the heme-group is positioned between MAMC and W128, the tryptophan emission will rather transfer its energy to heme instead of to MAMC. An explanation for the reduced tryptophan emission intensity upon the addition of MAMC may be a conformational change in the protein, repositioning the tryptophan residues closer to quenching amino acids or the heme-moiety.
The rmsd values of κ^2/r^6 give the width of the distribution around the average value and are an indication of flexibility of the protein. As is seen in Table 3, the relative rmsd values are not much different for six tryptophans with or without MAMC present. Monitoring of the positions of the tryptophan transition dipole moments yielded the largest fluctuations for W262 for the substrate-free CYP2D6, and for W75 in the presence of MAMC. However, the

fluctuations are smaller than 0.5 nm, which is small on the scale of the total protein (about 7 nm diameter).

(c) *MAMC to heme*. Also for MAMC acting as the donor and the heme group as the acceptor, the spectral overlap is extensive. The 35% reduction of the MAMC emission intensity in presence of both wild-type CYP2D6 and W128F mutant indicate that, indeed energy transfer takes place. For the MAMC-heme pair the predicted κ^2/r^6 value is very high. The values for tryptophan to MAMC are in general relatively small; also here the highest value is found for W128, which is the closest to the active site. The MD simulations of r^6 and κ^2 revealed a FRET efficiency of almost 100%, meaning that the excitation energy is completely transferred from MAMC to the heme and that no emission of MAMC when bound in the active site can be seen at all. This would explain why the lifetimes of MAMC in presence of CYP2D6 are not shortened and why the quenching properties are not changed: emission is only observed from unbound substrate. Thus, from the intensity reduction in MAMC emission (Table 1), it can be concluded that about 35% of the total amount of MAMC added to the sample is bound to CYP2D6, both for wild-type and W128F mutant. This is also reflected in the similar activities. Unfortunately, this explanation also implies that the emission spectra do not reveal any information on the properties of bound MAMC. On the basis of these results, MAMC to enzyme dissociation constants can be estimated using Equation 7:

$$K_d = \frac{[S][P]}{[SP]} = \frac{[S_0 - x][P_0 - x]}{x} \qquad (7)$$

S_0 and P_0 are the initial MAMC and enzyme concentrations (resp. 2 µM and 1 µM) and x is the concentration of MAMC bound in the active site. It is calculated that Kd = 0.56 ± 0.10 µM for both wild-type and W128F mutant CYP2D6.

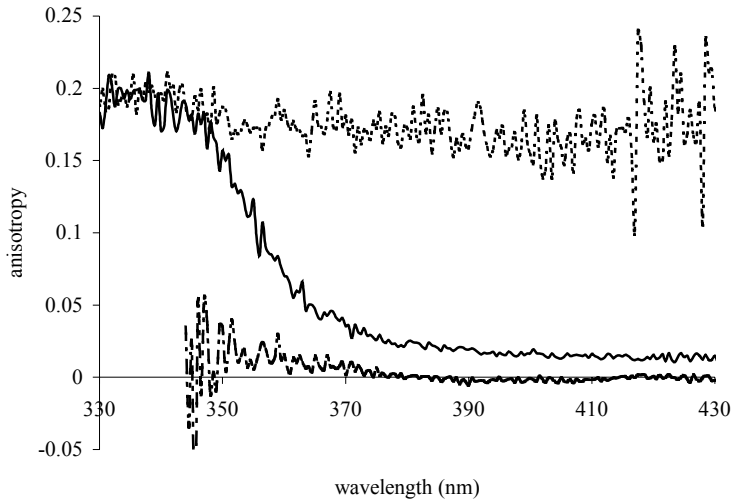

Figure 4: Steady-state anisotropy traces of 1 µM wild-type CYP2D6 (dotted line), 2 µM MAMC (dashed line) and the mixture of both (black line).

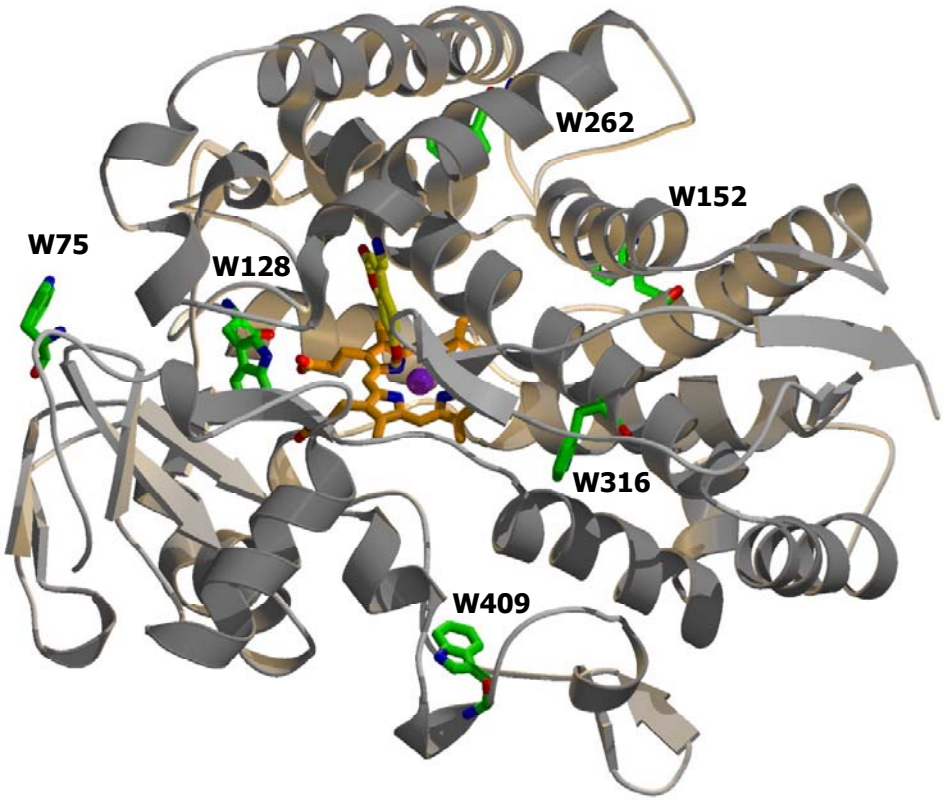

Figure 5: Homology model of CYP2D6 based on rabbit CYP2C5, indicating the positions of the six tryptophans, the heme-group and the substrate MAMC. W29 is not present in the homology model. A colored version of the figure is shown in the Appendix of this thesis.

Table 4: Summary of the three types of MAMC in the presence of CYP2D6.

	MAMC type	WT	W128F
I	Unbound	62.6 ± 2.0 %	62.4 ± 2.1 %
II	Bound in active site	35.0 ± 1.5 %	35.2 ± 1.6 %
III	Associated to enzyme	2.4 ± 0.5 %	2.4 ± 0.5%

Anisotropy

The results of steady-state anisotropy experiments are shown in Figure 4. The anisotropy of the tryptophan residues in the protein is about 0.2, as is expected for tryptophans rotating slowly on the fluorescence lifetime-scale [26]; the slow rotation is caused by overall tumbling of the protein, side-chain rotations are too fast to be seen. Free MAMC in solution rotates also much faster than its fluorescence decay, and indeed no residual anisotropy is observed.

Although the analysis of FRET suggests that MAMC bound to CYP2D6 will not contribute to the emission spectrum at all, a residual anisotropy of 0.015 is seen in the steady-state

anisotropy traces of both wild-type and W128F CYP2D6. This anisotropy can most probably be explained by invoking a third type of MAMC present in the sample: MAMC that is also bound in some way to CYP2D6 (to be denoted as "associated MAMC", Table 4). Its emission will be partly polarized, as it rotates with the enzyme, but it is not located close enough to the heme to be quenched by FRET. Maybe the substrate first binds to the access channel of the enzyme, which undergoes a conformational change before allowing it to enter [43, 44], or it is located in the access channel. Using equations 5 and 6 and the initial anisotropy r_0 = 0.39, the ratio of free MAMC to associated MAMC is calculated to be 41 ± 6, implying that 2.4 ± 0.5 % of the amount of MAMC that is not bound in the active site is associated in another way to the protein. As these MAMC molecules will experience a slightly more apolar environment, their emission is blue-shifted, as can be seen in Figure 2. However, the observed shift of 6 nm is relatively large, if only 2.4% of MAMC is associated to the enzyme. Presumably the associated MAMC molecules still have a large degree of rotational freedom, causing the amount to be underestimated when calculated from anisotropy experiments.

Conclusions

Wild-type and W128F mutant CYP2D6 were investigated by steady-state and time resolved fluorescence experiments to determine the extent of conformational changes in the protein, and the properties of MAMC upon binding. Because both the enzyme and the substrate contain fluorophores, it was possible to study emission properties of both compounds. The experiments do not show indications for large scale conformational changes in CYP2D6 in the presence of the substrate MAMC: there are only small changes in emission maxima and lifetimes when MAMC is present. However, the tryptophan residues in substrate-bound enzyme are quenched less efficiently than in substrate-free CYP2D6, which may be caused either by shielding of the tryptophans by MAMC or a "contraction" of the structure, induced by binding of the substrate. MD simulations indicated that the tryptophan residues are more flexible in the presence of MAMC, but these changes are small on the scale of the total protein; no large fluctuations in protein structure are found. Mutagenesis of more tryptophan residues would be helpful in the assignment of lifetimes to individual residues, and may provide more information on possible local conformational changes in the enzyme upon substrate binding. Several FRET pathways were evaluated from which was concluded that emission of MAMC when bound to CYP2D6 is completely transferred to the heme, and is therefore not observed. From anisotropy experiments it could be inferred that not all of the observable MAMC is free in solution, but that at least 2 % is associated to the protein. No differences were found in the dissociation constants.

Acknowledgements

We thank Ed Groot for his help in expressing and purifying the enzymes.

References

1. Zanger UM, Raimundo S and Eichelbaum M, Cytochrome P450 2D6: overview and update on pharmacology, genetics, biochemistry. *Naunyn Schmiedebergs Arch Pharmacol* **369:** 23-37, 2004.
2. Shimada T, Yamazaki H, Mimura M, Inui Y and Guengerich FP, Interindividual variations in human liver cytochrome P450 enzymes involved in the oxidation of drugs, carcinogens and toxic chemicals: studies with liver microsomes of 30 Japanese and 30 Caucasians. *J Pharmacol Exp Ther* **270:** 414-23, 1994.
3. Ingelman-Sundberg M, Pharmacogenetics of cytochrome P450 and its applications in drug therapy: the past, present and future. *Trends Pharmacol Sci* **25:** 193-200, 2004.

4. de Graaf C, Vermeulen NPE and Feenstra KA, Cytochrome P450 in silico: an integrative modeling approach. *J Med Chem* **48:** 2725-55, 2005.
5. Prasad S, Mazumdar S and Mitra S, Binding of camphor to Pseudomonas putida cytochrome p450(cam): steady-state and picosecond time-resolved fluorescence studies. *FEBS Lett* **477:** 157-60, 2000.
6. Prasad S and Mitra S, Role of protein and substrate dynamics in catalysis by Pseudomonas putida cytochrome P450cam. *Biochemistry* **41:** 14499-508, 2002.
7. Beechem JM and Brand L, Time-Resolved Fluorescence of Proteins. *Annual Review of Biochemistry* **54:** 43-71, 1985.
8. Eftink MR, The use of fluorescence methods to monitor unfolding transitions in proteins. *Biochemistry-Moscow* **63:** 276-284, 1998.
9. Engelborghs Y, Correlating protein structure and protein fluorescence. *Journal of Fluorescence* **13:** 9-16, 2003.
10. Wester MR, Johnson EF, Marques-Soares C, Dansette PM, Mansuy D and Stout CD, Structure of a substrate complex of mammalian cytochrome P450 2C5 at 2.3 A resolution: evidence for multiple substrate binding modes. *Biochemistry* **42:** 6370-9, 2003.
11. Williams PA, Cosme J, Ward A, Angove HC, Matak Vinkovic D and Jhoti H, Crystal structure of human cytochrome P450 2C9 with bound warfarin. *Nature* **424:** 464-8, 2003.
12. Scott E, He Y, Wester MR, White M, Chin C, Halpert J, Johnson EF and Stout CD, An open conformation of mammalian cytochrome P450 2B4 at 1.6-A resolution. *Proc Natl Acad Sci U S A* **100:** 13196-201, 2003.
13. Yano JK, Wester MR, Schoch GA, Griffin KJ, Stout CD and Johnson EF, The structure of human microsomal cytochrome P450 3A4 determined by X-ray crystallography to 2.05-A resolution. *J Biol Chem* **279:** 38091-4, 2004.
14. Weber G and Teale FJW, Electronic Energy Transfer in Haem Proteins. *Discuss Faraday Soc***:** 134-141, 1959.
15. Gryczynski Z, Lubkowski J and Bucci E, Intrinsic fluorescence of hemoglobins and myoglobins. *Fluorescence Spectroscopy* **278:** 538-569, 1997.
16. Hochstrasser RM and Negus DK, Picosecond fluorescence decay of tryptophans in myoglobin. *Proc Natl Acad Sci U S A* **81:** 4399-403, 1984.
17. Onderwater RC, Venhorst J, Commandeur JNM and Vermeulen NPE, Design, synthesis, and characterization of 7-methoxy-4-(aminomethyl)coumarin as a novel and selective cytochrome P450 2D6 substrate suitable for high-throughput screening. *Chem Res Toxicol* **12:** 555-9, 1999.
18. Venhorst J, Onderwater RC, Meerman JH, Vermeulen NPE and Commandeur JNM, Evaluation of a novel high-throughput assay for cytochrome P450 2D6 using 7-methoxy-4-(aminomethyl)-coumarin. *Eur J Pharm Sci* **12:** 151-8, 2000.
19. Eftink MR and Ghiron CA, Exposure of tryptophanyl residues in proteins. Quantitative determination by fluorescence quenching studies. *Biochemistry* **15:** 672-80, 1976.
20. Lakowicz JR, Quenching of fluorescence. In: *Principles of fluorescence spectroscopy*, pp. 257-95. Plenum Press, New York, 1983.
21. Lehrer SS, Solute perturbation of protein fluorescence. The quenching of the tryptophyl fluorescence of model compounds and of lysozyme by iodide ion. *Biochemistry* **10:** 3254-63, 1971.
22. Keizers PHJ, de Graaf C, de Kanter FJJ, Oostenbrink C, Feenstra KA, Commandeur JNM and Vermeulen NPE, Metabolic regio- and stereoselectivity of cytochrome P450 2D6 towards 3,4-methylenedioxy-N-alkyl-amphetamines: in silico predictions and experimental validation. *J Med Chem* **48:** 6117-6127, 2005.
23. Keizers PHJ, Lussenburg BMA, de Graaf C, Mentink LM, Vermeulen NPE and Commandeur JNM, Influence of phenylalanine 120 on cytochrome P450 2D6 catalytic selectivity and regiospecificity: crucial role in 7-methoxy-4-(aminomethyl)-coumarin metabolism. *Biochem Pharmacol* **68:** 2263-2271, 2004.
24. Omura T and Sato R, The carbon monoxide-binding pigment of liver microsomes. I. Evidence for its hemoprotein nature. *J Biol Chem* **239:** 2370-8, 1964.

25. Beechem JM, Global analysis of biochemical and biophysical data. *Methods Enzymol* **210:** 37-54, 1992.
26. Valeur B, *Molecular fluorescence: principles and applications*. Wiley-VCH, 2002.
27. Cheung HC, Resonance energy transfer. In: *Topics in fluorescence spectroscopy 2: Principles* (Ed. Lakowicz JR). Plenum Press, New York, 1991.
28. Morris GM, Goodsell DS, Halliday RS, Huey R, Hart WE, Belew RK and Olson AJ, Automated docking using a Lamarckian genetic algorithm and an empirical binding free energy function. *J Comput Chem* **19:** 1639-1662, 1998.
29. Jones G, Willett P, Glen RC, Leach AR and Taylor R, Development and validation of a genetic algorithm for flexible docking. *J Mol Biol* **267:** 727-48, 1997.
30. Berendsen HJC, Postma JPM, van Gunsteren WF and Hermans J, Interaction models for water in relation to protein hydration. In: *Intermolecular forces* (Ed. Pullman B), pp. 331-42. Reidel, Dordrecht, 1981.
31. van Gunsteren WF, Billeter SR, Eising AA, Hünenberger PH, Krüger P, Mark AE, Scott WRP and Tironi IG, Biomolecular simulation: The GROMOS 96 manual and user guide. In: *Vdf Hochschulverlag AG an der ETH Zürich*, Zürich, 1996.
32. Daura X, Mark AE and van Gunsteren WF, Parametrization of aliphatic CHn united atoms of GROMOS96 force field. *J Comput Chem* **19:** 535-547, 1998.
33. Schuler LD and van Gunsteren WF, On the choice of dihedral angle potential energy functions for n-alkanes. *Mol Simulation* **25:** 301-19, 2000.
34. Lindahl E, Hess B and van der Spoel D, GROMACS 3.0: a package for molecular simulation and trajectory analysis. *J Mol Model* **7:** 306-317, 2001.
35. Callis PR, 1La and 1Lb transitions of tryptophan: applications of theory and experimental observations to fluorescence of proteins. *Methods Enzymol* **278:** 113-50, 1997.
36. Maroncelli M and Fleming GR, Picosecond Solvation Dynamics of Coumarin-153 - the Importance of Molecular Aspects of Solvation. *Journal of Chemical Physics* **86:** 6221-6239, 1987.
37. Lee B and Richards FM, The interpretation of protein structures: estimation of static accessibility. *J Mol Biol* **55:** 379-400, 1971.
38. Lakowicz JR, Protein fluorescence. In: *Principles of fluorescence spectroscopy*, pp. 341-79. Plenum Press, New York, 1983.
39. Sharma VK, Saharo PD, Sharma N, Rastogi RC, Ghoshal SK and Mohan D, Influence of solvent and substituent on excited state characterstics of laser grade coumarin dyes. *Spectrochimica Acta Part a-Molecular and Biomolecular Spectroscopy* **59:** 1161-1170, 2003.
40. Stortelder A, Buijs JB, Bulthuis J, van der Vies SM, Gooijer C and van der Zwan G, Time-resolved fluorescence of the bacteriophage T4 capsid protein gp23. *J Photochem Photobiol B* **78:** 53-60, 2005.
41. Larsen OFA, van Stokkum IHM, Pandit A, van Grondelle R and van Amerongen H, Ultrafast polarized fluorescence measurements on tryptophan and a tryptophan-containing peptide. *Journal of Physical Chemistry B* **107:** 3080-3085, 2003.
42. Chen Y and Barkley MD, Toward understanding tryptophan fluorescence in proteins. *Biochemistry* **37:** 9976-82, 1998.
43. Ludemann SK, Lounnas V and Wade RC, How do substrates enter and products exit the buried active site of cytochrome P450cam? 1. Random expulsion molecular dynamics investigation of ligand access channels and mechanisms. *J Mol Biol* **303:** 797-811, 2000.
44. Ludemann SK, Lounnas V and Wade RC, How do substrates enter and products exit the buried active site of cytochrome P450cam? 2. Steered molecular dynamics and adiabatic mapping of substrate pathways. *J Mol Biol* **303:** 813-30, 2000.

Summary, conclusions and perspectives

Chapter 9

Summary

Cytochrome P450 2D6 (CYP2D6) is one of the most important enzymes in human drug metabolism. It is involved in the metabolism of a large number of clinically relevant drugs and furthermore, due to genetic polymorphisms there is a wide variability in the enzyme activity in different human populations [1-3]. It would be a great advantage if the metabolism of new chemical entities and drug-candidates by CYP2D6 could be rationalized and predicted in the early stages of drug discovery and development. A better understanding of the structure and functioning of CYP2D6 has been the major objective of this thesis. This goal was approached, by studying the most dominant factors that determine the substrate binding, the catalytic activity, and the regio- and stereoselectivity of CYP2D6.

First of all, the active site topology may dictate substrate binding and conversion by specific interactions with the compound, or by steric restriction. At second, the nature of oxygenating species can determine CYP activity and regioselectivity. At third, it is thought that the heme configuration can also influence the activity. Finally, the overall changes in conformation of the CYP during the catalytic cycle may allow for substrates to enter the active site. Furthermore, substrate mobility in the active site may determine the regioselectivity.

To address the impact of these factors on the activity and the selectivity of CYP2D6, the enzymology of site-directed mutants of CYP2D6 was studied and various spectroscopic techniques were used to examine the wild-type and mutants of the enzyme. These experimental techniques were complemented by computational techniques, to rationalize the findings and to predict the enzyme and substrate conformations.

In **Chapter 1** CYPs are introduced and their role in drug metabolism is explained. It is shown that in humans only a few CYP isoforms are involved in the oxidative metabolism of about 90% of all prescribed drugs and that in this process, the isoform CYP2D6 is one of the most important ones. Although the hepatic CYP2D6 expression levels are relatively low, the enzyme is involved in the metabolism of about 30% of the currently marketed drugs. Furthermore, the enzyme is known for its polymorphisms. This leads to an increased metabolite formation of drugs that are predominantly metabolized through CYP2D6 dependent pathways by individuals having the ultrarapid metabolizer phenotype, while individuals having the poor metabolizer phenotype, hardly metabolize these drugs. This of course has a big impact on the wanted effects of a drug, and also on unwanted side effects due to improper dosing. Clearly there is a need for structural data on CYP2D6 in order to rationalize and predict how it metabolizes its substrates. In the absence of crystallographic data, CYP2D6 has been subject of elaborate pharmacophore and homology modeling studies for rationalization and predictive purposes. Due to the availability of better templates, the homology modeling kept evolving; so more experimental validation by site-directed mutagenesis was needed. The quality of the models is discussed and an overview of the mutations is given.

Spectroscopic and other biophysical techniques that have been used to study structural aspects of CYPs are also summarized in Chapter 1. Besides for the validation of computational models of CYPs, spectroscopic data can also be used to gain complementary information on CYPs, like the characteristics of the porphyrin prosthetic group. So far, the applications of these techniques have predominantly been restricted to studies on bacterial CYPs. Due to improved expression and purification methodologies, it has become possible to study human CYPs in a spectroscopic way too.

In **Part I** of this thesis, entitled **Key determinants of CYP2D6 activity**, site-directed mutagenesis and enzyme kinetic analysis were used to study the influence of the active site topology, and the role of multiple oxygenating species on the activity of CYP2D6. The active site residues F120, F483, and T309, are introduced as being crucial for the activity of CYP2D6.
In **Chapter 2**, the role of CYP2D6 active site residue F120 in ligand binding and catalysis was experimentally examined by mutating it into an alanine. Typical CYP2D6 substrates generally contain a basic nitrogen atom at about 7 Å, and an aromatic moiety adjacent to the site of metabolism. In homology modeling studies it has been suggested that there may be an important role for F120 in fixation of this substrate aromatic moiety [4]. Strikingly, the F120A mutation led to a completely abolished 7-methoxy-4-(aminomethyl)-coumarin (MAMC) *O*-demethylating activity of CYP2D6. On the other hand, bufuralol metabolism was hardly affected as was dextromethorphan *O*-demethylation. However, the F120A mutant also formed 3-hydroxymorphinan, i.e. double demethylated dextromethorphan, which was not detected using wild-type CYP2D6. 3,4-methylenedioxymethamphetamine (MDMA or XTC) was *O*-demethylenated to 3,4-dihydroxy-methamphetamine by both mutant and wild-type CYP2D6. In addition the F120A mutant formed two additional metabolites: 3,4-methylenedioxyamphetamine and N-hydroxy-3,4-methylenedioxymethamphetamine. Such substrate dependent effects of this mutation were not described before for any CYP2D6 mutant. Studying the inhibition of dextromethorphan *O*-demethylation, a 6-fold decreased affinity of the F120A mutant for quinidine was found, due to the loss of the specific aromatic interaction, as was predicted using the homology model [4]. These data indicated for the first time the importance of F120 in the selectivity and regiospecificity in substrate binding and catalysis by CYP2D6. During writing and publishing of Chapter 2 [5], also other groups reported mutagenesis studies on F120 [6, 7], and very recently we performed additional studies to the role of F120 [8, 9], confirming our findings.
According to the CYP2C5 based CYP2D6 homology models, a second phenylalanine residue appered to be positioned in the active site, besides F120. This residue, F483, was examined in **Chapter 3**. It was hypothesized that F483 also would play an important role in the interaction with the aromatic moiety of typical CYP2D6 substrates. Experimental data to support this hypothesis, however, was not yet available. In fact, in the only study performed, mutation of F483 to isoleucine or tryptophan did not affect the 1'-hydroxylation of bufuralol at all [10]. In Chapter 3, substrate binding and oxidative metabolism by wild-type and F483A mutant CYP2D6 was experimentally examined. The F483A mutation resulted in a 30-fold lower V_{max} for bufuralol 1'-hydroxylation, while the K_m was hardly affected. The V_{max} for MDMA *O*-demethylenation on the other hand decreased only two-fold, whereas the effect on the K_m was much larger. For dextromethorphan, in addition to dextrorphan (*O*-demethylation) and 3-methoxymorphinan (*N*-demethylation), two other metabolites were formed that were not detected for the wild-type enzyme. The substrate MAMC was not metabolized at all by the F483A mutant CYP2D6, as we also reported for the F120A mutant. The presented data show that next to F120, residue F483 plays an important

role in the metabolism of typical CYP2D6 substrates. This influence of F483 on the oxidative metabolism by CYP2D6 was found to be substrate-dependent, like for F120. Besides the previously described active site carboxylates D301 and E216 [11, 12], we have now introduced the two phenylalanines F120 and F483 as key determinants for CYP2D6 activity [13].
In the previous two chapters, the critical roles residues F120 and F483 play in the oxidative metabolism of MAMC by cytochrome P450 2D6 (CYP2D6) were reported. In **Chapter 4**, a series of *N*-alkyl-7-methoxy-4-(aminomethyl)-coumarins (MAMC-analogs) were used as substrates for the F120A and F483A mutants, in order to further probe the CYP2D6 active site by increasing the substrate *N*-alkyl chain. The F120A and F483A mutants of CYP2D6 displayed significant activity towards the MAMC-analogs. This indicated that additional substrate interaction points are present in the CYP2D6 site, which add in the accommodation of the longer chain MAMC-analogs in a reactive conformation. Automated docking studies of the MAMC-analogs in the CYP2D6 homology model suggested a distal hydrophobic active site binding cleft for the substrate *N*-alkyl chains, consisting of the residues L213 and V308. Therefore, we propose L213 and V308 to be important as distal active site restricting residues, involved in binding to the larger substrates via hydrophobic interactions. Future site-directed mutagenesis studies should confirm this hypothesis.

The residues studied so far are all involved in binding the substrates in the active site of CYP2D6, as shown in Figure 1. Besides residues determining the active site topology, other active site residues may be involved in the mechanism of oxidation, by being involved in oxygen, proton and electron donation to the heme. Based upon sequence alignments and homology modeling, we proposed threonine 309 in CYP2D6 to be the conserved I-helix threonine, which is supposed to play a role in dioxygen activation by CYPs [14]. In **Chapter 5**, T309 was therefore mutated into a valine and subsequently, the binding and metabolism of model substrates was studied. The T309V mutant of CYP2D6 displayed a strong shift from *O*-dealkylation to *N*-dealkylation reactions in oxidation of dextromethorphan and MDMA. This could be explained by an elevated ratio of hydroperoxo-iron to oxenoid-iron of the oxygenating species. In consistence, using CuOOH, which directly forms the oxenoid-iron, the T309V mutant again selectively catalyzed these *O*-dealkylation reactions. The changed ratio of oxygenating species could also explain the decreased activity and changed regioselectivity that was observed in MAMC and bufuralol oxidation respectively by the T309V mutant. Interestingly, the T309V mutant always showed a significantly increased, up to 75-fold, higher activity compared to the wild-type enzyme when using CuOOH. With these results, a residue of CYP2D6 involved in the mechanism of oxidation was introduced. We have shown that T309 in CYP2D6 is involved in maintaining the balance of multiple oxygenating species and thus influences substrate and regioselectivity [15].

In **Part II** of this thesis, entitled **Spectroscopy and modeling of CYP2D6**, the purified wild-type and mutants of CYP2D6 were subjected to several spectroscopic techniques. Spin lattice relaxation NMR was used to correlate the active site orientation of substrates to the CYP2D6 catalytic regioselectivity. Resonance Raman spectroscopy was used to study the effects of the T309V mutation, known to cause changed activity, on the heme configuration of CYP2D6. Fluorescence spectroscopy was used to study the impact of substrate binding on the conformation of the apoprotein of CYP2D6. Furthermore, substrate affinity and active site dynamics were studied using the intrinsic fluorescence of the substrate. The homology model of CYP2D6 was used to relate the spectroscopy to protein structure, and also to calculate ideal substrate binding conformations and positions of amino acids.

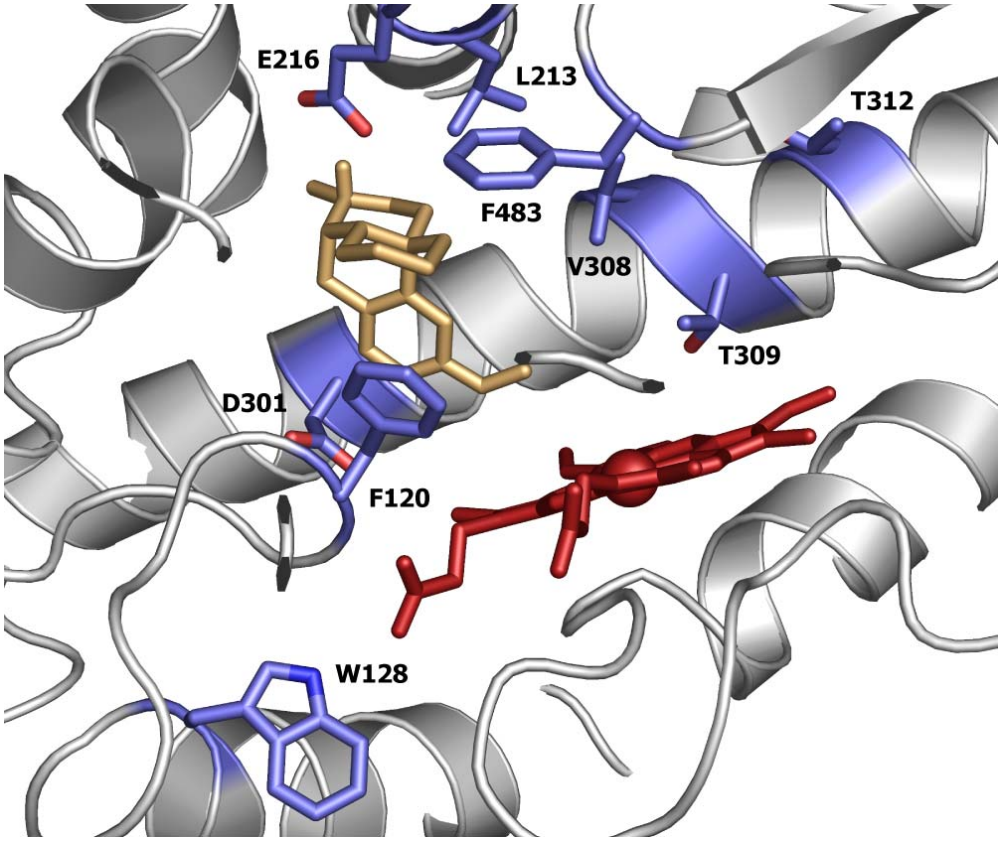

Figure 1: The CYP2D6 active site (heme in center, Fe as sphere) according to the homology model [16], with dextromethorphan bound according to automated docking (GOLD-Chemscore), showing the key residues involved in enzyme activity and the other residues that have been mutated in this thesis. F120, F483, L213, and V308 are identified as being involved in steric restriction and/or hydrophobic interaction with substrates, E216 is interacting with basic substrate N-atoms, D301 interacts with the backbone of F120, W128 interacts via H-bonds with the pyrrole C-propionate and was mutated to a phenylalanine in Chapter 8, which did not affect the activity, and T312 was mutated to a valine in Chapter 5, which did not affect activity either. The figure, of which a colored version is shown in the Appendix of this thesis, was made using Pymol 0.98.

In **Chapter 6**, a series of 3,4-methylenedioxy-*N*-alkylamphetamines (MDAAs) were automatically docked and subjected to molecular dynamics (MD) simulations in a CYP2D6 protein model. The predicted substrate binding orientations, sites of oxidation and relative reactivities were compared to experimental data of the wild-type and the F120A mutant of CYP2D6. Automated docking results were not sufficient to accurately rationalize experimental binding orientations of MDMA in the two enzymes as measured with spin lattice relaxation NMR. Therefore, the docking results were used as starting structures for MD simulations. Predicted binding orientations of MDMA and the sites of oxidation of the MDAAs derived from MD simulations matched well with the experimental data. It appeared

that the experimental results were best described in MD simulations considering the nitrogen-atoms of the MDAAs in neutral form. Apparently, the CYP2D6 active site pH is different from the enzyme environment, since at pH 7.4 the basic *N*-atom of the MDAA's is expected to be protonated. Differences in regioselectivity and stereoselectivity in the oxidative metabolism of the MDAAs by the F120A mutant of CYP2D6 were correctly predicted from the MD simulations, and the effects of the F120A mutation could be rationalized as well. F120 was found to interact with the substrates by π–stacking. The combination of automated docking of substrates, with MD simulations in the CYP2D6 homology model was a very successful way to predict sites of metabolism, and is a promising novel approach to use for other protein-ligand complexes as well [16].

In **Chapter 7**, resonance Raman (RR) spectroscopy was used to study the effects of the T309V mutation in CYP2D6 on the heme prosthetic group characteristics. In Chapter 4, we hypothesized that T309 in CYP2D6 is involved in the determining the balance of different activated oxygen species. The RR spectra of wild-type and the T309V mutant of CYP2D6 revealed that in the wild-type enzyme a five coordinated high spin (5cHS) species is present in the absence of substrate, whereas in the T309V mutant only a six coordinated low spin (6cLS) species was observed. The addition of saturating amounts of the substrate dextromethorphan led to the formation of more 5cHS species in both the enzymes, however, the difference between wild-type enzyme and mutant was still significant. The T309V mutation had no effect on the CO-Fe stretching frequency in the spectrum of CO bound ferrous CYP2D6, indicating that this residue does not directly influence the hydrophobicity of a heme-bound axial ligand. So T309 influences the spin state in CYP2D6, but is at a too large distance from the axial heme ligand, i.e. CO or O_2, to directly interact with it. Therefore it is thought to be involved in maintaining a network of hydrogen bonds through water molecules in the enzyme active site [17]. Whether this role influences the changed activity of the T309V mutant, or whether it is a secondary, not related effect, remains to be resolved. This is the first time that an effect of the conserved I-helix threonine on the heme spin state is reported for a CYP.

Enzyme structure and dynamics may play a main role in substrate binding and the subsequent steps in the CYP catalytic cycle. In **Chapter 8**, for the first time changes in the apoprotein conformation of CYP2D6 upon binding of a substrate were studied. Steady-state and time-resolved fluorescence methods were used, focusing not only on the emission of the tryptophan residues, but also on emission of the substrate. As a substrate MAMC was selected, a compound exhibiting native fluorescence. Next to the wild-type enzyme, the W128F mutant of CYP2D6 was studied. W128 is the tryptophan residue most close to the heme (Figure 1), therefore its fluorescence is expected to be quenched extensively, and to have a short lifetime. A mutation to another bulky but non-fluorescent phenylalanine residue at position 128, would validate this hypothesis. After binding of MAMC, a variety of energy transfer possibilities exist, and molecular dynamics (MD) simulations were performed to calculate distances and relative orientations of donors and acceptors. Energy transfer from W128 to the heme indeed appeared to be important; its emission was related to the shortest of the three average tryptophan fluorescence lifetimes observed for CYP2D6. Energy transfer from MAMC to the heme was very efficient as well: when bound in the active site, the emission of MAMC was fully quenched. Steady-state anisotropy revealed that besides the MAMC in the active site, another 2% of MAMC was bound to wild-type CYP2D6 outside of the active site. The tryptophan residues in CYP2D6 appeared to be less accessible for the external quenchers iodide and acrylamide in presence of MAMC, indicating a tightening of the enzyme structure upon substrate binding. However, the changes in the overall enzyme structure were not large, since the emission characteristics of the enzyme

were not very different in the presence of MAMC [18]. More extensive studies are needed to reveal the importance of apoprotein conformational changes during the rest of the catalytic cycle of mammalian CYPs, and upon the binding of larger substrates. Nevertheless, in this chapter the necessary tools have been introduced.

Conclusions and perspectives

The major objective of the research described in this thesis, was to increase the understanding of the structure in relation to the catalytic activity of CYP2D6. Structural data is necessary for the rationalization of the oxidative metabolism of compounds by this enzyme and can eventually lead to a way of prediction of substrate, regio- and stereoselectivity in catalysis by the enzyme. In this thesis several aspects have been investigated that may influence CYP2D6 activity: (i). The active site topology was examined making use of site-directed mutagenesis and spin lattice relaxation NMR, in combination with homology modeling. (ii). The influence of the balance of multiple oxygenating species on CYP2D6 was studied in relation to the role of residue T309. (iii). The changes in the heme configuration of CYP2D6 upon substrate binding and active site mutagenesis were investigated using RR spectroscopy. (iv). Finally, protein conformational changes and substrate dynamics were studied making use of the native fluorescence of the endogenous tryptophan residues. In the following sections general conclusions based upon the findings in the experimental chapters will be drawn and related to future research.

Homology model versus crystal structure of CYP2D6

In the process of writing the last parts of this thesis, the first X-ray structure of CYP2D6 was reported [19]. This substrate-free structure (PDB file 2F9Q) shows the characteristic fold as seen in other CYP members and shows a very high similarity to the homology model used in this thesis; after fitting, 88% of all Cα-atoms of the model are within 2Å of their crystallized counterparts. There are however also some significant differences between the two structures. In the allover structures, relatively large differences are found between the B' helix and in the F-G helical region. The differences can partly be explained by the low resolution of the crystal structure of CYP2D6 at some regions (F-G loop, N-terminus). Another crucial difference is that for the homology model the substrate-bound crystal structure of CYP2C5 was used, so the model is biased towards a substrate bound structure. This can clearly be observed from the position of F483 in the protein model. The active site residues in the homology model that have been mutated, or otherwise mentioned in this thesis have been aligned to their crystal structure positions in Figure 2. The phenyl-ring of F483 is twisted about 90° in the two structures. A similar difference is observed when comparing the crystal structures of substrate bound and substrate free CYP2C9 (PDB files 1OG5 and 1R9O respectively [20]). In CYP2C9 a homologous phenylalanine residue, F476, is present in the active site, which is twisted to the same extent upon substrate binding. The other active site residues are in general in almost identical positions in the model as in the X-ray structure. So while there already is high similarity between the crystal structure of CYP2D6 and the homology model used in this thesis, the homology model probably even better represents a substrate-bound enzyme. The resolving of the crystal structure of CYP2D6 increased the confidence in the quality of our homology model, and our interpretations of it, used in this thesis.

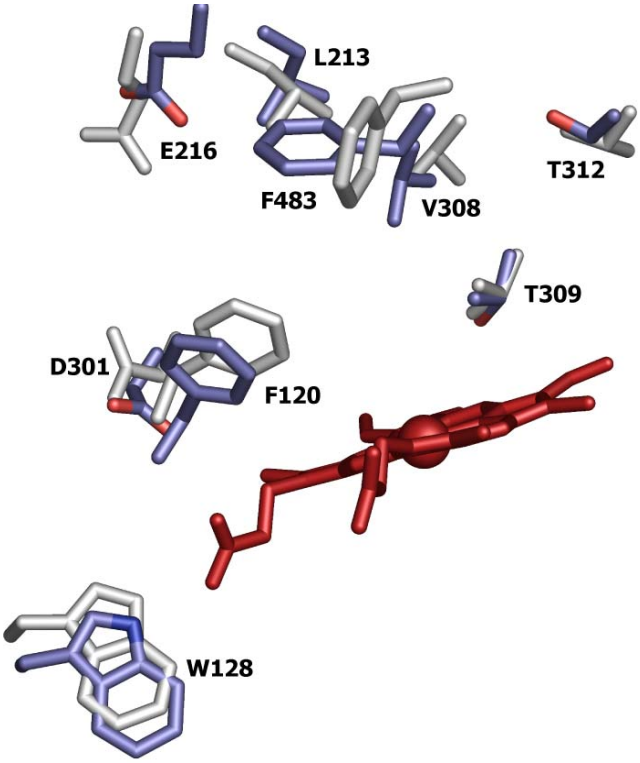

Figure 2: Overlay of the active site residues examined in this thesis from the homology model [16] in dark, and from the crystal structure of CYP2D6 [19] in light, around the modeled heme (Fe as sphere). The figure, of which a colored version is shown in the Appendix of this thesis, was made using Pymol 0.98.

Present research versus the CYP catalytic cycle

The general overall reaction CYPs catalyze can be schematically represented in a catalytic cycle, in which each step represents a change in the heme configuration (Chapter 1 and [21]). The research described in this thesis involves different parts of the catalytic cycle of CYP2D6. In Figure 3, it is indicated which stages of the catalytic cycle are studied in the experimental chapters. The cycle starts with the binding of a substrate (Stage 1-2). Substrate binding is the easiest step to follow by spectroscopic means, and has been studied in all chapters. In Chapter 7, the binding of the artificial ligand CO to the heme was investigated by RR spectroscopy, as a model for the binding of O_2. In Chapter 5, the reactivities of the oxygenating species, stages 5-7 in the cycle, have been studied in relation to residue T309.

The boxes representing the experimental chapters include all stages of the cycle in Figure 3, indicating that in this thesis a large part of the cycle has been under examination. On the other hand, the reactions leading from one stage to the next have not been addressed in detail in this thesis. For example, the ways of entrance of substrate, electrons, oxygen, and protons were not examined. Nor were studied product egress, or the velocities of individual steps. Therefore there is still much experimental and computational research to be done, not only for CYP2D6, but also for CYPs in general. The mechanistic understanding and

experimental validation of the CYP catalytic cycle is a near future goal for CYP research [22]. Due to the improving of freeze-quenching and stop-flow techniques, it has recently become possible to study most stages of the cycle spectroscopically (Chapter 1 and [23]). Also recently, crystal structures of CYPs with oxygen heme-bound have become available (Chapter 1 and [24]), enabling to study protein conformational changes during the catalytic cycle. It will soon become possible to calculate the electronic structures of all intermediates of the cycle, as was recently shown possible for example, for Stage 7 of human CYPs [25]. New methods are being developed for this goal also within the CCM research program [26]. Finally, the relevance of the experimentally observed intermediates will be related to the eventual activity of the enzyme.

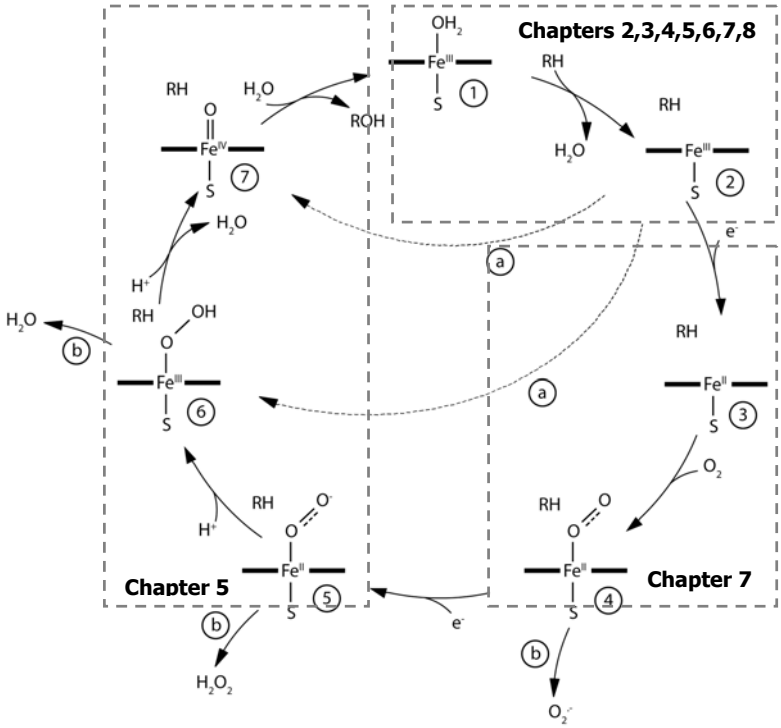

Figure 3: The catalytic cycle of CYPs, as discussed in Chapter 1. Dashed boxes indicate what stages are investigated in each experimental chapter.

Allosterism and suicide inhibition

In this thesis, allosteric effects on product formation by CYP2D6 are reported (Chapter 4). A second substrate-binding site is proposed for CYP2D6, as an explanation for the atypical kinetics in formation of 6-OH-bufuralol. In a former study, potentiation of MAMC *O*-demethylation by CYP2D6, when co-incubated with the substrates sparteine or phenformine, was already reported [4]. Furthermore, an additional CYP2D6 binding-site is proposed for MAMC in Chapter 8. It is known that CYP3A4 although having in crystallized form a relatively small active site [27], is well capable of binding more than one substrate simultaneously [28]. Also crystal structures of CYP2C9 suggest that more than one ligands fit together in the enzyme active site [20]. The capability of CYP2D6 to bind several substrates at the

same time, may potentially have a great impact on the prediction of CYP2D6 mediated metabolism and thus on the extrapolation of *in vitro* experiments to *in vivo* extrapolations [29]. Obviously more experimental and computational research is needed to investigate the nature of the observations of allosterism in CYP2D6.
Another issue of high interest in CYP research is suicide inhibition; the process in which the product formed by a CYP covalently binds to the enzyme thus disabling it to metabolize any other substrate. Besides being involved in activating heme-bound oxygen, the conserved I-helix threonine of CYPs was shown to be involved in irreversible inhibition in CYP2B4 [30], and in CYP2E1 [31]. In the case of CYP2D6, time-dependent inhibition has been described for a number of substrates, including methylenedioxy-containing compounds like MDMA [32], and paroxetine [33]. Using the T309V and T312V mutants of CYP2D6 to study the inhibition of suicide inhibitors like MDMA could reveal the mechanism of this inhibition.

Progress in molecular modeling
The mutagenesis studies in the first part of this thesis were guided by predictions from the homology model of CYP2D6. The experimental observations that residues F120, F483 and T309 had large effects on the CYP2D6 activity, in a way matching with what was predicted, can therefore be seen as the validation of the computer model. Thus, with confidence the model could be used to predict active site substrate orientations and enzyme residue conformations in the following chapters.
The approach of combining automated docking and MD simulations in a protein model as described in Chapter 6 was a successful way to rationalize the oxidative metabolism of a series of 3,4-methylenedioxy-*N*-alkylamphetamines (MDAAs) by CYP2D6. The differences in oxidative metabolism of these closely related substrates could be predicted in terms of regioselectivity and stereoselectivity. Furthermore, the effects of the active site F120A mutation on the substrate selectivity could be rationalized. The presented integrated modeling method is apparently a promising tool in the prediction of the metabolic properties of new (drug-like) compounds by CYP2D6 and may very well be applicable for other drug metabolizing enzymes as well.
Using substrate active site orientations as determined using spin lattice relaxation NMR to rationalize the effects of active site mutations, was found to have its limitations. The experimentally determined orientations of both enantiomers of MDMA in the active sites of wild-type and F120A mutant CYP2D6 were not as different as expected, based on the measured product formation by the enzymes. Relatively small substrates, like MDMA, may have more than one energetically favorable binding orientation and may be highly mobile within the active site. This was confirmed by the automated docking, where several distinct modes of binding could be appointed for MDMA and its analogs in the active site of both enzymes. Furthermore, in the MD simulations complete conversions of orientations were observed. Despite this apparent disadvantage, the performed spin lattice relaxation NMR experiments were useful, since they could be used well to validate the molecular modeling procedure. However, to study the effects of an active site mutation on substrate orientation other experimental techniques (i.e. anisotropy, see Chapter 8) may be better suited.
One aspect that was not taken into account in Chapter 6 was the relative reactivity of the various atoms in substrates. The ease of hydrogen abstraction or electron abstraction may very well determine product formation [34, 35]. In the case of the MDAA's in Chapter 6, this is probably not the rate-determining factor, for the molecular modeling was well capable to predict sites of oxidation. But to predict sites of metabolism of a wide variety of compounds energy barriers for hydrogen and electron abstraction should be calculated and added to the molecular modeling procedure.

Spectroscopy on CYP

Various techniques, i.e. spin lattice relaxation NMR, resonance Raman scattering and fluorescence spectroscopy have been applied to CYP2D6 in this thesis, in order to validate predictions about the enzyme based upon its homology model. Besides this validation of a model that is practically useful for pharmaceutical research, these techniques were also chosen to explore more fundamentally how a heme-containing enzyme works.

It is shown that RR spectroscopy is a useful tool in studying in detail the characteristics of the porphyrin prosthetic group. Small differences in spin state (Chapter 7) and conformations of vinyl and propionate side-chains [36], can be detected at room temperature, using a minimal amount of enzyme. Although absorbance spectroscopy is more sensitive than RR, it cannot be used to distinguish small changes in spin state nor can it be used to study porphyrin side chain conformations. EPR can be used to sensitively measure spin state but has the disadvantage that it can only be used at low temperatures, which may influence the spin and substrate binding equilibria.

RR spectroscopy yields information complementary to that obtained by homology modeling. The homology model does not contain information about the heme configuration, but quantum mechanical/molecular mechanics (QM/MM) methods can be used instead [37]. For instance, to determine the influence of T309 on the heme spin state (Groenhof et al., unpublished results).

Interestingly, the active site residues may have an indirect influence on the heme reduction potential. In CYP102, it was shown that mutation of residue F393, neighboring the heme ligating residue C400, led to changes in the reduction potential and catalytic activity [38]. Although in CYP2D6 F120 and F483 are positioned on the other side of the heme, it would be interesting to see the influence of the alanine mutations on the heme reduction potential. The cause of the change in reduction potential of the F393 mutants of CYP102 was suggested to be a steric interaction between the residue and the heme vinyl side-chains [36]. In CYP2D6 no changes in the vinyl conformations were observed after the F120A mutation [9], nor after the F483A mutation (unpublished results). So if only steric interaction with the vinyl groups could be responsible for a changed reduction potential, then this is unlikely for CYP2D6 after the F120A and F483A mutations.

It is necessary to study mammalian CYPs in a more fundamental way as well, instead of restricting the fundamental research on CYPs to relatively easily produced bacterial isoforms of the enzyme family. The steady-state and time-resolved fluorescence experiments on CYP2D6 revealed small-scale conformational changes in CYP2D6 upon binding of MAMC (Chapter 8). This result was somewhat surprising since larger conformational changes were reported previously for CYP101 upon substrate binding [39]. These results might therefore be indicative that CYP101 is not a good model for the dynamics of mammalian CYPs.

To really study the dynamics of CYPs during the whole catalytic cycle, a trigger like an electron donating substrate [40] or a temperature jump [41], is needed. Then, the fluorescence techniques described in Chapter 8 are well suited to study CYP2D6 time resolved. Also when CYP2D6 is immobilized on a silver electrode, surface enhance RR scattering (SERRS) is possible (Bonifacio et al. unpublished results). The electrode might then be used to trigger the catalytic cycle, during which the SERR spectra of the enzyme can be followed in time.

CYP2D6 as a model

In this thesis, expression, mutagenesis, enzymology, spectroscopy, and molecular modeling have been used as tools to learn more about how the enzyme CYP2D6 metabolizes its

substrates. By combining these techniques we were able to make a well validated model of CYP2D6, usable to predict binding [42], and metabolism [16] of model substrates and unknown compounds. The fact that the model is of high quality is confirmed by the recently resolved crystal-structure of the enzyme [19]. Therefore it can be concluded that the combining of homology modeling with site-directed mutagenesis studies, enzymology and various spectroscopical studies, as has been the aim of this thesis, is an excellent way to study enzymes and is a very promising approach to use for other proteins, of which structural information is lacking, as well.

References

1. Vermeulen NPE, Prediction of drug metabolism: the case of cytochrome P450 2D6. *Curr Top Med Chem* **3:** 1227-39, 2003.
2. Zanger UM, Raimundo S and Eichelbaum M, Cytochrome P450 2D6: overview and update on pharmacology, genetics, biochemistry. *Naunyn Schmiedebergs Arch Pharmacol* **369:** 23-37, 2004.
3. Ingelman-Sundberg M, Genetic polymorphisms of cytochrome P450 2D6 (CYP2D6): clinical consequences, evolutionary aspects and functional diversity. *the Pharmacogenomics Journal* **5:** 6-13, 2005.
4. Venhorst J, ter Laak AM, Commandeur JNM, Funae Y, Hiroi T and Vermeulen NPE, Homology modeling of rat and human cytochrome P450 2D (CYP2D) isoforms and computational rationalization of experimental ligand-binding specificities. *J Med Chem* **46:** 74-86, 2003.
5. Keizers PHJ, Lussenburg BMA, de Graaf C, Mentink LM, Vermeulen NPE and Commandeur JNM, Influence of phenylalanine 120 on cytochrome P450 2D6 catalytic selectivity and regiospecificity: crucial role in 7-methoxy-4-(aminomethyl)-coumarin metabolism. *Biochem Pharmacol* **68:** 2263-2271, 2004.
6. Flanagan JU, Marechal JD, Ward R, Kemp CA, McLaughlin LA, Sutcliffe MJ, Roberts GC, Paine MJ and Wolf CR, Phe120 contributes to the regiospecificity of cytochrome P450 2D6: mutation leads to the formation of a novel dextromethorphan metabolite. *Biochem J* **380:** 353-60, 2004.
7. Masuda K, Tamagake K, Okuda Y, Torigoe F, Tsuzuki D, Isobe T, Hichiya H, Hanioka N, Yamamoto S and Narimatsu S, Change in enantioselectivity in bufuralol 1''-hydroxylation by the substitution of phenylalanine-120 by alanine in cytochrome P450 2D6. *Chirality* **17:** 37-43, 2005.
8. van Waterschoot RAB, Keizers PHJ, de Graaf C, Vermeulen NPE and Tschirret-Guth RA, Topological Role of Cytochrome P450 2D6 Active Site Residues. *Arch Biochem Biophys* **447:** 53-58, 2006.
9. Bonifacio A, Keizers PHJ, Vermeulen NPE, Gooijer C, Commandeur JNM and van der Zwan G, Binding of bufuralol, dextromethorphan and 3,4-methylenedioxymethylamphetamine to wild-type and F120A mutant cytochrome P450 2D6 studied by resonance Raman spectroscopy. *Biochem Biophys Res Commun* **343:** 772-779, 2006.
10. Smith G, Modi S, Pillai I, Lian LY, Sutcliffe MJ, Pritchard MP, Friedberg T, Roberts GC and Wolf CR, Determinants of the substrate specificity of human cytochrome P-450 CYP2D6: design and construction of a mutant with testosterone hydroxylase activity. *Biochem J* **331:** 783-92, 1998.
11. Paine MJ, McLaughlin LA, Flanagan JU, Kemp CA, Sutcliffe MJ, Roberts GC and Wolf CR, Residues glutamate 216 and aspartate 301 are key determinants of substrate specificity and product regioselectivity in cytochrome P450 2D6. *J Biol Chem* **278:** 4021-7, 2003.
12. Guengerich FP, Hanna IH, Martin MV and Gillam EM, Role of glutamic acid 216 in cytochrome P450 2D6 substrate binding and catalysis. *Biochemistry* **42:** 1245-53, 2003.
13. Lussenburg BMA, Keizers PHJ, de Graaf C, Hidestrand M, Ingelman-Sundberg M, Vermeulen NPE and Commandeur JNM, The role of phenylalanine 483 in cytochrome P450 2D6 is strongly substrate dependent. *Biochem Pharmacol* **70:** 1253-61, 2005.

14. Coon MJ, Vaz AD, McGinnity DF and Peng HM, Multiple activated oxygen species in P450 catalysis: contributions To specificity in drug metabolism. *Drug Metab Dispos* **26:** 1190-3, 1998.
15. Keizers PHJ, Schraven LHM, de Graaf C, Hidestrand M, Ingelman-Sundberg M, van Dijk BR, Vermeulen NPE and Commandeur JNM, Role of the conserved threonine 309 in mechanism of oxidation by cytochrome P450 2D6. *Biochem Biophys Res Commun* **338:** 1065-74, 2005.
16. Keizers PHJ, de Graaf C, de Kanter FJJ, Oostenbrink C, Feenstra KA, Commandeur JNM and Vermeulen NPE, Metabolic regio- and stereoselectivity of cytochrome P450 2D6 towards 3,4-methylenedioxy-N-alkyl-amphetamines: in silico predictions and experimental validation. *J Med Chem* **48:** 6117-6127, 2005.
17. Haines DC, Tomchick DR, Machius M and Peterson JA, Pivotal role of water in the mechanism of P450BM-3. *Biochemistry* **40:** 13456-65, 2001.
18. Stortelder A, Keizers PHJ, Oostenbrink C, de Graaf C, de Kruijf P, Vermeulen NPE, Gooijer C, Commandeur JNM and van der Zwan G, Binding of 7-methoxy-4-(aminomethyl)-coumarin to wild-type and W128F mutant cytochrome P450 2D6 studied by time resolved fluorescence spectroscopy. *Biochem J* **393:** 635-643, 2006.
19. Rowland P, Blaney FE, Smyth MG, Jones JJ, Leydon VR, Oxbrow AK, Lewis CJ, Tennant MG, Modi S, Eggleston DS, Chenery RJ and Bridges AM, Crystal structure of human cytochrome P450 2D6. *J Biol Chem* **in press**, 2006.
20. Williams PA, Cosme J, Ward A, Angove HC, Matak Vinkovic D and Jhoti H, Crystal structure of human cytochrome P450 2C9 with bound warfarin. *Nature* **424:** 464-8, 2003.
21. White RE and Coon MJ, Oxygen activation by cytochrome P-450. *Annu Rev Biochem* **49:** 315-56, 1980.
22. Guengerich FP, Cytochrome P450: what have we learned and what are the future issues? *Drug Metab Rev* **36:** 159-97, 2004.
23. Spolitak T, Dawson JH and Ballou DP, Reaction of ferric cytochrome P450cam with peracids. *J Biol Chem* **280:** 20300-20309, 2005.
24. Nagano S, Cupp-Vickery JR and Poulos TL, Crystal structures of the ferrous dioxygen complex of wild-type cytochrome P450eryF and its mutants, A245S and A245T: investigation of the proton transfer system in P450eryF. *J Biol Chem* **280:** 22102-7, 2005.
25. Bathelt CM, Zurek J, Mulholland AJ and Harvey JN, Electronic structure of compound I in human isoforms of cytochrome P450 from QM/MM modeling. *J Am Chem Soc* **127:** 12900-12908, 2005.
26. Swart M, Groenhof AR, Ehlers AW and Lammertsma K, Validation of exchange - Correlation functionals for spin states of iron complexes. *Journal of Physical Chemistry A* **108:** 5479-5483, 2004.
27. Williams PA, Cosme J, Vinkovic DM, Ward A, Angove HC, Day PJ, Vonrhein C, Tickle IJ and Jhoti H, Crystal structures of human cytochrome P450 3A4 bound to metyrapone and progesterone. *Science* **305:** 683-6, 2004.
28. Wang RW, Newton DJ, Liu N, Atkins WM and Lu AY, Human cytochrome P-450 3A4: in vitro drug-drug interaction patterns are substrate dependent. *Drug Metab Dispos* **28:** 360-6, 2000.
29. Wienkers LC and Heath TG, Predicting in vivo drug interactions from in vitro drug discovery data. *Nature rev. drug discov.* **4:** 825-833, 2005.
30. Roberts ES, Pernecky SJ, Alworth WL and Hollenberg PF, A role for threonine 302 in the mechanism-based inactivation of P450 2B4 by 2-ethynylnaphthalene. *Arch Biochem Biophys* **331:** 170-6, 1996.
31. Blobaum AL, Kent UM, Alworth WL and Hollenberg PF, Novel reversible inactivation of P450 2E1 T303A by tert-butyl acetylene: The role of threonine 303 in proton delivery to the active site of cytochrome P450 2E1. *J Pharmacol Exp Ther*, 2004.
32. Heydari A, Yeo KR, Lennard MS, Ellis SW, Tucker GT and Rostami-Hodjegan A, Mechanism-based inactivation of CYP2D6 by methylenedioxymethamphetamine. *Drug Metab Dispos* **32:** 1213-7, 2004.
33. Bertelsen KM, Venkatakrishnan K, Von Moltke LL, Obach RS and Greenblatt DJ, Apparent mechanism-based inhibition of human CYP2D6 in vitro by paroxetine: comparison with fluoxetine and quinidine. *Drug Metab Dispos* **31:** 289-93, 2003.

34. Ebner T, Meese CO and Eichelbaum M, Mechanism of cytochrome P450 2D6-catalyzed sparteine metabolism in humans. *Mol Pharmacol* **48:** 1078-86, 1995.
35. Krauser JA and Guengerich FP, Cytochrome P450 3A4-catalyzed testosterone 6beta-hydroxylation stereochemistry, kinetic deuterium isotope effects, and rate-limiting steps. *J Biol Chem* **280:** 19496-506, 2005.
36. Chen Z, Ost TW and Schelvis JP, Phe393 mutants of cytochrome P450 BM3 with modified heme redox potentials have altered heme vinyl and propionate conformations. *Biochemistry* **43:** 1798-808, 2004.
37. Groenhof AR, Swart M, Ehlers AW and Lammertsma K, Electronic ground states of iron porphyrin and of the first species in the catalytic reaction cycle of cytochrome P450s. *J Phys Chem A* **109:** 3411-3417, 2005.
38. Ost TW, Clark J, Mowat CG, Miles CS, Walkinshaw MD, Reid GA, Chapman SK and Daff S, Oxygen activation and electron transfer in flavocytochrome P450 BM3. *J Am Chem Soc* **125:** 15010-20, 2003.
39. Prasad S and Mitra S, Role of protein and substrate dynamics in catalysis by Pseudomonas putida cytochrome P450cam. *Biochemistry* **41:** 14499-508, 2002.
40. Dunn AR, Dmochowski IJ, Winkler JR and Gray HB, Nanosecond photoreduction of cytochrome p450cam by channel-specific Ru-diimine electron tunneling wires. *J Am Chem Soc* **125:** 12450-6, 2003.
41. Narasimhulu S and Willcox JK, Temperature-jump relaxation kinetics of substrate-induced spin-state transition in cytochrome P450 (comparison of the wild-type and C334A mutant P450(CAM) and P450(2B4)). *Arch Biochem Biophys* **388:** 198-206, 2001.
42. de Graaf C, Oostenbrink C, Keizers PHJ, van der Wijst T, Jongejan A and Vermeulen NPE, Catalytic site prediction and virtual screening of cytochrome P450 2D6 substrates by consideration of water and rescoring in automated docking. *J Med Chem* **49:** 2417-2430, 2006.

Het peilen van menselijke cytochromen P450: analyse van CYP2D6 met behulp van mutaties en spectroscopie

In het dagelijks leven wordt de mens voortdurend blootgesteld aan giftige stoffen, zoals bijvoorbeeld uitlaatgassen, verbrandingsresten in voeding, maar ook andere giftige bestanddelen van planten en dieren, die via de voeding in de mens belanden. In het lichaam zijn daarom mechanismen aanwezig, die ervoor zorgen dat dergelijke stoffen zo min mogelijk schade kunnen veroorzaken. Deze ontgiftigings-processen vinden in het ganse lichaam plaats, maar met name in de lever. Daar komen via het bloed de meeste lichaamsvreemde stoffen vroeger of later terecht en daar is dan ook de concentratie van ontgiftende enzymen het hoogst. Enzymen zijn eiwitten die een chemische reactie kunnen versnellen. Een van de belangrijkste groepen ontgiftigings-enzymen zijn de zogenaamde cytochromen P450 (CYPs). Deze enzymen ontlenen hun naam aan hun kleur (het woord cytochroom is afgeleid uit het Grieks en staat voor kleurgevend aan cel, de P staat voor pigment), en aan hun unieke eigenschap dat ze licht met een golflengte van 450 nm selectief kunnen absorberen. Helaas zijn er ook stoffen die wel degelijk goed (kunnen) zijn voor het lichaam, maar die toch door CYPs worden herkend als mogelijk giftig, en dus worden afgebroken. Hierbij kan gedacht worden aan medicijnen. Om een medicijn goed te laten werken, is het een voordeel als deze zo min mogelijk wordt afgebroken. Dan kan de dosering omlaag en is er minder kans op bijwerkingen.
Er zijn ongeveer 60 menselijke CYP enzymen bekend waarvan de unieke vorm CYP2D6 één van de belangrijkste is wat betreft de afbraak van medicijnen. Ongeveer een derde deel van de medicijnen die momenteel worden voorgeschreven, wordt door CYP2D6 aangevallen en omgezet in een stof die uiteindelijk makkelijker via de urine het lichaam kan verlaten. Daarnaast is het ook nog eens zo dat bij verschillende personen, de hoeveelheid van CYP2D6 verschillend is. Dit is erfelijk bepaald en heeft een grote invloed op het vaststellen van een goede dosering van medicijnen voor iedere individuele patiënt.
Cytochromen P450 zijn enzymen met een kleur. Net als hemoglobine, het eiwit dat bloed haar rode kleur geeft, bevat cytochroom P450 ijzer. Vandaar dat gezuiverd CYP2D6 een rood/bruine kleur heeft, zoals de kaft van dit boekje. En net zoals het ijzer op de kaft van dit boekje verroest is door het reageren met zuurstof (oxidatie), zo kan ook CYP2D6 zuurstof binden, wat nodig is voor de activiteit van het enzym. CYP2D6 (en andere CYPs) splitst zuurstof; $O_2 \rightarrow 2O$, en bouwt één atoom daarvan in het medicijn. Zo wordt het medicijn vaak beter wateroplosbaar en dus makkelijker uit te scheiden.

Het is dus niet alleen een wetenschappelijke uitdaging, maar het heeft ook een direct praktisch nut om te weten hoe het enzym CYP2D6 werkt. Als dat bekend is, dan kan van tevoren worden voorspeld of een nieuw medicijn door CYP2D6 zal worden afgebroken. Eventueel kan het ontwerp van zo een stof hierop worden aangepast zodat dat niet meer het geval zal zijn. Natuurlijk bepaald niet enkel CYP2D6 het lot van een medicijn door een mens geslikt. Desalniettemin was dat de afgelopen vier jaar, en samengevat in dit boekje, wel de centrale vraag: hoe werkt CYP2D6?

Om met behulp van experimenten een antwoord op deze vraag te kunnen geven was in de eerste plaats het enzym zelf nodig in een reageerbuis. Bij een gebrek aan vrijwilligers is er voor gekozen CYP2D6 recombinant te maken. Het gen coderend voor CYP2D6 is gekloneerd

in bacteriën. Dit kloneren heeft als bijkomend voordeel dat het enzym te manipuleren is. Zo kunnen er kleine wijzigingen aangebracht worden, mutaties, waarbij gekeken kan worden wat het effect is op de medicijn-afbrekende activiteit. Deze experimenten zijn beschreven in Deel I van dit boekje.
In de hoofdstukken 2 en 3 hebben we door middel van het aanbrengen van mutaties aangetoond dat CYP2D6 een tweetal specifieke plekken heeft, die cruciaal zijn voor activiteit. Deze plekken, de aminozuren fenylalanine 120 en 483 zijn er voor nodig om een stof (het medicijn) op de goede plek aan CYP2D6 te laten binden, zodat het kan worden afgebroken. Vervolgens hebben we in hoofdstuk 4 aangetoond dat fenylalanines 120 en 483 niet exact dezelfde functie hebben en bovendien hebben we laten zien dat er meerdere aminozuren van belang zijn voor het binden van stoffen. Met de aminozuren reeds genoemd in de literatuur en degenen geïntroduceerd in de hoofdstukken 2 t/m 4 denken we dat de plekken in CYP2D6, die van belang zijn voor het binden van stoffen, voor het grootste deel in kaart zijn gebracht.
Ook in hoofdstuk 5 hebben we een mutatie aangebracht in CYP2D6, dit keer aan aminozuur threonine 309. Door middel van deze mutatie hebben we de activiteit van CYP2D6 kunnen veranderen, ofschoon de stoffen nog wel gewoon aan het enzym konden binden. Door naar specifieke reacties te kijken en deze te vergelijken met reeds beschreven onderzoek hebben we aannemelijk gemaakt dat threonine 309 betrokken is bij de activering van zuurstof in CYP2D6. De manier waarop zuurstof wordt geactiveerd is bepalend voor welke reactie het enzym uitvoert.

Dat CYP2D6 een atoom ijzer bevat is een prettige eigenschap voor het doen van onderzoek aan dit enzym. Hierdoor zijn kleine veranderingen aan het enzym (denk aan het binden van zuurstof of van een medicijn) namelijk gemakkelijk te meten, mits er aan het ijzer of de directe omgeving daarvan iets verandert. Dan namelijk verandert de exacte kleur van het enzym (de absorptiegolflengte verschuift), of de magnetische eigenschappen veranderen, of de trillingen van het ijzer in het enzym veranderen. Deze eigenschappen zijn bestudeerd (spectroscopisch) in deel II van dit boekje.
Zoals een kleine ijzeren spijker of een naald zich richt wanneer het bij een magneet wordt geplaatst, zo is ook het cytochroom P450 door zijn ijzeratoom, (para)magnetisch. Als er een medicijn aan het cytochroom P450 gebonden is, dan voelt deze stof als het ware het paramagnetische effect van het cytochroom P450 in een magneetveld. Dit effect is sterk afstandsafhankelijk en omdat het van één punt afkomstig is, het ijzeratoom, is door het meten van kernspin resonantie (NMR) de oriëntatie van het medicijn ten opzichte van het ijzer atoom te meten. Door in hoofdstuk 6 gebruik te maken van deze techniek, was het mogelijk een computermodel van CYP2D6 te valideren, waarmee de binding en oriëntaties van medicijnen in het enzym kunnen worden bepaald. Zo kon worden aangetoond, dat met het computer model goed te voorspellen viel hoe XTC en verwante stoffen door CYP2D6 worden afgebroken. XTC is nu bekend als feestdrug, maar is ooit ontwikkeld als medicijn tegen eetstoornissen. Daarnaast konden we met het computermodel het effect van de mutatie van fenylalanine 120 uit hoofdstuk 2 verklaren.

Alle moleculen trillen bij kamertemperatuur, zo ook CYP2D6. De frequenties waarmee trillingen van moleculen plaatsvinden, hangt af van de chemische structuur van de moleculen. De bindingen tussen atomen kunnen wat dat betreft vergeleken word met een gewicht aan een veer; het gewicht en de sterkte van de veer bepalen de heftigheid en levensduur van de trilling. In hoofdstuk 7 hebben we gekeken naar de frequenties waarbij CYP2D6 trillingen veroorzaakt na activering met behulp van een laser (resonantie Raman

spectroscopie). Daarbij hebben we met name gekeken of er een verschil was tussen het gewone, natuurlijke enzym en de T309V mutant, zoals we die hebben gemaakt in hoofdstuk 5. We hebben een aantal typische verschillen gevonden die veroorzaakt werden door de mutatie. Daaruit hebben we geconcludeerd dat het aminozuur T309 naast het activeren van zuurstof, ook betrokken is bij de organisatie van de watermoleculen in het enzym rondom het ijzeratoom. Uit andere studies blijkt dat dit van grote invloed kan zijn op de werking van andere CYP enzymen. Er was nog niet eerder onderzoek verricht naar dergelijke trillingen van CYP2D6. De relevantie van de verschillen die wij hier rapporteren na mutatie van T309 moet dus nog verder worden onderzocht.

Als een medicijn bindt aan CYP2D6 zodat het kan worden omgezet in een stof die makkelijk uit te scheiden is, dan zou je kunnen verwachten dat CYP2D6 van vorm veranderd, als een soort happende 'Pacman' die een blokje op eet. Het medicijn moet namelijk diep in CYP2D6 bij het ijzeratoom worden gebracht, want daar vindt de reactie plaats, en vervolgens moet het gevormde product weer uit het enzym. De medicijnen kunnen vrij grote moleculen zijn, terwijl CYP2D6 geen grote openingen heeft naar het goed beschermde ijzer atoom toe, vandaar de analogie met een happende Pacman. In hoofdstuk 8 hebben we geprobeerd deze mogelijke vormveranderingen in kaart te brengen. Daarbij hebben we weer gebruik gemaakt van het computermodel van CYP2D6 en we hebben het gemeten. Er zijn namelijk aminozuren in CYP2D6 die fluorescerend zijn; tryptophanen. Als deze worden beschenen met licht van een bepaalde golflengte dan zenden ze vervolgens zelf ook licht uit van een andere golflengte. De fluorescentie van deze tryptophanen kan vervolgens worden gedoofd door het ijzer bevattende centrum van het CYP2D6. Deze uitdoving vindt meer plaats indien de tryptophanen dichterbij het ijzeratoom zijn, en de uitdoving van de fluorescentie is dus een maat voor de afstanden in CYP2D6 van de tryptophanen naar het ijzeratoom. Door de fluorescentie van CYP2D6 te meten in aan en afwezigheid van een model-medicijn, hebben we kunnen vaststellen dat CYP2D6 een klein beetje van vorm veranderd als het een medicijn bindt. Deze vormveranderingen hebben we beschreven in hoofdstuk 8.

Door het doen van de experimenten beschreven in dit boekje, zijn we wijzer geworden over hoe CYP2D6 precies werkt. Daarnaast is het belangrijk dat we met de beschreven experimenten hebben laten zien dat ons computermodel van CYP2D6 in hoge mate overeenkomt met de werkelijkheid. Een computermodel van een eiwit is relatief gemakkelijk gemaakt, maar de kwaliteit van een model wordt bepaald door experimentele validatie.
Door de technieken die we hebben gebruikt ook te gaan toepassen op andere CYPs en andere medicijn-afbrekende enzymen, kan uiteindelijk een soort virtuele lever ontwikkeld worden. Daarmee kan tevoren worden nagegaan of een nieuw ontworpen molecuul met medicinale potentie niet wordt afgebroken alvorens het gewenste effect wordt verkregen. Bovendien kunnen er suggesties worden gedaan hoe het nieuwe medicijn zo aan te passen, dat het minder zal worden afgebroken. Door de ontwikkeling van deze modellen vallen betere medicijnen te ontwikkelen, met minder bijwerkingen, en uiteindelijk toegespitst op individuele patiënten.

List of publications

Keizers PHJ, Lussenburg BMA, de Graaf C, Mentink LM, Vermeulen NPE and Commandeur JNM, Influence of phenylalanine 120 on cytochrome P450 2D6 catalytic selectivity and regiospecificity: crucial role in 7-methoxy-4-(aminomethyl)-coumarin metabolism. *Biochem Pharmacol* **68**: 2263-2271, 2004.

Keizers PHJ*, de Graaf C*, de Kanter FJJ, Oostenbrink C, Feenstra KA, Commandeur JNM and Vermeulen NPE, Metabolic regio- and stereoselectivity of cytochrome P450 2D6 towards 3,4-methylenedioxy-N-alkyl-amphetamines: in silico predictions and experimental validation. *J Med Chem* **48**: 6117-6127, 2005. * *contributed equally*

Keizers PHJ, Schraven LHM, de Graaf C, Hidestrand M, Ingelman-Sundberg M, van Dijk BR, Vermeulen NPE and Commandeur JNM, Role of the conserved threonine 309 in mechanism of oxidation by cytochrome P450 2D6. *Biochem Biophys Res Commun* **338**: 1065-74, 2005.

Lussenburg BMA, Keizers PHJ, de Graaf C, Hidestrand M, Ingelman-Sundberg M, Vermeulen NPE and Commandeur JNM, The role of phenylalanine 483 in cytochrome P450 2D6 is strongly substrate dependent. *Biochem Pharmacol* **70**: 1253-61, 2005.

Stortelder A*, Keizers PHJ*, Oostenbrink C, de Graaf C, de Kruijf P, Vermeulen NPE, Gooijer C, Commandeur JNM and van der Zwan G, Binding of 7-methoxy-4-(aminomethyl)-coumarin to wild-type and W128F mutant cytochrome P450 2D6 studied by time resolved fluorescence spectroscopy. *Biochem J* **393**: 635-643, 2006. * *contributed equally*

van Waterschoot RAB, Keizers PHJ, de Graaf C, Vermeulen NPE and Tschirret-Guth RA, Topological Role of Cytochrome P450 2D6 Active Site Residues. *Arch Biochem Biophys* **447**: 53-58, 2006.

de Graaf C, Oostenbrink C, Keizers PHJ, van der Wijst T, Jongejan A and Vermeulen NPE, Catalytic site prediction and virtual screening of cytochrome P450 2D6 substrates by consideration of water and rescoring in automated docking. *J Med Chem* **49**: 2417-2430, 2006.

Bonifacio A, Keizers PHJ, Vermeulen NPE, Gooijer C, Commandeur JNM and van der Zwan G, Binding of bufuralol, dextromethorphan and 3,4-methylenedioxymethylamphetamine to wild-type and F120A mutant cytochrome P450 2D6 studied by resonance Raman spectroscopy. *Biochem Biophys Res Commun* **343**: 772-779, 2006.

Keizers PHJ, van Dijk BR, de Graaf C, Lussenburg BMA, Vermeulen NPE and Commandeur JNM, Metabolism of N-substituted 7-methoxy-4-(aminomethyl)-coumarins by cytochrome P450 2D6 mutants indicates additional substrate interaction points. *Xenobiotica* in press, 2006.

Keizers PHJ, Bonifacio A, Gooijer C, Vermeulen NPE, van der Zwan G and Commandeur JNM, Threonine 309 stabilizes the high spin state in cytochrome P450 2D6: a resonance Raman scattering study. in prep., 2006.

Curriculum Vitae

Peter Henricus Jozef Keizers was born on September 11th 1975 in Stad Delden. In 1993 he graduated from highschool (Atheneum) at the Twickel College in Hengelo (Ov). In the same year he started studying Medical Biology at the Utrecht University, which he changed for Chemistry at the Hogeschool van Utrecht after one year. He did his major in Biochemistry, for which he spent his internship at the Cell Biology group of Dr. Eric Ronken at the Pharmacology department of Solvay Pharmaceuticals in Weesp. The project involved studying signal transduction from G-protein coupled receptors (GPCRs) to the immediate early gene *c-fos*. In 1998 he started working as a Research Assistant at the Biotechnology department of Solvay Pharmaceuticals, where he developed novel assays to study GPCR ligand interactions and the receptor signal transduction. In the meanwhile, in 1999, he started studying Chemistry at the Utrecht University. For this study, he did his major at the department of Biochemistry of Lipids, of the Center for Biomembranes and Lipid Enzymology (CBLE), under supervision of Prof. Dr. Karel Wirtz and Dr. Gerry Snoek. The subject of this study was searching ligands for an orphan GPCR with a newly developed MAPK phosphorylation ELISA assay. The experimental work was performed at Solvay's under supervision of Dr. Gerard Dijkstra. He did his PhD research described in this thesis from July 2001 till September 2005 at the division of Molecular Toxicology, of the Leiden Amsterdam Center for Drug Research (LACDR), at the department of Chemistry and Pharmaceutical Sciences of the Vrije Universiteit Amsterdam, under the supervision of Prof. Dr. Nico P.E. Vermeulen, Dr. Jan N.M. Commandeur, and Prof. Dr. Saskia M. van der Vies. Currently, he is holding a postdoctoral position in the Metalloprotein group of the Leiden Institute of Chemistry.

Nawoord

In dit boekje heb ik vier jaar onderzoek samengevat, met de nadruk op de dingen die gelukt zijn natuurlijk. Bij het doen van de proefjes en alles wat daar bij komt kijken, zoals plezier, heb ik veel bijval gehad van anderen en die wil ik daar dan ook bij deze van harte voor danken. Een aantal mensen wil ik op deze plek daarvoor met naam noemen.
Nico, promotor is een benaming die letterlijk op jou slaat, met veel enthousiasme had je het project waar mogelijk altijd alvast verkocht en mijn naam ook al laten vallen, erg vleiend en af en toe ook handig. Dank dat je me hebt aangenomen en voor de vrijheid het onderzoek zelf vorm te geven. Jan, dank voor het zijn van mijn copromotor. We waren het niet altijd eens, maar een compromis was wel altijd te vinden. Je kritische blik is erg leerzaam geweest. Saskia, dank voor het zijn van tweede promotor. Je was met name als trekker van het CCM programma betrokken bij het project. Dank voor het opzetten van het ambitieuze project en de verschillende partijen bij elkaar te houden. Alois en Chris, paranimfen, doorgewinterde verhuizers, bergbeklimmers. Tussen de sigaren en drank door hebben we menig discussie gevoerd, waaronder ook wetenschappelijke. Veel dank voor de goede tijden. Jeroen en Sebas, het was me een genoegen samen de nieuwe batch MolTox aio's te vormen. De cursussen en meetings in Londen, Noordwijkerhout, Lunteren, en bij Bolt Thrower waren mede door jullie de moeite waard. Een van de doelen van het CCM project was de samenwerking tussen de verschillende disciplines te intensiveren. Dat is goed gelukt, vooral door de inzet van de deelnemers. Aike, André, Andreas, Bart, Cees, Gert, Harm, Johnny, Koop, Marcel, Mirka, Patrick en Stéphane, allen dank voor de samenwerking. Natuurlijk ook dank aan alle mensen die in mijn tijd in of rond het Moltox lab werkzaam waren en bijdroegen aan wetenschap en gezelligheid; Aldo, Anton, Barbara, Chris O., Eva, Francine, Hande, Hilmi, Jelle, Jennifer, Laura, Marola, Martijn, Micaela, Peter S., Regina en Robert. Ed, je hebt veel enzym voor me geproduceerd, voor mij en mijn opvolgers erg handig. Veel dank voor je hulp. Frans, dank voor de hulp met de NMR metingen. Magnus and Mats, thanks for the collaboration. Ik heb met veel studenten mogen werken gedurende het project; Ayla, Ben, Jon, Letty, Loek, Mirabela, Nazha, Petra, Roos en Saskia, dank voor jullie inzet en wat jullie mij hebben geleerd. Familie en vrienden, dank voor de getoonde interesse in het meestal onbegrijpelijke gespeel wat ik als werk doe. Es, dank voor alles!

List of abbreviations

ADHD	attention deficit/hyperactivity disorder
AU	arbitrary units
BF	bufuralol
BHAMC	N-butyl 7-hydroxy-4-(aminomethyl)-coumarin
BMAMC	N-butyl 7-methoxy-4-(aminomethyl)-coumarin
cDNA	copy Deoxyribose Nucleic Acid
CPR	cytochrome P450 NADPH-reductase
CuOOH	cumene hydroperoxide
CYP	cytochrome P450
D301Q	aspartic acid 301 → glutamine
DX	dextromethorphan
EHAMC	N-ethyl 7-hydroxy-4-(aminomethyl)-coumarin
EMAMC	N-ethyll 7-methoxy-4-(aminomethyl)-coumarin
F120A	phenylalanine 120 → Alanine
F483A	phenylalanine 483 → alanine
FRET	Förster resonance energy transfer
FU	fluorescence units
HAMC	7-hydroxy-4-(aminomethyl)-coumarin
KPi buffer	50 mM potassium phosphate buffer, pH 7.4
MAMC	7-methoxy-4-(aminomethyl)-coumarin
MAO	monoamine oxidase
MD	molecular dynamics
MDA	methylenedioxyamphetamine
MDAAs	N-alkyl 3,4-methylenedioxymethylamphetamines
MDEA	N-ethyl 3,4-methylenedioxymethylamphetamine
MDMA	3,4-methylenedioxymethylamphetamine
MDPA	N-propyl 3,4-methylenedioxymethylamphetamine
MHAMC	N-methyl 7-hydroxy-4-(aminomethyl)-coumarin
MMAMC	N-methyl 7-methoxy-4-(aminomethyl)-coumarin
NADPH	reduced nicotinamide adenine dinucleotide phosphate
NMR	nuclear magnetic resonance
N-OH-MDMA	N-hydroxy 3,4-methylenedioxymethylamphetamine
3,4-OH-MDA	3,4-hydroxymethylamphetamine
PHAMC	N-propyl 7-hydroxy-4-(aminomethyl)-coumarin
PMAMC	N-propyl 7-methoxy-4-(aminomethyl)-coumarin
RR	resonance Raman
T309V	threonine 309 → valine
T312V	threonine 312 → valine
t_R	retention time
W128F	tryptophan 128 → phenylalanine

Color figures

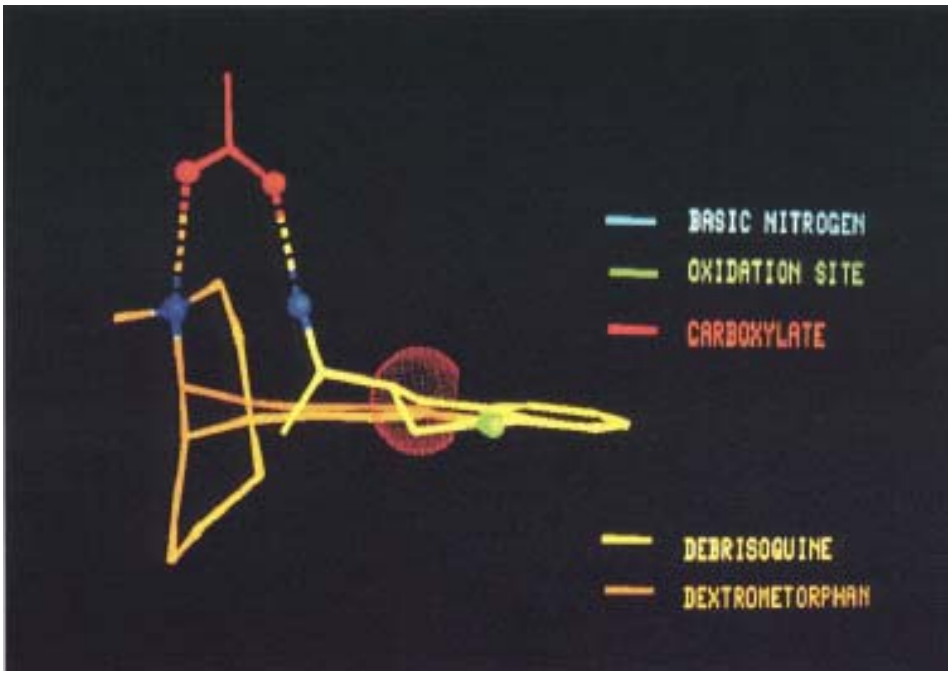

Chapter 1, Figure 4: Conformations of the template substrates debrisoquine and dextromethorphan used to construct the pharmacophore model of CYP2D6. The sites of oxidation are fixed and the red dotted surface represents a part in the molecule where all substrates exhibit a negative electrostatic potential.

A

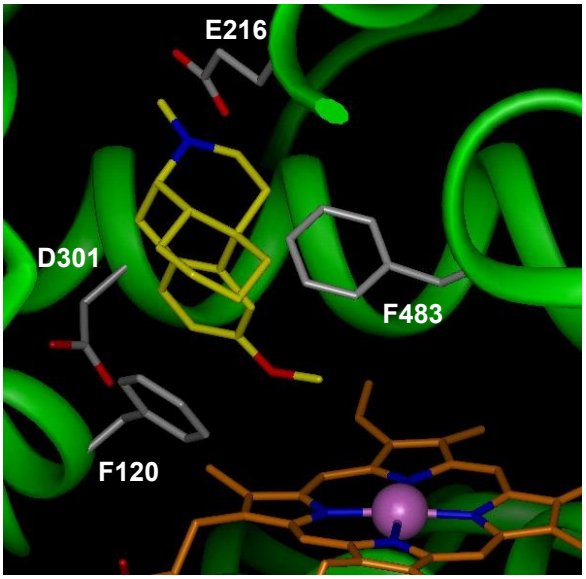

B

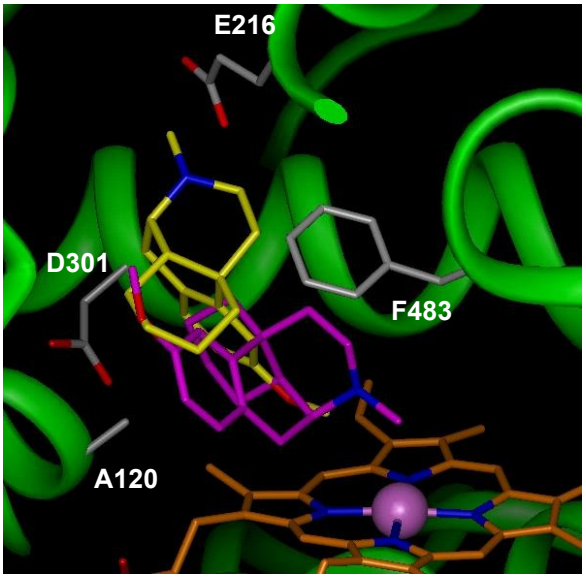

Chapter 2, Figure 4: Binding orientation of dextromethorphan automatically docked in the active site of the homology models of CYP2D6 using Autodock with standard conditions. In wild-type CYP2D6 the orientation of dextromethorphan (in yellow) with its O-methyl pointing towards the heme is favored (A), in the F120A mutant two distinct orientations, supporting both N-demethylation (in magenta) as *O-*demethylation (in yellow) were found (B).

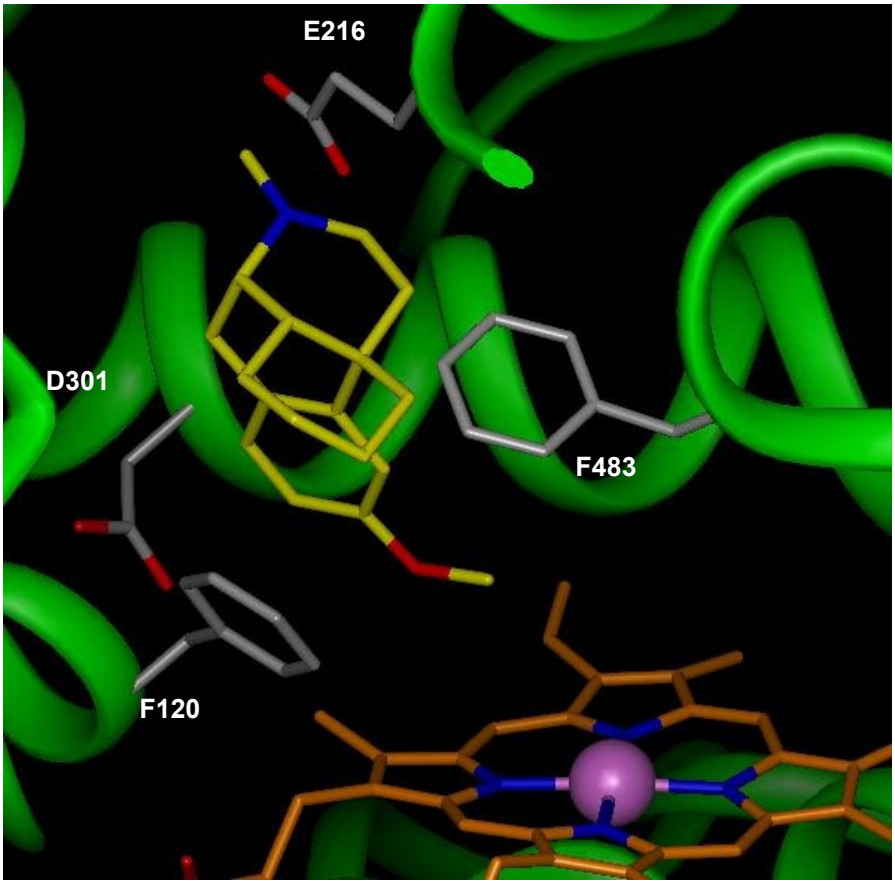

Chapter 3, Figure 1: The active site of the homology model of CYP2D6 [5], showing the active site residues F120, E216, D301 and F483. The pink ball is the heme iron atom. In yellow, the substrate dextromethorphan is depicted.

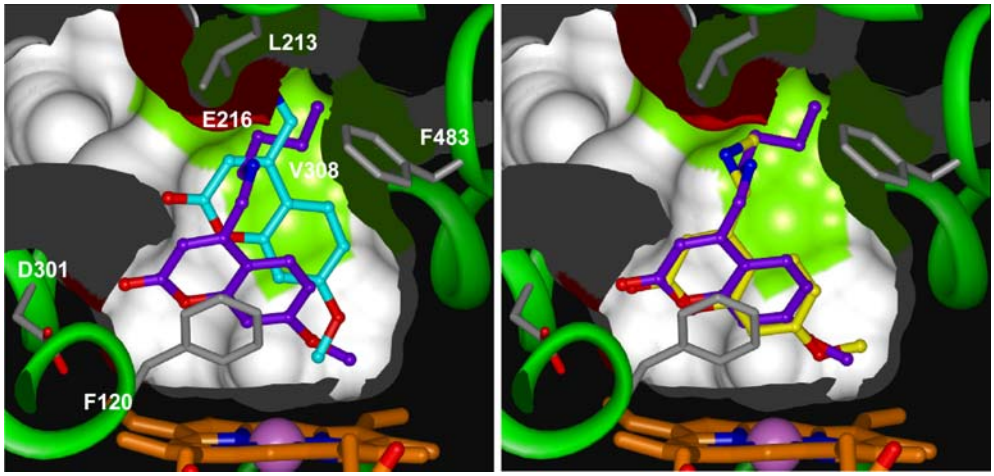

Chapter 4, Figure 3: MAMC (cyan) and BMAMC (purple) (left panel), and MMAMC (yellow) and BMAMC (purple) (right panel), docked into the CYP2D6 homology model as described in the Methods section. The molecular Connoly surface of the active site of CYP2D6 is depicted; the surfaces of carboxyl oxygen atoms of D301 and E216, and the apolar sidechain atoms of L213, V308, and F483 are colored red and green, respectively. Amino acid side chains involved in substrate binding are shown as sticks. For reasons of clarity, only the locations of E216 and V308 are indicated.

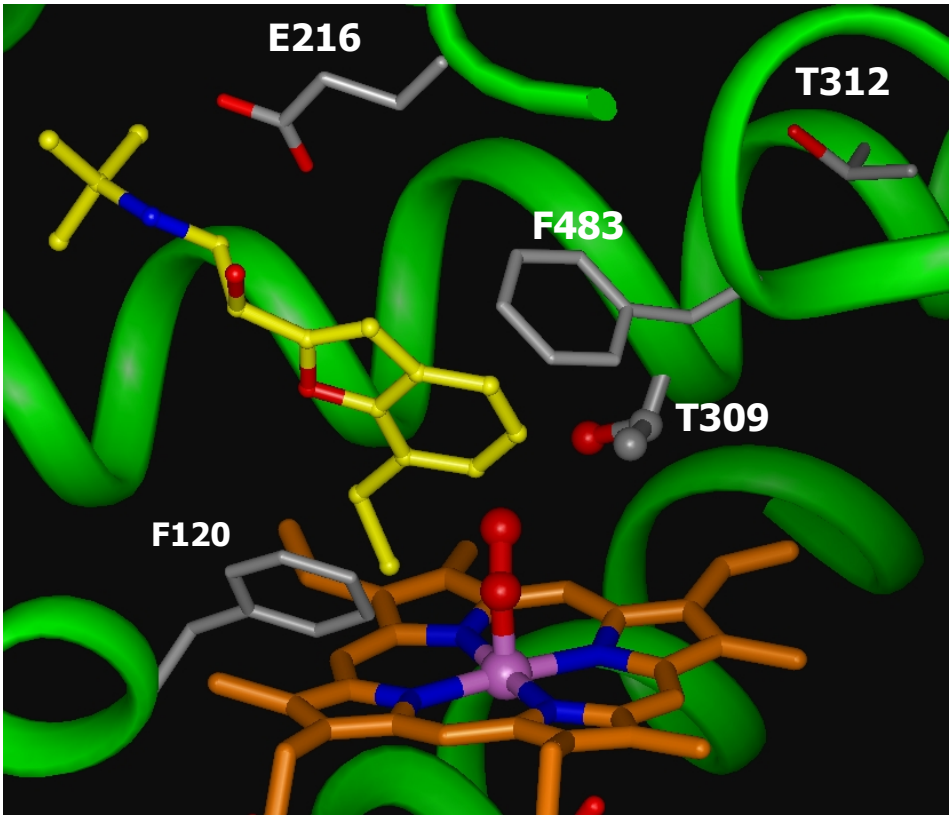

Chapter 5, Figure 1A: Protein model displaying the active site of CYP2D6 with dioxygen and S-bufuralol bound, showing the positions of the substrate interacting residues F120, F483 and E216, the conserved putative oxygen activating T309, and conserved T312.

A

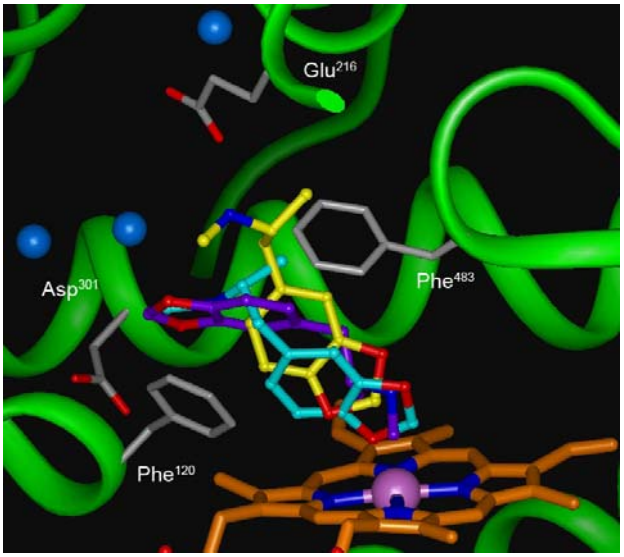

B

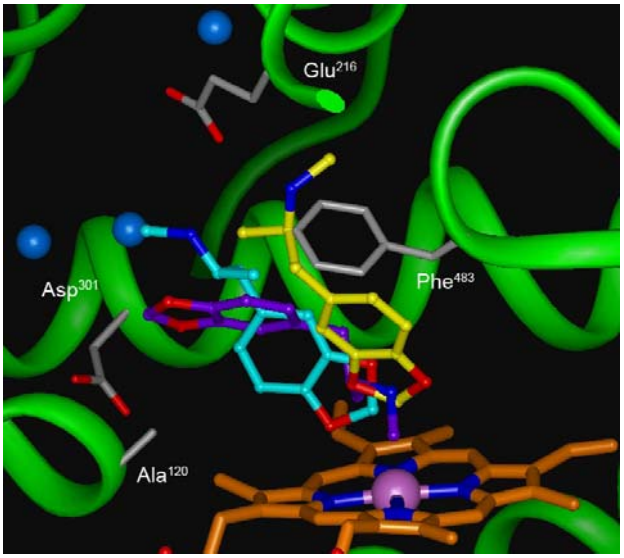

Chapter 6, Figure 6: Molecular dynamics (MD) simulations starting orientations of charged R-MDMA, generated by automated docking studies in wild-type (A) and F120A mutant (B) CYP2D6 homology models. Two orientations are corresponding to O-demethylenation, with the substrate nitrogen-atom either in close contact with E216 (pose 1, in yellow) or placed between E216 and D301 (pose 2, in cyan). A third orientation is corresponding to N-demethylation or N-hydroxylation (pose 3, in purple). Water oxygen atoms, as predicted by GRID (see Materials and Methods section), are depicted in blue.

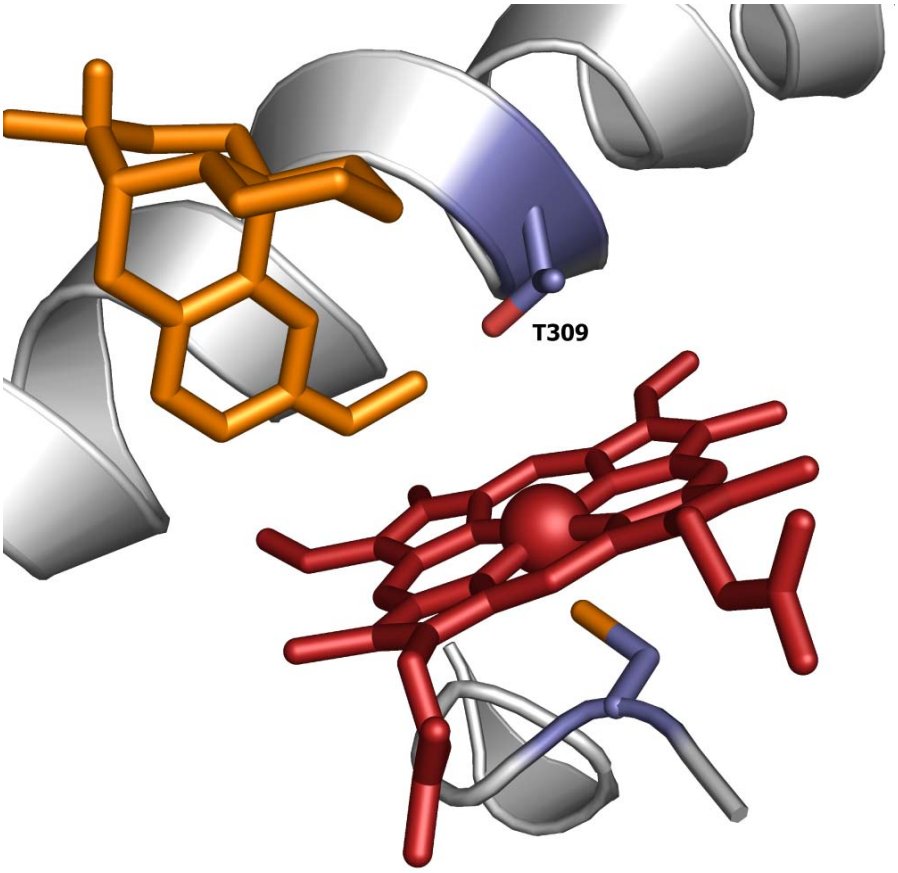

Chapter 7, Figure 6: Protein model displaying the active site of CYP2D6 with dextromethorphan bound. The porphyrin is shown in red with Fe as a sphere, the Fe coordinating C443 is shown and the putative oxygen activating T309.

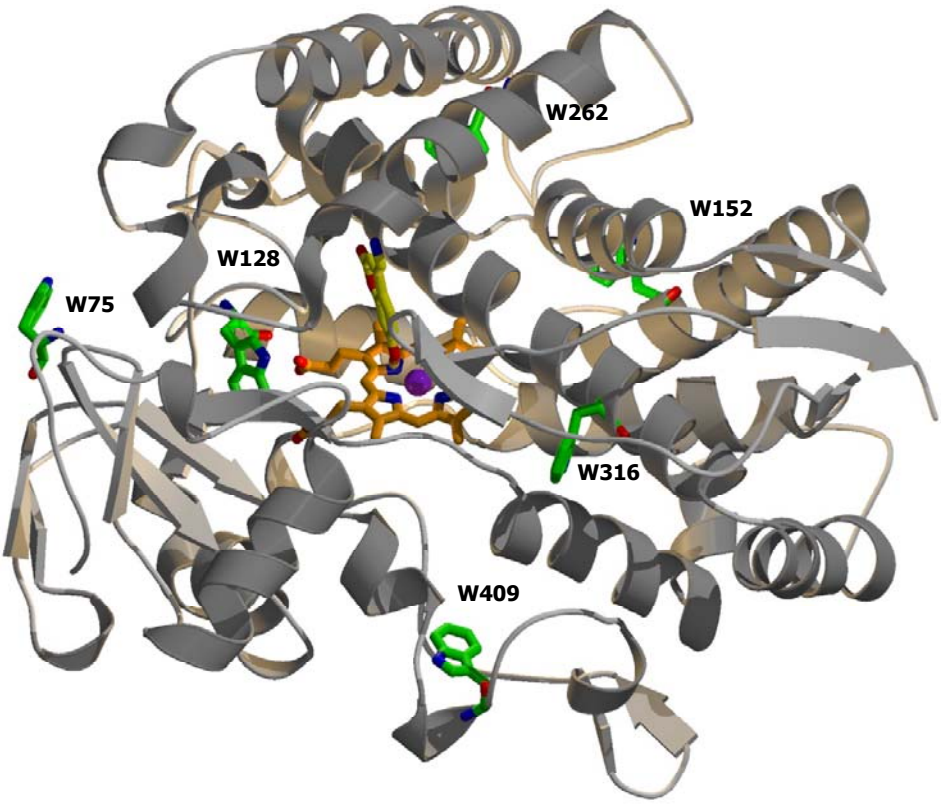

Chapter 8, Figure 5: Homology model of CYP2D6 based on rabbit CYP2C5, indicating the positions of the six tryptophans (red; purple for W128), the heme-group (green) and the substrate MAMC (yellow). W28 is not present in the homology model.

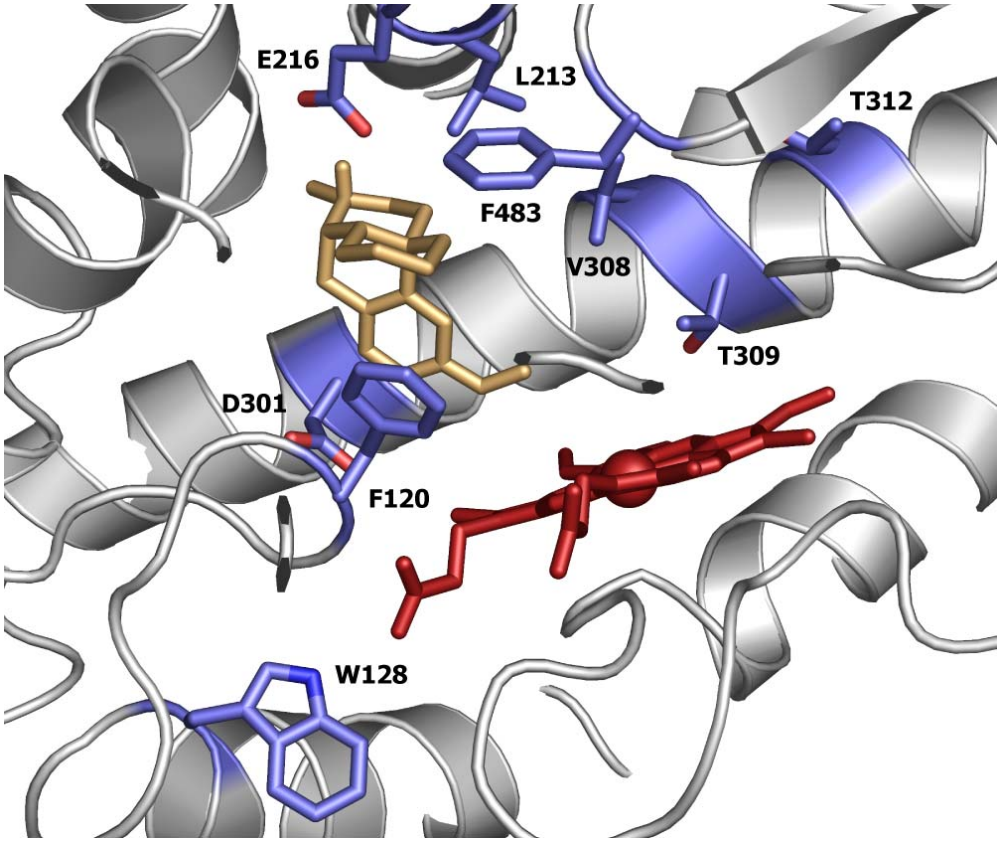

Chapter 9, Figure 1: The CYP2D6 active site (heme in red, Fe as sphere) according to the homology model, with dextromethorphan (in orange) bound according to automated docking (GOLD-Chemscore), showing the key residues involved in enzyme activity and the other residues that have been mutated in this thesis. F120, F483, L213, and V308 are identified as being involved in steric restriction and/or hydrophobic interaction with substrates, E216 is interacting with basic substrate N-atoms, D301 interacts with the backbone of F120, W128 interacts via H-bonds with the pyrrole C-propionate and was mutated to a phenylalanine in Chapter 8, which did not affect the activity, and T312 was mutated to a valine in Chapter 5, which did not affect activity either. The figure was made using Pymol 0.98.

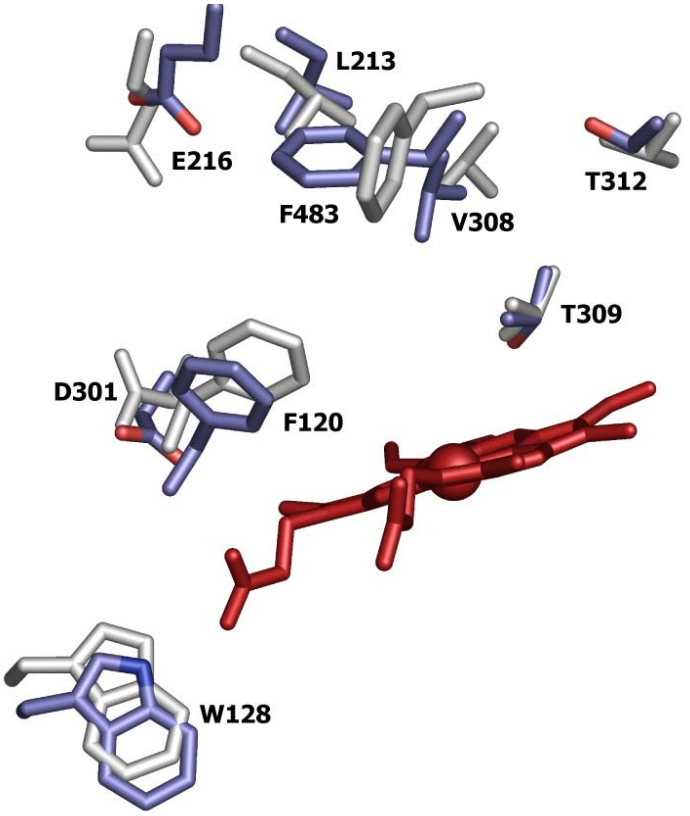

Chapter 9, Figure 2: Overlay of the heme (red, Fe as sphere) and the active site residues examined in this thesis from the homology model, depicted in blue, and from the crystal structure of CYP2D6, depicted in gray. The figure was made using Pymol 0.98.